UNIVERSITY OF BELGRADE

FACULTY OF TECHNOLOGY AND METALLURGY

Luka V. Živković

A METHODOLOGY FOR REACTOR SYNTHESIS BASED ON PROCESS INTENSIFICATION CONCEPTS AND APPLICATION OF OPTIMIZATION METHODS

Doctoral Dissertation

Belgrade, 2019

УНИВЕРЗИТЕТ У БЕОГРАДУ

ТЕХНОЛОШКО-МЕТАЛУРШКИ ФАКУЛТЕТ

Лука В. Живковић

МЕТОДОЛОГИЈА ЗА СИНТЕЗУ РЕАКТОРА ЗАСНОВАНА НА КОНЦЕПТИМА ИНТЕНЗИФИКАЦИЈЕ ПРОЦЕСА И ПРИМЕНИ МЕТОДА ОПТИМИЗАЦИЈЕ

докторска дисертација

Београд, 2019

Commission

_____

Prof. Dr. Nikola Nikačević (Mentor)
University of Belgrade / Faculty of Technology and Metallurgy

_____

Prof. Dr. Menka Petkovska
University of Belgrade / Faculty of Technology and Metallurgy

_____

Assist. Prof. Dr. Blaž Likozar, Senior Scientific Associate
National Institute of Chemistry, Ljubljana / Department of Catalysis and Chemical Reaction Engineering

Date **Ph.D. Student**

_____ _____
Luka Živković, dipl. ing.

Acknowledgments

I want to thank my Mentor, Prof. Dr. Nikola Nikačević, for his patience, support, advice, and help during the work on this thesis.

I would also like to thank Prof. Dr. Menka Pekovska for her advice, opportunity to work under her guidance, and participate in Process Control classes.

I am grateful to all members of the Department of Catalysis and Chemical Reaction Engineering in National Institute of Chemistry in Slovenia for their warm hospitality and opportunity to work in their team.

Finally, I would like to thank my family for giving me support through all these years.

Abstract

In this Ph.D. thesis, a new methodology for **Re**actor **Sy**nthesis Based on **P**rocess **I**ntensification Concepts and Application of **O**ptimization Methods (ReSyPIO) is presented and applied to two different cases.

In **Chapter 1: Introduction – Motivation and Objectives**, the motive for the research is presented, and Hypotheses are formulated. The ReSyPIO methodology that rests upon these Hypotheses and consists of three consecutive stages is briefly described in this Chapter. The first stage encapsulates all present phases and phenomena inside the reactor functional building block, called module. Modules come as a direct result of a conceptual representation of the analyzed system. In the second stage, modules are further segmented if needed and interconnected, creating a reactor superstructure that is mathematically described for all desirable operating regimes. In the last stage of the ReSyPIO methodology, the optimal structure, operating conditions, and the operational regime are determined with the use of rigorous optimization. All three stages of the ReSyPIO methodology have a backflow, meaning that if analysis leads to impractical, nonfunctional or inefficient results, modifications in reactor superstructure and modules can be made. The objective is to conceptually and numerically derive the most efficient reactor structure and a set of operating conditions that would be used as a starting point in the future reactor design.

Chapter 2: Literature Review is used to cover and review the most important research published in the area of Process Intensification and different Process System Engineering techniques. Different approaches and studies present in academia are highlighted and their elements compared with the presented ReSyPIO methodology with the accent on its advantages and contribution to the engineering science community.

Also, in this Chapter, an array of well researched analytical and numerical approaches is presented that could be used in the future to strengthen the ReSyPIO methodology further and facilitate its easier application.

In **Chapter 3: Description of the ReSyPIO Methodology** Reactor Synthesis based on Process Intensification and Optimization of Superstructure is explained in detail, with a graphical representation of the main building block, called Phenomenological Module. A general explanation is given on how to form a reactor superstructure and mathematically describe it with sets of material and energy balance equations that correspond to a number of present phases and components in the system.

The ReSyPIO methodology is first applied to a generic case of two parallel reactions in **Chapter 4**, called **Application of the ReSyPIO Methodology on a Generic Reaction Case**. The case corresponds to two parallel reactions that could be found in the fine chemical industry. The reactions are endothermic and slow with the undesired product. After the application of the ReSyPIO methodology, an optimal reactor structure consisting of a segmented module with 17 side inlets for the reactant and heat source is obtained. It is recommended for the reactor to work in a continuous steady-state mode as the dynamic operation would not lead to a sufficient increase in reactor efficiency.

In **Chapter 6: Reactor Synthesis for Hydrogen Production Through Sorption– and Membrane–Enhanced Water–Gas Shift Reaction**, the ReSyPIO methodology is applied on an industrially relevant case for which detailed experimental research was conducted, published and included in **Chapter 5: Experimental Research on Sorption-Enhanced Water–Gas Shift Reaction**. Steady-state experiments were performed for determination of water-gas shift kinetic parameters in a packed bed reactor. Additionally, dynamic experiments were conducted to determine diffusion parameters of sorption-enhanced water-gas shift reaction. Both types of experiments showed that water-gas shift reaction and hydrogen production could be significantly improved by a sorption-enhanced process with calcium oxide used as the sorbent.

Estimated kinetic and diffusion parameters are then used to screen all phenomena and create modules that can also include a possibility of hydrogen removal with Palladium membrane. After reactor superstructure creation and rigorous multi-objective optimization, the results show that the most significant reactor efficiency can be achieved in a reactor with two modules with sorption and no membrane.

In **Conclusions**, main advantages and challenges of the proposed ReSyPIO methodology are listed with the prospects for future use and possible integration with other Process System Engineering methods.

Keywords

- reactor synthesis
- process intensification
- process integration
- dynamic optimization
- multi-objective optimization
- water-gas shift reaction
- sorption-enhanced reaction
- membrane reactor
- trickle solids reactor

Сажетак

У овој докторској дисертацији је представљена и примењена нова методологија за синтезу реактора заснована на концептима интензификације процеса и примени различитих оптимизационих техника (***Re****actor* ***Sy****nthesis Based on* ***P****rocess* ***I****ntensification Concepts and Application of* ***O****ptimization Methods* – ReSyPIO).

У поглављу **Увод – Мотивација и циљеви**, формиране су хипотезе на којима почива ReSyPIO методологија и дата је мотивација за истраживање. ReSyPIO методологија је укратко представљена и описана кроз три узастопне етапе. Прва етапа уоквирава све присутне фазе и феномене у реактору унутар функционалних градивних јединица, названих модули. Модули представљају резултат концептуалног приказа анализираног система. У другој етапи, модули се по потреби могу даље поделити у сегменте и међусобно повезати, креирајући суперструктуру реактора. Суперструктура је математички описана за све режиме рада реактора од интереса. У последњој етапи ReSyPIO методологије, оптимална структура, услови и режим рада реактора су одређени применом ригорозне оптимизације. Све три етапе ReSyPIO методологије имају повратни ток, што значи да уколико анализа води ка непрактичним, нефункционалним или неефикасним решењима, модификација математичког модела, суперструктуре и/или модула је могућа. Циљ примене ReSyPIO методологије је да се концептуалним и нумеричким приступом дође до оптималне препоруке за структуру реактора, оперативне услове и режим рада, која би била почетна претпоставка у будућем дизајну уређаја.

Преглед литературе даје опис и приказ свих истраживања од интереса, из области Интензификације процеса и Теорије и анализе процесних система. Наглашени су различити приступи и студије присутне у истраживачкој

заједници, а њихови елементи упоређени са представљеном ReSyPIO методологијом са акцентом на предностима и научном доприносу. У овом поглављу је дат и низ добро истражених аналитичких и нумеричких приступа који би могли да буду коришћени у оквиру ReSyPIO методологије и олакшају њену примену.

У поглављу **Опис ReSyPIO методологије**, је детаљно објашњена синтеза реактора заснована на концептима интензификације процеса и оптимизацији суперструктуре. Прво је дата процедура за графичку и концептуалну репрезентацију система, преко главних градивних јединица, феноменолошких модула. Потом је објашњено како се креира суперструктура реактора. На крају је дат уопштен поступак за математички опис суперструктуре преко скупова једначина материјалног и енергетског биланса, чији број зависи од броја присутних фаза и компонената у систему.

ReSyPIO методологија је први пут примењена на случају две генеричке паралелне реакције у поглављу под називом **Примена ReSyPIO методологије на случају генеричке реакције**. Овај случај одговара реакцијама које се могу наћи у индустрији финих хемикалија. Реакције су ендотермне и споре, при чему је кинетички фаворизовано креирање нежељеног производа. Након примене ReSyPIO методологије, добијена је оптимална структура реактора која се састоји од сегментисаног модула са 17 улаза за извор топлоте и реактант који се дозира. Предложено је да реактор ради континуално, у стационарном режиму рада, јер би динамички режим рада резултовао недовољним повећањем ефикасности реактора.

У поглављу **Синтеза реактора за производњу водоника реакцијом водене паре побољшане сорпцијом и мембранском сепарацијом**, ReSyPIO методологија је примењена на случају од индустријског значаја, за који је детаљно експериментално истраживање урађено, објављено и описано у претходном поглављу под називом, **Експериментално истраживање реакције воденог гаса побољшане сорпцијом**.

Урађени су експерименти у стационарном стању, у реактору са пакованим слојем, ради одређивања кинетичких параметара реакције воденог гаса, и динамички експерименти помоћу којих су естимирани дифузиони параметри када је иста реакција побољшана сорпцијом. Обе врсте експеримената су показале да се реакција воденог гаса и производња водоника могу унапредити у значајној мери, укључивањем сорпције на калцијум оксиду. Естимирани кинетички и дифузиони параметри су потом коришћени за прву етапу ReSyPIO методологије, тј. преглед, одабир и анализу феномена, уз остављену могућност уклањања водоника путем мембранске сепарације. Након креирања суперструктуре реактора и ригорозне мултиобјектне оптимизације, резултати су показали да се највећа ефикасност реактора може остварити уколико се он састоји од два модула без мембране, са присутном сепарацијом.

У **Закључцима**, је дат преглед главних предности и недостатака примењене ReSyPIO методологије, са перспективом будуће примене и могуће интеграције са другим методама из области Теорије и анализе процесних система.

Кључне речи

- синтеза реактора
- интензификација процеса
- интеграција процеса
- динамичка оптимизација
- мултиобјектна оптимизација
- реакција водене паре
- реакција побољшана сорпцијом
- мембрански реактор
- реактор са падајућим честицама

Table of Contents

1. Introduction – Motivation and Objectives

"One's judgments are always based on what comes to mind."

Daniel Kahneman, the famous Israeli-American behavioral economist, said that *"people are not accustomed to thinking hard and are often content to trust a plausible judgment that comes to mind."* He further added in his *Model of Judgment Heuristics* that people *"rely on a limited number of heuristic principles which reduce the complex tasks of assessing probabilities"* [1].

The subject of this thesis is to develop and apply a new methodology for reactor conceptual design. So far, the traditional selection of reactors in the chemical industry has been mostly based on experience, thus giving a narrow pallet of choices according to which, the judgment is to be made. The goal of this thesis is to try to widen the range of choices for decision-making. The choices are to be derived as objectively as possible by developing a network of possible solutions. This network will then be subjected to a rigorous optimization to obtain an optimal recommendation or set of recommendations for the reactor structure and its operating conditions. The range of choices and decision-making is therefore not based solely on heuristics, i.e., existing solutions in chemical engineering, but on what could give the maximum theoretical efficiency. This conceptual solution is to be used as a starting point in the more detailed reactor and device design.

Limited resources and continually increasing global population and production costs have led to a greater need for more efficiency in the industry. The processes used in production require constant upgrades, changes, and innovative solutions to keep up with the fast pace of changing global needs. As a result, existing technologies and processes are enhanced with the use of concepts of process intensification (PI) and the application of different process system engineering (PSE) techniques.

The application of PI concepts and PSE techniques has led to significant contributions in the area of the conceptual design of a new type of reactors and increased efficiency of the process. The exclusive combination and integration of PI concepts and different PSE techniques, which allows for a unique conceptual way of problem formulation and solving, is the cornerstone of the proposed methodology. The result is not a product of solely "what comes to mind" but of a theoretical and rigorous optimization analysis.

The methodology for reactor synthesis based on process intensification concepts and application of optimization methods, or shortly ReSyPIO, and the thesis, rest on the following starting hypotheses:

Hypothesis I: Reactor or reaction system is defined as a control volume where a reaction process or set of reaction accompanying processes occur. This system can be conceptually synthesized.

Hypothesis II: A methodology based on different mathematical and engineering techniques can be derived. This methodology would give a recommendation for the structure and operating conditions of the reaction system defined by *Hypothesis I*.

Hypothesis III: The main building blocks of the reaction system defined by *Hypothesis I* are phenomenological modules. Modules consist of phases in which different phenomena occur. Phenomena are processes of interest in the synthesized reaction system. They can represent chemical reaction, mass transfer (convection and diffusion), heat transfer (convection, conduction, radiation or other heat sources/sinks), phase change (melting, condensation, evaporation, sublimation or crystallization) and surface phenomena (adsorption, desorption, capillary effects, adhesion, abrasion, agglomeration etc.).

Hypothesis IV: Phenomena of interest in the phenomenological module defined by *Hypothesis III* can be mathematically described. The reaction system defined by *Hypothesis I* can be subsequently represented with a mathematical model or set of models that would not presuppose the layout of modules inside the reactor (superstructure) or its operating conditions.

Hypothesis V: The model or models that mathematically define the reactor are robust for optimization. The applied optimization methods result in optimal reaction system structure and the operating conditions that give the highest theoretical efficiency. The efficiency is defined according to process requirements and overall production goals. The optimal result presents a recommendation or the first step in reactor design.

The ReSyPIO methodology is split into three different stages. The first stage, called *Phenomena Screening*, is conceptual and consists of the analysis of the reaction and all accompanying processes of interest that would improve the reaction. During this stage, phenomenological modules (*Hypothesis III*) are defined. Modules serve as building blocks, or conceptual sets of present phases and phenomena. In the following stage, which is both conceptual and mathematical, the superstructure of the reactor is derived. The superstructure is mathematically described with one, or several models (*Reactor System Superstructure and Mathematical Modeling*) needed to cover all operational regimes of interest. In the last, numerical stage of the ReSyPIO methodology, called *Optimization*, different PSE techniques are applied to obtain the optimal reactor structure and operating conditions. Three stages are, therefore, unique: conceptual, mathematical, and numerical stage. If one of them leads to an undesired or impractical solution, the user can reassess the work done in the previous stage. The stage-backflow allows the user to rethink the conceptual foundation (proposed module) in the first stage if it cannot be mathematically described (the second stage) or numerically leads to no improvements (the third

stage). The user can also change the mathematical model (the second stage) if the used numerical integration techniques and software fail to give any solution. In the end, the user can always try other numerical methods or combine them with analytical PSE techniques, if available. All three stages of the ReSyPIO methodology, including their steps, will be presented on two separate cases: a general example of two parallel reactions, and an industrially relevant process of hydrogen production through water-gas shift reaction. The industrial case was experimentally analyzed to estimate all kinetic and diffusion parameters needed for the application of this methodology. All guidelines about the general applicability of the ReSyPIO methodology and overall conclusions are presented at the end.

The scientific contributions of the thesis are reflected in (to be) published research articles [2-4]. Among the first contributions is the development and presentation of a new methodology for conceptual reactor synthesis [2]. The ReSyPIO methodology is unique among other present reactor synthesis methods because it can simultaneously cover all three aspects of a reaction system: its structure, operating conditions, and operational regime, and uses rigorous optimization to derive the recommendation that is to be used for future device design. Its uniqueness is reflected in the fact that it covers all four PI domains: structural, synergetic, dynamic, and energetic. The contemporaneity of the ReSyPIO methodology is seen in its application on an industrial case of hydrogen production [4]. Hydrogen is a vital element of a sustainable energy system and causes no harmful effects on the environment. As a fuel, hydrogen can be produced in different ways, one being through the water-gas shift reaction. A detailed experimental investigation of this reaction was conducted, as well as sorption-enhanced water-gas shift reaction [3]. Kinetic and diffusion parameters were estimated for an industrial iron-chromium catalyst and calcium oxide sorbent. This gave more insight into the advantages of sorption-enhanced water-gas shift reaction and provided the scientific community with experimental and estimation data for further investigations in this field. The data was then used to propose an original recommendation for the hydrogen production reactor design [4], which is the final contribution of this thesis.

2. Literature Review

The increase in global demand for products of any kind, limited resources, and environmental concerns have entailed a need to improve the existing production processes radically, i.e., intensify them (Process Intensification, PI) and apply different process system engineering methods (Process System Engineering, PSE) [5]. PI pertains to process development that leads to smaller equipment, i.e., reduction in size, improved control of reaction kinetics, higher energy efficiency, and reduced capital costs. While the word "intensification" is analogous to enhancement, PI pertains to all active and passive methods to achieve a smaller, more efficient, cheaper, and environmentally friendly process [6].

Activities within designing process systems include process design, optimal arranging and system operations planning as well as optimal management. Most PSE methods describe the behavior of the system as a whole and emphasize how individual system components and their interaction contribute to increasing or decreasing system efficiency [7]. The chemical reactor is the major part of a system in the chemical processing industry whose efficiency widely affects the economic profit of the whole process [6]. The reactor itself or the reaction system can be viewed as a processing device that should be devised, designed, and controlled. The traditional design of reactors in the industry involves the steps shown in Figure 2.1 [8].

From Figure 2.1 it follows that the first step in the traditional design is choosing device type based on the already existing experience, i.e., heuristics. This choice is usually reduced to two basic classes of reactors: with batch or continuous mode of operation. The next step is to design the device for the given case, that is, to obtain optimal geometric and physical sizes of the reaction system. The final step is to analyze the formed reactor stability and the control system design. Such an approach yields reactors that are applicable in practice but leaves little space for creativity in terms of their structure and modes of operation.

The increase in the efficiency of such designed devices is reduced to modifying the input values and reaction parameters (e.g., a type of catalyst and the introduction of parallel reactions) after their finalization.

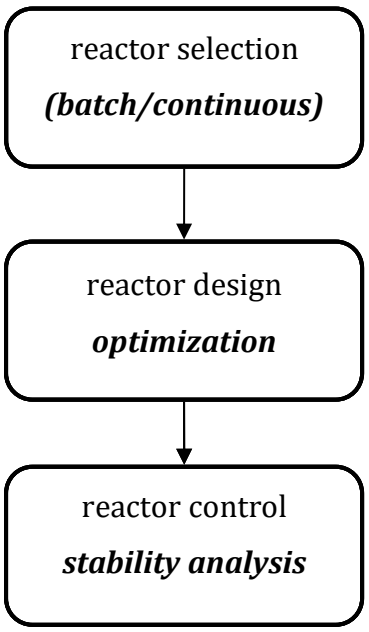

Figure 2.1 - Traditional approach to reaction system synthesis [8]

Using PSE techniques, it is possible to achieve greater integration of process elements, to determine the potential for theoretically highest possible improvement, and to design the process and device [9]. In the academic sphere, there are a large number of proposed methodologies for integrated design and control of the system [10, 11] and integrated reactor operation and design [12].

Over the following several Sections, past and recent publications will be covered in the PI and PSE domain. Firstly, PI will be defined as the means of enhancing processes, and its brief history will be given. Then PSE will be covered as a means of achieving novel ways to intensify processes, and in the end, challenges and prospects for the future will be included.

2.1 Chemical Engineering and Process Intensification

In the late 1950s, professors from the University of Wisconsin, Byron Bird, Warren Stewart, and Edwin Lightfoot highlighted the importance of a better understanding of mass, heat, and momentum transfer [13]. Their well-known textbook "Transport Phenomena" [14] influenced chemical engineering to the extent that it enabled defining generalized equations. Before them, the transfer of different sizes in the process was described at a quantitative level and for a narrow range of operations and devices. In the same period, professors from the University of Minnesota, Neal Amundson and Rutherford Aris, have increased the significance of mathematical modeling in chemical engineering [13]. Two significant releases in 1956, "Unit Operations of Chemical Engineering," by Warren Mccabe, Julian Smith and Peter Harriott [15], and "Chemical Engineering Kinetics" by Joseph Smith [16], have changed how chemical engineering is taught. The first book has retained its importance in education to this day, while the second book first presents chapters in the field of reactor design so that it could be referred to as an introduction to "reaction engineering" [17]. The first comprehensive reaction engineering book was published in 1962 by a professor from the University of Oregon, Octave Levenspiel. His book "Chemical Reaction Engineering" [18] has become a standard in this field and retained its popularity in the 21st century. In the next two decades, detailed research on the dynamic behavior of chemical reactors has been carried out [13]. The works of Gilles et al. [19, 20] have enriched the field of chemical engineering by introducing new concepts of control theory for reactor stability analysis. The development of computers and information followed the parallel progress of chemical engineering and the introduction of new concepts in the field of analysis, dynamics, and control of reactors and software technologies [13]. The development continued until the moment of overlapping and the initial influence of computers in chemical engineering, or the creation of computer-aided process modeling field [21].

The end of the 20th century was marked by the development of sophisticated commercial software programs for process simulation. The growth of calculating speed, high memory capacity and the availability of computers were accompanied by their application in cases of complex modeling problems, analysis of highly complex reaction networks and, finally, optimization of multi-stage processes. Today, although the field of chemical engineering is technically more mature and highly sophisticated compared to the half-century ago, the concept of unit operations continues to play a significant role in chemical engineering and reactor design [13].

2.1.1 Process Intensification – Definition and Classification

The notion of process intensification was first used in Eastern Europe, in the work of Polish Leszczynski "Role of chemical engineering and chemical process machinery in industrial application and in process intensification" in 1973 [22]. The meaning of this term was defined as process "improvement" or "enhancement." In modern terms, process intensification, as "drastic" process improvement, was first presented in the work of Colin Ramshaw on the research of the application of centrifugal fields in distillation processes in the eighties of the last century [23]. The work aimed to significantly reduce plant sizes and installation costs [24]. In the 1990s, the interest of the academic community and the industry in process intensification was multiplied. The high interest was reflected in the number of papers that could be found on the Internet. A simple search on publications related to process intensification resulted in four papers that were published between 1966 and 1975, 15 papers in the next ten years, 25 papers between 1986 and 1995, 49 papers between 1996 and 2000, and between 30 and 70 papers published each following year [13]. A significant increase in the number of publications was contributed by the holding of the first Conference on Process Intensification in 1995, while the first manuals and books in this field were published by authors Stankiewicz [24], Moulijn [25] and Keil [26].

In his work [27], Stankiewicz defines process intensification as "a field consisting of the development of novel apparatuses and techniques that compared to commonly used today are expected to bring dramatic improvements in manufacturing and processing, substantially decreasing equipment–size/production–capacity ratio, energy consumption or waste production and ultimately resulting in cheaper, sustainable technologies." In the same paper, a clear distinction was made between process intensifying equipment (e.g., specialized membranes and carriers) and process intensifying methods. The methods, among others, include multifunctional reactors [28-31], hybrid separations [32-36] and alternative energy sources [24, 37]. Authors Sadukhan and Bhat [38] define process intensification as a useful strategy for achieving increased energy efficiency by reducing resistance to mass and energy transfer. Reduction in resistance is achieved by overcoming thermodynamic constraints through integrated design and technological operations. Since there is no universally accepted and precise definition of process intensification, it is used as a collective term for a broad spectrum of methods aimed at increasing process efficiency. Therefore, popular expressions in the industry and science such as "cheaper, smaller, cleaner" are often identified with process intensification [13]. In 2009, Gerven and Stankiewicz [39] further broadened the term process intensification and represented it as a progress area for chemical engineering research.

The area of process intensification [40] can be viewed according to the scale of the process (molecular processes at the smallest scale and plant processes at the largest scale), domain (spatial, thermodynamic, functional and time domain) and principle. The four main principles of process intensification are defined as [39]:

1. Maximizing the effectiveness of intra- and intermolecular events;
2. Giving each molecule the same processing experience;
3. Optimizing the driving forces at every scale and maximizing the specific surface area to which these forces apply;
4. Maximizing the synergistic effects from partial processes.

2.1.2 Process-Intensifying Equipment and Methods

Process-intensifying equipment refers to all novel single-function reactors, intensive mixing, and heat- and mass-transfer devices [27]. They differ from the process-intensifying methods by not including anything other than the reaction in the device. In Table 2.1, three basic ways to achieve process intensification in devices are shown: equipment miniaturization; exclusive selection of geometric structures for reactors; and thermal integration [13]. Although many of the listed process-intensifying equipment are present in academia for years, they are yet to be applied in the industry [13, 40].

Table 2.1 – Three ways to intensify processes in the equipment

1. Equipment miniaturization [41-44]	
micro reactors [41, 45-50]	micro mixers [51, 52]
micro heat exchangers [53, 54]	micro separators [55, 56]
2. Selection of geometric structures [57]	
monolithic structures [58, 59]	foam structures [60-62]
structured packages [63, 64]	nanofibers [65, 66]
3. Thermal integration [67, 68]	
coupling of reactions [69-71]	microchannel converters [72, 73]
counter-current heat-exchange reactors [74, 75]	use of inert adsorbents for desorption cooling [76]

Process-intensifying methods are all approaches to incorporate several functions into one device, alternative methods for mass, heat and momentum transfer, designs involving hybrid separations and methods for intensification in thermodynamic and time domain [27]. In Table 2.2, an overview of methods for multifunctional reactors, or rearrangement of the defined process flows and lumped reactive processes [13], alternative methods for the mass, heat and momentum transfer [77] and hybrid separations that encompass all individual separations [78] that can also be coupled [35, 36] is given. For the ReSyPIO methodology, presented in this thesis, of particular importance are multifunctional reactors, which belong to the previously mentioned synergetic domain of PI. As stated by Tian et al., multifunctional reactors allow the synergy between multifunctional phenomena at a different time and spatial scales, thus enhancing the mass, heat, and momentum transfer. When combined with miniaturization (structural PI domain), they can result in devices with improved performances in energy systems. Such is the example of gas to liquids (GTL) process that uses high-temperature multifunctional microsystems for syngas production [79].

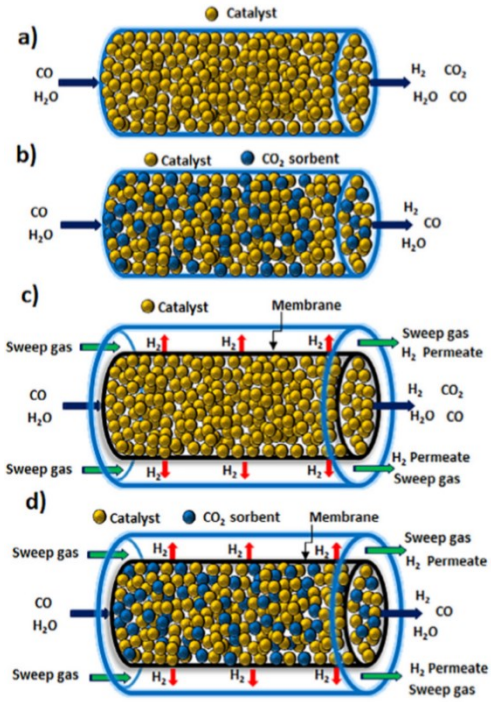

Figure 2.2 – Water-gas shift reaction in:
a) traditional reactor;
b) sorption-enhanced reactor;
c) membrane-enhanced reactor; and
d) sorption-, and membrane-enhanced reactor [80]

Table 2.2 – Different process-intensifying methods

Methods for multifunctional reactors	
Process flows rearrangement [81, 82]	Combined reactive processes [80, 83-86]
reverse-flow reactors [87, 88] segmented flow reactors [102-104] helix flow reactors [114-116] process retrofitting [119]	reactive distillation [89-101] reactive adsorption [29, 105-113] reactive extraction [117, 118] reactive crystallization [120, 121] reactive filtration [122, 123] reactive fragmentation [124, 125] reactive ejection [126, 127] chromatographic reactors [128, 129] membrane reactors [30, 130-138] fuel cells [139, 140]
Methods for the mass, heat and momentum transfer	
Alternative energy sources	Artificial gravitational fields
microwaves [141, 142] photochemical induction [144, 145] ultrasound [148, 149] hydrodynamic cavitation [152, 153] electrothermal desorption [154]	centrifugal fields [23, 143] electric fields [146, 147] magnetic fields [150, 151]
Methods for coupling of separation processes (hybrid separations)	
extraction distillation [155, 156] crystallization-distillation [34] adsorptive distillation [162, 163] pervaporation membranes [167-171]	membrane separation [157-159] membrane adsorption [160, 161] membrane distillation [164-166] liquid emulsion membranes [172, 173]
Methods in the thermodynamic domain	
ionic liquids [174-176] microemulsions [179, 180]	supercritical fluids [177, 178] phase transfer catalysts [181, 182]

Syngas can also be produced by the so-called water-gas shift reaction. The production can be realized in both traditional reactor and multifunctional reactors that combine several processes into a single device, shown in Figure 2.2. As published by Soria et al. in 2019, hydrogen production can be significantly increased in multifunctional reactors at specific operating conditions when compared to a traditional reactor. For their analysis, the authors have compared hydrogen production in reactors where the reaction was combined with CO_2 sorption, H_2 separation, and both sorption and membrane separation [80]. However, the authors did not do rigorous optimization and reactor synthesis, as was done in Chapter 6 of this thesis. Instead, they did an experimental analysis of the before mentioned hybrid multifunctional reactors.

Methods for intensification in the thermodynamic domain, also given in Table 2.2, refer mostly to processes occurring within the scope of a phase, as well as processes between two or more phases [183]. Solutions at this level are a direct result of thermodynamic constraints. Examples of process intensification in the thermodynamic domain are different uses of new reaction mediums and phase transfer catalysts [181, 182] with the goal to improve the process on the level of a group of molecules forming the thermodynamic phase [13].

Process-intensifying methods in the time domain are mostly done on a scale of processing units and plants [184]. At the plant level, it is possible to examine the connections between the devices and operations and analyze the entire process scheme. A large part of process intensification at this level is reduced to the scheduling of operations within the plant and the potential integration of multiple operations within multifunctional devices [25]. Observing the operating mode of the plant or part of the plant, dynamic or transient operating modes [185] are the most common type of process intensification in the time domain.

Also important is the intensification in the time domain on the milli scale [186, 187]. It can involve the enhancement of reactor efficiency by applying different periodic changes to the inlet variables. As published by Nikolić and Petkovska in 2016, the reactor's efficiency in a dynamic operating regime can be improved when compared to steady-state operation. The improvement comes from the nonlinear response of the reactor to a forced periodic change of the inlet variables. The amplitudes of the change, frequency, and the phase difference are carefully selected in order to ensure maximum improvement [188]. All of this is achieved by applying a PSE mathematical technique, called Nonlinear Frequency Response (NLFR) Method, devised by Professor Petkovska and published in Chapter 14, Evaluation of Periodic Processes, of the book "Periodic Operation of Reactors," by Silveston and Hudgins [189]. The NLFR method has greatly inspired how reactor operating regime was determined in this thesis and will be more explained in the last Section of this Chapter.

2.2 Process Synthesis and Design

The term process synthesis refers to a field aimed at obtaining alternative process flow schemes and choosing the optimal structure [190]. The optimal structure is achieved in relation to the objective function, which is most often of a techno-economic nature. There are many suggested methodologies for process synthesis, and most of them are based on integrated optimization methods [191-195]. Unlike process synthesis, process design goes a step further in terms of obtaining an optimal solution for the device that should constitute one process and can be presented by the following steps [196]:

1. problem definition
2. solution synthesis
3. proposed solution analysis
4. evaluation and optimal design
5. design analysis and report

From the above, it follows that process design is based on the synthesis of one or more specific proposed solutions for the given problem [197]. In order to obtain an optimal solution, it is necessary, during synthesis, to use a conceptual process design that is based on the optimization of the superstructure of processes [198, 199]. To summarize, one can view process synthesis and design as a part of process development [200]. The goal is to generate feasible flowsheet variants and to optimize them concerning specific objective. The set objectives are mostly related to economics but also deal with environmental impact and safety. Process synthesis and design can refer to reaction network design [201] and solvent selection [202, 203], integration of solvent and process design [204-208], solvent selection and energy integration [209], but also innovative equipment design, as shown in Figure 2.3 [210].

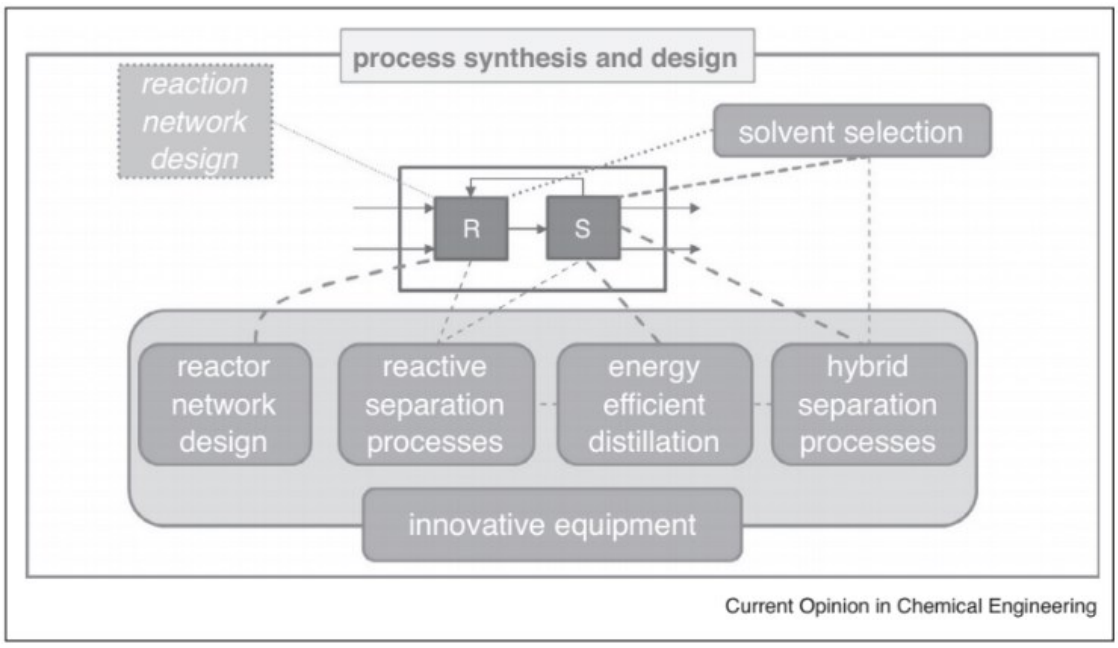

Figure 2.3 – Synthesis and design of reaction (R) and separation (S) sections [210]

Traditionally, the conceptual process design consists of the following steps:

1. The process engineer generates all possible variations of technological-operational schemes for the given case;
2. The superstructure is formed by connecting operations in all possible ways;
3. The mathematical model is compiled for the formed superstructure;
4. The objective function is defined (as the cost function) along with all technical and functional constraints;
5. The selected operating variables are optimized using mixed-integer nonlinear programming, and an optimal superstructure is obtained based on the results.

From the first step, the conceptual design is mainly based on the concept of unit operations and represents any process as a series of unit operations. It can be based either on optimization (optimization-based superstructure) or experience (heuristics) [211].

Conceptual methods based on optimization require process representation in the form of a superstructure made up of combinations of process flows and operations [211]. Their advantage is reflected in the applicability to many problems and rigorous analysis. The disadvantage is the absence of an automatic generation of process flows, which would cover all possible combinations, as well as the complexity of calculation requiring the use of expensive computers and software [25]. A conceptual design based on transfer phenomena stands out among optimization methods. It starts from the lowest level of aggregation and consists of analyzing the problem at the phenomenological level, grouping the phenomena, and analyzing the operation conditions (concentration and temperature analysis) [212]. In addition to this type of design, there is also a technique for analyzing the extreme mean value. It is used when the initial state of the reactants and the state of the product are known, so the optimal superstructure and devices are obtained from these data [25].

Within process synthesis, the synthesis of reaction networks is distinguished as a separate area with many published articles [5, 213-218]. The reaction networks synthesis aims to identify reactor structures that would yield high efficiency, at the expense of the effects of mixing, current flow changes, introduction of recycles and temperature effects, such that the system efficiency is increased at the expense of the observed objective functions [25]. Within reaction network synthesis, process design from phenomena blocks might be the key to new and innovative configurations, as well as novel equipment solutions. Phenomena blocks allow for abstract representations of the process, which could bear the largest potential for innovation [210]. Same was concluded by Anantasarn et al., who developed a systematic synthesis-intensification framework for more sustainable design [219]. The presented framework operates on three process intensification scales or unit operations scale, task scale, and phenomena scale. The authors stated that the most sustainable and innovative solutions could be generated by performing process intensification at the lowest, phenomena scale.

Tian et al. [220] conceded on this point and further added that while process intensification offers the potential to reduce the energy consumption and production cost, optimization techniques allow for state-of-the-art solutions. They define three key questions that remain to be answered:

1. How to efficiently screen an ample design space and systematically derive intensified and modular designs?
2. How to estimate the feasibility and cost of new intensified designs?
3. How to ensure that derived structures are operable and optimal in their expected functional state?

Tian et al. concluded that among ideas that have emerged to address these three questions, the most important ones are in the area of process synthesis on the phenomena level. This type of conceptual process design goes beyond conventional unit operations and explores intensification options at the lower aggregation level. This leads to innovative and novel process structures, while further research remains to be done to guarantee their operational performance [79]. Most of the further literature review in this Chapter will be focused on different methods of process synthesis in single-phase and multi-phase systems with existing examples from academia.

2.2.1 Synthesis in Single-Phase Systems

Almost all efforts in the area of reaction networks synthesis have been focused on studying single-phase systems [25]. Methods in this area can be classified into two categories: graphic synthesis methods and superstructure optimization-based methods. Author Glasser [221] was the first to develop graphical methods by upgrading the theory of Horn [222], which later became known as the "attainable region methods" (AR). The principle is based on the graphic structure of the problem skeleton within the allowed thermodynamic and reaction limits, i.e., attainable region. Cases in which a multi-dimensional view is required can face solution implementation problems. Also, the method can provide impractical complex solutions with multiple units of plug flow (PFR) and continuous stirred-tank reactors (CSTR) and complicated ways of introducing reactants. Despite many limitations, numerous studies on graphic methods for synthesis of reaction networks have been continuously carried out [223-229].

Authors Achenie and Biegler [213, 230, 231] first synthesized practical reactor superstructures using optimization. They developed four different superstructures using models: Plug flow with axial dispersion, a plug flow reactor (PFR), a reactor with recycle stream, and a model with reduced environmental impact. Afterward, using optimization methods in the form of non-linear programming, i.e., NLP algorithm, they identified the most desirable superstructure for reactor design. Kokossis and Floudas [214, 215, 232] were the first to present the idea that reaction networks should be displayed through a model that would be optimized using the MINLP algorithm. They replaced detailed with simpler models using generic structures sufficient to estimate the limiting system efficiency and hence the potential of each superstructure for design purposes. Also, the components of the system were replaced with CSTR cascades. The superstructure consisting of ideal CSTR and PFR elements allowed for all possible connections of such elements (Figure 2.4) and then it was modeled and optimized using the MINLP algorithm.

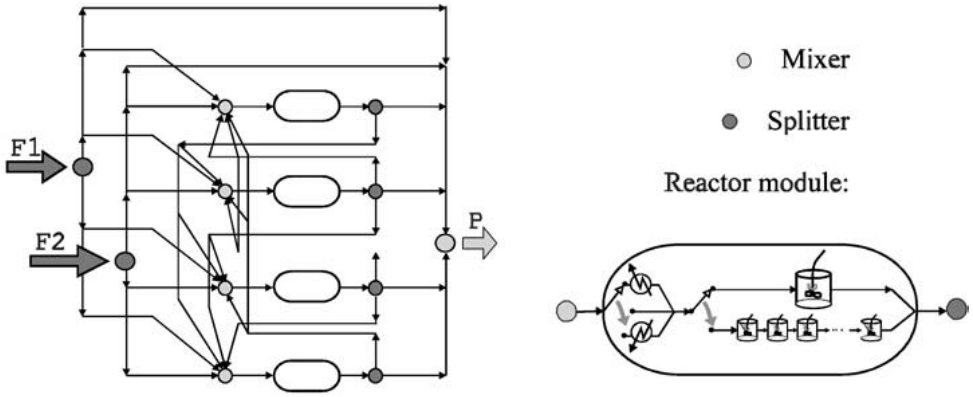

Figure 2.4 - Example of reactor superstructure [216]

Schweiger and Floudas [217] used the same method by replacing ideal PFR elements with distributed tubular elements. In 1999, authors Marcoulaki and Kokossis presented a synthesis method using the targeting and screening concept. Targeting determines the limiting elements for efficiency, i.e., obtains the maximum theoretical efficiency, while screening systematically develops and selects design candidates leaning to that efficiency [216].

The MINLP and NLP algorithms did not prove to be suitable for synthesizing non-linear, discontinuous, and distributed parameter systems. Mathematical programming requires staring points for numerical calculations and interrupts the search at the nearest local optimum. Therefore, the obtained solution could be significantly improved if the starting point for optimization was different. On the other hand, it has been demonstrated that the use of stochastic optimizations on particularly non-linear models achieves safe results not limited by the dimensions and size of the problem [216].

Marcoulaki and Kokossis applied stochastic optimizations to the problem of synthesizing a single-phase reaction network [216] on numerous superstructures in order to reach the desired design candidates by targeting [214].

To illustrate their methodology, they used a reaction mechanism consisting of four reactions:

$$2A \xrightarrow{k_1} B \tag{2.1}$$

$$B \xrightarrow{k_2} C \tag{2.2}$$

$$A \xrightarrow{k_3} D \tag{2.3}$$

$$2B \xrightarrow{k_4} E \tag{2.4}$$

with the reaction orders corresponding to respective stoichiometry. The goal of the optimization was to find the maximum concentration of component B [216]. The theoretical efficiency of the system was determined by a series of stochastic optimizations. The authors used several configurations, and the optimal result consisted of regular CSTR and ideal PFR connections. Although no novel structure came out as the result of this research, it remained significant in process synthesis history because of the application of stochastic algorithms.

2.2.2 Synthesis in Multi-Phase Systems

Multiphase reactors are the most commonly used reaction systems in the chemical processing industry [225, 233]. The presence of multiple phases in the system gives additional degrees of freedom that can be used in process synthesis. Also, a larger number of phases involves a much larger number of connections that can be formed in reaction networks compared to single-phase systems as well as more sophisticated mathematical models describing the phenomena of mass transfer and momentum transfer. Authors Mehta and Kokossis [234] presented a systematic methodology for the synthesis of multiphase chemical reaction networks. The methodology is based on the analysis of conventional industrial reactors such as bubble columns, co- and counter-current packed columns, mixed reactors, and some parts of devices which would lead to the improvement of the multiphase reaction process efficiency.

Connections between different parts of the device are linked in a superstructure which is then optimized to determine which type of device suits best the given case. Ideal CSTR and PFR elements are used as construction units of such a superstructure (Figure 2.5).

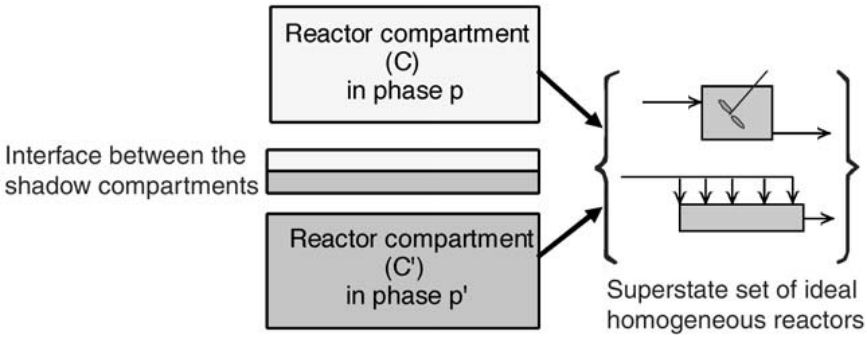

Figure 2.5 - Construction units of the multiphase reactor superstructure [235]

Non-isothermal systems are represented by insertion of the following temperature elements into the construction units of the superstructure: elements that represent temperature profiles (profile-based approach) or heating/cooling elements (unit operation-based approach). In order to facilitate modeling of such systems, an assumption about thermal equilibrium between different phases is introduced. More details about the synthesis of non-isothermal homogeneous and multiphase reactors can be found in a paper of Mehta and Kokossis [236]. Stochastic optimizations and simulated annealing (SA) algorithm were used to obtain optimal superstructures. The SA algorithm is based on the random development of the state, which is changed step-by-step (stepwise modification). The stochastic optimizations result in several solutions with similar efficiencies. Such solutions can be further improved during design by using deterministic methods and more precise models.

A special category of multi-phase systems in process synthesis belongs to complex distillation [237]. Despite advances in separation technology, distillation is still the most commonly used operation in chemical plants [25]. Therefore, many methods focus on the development of complex distillation, which involves the use of more complex columns that would reduce mixing losses, use liquid and steam more efficiently and lead to efficiency improvement [238]. Although it shows great potential for energy savings, the application of complex distillation is limited due to its complex structure in the domain of synthesis and design. Issues with the mode of operation, resulting from the complicated system dynamics, are the main obstacle in the synthesis and prevent its more common application in the industry. Optimization methods use superstructures to represent complex configurations [239-241]. Thus, a group of authors proposed differential superstructures and developed MINLP models for the synthesis of distillation systems [218, 242-246]. However, as superstructures are inspired by the already existing technology, solutions obtained in all of these studies were generally conventional solutions, rather than innovative designs that would significantly improve the process efficiency in the industry.

Papalexandri and Pistikopoulos [247] as well as Shah and Kokossis [248, 249] first presented a superstructure composed of multipurpose heat and mass transfer modules and put a focus on the operations of such units. For the needs of optimizing the superstructure, they used the MINLP algorithm. However, there remains some room for more considerable progress in the field of new methods that would use synthesized superstructures and not conventional solutions from the industry.

2.2.3 Novel Approaches in Process Synthesis

An example of a novel approach to the conceptual reactor design is the scientific work of Peschel et al., presenting the optimal design methodology based on the concept of elementary process functions [212]. The concept aims to determine the best reaction route in the thermodynamic state space. The route is created by manipulating fluxes that affect the movement of a tracked fluid element through the reactor. The methodology is divided into three levels:

The first level: Comparison of different concepts for integration and improvement, and formulation of the general ideal model. Dynamic optimization of an ideal model (unlimited fluxes) with fluxes as optimization variables (improved fluxes).

The second level: Determining the best optimization variables for achieving the desired flux, and constraint analysis. The model includes transfer phenomena.

The third level: Development of the optimal technical reactor based on the best profile of the control variables.

The application of the proposed methodology is independent of existing solutions and can result in both traditional and innovative reactor concepts. It allows the selection of the most efficient reactor from an economical point of view. The given methodology was firstly tested in the case of sulfur dioxide oxidation. After the first level was applied, three solutions were obtained.

The first solution was an adiabatic reactor and a cooler (connected in series). The second solution was a polytropic reactor with a constant cooling temperature within which the reaction and cooling are integrated without heat flux control, and the third solution was an integrated reactor and cooler with controlled heat flux, to examine the potential of distributed cooling.

The second level of the methodology dealt with ways to achieve the desired heat fluxes, while in the third step, a technical solution for the reactor was developed, presented with three segments in Figure 2.6. For the first segment, the constant maximum ambient temperature was found to be optimal, in the second segment distributed cooling was necessary, while the third segment could be approximated either with a constant cooling temperature or with a slightly decreasing cooling temperature.

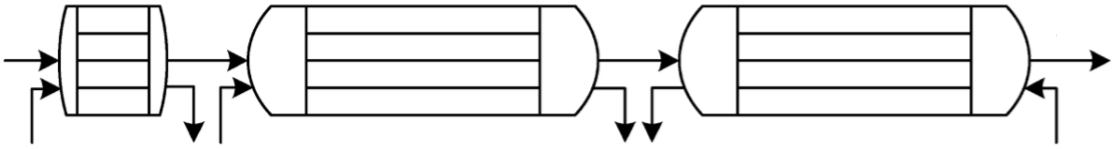

Figure 2.6 - Possible technical approximation of the optimal process route [212]

Given the fact that methodology uses Lagrange's formulation of the governing equations, it can be applied only to the design of batch reactors and continuous reactors [212].

In another study by the same authors and Florian Karst [250], the methodology was expanded with the concepts of process intensification and tested on the case of the synthesis of reactors for ethylene oxidation.

The updated methodology consisted of three consecutive stages:

1. Finding the optimal route in the state space – setting governing equations, reaction kinetics, and thermodynamic constraints;
2. Selecting a schematic reactor – defining the catalyst density and including the mass and heat transfer in order to calculate the impact of the resistances on transfer and to obtain the boundaries of specific surfaces;
3. Selecting the best possible reactor – approximating the control variable profiles, validating the design by calculating the nonideality.

The proposed methodology was also used to define the optimal design of a multiphase reactor [251], for which many other optimization methods can be found [236, 252, 253]. In 2018, within the same framework of elementary process functions, Kaiser et al. presented an approach to obtain reaction network candidates by using dynamic optimization of a batch process scheme. As before, optimal mass and energy control fluxes were used for analysis and determination of the attainable region [254]. Xie and Freund continued the work on the extension of the methodology based on elementary process functions [255, 256]. In their latest work, they applied it on the process of chemisorption of carbon dioxide in a multiphase reactor. The methodology was changed so that each phase is represented with one fluid element, and each fluid element is subject to its own internal and external fluxes and transfer fluxes between two elements. In order to enable transfer limitations, each element can feature an internal gradient. As a result, the performance improvement up to 38 % was reported for the investigated cases [256].

Perhaps the most interesting example from the view of this thesis is the paper published by Demirel et al. in 2017. The authors presented a novel method for systematic process design and intensification, based on building blocks. These building blocks can be linked to process phenomena, tasks, and unit operations [257].

Blocks of the same type result in the classical unit, while blocks of different types result in an intensified unit. The authors give a detailed description of how blocks can be formed to represent different phenomena, how process units and flowsheets are depicted, and how all of that makes a superstructure (Figure 2.7).

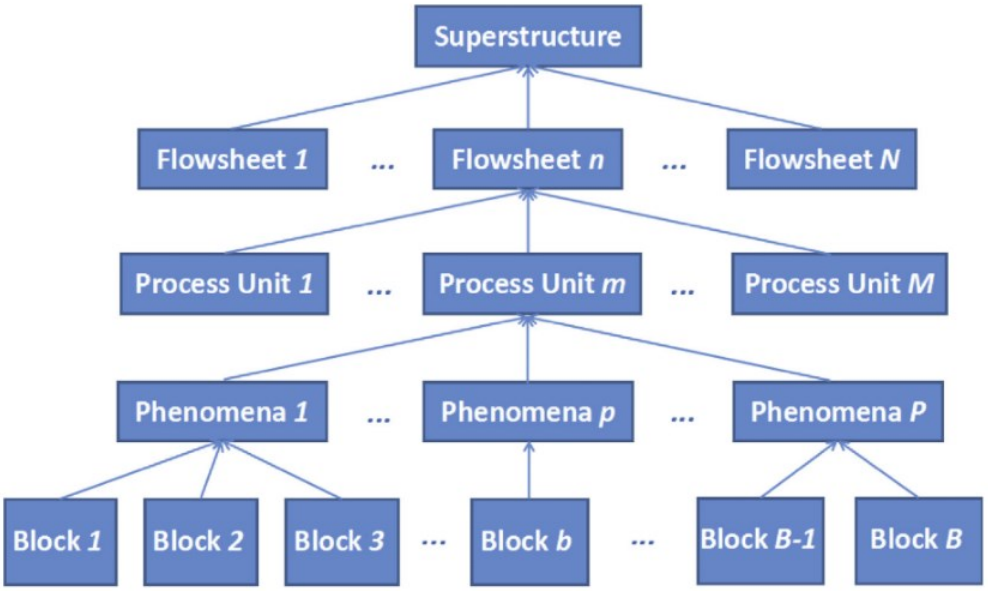

Figure 2.7 – Superstructure creation by using building blocks [257]

Demirel et al. use single mixed-integer nonlinear optimization (MINLP) of the superstructure and acknowledge that challenges remain in achieving global optimality. This is due to the nonlinearity and nonconvexity of the defined model. It poses a big numerical challenge in achieving an optimal solution without a good starting point [257]. Using a starting point is opposite to the authors' intent to obtain novel and new configurations which are independent of the user input. The same methodology was later used in a process integration study published by Li et al. [258].

Optimization challenges listed by Demirel et al. were partly bypassed by Kuhlmann and Skiborowoski who used a combination of stochastic and deterministic optimization, an approach similar to the one used in his thesis [259].

The authors applied a memetic algorithm which consists of an evolutionary algorithm that addresses the combinatorial complexity of the superstructure, and a local deterministic optimization approach that minimizes the objective function by modifying the operating conditions. However, they presented their methodology for process synthesis based on phenomena building blocks on a simple nonreactive case study of ethanol dehydration [259].

In another study, Kuhlmann et al. applied the same methodology on the case of transesterification of propylene carbonate with methanol. The authors concluded that the complexity of the superstructure optimization approach significantly limited the size of the problem and lead to the exclusion of some promising solutions already present in academia. They further added that future work would be focused on the expansion of the problem size and extension of their phenomena building blocks methodology [260].

A different approach was suggested by Tula et al., who developed a process-group contribution method for process flowsheet synthesis. Even though the proposed method is component independent and can be applied to any system of the same properties, the generation of feasible flowsheets heavily depends on the database of existing building blocks called process-groups. Also, this method does not explore the process at the lower, phenomena level [261], unlike the proposed methodology in this thesis. Tula et al. later extended the developed model to perform process synthesis-intensification for selection of more sustainable process design on the case of bio-diesel production. Their extension incorporated existing process group-contribution method into a synthesis-intensification framework [262].

2.3 Challenges and Future Prospects

As described in Section 2.2, optimization has become an invaluable tool for obtaining the optimal process design within the field called Process Systems Engineering (PSE) [37, 263, 264]. Although initially it represented a method of interest only in the academic sphere, it has an increasing influence in the industry [265]. Still, the more widespread use of optimization in the industry depends on strengthening three key pillars:

1. Accessibility
2. Alignment and Information Availability
3. Awareness and Training

The first pillar ensures the easy-to-use interface, customer support, and adequate representation of results. The second pillar involves sharing of optimization-relevant information between all involved in the process design. However, this could potentially endanger the confidentiality policy in the industry. The last pillar addresses the current low and limited application of optimization methods in undergraduate and graduate engineering curriculum [266].

Nonlinear optimization is essential when it comes to decision-making tasks in process design and operations. Future development of nonlinear optimization algorithms will lead to faster solution strategies, tackling larger process system models at both time and length scales, as well as quickly analyzing dynamic systems [267].

When solving complex problems involving planning an operation of a multi-product plant [268-270], optimization is the only tool which can contribute to achieving a satisfactory result.

Considering the many criteria that must be calculated, solutions can be put in the form of a Pareto set of functions which are then used for multi-objective optimization. Since a large number of local minima/maxima is possible, the multi-objective genetic algorithm (moGA) can be used as an algorithm for finding a global optimum [271]. It is up to the process engineer to choose which functions from the Pareto set will be favored, all depending on whether he/she wants maximum profit/productivity or minimum harmful environmental impact of production [272-276]. However, the reactor design that entails the simultaneous determination of both reactor structure, operational parameters, and the operational regime, would significantly increase the number of variables that ought to be optimized. So far, optimization methods have been successfully applied only on relatively simple reactor structures [210]. Consideration of both operational regime and structure would mean that the optimization problem would have to be tackled by solving potentially complex systems of ordinary or partial differential equations, posing yet another expensive and time-consuming obstacle in numerical integration and optimization.

For process dynamics analysis, in addition to numerical methods [186, 277], analytical methods [188, 189, 278-294] can also be used. An example is the Nonlinear Frequency Response (NLFR) method, mentioned in Section 2.1.2. The NLFR method is based on nonlinear frequency response and the concept of higher-order frequency transfer functions (FRFs). It has been proven to be an excellent tool for analyzing weakly nonlinear systems. The frequency response, in addition to the first harmonic, contains a non-periodic (DC) component and a theoretically infinite number of higher harmonics. By applying the concept of higher order FRFs the model of a weakly nonlinear system can be replaced by an infinite series of linear models of different orders (in the frequency domain, FRFs of different orders). These FRFs are directly related to the DC component and different harmonics of the system response to the periodic input change.

Thanks to these characteristics, the NLFR method is a useful PSE technique for analyzing weakly nonlinear adsorption systems [278, 280-283, 290, 293, 295, 296], identifying kinetic mechanisms [289], estimating equilibrium and kinetic parameters from experimental data [288], and most importantly for this thesis, analyzing periodic operations of reactors [188, 279, 284-287, 291, 292].

Using the NLFR method, it is possible to determine whether switching from an optimal stationary operation to an operation in which inputs periodically change around an optimal stationary state increases reactor efficiency or not. The non-periodic (DC) component obtained by applying the NLFR method corresponds to the time-averaged difference between the newly-established pseudo-stationary periodic state and the optimal stationary state (Δ in Figure 2.8), the sign of which indicates whether the reactor performance has improved or not. The non-periodic component of the FR response is approximately proportional to the asymmetrical second-order frequency response function and the square of the input amplitude, so the whole procedure for evaluating the potential of the periodic operation for improving the reactor performance is reduced precisely to determining and analyzing the sign of this function and its absolute value. For example, if the asymmetrical second order FRF corresponds to the outlet concentration of the reactant, its negative sign corresponds to higher conversion in the periodic regime (the case shown in Figure 2.9).

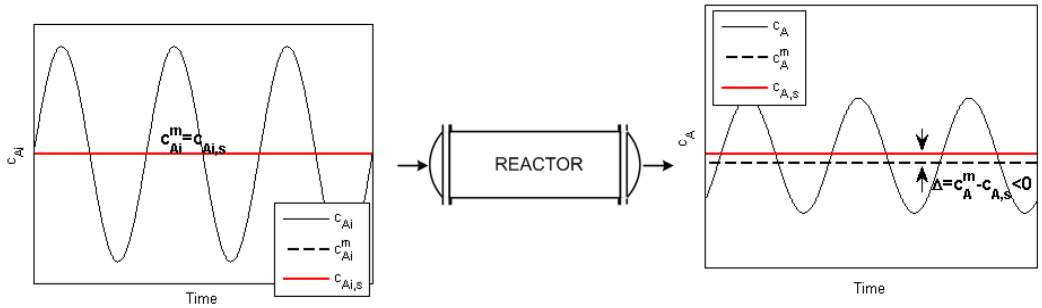

Figure 2.8 – Example of periodic operation of a reactor with increased conversion of A owing to a periodic modulation of the concentration of A in the feed stream, (Δ< 0) [189]

The procedure for derivation of the FRFs necessary for applying the NLFR method is standard and starts from the nonlinear model equations [189]. One step of this procedure is a change of the domain (from time to frequency) in which the model defined as a system of nonlinear ordinary differential equations is converted into a larger system of linear algebraic equations, thus removing the problems of slow, ineffective or unreliable numerical computations. By automating the procedure for derivation of the needed FRFs and fusion with existing optimization methods, it would be possible to reliably determine an optimal operational regime and its parameters in a short time. Furthermore, this could then be integrated into already used optimization for reactor structure, making it a potentially indispensable fast tool for simultaneous determination of reactor structure, operational regime, and its parameters. However, the result would still depend on how well the fundamental first principle mathematical model describes the system of interest.

The first principle models, which rely on complex mathematically driven equations, are usually used to investigate the viability and exact applicability of an employed method. These models depend on accurate knowledge of the parameters and the interaction between them. With the rise of computational intelligence and machine learning techniques, a new area of applied artificial intelligence (AI) is giving researchers an alternative [297].

For years, machine-assisted approaches have been developed in the field of chemical synthesis [298], tailor-making microstructures and polymerization [299], and modeling the physical and chemical behavior of compounds [300]. The rise of AI can be split into three different eras: the first two are the expert systems in the 1980s and neural networks in the 1990s, and the third, current one, is the deep learning and data science era. Although the first two eras have not brought revolutionary changes to chemical engineering, it can be expected that highly increased computational power, software accessibility, and reduced costs, will create favorable conditions for AI to play a more significant role in the research community and future industry [301].

With the use of stochastic methods and the AI, one can maximize the use of a human resource by increasing efficiency and giving researches more time to think, plan, and come to fast conclusions. Big data analysis and information processing also allow for easier and faster collaboration between the different disciplines, which leads to synergetic benefits [298]. While stochastic models are very successful at predictions, the first principle models still have advantages when it comes to getting a more profound understanding of how the system behaves. This is the reason why hybrid, or so-called surrogate models (a combination of stochastic, empirical, and deterministic models), are sometimes used when model uncertainties need to be accounted for [302].

3. Description of the ReSyPIO Methodology

As covered in Chapter 2, the existing methodologies for reactor synthesis that are present in academia rarely combine different process intensification (PI) principles with multiple process system engineering (PSE) techniques. Nevertheless, it is worth investigating what the possible theoretical enhancement of a reaction system with different integrated PI principles would be. This kind of investigation, which includes a systematic approach to PI and the use of techniques of PSE for the integration of different PI methods, is in the focus of the new methodology for reactor synthesis based on process intensification concepts and application of optimization methods (ReSyPIO), presented in this thesis. Since the combination of PI methods in one system is currently difficult to realize and experimentally prove, it is valuable to use modeling and optimization for approximate initial prediction of a reaction enhancement potential. Many PI investigations and state-of-the-art modeling of individual PI methods provide reliability to perform such a complex and multifunctional analysis. Therefore, proven PI approaches and models should be used in superstructure optimization of potentially improved or novel reactor types [2].

The foundations of the ReSyPIO methodology are first presented in review and position paper by Nikačević et al. [303], and elaborated in several conference proceedings by Nikačević et al. [8, 304-306]. However, the full description and formulation, presented in this Chapter, was published by Živković and Nikačević in 2016 [2]. The ReSyPIO methodology uses PI concepts within the structural, temporal, synergetic, and energetic domain for the synthesis of the reaction system macroscopic superstructure, which is then subjected to optimization. Thus, by the simultaneous use of different PI concepts and PSE techniques of reactor network synthesis, superstructure creation, and different optimization techniques, the theoretical potential for overall reaction system improvement is to be attained. The improvement potential should be higher than the enhancement in case of using a single PI method in a reactor, and significantly higher than the sole optimization of the conventional reactors (without PI concepts applied).

The conceptual method for reactor synthesis (shown in Figure 3.1) consists of three stages containing intermediate steps in which PI concepts are considered simultaneously through phenomenological modules and integrated into a reactor superstructure that is optimized.

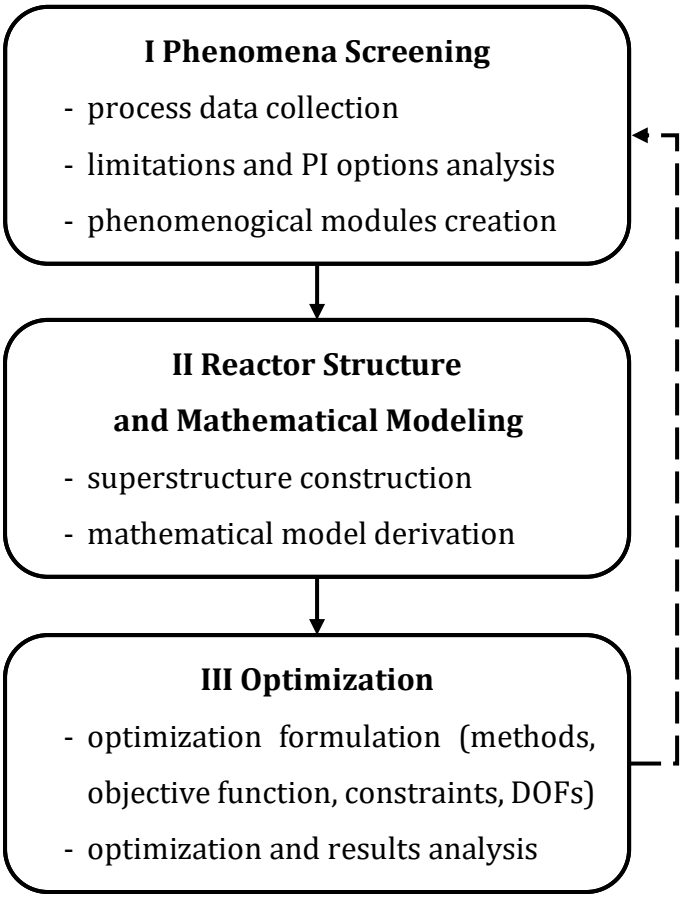

Figure 3.1 – The proposed method for conceptual reactor synthesis [2]

3.1 Phenomena Screening

The first stage of the proposed ReSyPIO methodology is Phenomena Screening. The first step of this stage is gathering the information that defines and eventually limits the reaction system of interest. These data include present reaction phases, reaction mechanism, kinetics, and its temperature and pressure dependence, possible chemical equilibrium, catalysts or solvents used, thermodynamics, such as phases' equilibrium, activities, the heat of reaction and other thermal properties.

In the second step of Screening, the gathered data are analyzed to define and consider all physically possible phenomenological, structural and dynamics alterations, and manipulations, which would enhance the reaction kinetics and thermodynamics desirably. Within this analysis, all PI options that match the system and may be considered in further stages are identified. Experimental research is conducted to collect all necessary kinetic, thermodynamic, heat, and mass transfer information. If required, new phenomena are acquired and added to overcome the current limitations.

In the third step, the phenomenological modules with the corresponding phases and present phenomena rates are defined. The phenomenological modules are functional parts of the reactor that can differ in 1) structure; 2) layout of phases; 3) presence or absence of phenomena inside the defined phases; and 4) operational parameters. The content and connections for the modules, listed above, are to be determined via optimization. Modules are based on data that are experimentally gathered and analyzed during the first two steps. Phases inside the modules present a volume in which all physical properties of the components making the phase can be uniform. Interactions between phases (e.g., two liquid or liquid and solid phase) take place because of the present phenomena and are mathematically described with phenomena rates.

In the unified graphical representation used in this work, phenomena modules are presented by purple rectangles, consisting of one or more phases (Figure 3.2). Phases are shown with a different color, and a name in the top left corner.

In Figure 3.2, an example of a phenomenological module is given with two phases, liquid (L) and gas (G) phase.

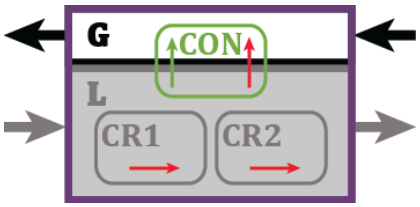

Figure 3.2 – A graphical example of the phenomenological module

L phase is shown with a gray area, and the G phase is shown with a white area. Inside these two phases, different phenomena can occur. Graphically, energy or heat transfer is depicted with red arrows, while the phenomena are depicted with marked rounded rectangles. Additionally, mass transfer between phases has a respective color arrow, depicting the direction of transfer. For the example shown in Figure 3.2, in L phase two chemical reactions occur, CR1 and CR2, depicted with gray rounded rectangles. These two reactions are exothermic and generate heat, which affects energy balance. This is marked with red arrows inside CR1 and CR2 rectangles. Apart from chemical reactions, convection phenomena, CON, take place in both phases (L and G). CON is shown with a green rounded rectangle present in both gray and white area in Figure 3.2. Thanks to CON both mass transfer from L to G phase (green arrow) and heat transfer (red arrow) occur. Of course, CON could also be conduction or diffusion, which would be described mathematically in a different way in the following stage. Apart from the layout of phases and phenomena in them, the primary inlet and outlet streams of the module are shown. In Figure 3.2, the module has a liquid phase inlet/outlet (gray arrows) and counter-current gas phase inlet/outlet (black arrows).

A more detailed graphical description of the phenomenological module, with present components, will be done in the next stage of the ReSyPIO methodology, before setting up the mathematical model of the system. This will be presented in the application of the ReSyPIO methodology for general reaction case, in Section 4.2, and industrial case application in Section 6.2.

The phenomena that are present in a module can be grouped in a chemical reaction (CR), mass transfer (MT), energy transfer (ET), phase change (PC), and in some cases surface phenomena (SP). Within these major groups, some of the specific phenomena that can be present within the module are listed in Table 3.1.

Table 3.1 - List of phenomena that exist in reaction systems and may constitute a phenomenological module [2]

Chemical reaction (CR)	Mass transfer (MT)	Energy transfer (ET)	Phase change (PC)	Surface phenomena (SP)
Non-catalyzed Catalyzed	Convection Diffusion	Convection Conduction Radiation Heat source (reactive, phase changing, electrical, microwave, shear, ultrasound)	Evaporation Melting Condensation Sublimation Solidification	Adsorption Desorption Capillary effects Adhesion Wetting Lubrication Abrasion Agglomeration Attraction

Momentum transfer and mixing are not considered and listed in Table 3.1, as ideal flow patterns (plug flow and ideal mixing) contribute to maximum theoretical efficiency in contrast to non-ideal flow conditions.

Nevertheless, pressure drop could be included when it is essential for the analysis, through semi-empirical equations (e.g., Ergun's equation for fixed bed).

If needed for additional feeding or recycling locations, modules can be further segmentized, i.e., divided into a number of segments. All segments that make a module have the same layout phases and phenomena rates. What makes them different is that each segment can have its inlet streams and be connected to other segments in different ways. The number of segments and their streams should be obtained by optimization.

Different phenomenological modules (and segments that constitute them) have different inner layouts of phases phenomena rates and can be connected and further optimized. Setting up the connections between modules and in-between segments belongs to the second stage, i.e., Superstructure Generation. Such an approach with reaction system modularization and subsequent segmentation allows for the study of the overall process intensification potential (simultaneous consideration of different PI approaches), as well as integration potential. Hence, a module should include not only phenomena rates and connections which define the conventional reaction process but also other physically realizable ones, derived by applying PI concepts. In the following examples, several general cases will be used to illustrate qualitatively the screening stage of the ReSyPIO methodology.

3.1.1. Examples of Phenomena Screening

Example 1: A liquid phase equilibrium reaction system with a solid catalyst

The first example considers a liquid phase equilibrium reaction system with a solid catalyst. Data gathered in the first step of the Phenomena Screening demonstrate that boiling points of the product and reactants differ considerably. Thus an option could be to evaporate the product and therefore shift the equilibrium beyond thermodynamic limitations. This analysis points to a reactive distillation (RD) process, in which the functional integration approach of PI is employed. There are several screening and synthesis methods, which resulted in RD solutions, offered in the literature [92, 97, 99, 307, 308]. Moreover, there are many realized industrial RD applications [90, 309], e.g., for the production of ethers (MTBE, ETBE, TAME, FAME), hydrogenation of aromatics, or hydrodesulfurization.

However, further analysis of the system shows that additional improvement could be considered, including the dynamic operation of the column with changeable volumes (capacities) of the liquid phase within the module [310, 311] which could result in energy savings (PI dynamic domain).

Importantly, Phenomena Screening for this example demonstrates that the mass transfer to the solid phase and adsorption/desorption are considerably faster than the reaction kinetics. Thus, the reaction can be treated as pseudo-homogeneous (liquid phase only), while the solid phase would not be considered (like in the above-cited articles).

As already explained, the phenomenological modules are defined in the third step of Phenomena Screening. A representative module has the liquid phase with two occurring reactions, convective mass, and heat transfer. It also has the gas phase with convective mass and heat transfer that is consequently connected with the liquid phase, in a similar way as the example shown in Figure 3.2.

The module, in this case, can be physically directly related to an RD column stage or tray. Within the following stages, superstructure optimization gives the optimal number of stages, i.e., the optimal arrangement of the modules and their optimal volumes and flow rates between them (dynamic domain) [310, 312].

Example 2: A gas phase equilibrium reaction with a solid catalyst

In the second example, a gas phase complex equilibrium reaction, catalyzed by a solid catalyst, can be intensified by removing the product. The reaction screening demonstrated that in this case, selective product removal might be achieved through membrane separation (PI synergetic domain). In Figure 3.3, a phenomenological module is given with the possible reactive separation. It consists of two gaseous phases, G1 (white area) and G2 (gray area) that are physically separated, and one solid phase, S (green area). Inside the G1 phase, a chemical reaction, CR, is taking place on a solid phase S (green area). Apart from the reaction, a separation through a membrane (MEM phenomena) is taking place between the phases G1 and G2. When defining the phases, with the membrane option, a second gaseous phase, introduced in the module, can contain sweep gas [313]. Both phases in this example are flowing in a co-current direction (black and gray arrows).

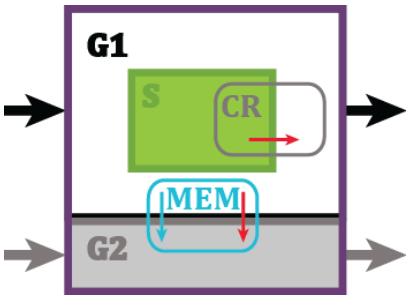

Figure 3.3 – A graphical example of a reactive-separation module

The module phase and phenomena layout, and orientation of the inlet and outlet streams are built upon the available experimental research data. It is because the Phenomena Screening stage solely depends on the gathered experimental information about the system. Thus, it will affect the details in which the corresponding phenomena rates will be modeled.

If experimental research was attained not just for the membrane separation but also for adsorption, these phenomena should be shown in Figure 3.3 as well. Industrial applications of this type of reaction can be found in energy and bulk chemistry sector, and some of them include steam methane reforming, for which membrane reactors [38, 314, 315] or reactors-adsorbers [112, 316] are exploited, then ammonia synthesis (membrane enhanced [317], sorption enhanced [28]) and methanol synthesis (sorption enhanced [318, 319], membrane/sorption [108], membrane [320]). Since a priori, it is not obvious which separation process is more advantageous, if enough experimental data is available both membrane and adsorption options should be optimized (with the same objective function and inlet/external conditions), and the results will show which would be techno-economically better. In the case of a sorption-enhanced system, a second solid phase is added in a module containing diffusion mass transfer and adsorption/desorption phenomena. The additional solid phase may be static (e.g., simulated moving bed [321], or moving (e.g., flowing particles concept [28, 318]). The modules with solid phases are differently described mathematically, according to their structure. Again, both cases should be subjected to optimization. Overall, for the second example, three reaction system options can constitute superstructures, which will be optimized and analyzed. The results provide an optimal reactor structure - the number of modules in series, with optimal reaction/separation combination (reactor structure - zones with reaction modules only / zones with combined reaction and separation and zones with separation only), and flow rates between the modules.

Example 3: A highly endothermic liquid phase reaction

In the third example, a highly endothermic liquid phase reaction, with relatively low throughput requirement, is screened. The critical aspect for this case, heat transfer, may be intensified through miniaturization (PI structural domain [41]). However, in this example, energy transfer ET (for endothermic reactions) may also be intensified by introducing an alternative heat source, such as microwaves or direct electric source (PI energetic domain [141]). Therefore, both cases (and possibly their combination) should be examined in a simultaneous investigation that will show which option has more potential [2].

In Figure 3.4, a module is shown with a liquid, L, phase (gray area) in which a chemical reaction (CR) takes place. L phase is heated by pressurized steam or W phase with a red arrow. Apart from this heating medium, another source is potentially added, which is a red rounded rectangle marked as MW, denoting a microwave source. The presence or absence of any of these phenomena and type of energy source should be determined with optimization.

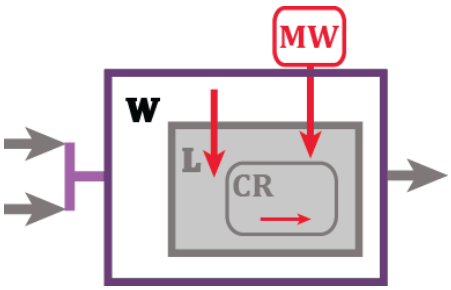

Figure 3.4 – A graphical example of the alternative energy source module

It should be noted that the mathematical models of the modules can differ considerably since micro-fluidic or surface capillary phenomena may exist in microreactors [103] in contrast to reactors of larger dimensions, while microwave heating includes different energy transfer mechanism (microwave heat source [141]) in contrast to conventional off-surface convection.

Applications can be found in organic chemical synthesis, and some examples include benzannulation reaction [322], Grignard reaction (exothermic, only miniaturization [323]), and synthesis of diaryl ethers [324].

Example 4: A reactive system with slow parallel reactions

The fourth illustrative example is a reactive system with slow parallel reactions, which can be found in various chemical and biochemical industry applications. This type of systems is usually operated in batch or semi-batch reactors, so it is worth investigating whether a continuous system would bring considerable improvements. Mainly, it would be interesting to compare whether distributed feeding of reactant is more favorable for the parallel reaction system than a fed-batch operation with dosing. It should be noted that in the case of a fed-batch system, only one module describes the whole system.
Generally, the number of modules can vary from one to up to several hundred, and this number should be the result of optimization (not fixed in advance). Moreover, dynamic operation (non-stationary feeding) of a continuous distributed system is another case which may have enhancement potential and could be investigated. The above considerations fall into PI structural and dynamic domains. A very similar example case will later be used in Chapter 4 as the detailed explanation and application of the method.

The advantage of the creation of the phenomenological module, or modularization, is that it provides simplicity for a future mathematical description of the system in which a modeler can easily later define intermediate inputs, outputs and recycles to each module. Moreover, it provides the flexibility, as a single optimization may derive a solution with one, several or many modules in series, which can be then physically realized as a single reactor or several reactors in series (or trays of distillation/extraction column as in the first example).

In conclusion, the goal of the Phenomena Screening stage is to:

1) gather all available experimental and previously researched information about the reaction process;
2) derive the number of present phases inside the module and determine their layout;
3) group phenomena that occur within the phases or can be introduced in the module;
4) show primary inlet and outlet streams into the module.

All of the beforementioned forms the base for the superstructure generation and modeling and optimization for maximum attainable improvement.

3.2 Reactor Structure and Mathematical Modeling

The second stage, shown in Figure 3.1, is the generation of the Reaction System Superstructure and Mathematical Modeling. In the first step, the formulated phenomenological modules are split into segments, if needed, and then arranged. The arrangement should define all realistically possible material and energy flow streams (connections). The flow streams connect the modules of the same type or may link the modules of different types. Thus, for a single-phase system, an arrangement of modules or segments in series represents the basic superstructure (if the phase and phenomena layout is the same). This corresponds to connections being the mass and energy flows from one segment to the adjacent one. For two or more phases, the number of connections and variations can become bigger, as there are several possible inlet streams. Furthermore, each segment can have additional inputs or outputs, in addition to the connections to the previous or following segments of one module. These additional streams could be recycling streams and side inputs or outputs.

The arrangement of modules in the superstructure and the respective feeds are also determined according to kinetic and thermodynamic limitations, observed in the Phenomena Screening stage. For instance, if needed, a module can be split into segments for parallel representation and in order to control residence time for a fixed or given molar flow rate (capacity) at the inlet. All parallel segments of one module have the same presence of phases and phenomena, as described in Section 3.1. Segments of different modules can vary in structure, presence of phases, and phenomena as well as operational variables. However, one should notice that the final layout of modules and the number of segments is to be determined using optimization. The flow streams, i.e., connections, are obtained through optimization of the flow rates (inlet streams). Thus, if optimization results in a zero flow rate for a particular connection, that stream would not exist. Nonexistant, or zero flow rate streams, are principally considered for additional input/output streams.

In some problems, the main streams, connecting the modules in series, can also be subjected to optimization, as in the first example from the Reaction Screening stage, for the dynamic option with changeable volumes - holdups of modules (trays) in an RD column [310, 311]. However, constructing a superstructure with all possible connections can result in a considerable optimization problem, which would be difficult to converge. Thus, only the connections that are physically achievable and valuable for analysis should be defined. For this purpose, information gathered during Phenomena Screening and consequent analysis is essential.

For the first example (a liquid phase equilibrium reaction system with a solid catalyst, Section 3.1.1), with one module, shown in Figure 3.2, the Phenomena Screening shows that side inputs (feed points) are a prospective option. Thus, these streams will be added to the segments of the module in the superstructure generation. On the other hand, the reaction mechanism shows that recycling would not bring improvements, and recycle screams are not included in the superstructure. A possible RD system with two catalytic reactions will have two different interacting phases. The superstructure consists of N segments connected in series, as shown in Figure 3.5.

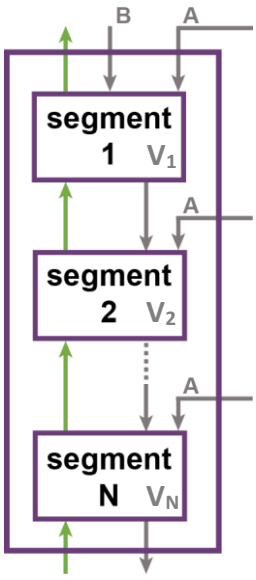

Figure 3.5 – A graphical example of the reactor superstructure made of one module, and N segments with optimized volumes

As described in Section 3.1 and shown in Figure 3.2, in the liquid (L) phase two reactions, CR1 and CR2, and convective mass and heat transfer, CON, may occur.
In the gas (G) phase, no reaction takes place, and there is merely convective heat and mass transfer of one component from L to G phase. The reactor superstructure is made of one module with N segments of the same type, connected in series (Figure 3.5). The volume of each segment is optimized. The gas phase (green line) and the liquid phase (gray line) have a counter-current flow. The reactants are fed into the first segment separately. Since in the Phenomena Screening stage, it was determined that component A is the limiting reactant, a possibility is left for A to be fed into each subsequent segment. Thus, the L phase inlet streams for the second and other segments consist of the outlet stream from the previous segment and reactant A inlet stream. These streams can vary in composition and flow rate, which is to be determined by optimization.

A presence of chemical reaction in a module (reactive stage with solid catalyst) is to be determined by optimization. For this, binary optimization variable can be used in each module, where 0 and 1 determine the absence or presence of reaction, respectively. Alternatively, since CR1 and CR2 are catalytic reactions, their presence can be determined by optimizing the amount of catalyst needed for each reaction. If no reaction is present, optimization should result in zero amount of catalyst for that phenomenological module. Thus, the final arrangement can consist of segments with one reaction, both reactions, and segments without a reaction. Separation (MT and HT) is present in the RD column module, more precisely in each segment of potentially different volume and liquid hold-up.

The reactant feed points and the overall number of modules and segments should be derived through optimization which can be integer type (with a binary variable) or non-integer type (all real variables). Mass and heat flow rates, input, and flow rates between modules and volumes of modules are typical continuous optimization variables.

For the mentioned improvement in PI dynamic domain, and consideration of dynamic operation, flow rates between the modules and volumes of modules are time-variant.

Having the reaction system superstructure constructed (e.g., Figure 3.5), the next and final step of this stage is to represent it with a governing mathematical model. Ideally, one mathematical model should be derived, as this is suitable for single optimization. However, in many cases, this is not possible, as it has been described in examples two, three, and four of the stage Phenomena Screening (Section 3.1.1).

In the second example, models of a membrane reactor, and an adsorber-reactor differ considerably, although they contain similar types of modules (with different phenomena and volume scales). In the third example, the phenomena in the modules, as well as their respective volumes, are different, so two models need to be derived.

In the fourth example, the system could be operated in discontinuous and continuous regimes. Thus, the mathematical model needs to cover possible time-dependent as well as time-independent cases. Generally, the aim is to define the minimal number of models which cover the screening options and are suitable for simultaneous optimization that produces directly comparable results. Moreover, the base case model should be defined and optimized for a fair comparison. It will be used for quantifying the overall intensification potential. Typically, the base case should be the one most currently used in industry, often not including PI features or methods. It should be underlined that this case must be optimized.

The mathematical models are derived on the level of the module or its corresponding segments. A more detailed graphical description of the module and its segments is drawn, with all component names, direction, and names for respective energy transfers.

The model contains $\sum_{p=1}^{P} M_p$ number of material balance equations where M_p is the total number of components in phase p, while P is the total number of phases. For the module or segment in which fluid is ideally mixed, the material balance for the amount of component j, n_j, that is changing in phase p is therefore generally defined as the sum of all phenomena rates, present in that phase:

$$\frac{dn_{j,p}}{dt} = \sum_{f=1}^{F_p} \phi_f \tag{3.1}$$

where t is time; ϕ_f is the rate of phenomena f; while Fp is the total number of phenomena present in phase p. Each phase should also have a total mass balance:

$$n_{tot,p} = \sum_{j=1}^{C_p} n_{j,p} \tag{3.2}$$

where $n_{tot,p}$ is the total amount for all components in phase p, and C_p is the total number of components in phase p. This means that, if separation is present, a well-posed system of equations will result in $n_{tot,p}$ becoming smaller for one phase, and in the same amount larger for the other, interacting phase.

Similarly, the energy balance equations for a well-mixed module or segment should be written. The energy balance contains P number of equations or one equation for each phase:

$$\frac{dU_{p1}}{dt} = \sum_{f=1}^{F_{p1}} \left(\phi_f \cdot \Delta H_f\right) + \sum_{p2=1}^{P} E_{p1p2} \tag{3.3}$$

where U_{p1} is the internal energy for the phase $p1$; ΔH_f is the energy per total amount in a phase, released or captured due to the phenomena rate ϕ_f; while E_{p1p2} is the heat transfer rate between interacting phases $p1$ and $p2$, such that:

$$E_{p1p2} = -E_{p2p1} \tag{3.4}$$

$$E_{p1p1} = E_{p2p2} = \cdots = E_{pPpP} = 0 \tag{3.5}$$

(a segment phase cannot exchange heat with itself).

The internal energy of the phase *p1*, U_{p1}, is connected to enthalpy, H_{p1}, with the following equation:

$$H_{p1} = U_{p1} + p_{p1} \cdot V_{p1} \tag{3.6}$$

where p_{p1} and V_{p1} are pressure and volume of phase *p1*, respectively.

Apart from these equations, the model can contain equations for mass and energy connections between modules, intermediary, and other equations that will be shown and explained in detail in Chapters 4 and 6. In the case when module or segment is distributed in space (one-dimensional, i.e., if the plug flow of phases is considered), the mass and energy equations become partial differential equations. However, the governing equations are of similar structure as Eq. 3.1-3.5, but for a single space-discretization element. The exact mathematical representation of a discrete element will depend on the discretization method.

3.3 Optimization

The third stage of the proposed ReSyPIO methodology (Figure 3.1) is the Optimization of the generic superstructure, which can also include the optimization of the regime of operation. In the first step, the objective function needs to be defined. The objective function is of technical and economical nature, as the purpose of the optimization is to get an optimal structure and operational regime that would correspond to the maximum theoretical efficiency, i.e., intensification potential. Notably, the objective function should contain the main physical and chemical output parameters that directly reflect the reactor economics, such as maximum desired productivity, minimum energy supply, minimum volumes, or surfaces. These factors are usually combined, but the aim is to formulate the objective function with a minimal number of weighting factors, as they are mostly valued arbitrarily (or approximately), which might cause some bias in the analysis.

In some cases, multi-objective optimization (MO) would be an option [307]. By using MO, one does not need weighing data for variables that comprise objective functions. Instead, sets of optimal results irrespective of the scale of the problem are attained [108, 325-327]. MO gives solutions named as Pareto optimal set such that any solution inside the set cannot be regarded as a better or worse solution than the others. All solutions of the set are connected by a curve called Pareto optimal front, and any point along this curve can improve the value of one objective function at the cost of the other [325]. For MO, a nondominated sorting genetic algorithm is usually used. Also called controlled, elitist genetic algorithm (NSGA), it can maintain satisfactory convergence of the nondominated front and an appropriate spread of the solutions [108].

When several models for the description of a reactor superstructure are needed, as explained in Section 3.1, special care should be taken in the objective function formulation.

In order to analyze different cases of operational regimes, they have to contain qualitatively comparable results. For example, a discontinuous (batch) case might have a time-dependent objective function so that time costs are included, while a continuous steady state (one or a series of CSTRs) will have a time-independent objective function. In order to compare different options, some parameters need to be fixed and identical for all cases, such as input flow rates (capacity) or volumes. The decision on which parameters are fixed depends on the goals of the optimization and, consequently, objective functions.

In the second step, constraints need to be defined. They are related to thermodynamic or kinetic limitations of the system (e.g., liquid phase reaction cannot occur at certain temperatures, and maximal allowable temperature for reaction), as well as the limitations of the equipment material (e.g., maximum allowed pressure or pressure drop, and minimal volume or surface). On the other hand, constraints need to be formulated for a wide enough range, in order not to limit the optimization to a small set of solutions.

In the third step, defining the degrees of freedom (DOF) for optimization is of special concern. DOF, i.e., optimization (or control) variables, are directly related to the Phenomena Screening stage, as well as to the Superstructure Generation and Modeling. Generally, more DOF allow for more innovative solutions and provide greater theoretical enhancement potential. On the other hand, too many DOF often result in optimization problems, such as too complex systems (impossible to solve or involving very slow and unstable convergence) or the existence of multiple solutions. Therefore, a balance should be achieved using a detailed DOF analysis. Some compromises may result in superstructure alteration and consequently subtraction of DOF, which could contribute to additional improvements. In practice, this may happen after a premature optimization with a larger number of DOF [2]. In some cases, the existence of multiple solutions can be analyzed and handled through lexicographical optimization [312].

After defining the objective functions, constraints, and DOF, numeric algorithms that will be used for optimization need to be selected. For complex superstructures, it is advisable to use stochastic optimization algorithms, such as genetic algorithm, simulated annealing, etc. which has been elaborated in detail in the literature [263, 328]. Stochastic algorithms are supposed to ensure global solutions, while deterministic ones may reach local solutions. Thus, in ReSyPIO methodology, for complex reaction systems, one could start with a genetic algorithm (GA) or other methods (simulated annealing, and Tabu search). Since GA can provide values of optimization variables and objective functions which are not accurate enough, it is an already established practice to perform deterministic optimization (MINLP, NLP) afterward, by using initial guesses from the previous GA optimization. For reaction systems that are inherently dynamic or entail non-stationary operational regimes, dynamic optimization (DO) needs to be employed.

The result of the ReSyPIO methodology should display theoretical intensification potential and provide enough information about the optimal structure and operational regime of such a reaction system. The goal of this analysis is to examine and point to innovative and physically realizable reaction systems which have a high economic potential for further development. For this purpose, the quantitative margin between the optimized base reaction case and the innovative intensified case should be large enough. If the innovative solution demonstrates satisfactory improvement, the next step would be more detailed modeling (e.g., CFD or other fundamental and rigorous approaches), simulation and possibly optimization, followed by pilot experimentation and proof of concept [2].

In the next Chapter, the ReSyPIO methodology will be presented in a generic case with two parallel reactions.

4. Application of the ReSyPIO Methodology to a Generic Reaction Case

The example used for illustration of the methodology for reactor synthesis based on process intensification concepts and application of optimization methods (ReSyPIO) was published by Živković and Nikačević in 2016 [2]. It is a generic case of two parallel reactions occurring in a liquid phase:

$$A + B \overset{k_1}{\rightarrow} C \tag{4.1}$$

$$B \overset{k_2}{\rightarrow} 2D \tag{4.2}$$

The desired reaction product is C (Eq. 4.1), while product D (Eq. 4.2) is undesired. Both reactions are of the second order, endothermic and slow, and correspond to systems that can be found in the fine chemical industry. The goal is to propose an optimal reaction system and operational regime in terms of general technical and economic performance (maximum production of C for minimum reactor volume and minimum consumption of energy), for a given input quantity (1 m^3) of reactant A. In the following Sections, all stages of the ReSyPIO methodology will be demonstrated in detail on this published example.

4.1 Phenomena Screening

Kinetic parameters and other physical properties used in this generic example are given in Table 4.1 (step 1 of Phenomena Screening). The values for the pre-exponential factor, activation energy, enthalpy of chemical reaction, density, and heat capacity were selected in order to kinetically and thermodynamically favor the second reaction, which results in the undesired product.

Table 4.1 - Kinetic and physical properties for the examined reaction system [2]

Chemical Reactions (CR) Kinetic Parameters

CR l	CR order	pre-exp. factor Aa_l, L/mol/h	activation energy Ea_l, kJ/mol	enthalpy of CR ΔHr_l, kJ/mol
(4.1)	2	101.55	7.51	-82.3
(4.2)	2	1603	10.94	-55.2

Mixture Physical Properties		Inlet Conditions	
ρ, kg/L	c_p, kJ/kg/K	$c_{A,1} = c_{B,1}$, mol/L	T_1, °C
1.05	2.35	10	20

The analysis of the reaction mechanism suggests that the required ratio of the desired and undesired product can be achieved by introducing distributed feeding, i.e., dosing of reactant B. This will minimize the production of undesired product D. Therefore, the feeding rate should be optimized. Furthermore, the optimal number of segments, and thus, feeding points will also be optimized. A higher number of segments reduces axial mixing in the reactor and consequently increases the reaction driving forces. Additionally, more feeding points allow for better control of the undesired reaction. On the other hand, after a certain point, the addition of new segments is not beneficial from the economic point of view. These potential improvements, which will be covered by optimization, fall into the structural domain of PI.

The analysis of the reaction kinetics constants (presented in Table 4.1) demonstrates that high temperature favors the second, undesired reaction, since $Ea_2 > Ea_1$. Higher temperatures, on the other hand, increase both reaction rates. Thus, heat input may be optimized to compromise these two opposite effects and consequently (economically) optimal performance may be attained. This consideration is associated with the energetic domain of PI.

Since the reactions are slow, in common engineering practice, a priori solution of choice would be the batch operating mode. A fed-batch operation would be chosen in the case of gradual dosing of reactant B. However, in the proposed ReSyPIO methodology, such choice is not adopted in advance, and both continuous and fed-batch operations are considered in the optimization. Furthermore, a continuous system for this reaction system can operate in the dynamic regime, with periodic changes of some inputs (feed rates and heating rates [189]). This could also provide additional improvements in the overall performance in comparison to commonly used fed-batch or steady-state operation. Therefore, all the listed options from the dynamic domain of PI will be considered and covered by optimization.

In the third and final step of the Screening, a representative phenomenological module is defined (Figure 4.1).

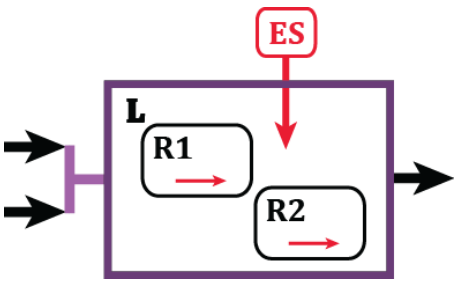

Figure 4.1 – Phenomenological module for the generic case study

Since both reactions occur in the same liquid phase and at the same time, only one type of module with a liquid (L) phase is enough for the representation of the system. The L phase is shown in Figure 4.1 as a white area within a purple rectangle denoting the borders of the module, or its control volume. Two reactions entail two different phenomena inside the module, named R1 and R2, both shown with their respective rounded rectangles. As the reactions are endothermic, heating will be required, so the energy source, ES, is also added (with its red arrow). ES is outside the boundaries of the module, meaning it will not be modeled in detail. Separation would not be beneficial, as both reactions are irreversible. Reactant A and B streams (black arrows) can be fed separately into the liquid phase of the module.

4.2 Reactor Structure and Mathematical Modeling

The first step of the next stage is the generation of the reaction system superstructure. Considering that only one type of a module with one phase is adopted and that adding a recycle is not beneficial for the reaction of interest, the general superstructure consists of a row or series of well-mixed segments of a module shown in Figure 4.2.

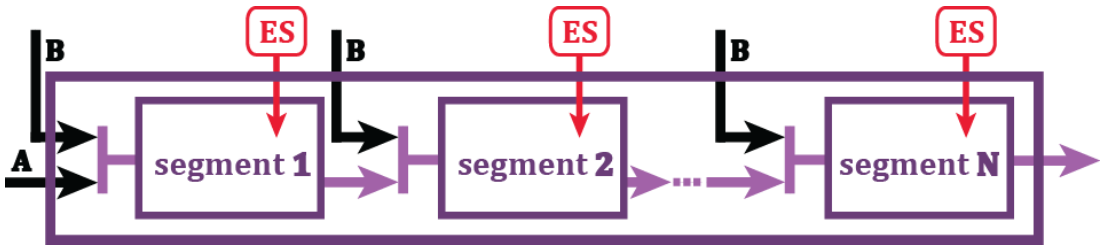

Figure 4.2 – The proposed superstructure of the analyzed reaction system

Reactant B needs to be dosed into the system in a distributed way in order to minimize the creation of the undesired product D. Therefore, multiple input streams of B are added, one to each segment. In the examined case, all segments of the module have two inlets (the mainstream and reactant B stream) and one outlet stream, as shown in Figure 4.2.

The second step of this stage entails the mathematical representation of the reaction system superstructure.

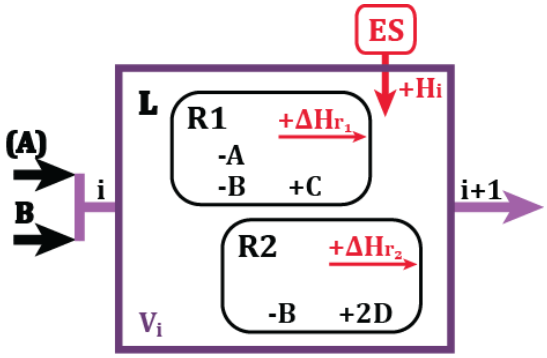

Figure 4.3 – Detailed graphical representation of segment i

For the purpose of mathematical modeling, the phenomenological module depicted in Figure 4.1 is segmented, and one representative segment (*i*) is described in detail in Figure 4.3. Inside the phenomena rectangles, the components with the corresponding stoichiometric coefficients are included (-A, -B and +C for R1). The segment inlet will be denoted in the equations with *i*, and the outlet with *i+1*.

The material balances for the segment *i*, shown in Figure 4.3, are mathematically described by four equations (for four components), where *j* = A, B, C, or D. It consists of the accumulation term (left-hand side) and the terms for inlet, outlet, and two phenomena rate elements (right side of the equation), respectively:

$$m \cdot \frac{d\left(V_i \cdot c_{j,i+1}\right)}{dt} = Q_i \cdot c_{j,i} - Q_{i+1} \cdot c_{j,i+1} + \phi_{R1}^{j,i} + \phi_{R2}^{j,i} \tag{4.3}$$

where $\phi_{R1,i}$ is the phenomena rate for reaction R1, while $\phi_{R2,i}$ is the phenomena rate for reaction R2, and component *j* in segment *i*:

$$\phi_{R1}^{j,i} = m \cdot V_i \cdot \upsilon_{R1,j} \cdot Aa_1 \cdot e^{-\frac{Ea_1}{R \cdot T}} \cdot c_{A,i+1} \cdot c_{B,i+1} \tag{4.4}$$

$$\phi_{R2}^{j,i} = m \cdot V_i \cdot \upsilon_{R2,j} \cdot Aa_2 \cdot e^{-\frac{Ea_2}{R \cdot T}} \cdot c_{B,i+1} \tag{4.5}$$

while the corresponding stochiometric coefficients for each component *j* are given in Figure 4.3:

$$\upsilon_{R1,A} = -1,\ \upsilon_{R1,B} = -1,\ \upsilon_{R1,C} = +1,\ \upsilon_{R2,A} = 0,\ \upsilon_{R2,B} = -1,\ ,\ \upsilon_{R2,C} = 0$$
$$\upsilon_{R2,D} = +2 \tag{4.6}$$

In Eq. 4.3-5, *m* is a binary segment identifier, signifying the presence (value 1) or absence (value 0) of the segment in the superstructure. The binary coefficients are introduced to facilitate the derivation of the optimal number of segments through optimization.

Since the volume of the segment changes for the discontinuous case, an additional equation of the total material balance is needed:

$$m \cdot \frac{dV_i}{dt} = Q_i + m \cdot Q_{B,i} - Q_{i+1} \tag{4.7}$$

The energy balance for the segment *i* is defined by one equation since only one phase is present. This equation consists of the terms for the inlet and outlet energy flow streams and three elements (three red arrows) that come from the heats of reaction R1 (ΔH_{r1}) and R2 (ΔH_{r2}) and heat inlet flow (H_i) from the energy source, ES:

$$\begin{aligned} \rho_{out} \cdot c_{p,out} \cdot m \cdot \frac{d(V_i \cdot T_{i+1})}{dt} = {} & Q_i \cdot \rho_{in} \cdot c_{p,in} \cdot T_i + m \cdot Q_{B,i} \cdot \rho_B \cdot c_{p,B} \cdot T_B - \\ & \rho_{out} \cdot c_{p,out} \cdot Q_{i+1} \cdot T_{i+1} + \\ & \Delta H_{r_1} \cdot \phi_{R1}^{C,i} + \Delta H_{r_2} \cdot \phi_{R1}^{D,i} + m \cdot H_i \end{aligned} \tag{4.8}$$

In this simplified generic case, the resistance to heat transfer is neglected, and uniform volumetric heating is considered (H_i). This is an idealized situation, which gives the maximal efficiency.

It should be emphasized that the ReSyPIO methodology does not imply a priori which general type of reactor will be exploited. For example, if the number of segments determined in the optimization is one (*N=1)*, then the physical reactor can be a fed-batch, or a continuous stirred-tank reactor (CSTR), operated in a steady- or dynamic-state. If the optimization converges to several segments in a row, then the system is continuous (steady-state or dynamic), which can be physically represented as a series of separate reactors. However, for the larger number of segments (above 10), the system could be physically realized as a tubular reactor, i.e., plug flow with axial dispersion (segments are not physically separated), which again could operate in a steady state or a deliberate unsteady state. Both the structure and the operational regime are determined simultaneously in the optimization, which is the following stage.

4.3 Optimization

The model presented in Section 4.2 is general enough to cover both discontinuous (fed-batch, without output flow) and continuous cases. According to the reaction screening, both cases are to be analyzed within the optimization step, along with continuous periodic operation. However, single optimization could not be set to cover all possible scenarios, as different optimization structures and methods are to be used for dynamic and steady-state cases. Therefore, three different optimizations for three cases will be defined and performed, i.e., fed-batch case (FB), continuous steady-state case (SS), and dynamic continuous case (DC). It should be underlined that all optimization parameters must be unified entirely in order to have fully comparable case results.

In order to have comparable results, the objective function (OF) needs to cover both time-dependent and independent cases. In general, it is defined (step 1) as:

$$OF = PRODUCTIVITY\ BENEFIT - ENERGY\ CONSUMPTION\ COST \tag{4.9}$$

Since component C is the desired product, only its productivity is beneficial. For the discontinuous operation (FB case), the objective function becomes:

$$OF_{FB} = \frac{c_{C,end}}{t_{end}} - C_H \cdot H_{tot} \tag{4.10}$$

while for the continuous steady-state (SS case) and dynamic continuous operation (DC case) it is, respectively:

$$OF_{SS} = \frac{c_{C,end} \cdot Q_{end}}{V_{tot}} - C_H \cdot H_{tot} \tag{4.11}$$

$$OF_{DC} = \frac{\left(c_{C,end} \cdot Q_{end}\right)^{mean}}{V_{tot}} - C_H \cdot H_{tot} \tag{4.12}$$

In Eq. 4.10-12, $c_{c,end}$ is the concentration of the desired product C at the end of FB operation, while in cases SS and DC it is the concentration at the outlet of the reactor (outlet of the last segment N). Constant C_H stands for energy consumption costs. The value of the coefficient C_H (1.4 mol/MJ) is chosen in such a way that energy consumption cost contributes to 25-30% of the overall productivity for examined cases. This is a realistic economic assumption, which may be applied to numerous reaction cases in the chemical industry.

It should be noted that the objective function can be defined differently to reflect other vital costs or revenues, including real prices when specific reaction system is a subject of analysis. By comparing OF for FB and SS case, it can be concluded that the maximal concentration of the desired product C at the end of the process in the FB case should be attained with minimal operation time, while in the SS case, the minimal residence time is required, which is analogous. For the DC case, a periodic change of the input variables is employed, which consequently leads to concentration and flow rates that vary over a sufficiently long time horizon. Thus, the mean values are accounted in the OF_{DC}, in order to examine the potential improvement. The input quantity of reactant A is fixed for all cases, which relates to the desired capacity of the process and ensures comparability.

The optimization constraints (step 2) reflect the process limitations (the maximally allowed temperature of the liquid phase) as well as the chemical limitations defined through the minimal selectivity and conversion:

$$T_i \leq 423.15 \text{ K} \tag{4.13}$$

$$sel = \frac{c_{C,end}}{c_{D,end}} \geq 8 \tag{4.14}$$

$$con = \frac{c_{A,0} - c_{A,end}}{c_{A,0}} \geq 0.80 \tag{4.15}$$

The selectivity, *sel*, is set high (Eq. 4.14), to achieve good control of the overall parallel reaction propagation and thus avoid subsequent separation of the undesired product. It should be underlined that conversion of A is not fixed, as optimization naturally drives the conversion to higher values in order to increase the productivity of C. However, constraint *con* (Eq. 4.15) is introduced to ensure the solutions in the high conversion regions, as there is a theoretical possibility for optimal solutions with low conversions and very short reaction times (Eq. 4.10-12).

In the third step, the optimization or control variables, i.e., DOF, are selected concerning the goal of getting the maximal theoretical efficiency for the given reaction case. Naturally, they differ within the optimization cases, although they essentially provide comparable results. For instance, in the FB case, the optimization or control variables are the input flow rates of the reactants A and B and the heat input. All these variables are time-dependent (overall quantity of A is fixed). In the SS case, the input variables are time-invariant, but they "vary in space" along with the series of segments (Figure 4.3). The DC case is optimized around the optimal SS case by periodically changing the inlet flow rates of the reactants A and B and the heat influx for each segment individually. This is achieved by the optimization of the amplitudes and phases and the frequency of periodic change for these three control variables:

$$Q_1 = Q_1^{ss} \cdot \left(1 + A \cdot cos(\omega \cdot t)\right) \tag{4.16}$$

$$Q_{B,i} = Q_{B,i}^{ss} \cdot \left(1 + A_{Q,i} \cdot cos(\omega \cdot t) + \varphi_{Q,i}\right) \tag{4.17}$$

$$H_i = H_i^{ss} \cdot \left(1 + A_{H,i} \cdot cos(\omega \cdot t) + \varphi_{H,i}\right) \tag{4.18}$$

Since the cross-effect of multiple periodic changes is the highest for the same frequency of the periodic changes of different inputs [329], a single frequency will be chosen through optimization for all variables in all segments.

The DOF for the three analyzed cases (discontinuous fed-batch, FB, continuous steady state, SS, and dynamic continuous, DC), as well as their lower and upper optimization bounds, are shown in Table 4.2.

Table 4.2 - Chosen control variables for three different operational regime cases of the reaction case and their upper and lower bounds [2]

	t $[h]$	$Q_{A,0}$ $[L/h]$	$Q_{B,i}$ $[L/h]$	H $[kW]$	V_{tot} $[m^3]$	N	ω $[rad/s]$	A_i	φ_i $[rad]$
FB	5	500	500	150					
	0	0	0	0					
SS			500*	150*	10	50			
			0	0	0	1			
DC							5	1	2π
							0	0	0

* per segment

The overall optimization is executed in a stepwise approach, with several optimizations, using numerical methods listed in Table 4.3. In the first step, the discontinuous FB case is optimized using dynamic optimization (DO) algorithm. The resulting fed-batch operation time, *t*, and the given (fixed) quantity of A are used to calculate the fixed input flow rate of the reactant A for SS, which provided the same capacities for both cases. In the second step, the stochastic genetic algorithm (GA) is used for obtaining a global solution for the SS case. GA is used because of a relatively complicated structure that can lead to local maximums if the MINLP is used. Subsequently, the results from GA are used as initial guesses for optimization variables in the mixed-integer nonlinear programming algorithm to confirm and refine the optimization results. The third and last step is the optimization of a continuous dynamic case around the optimal steady-state case, to check if there is any improvement if the reactor is switched to a periodic operation.

For this optimization, DO algorithms are used. The whole optimization algorithm is schematically shown in Figure 4.4.

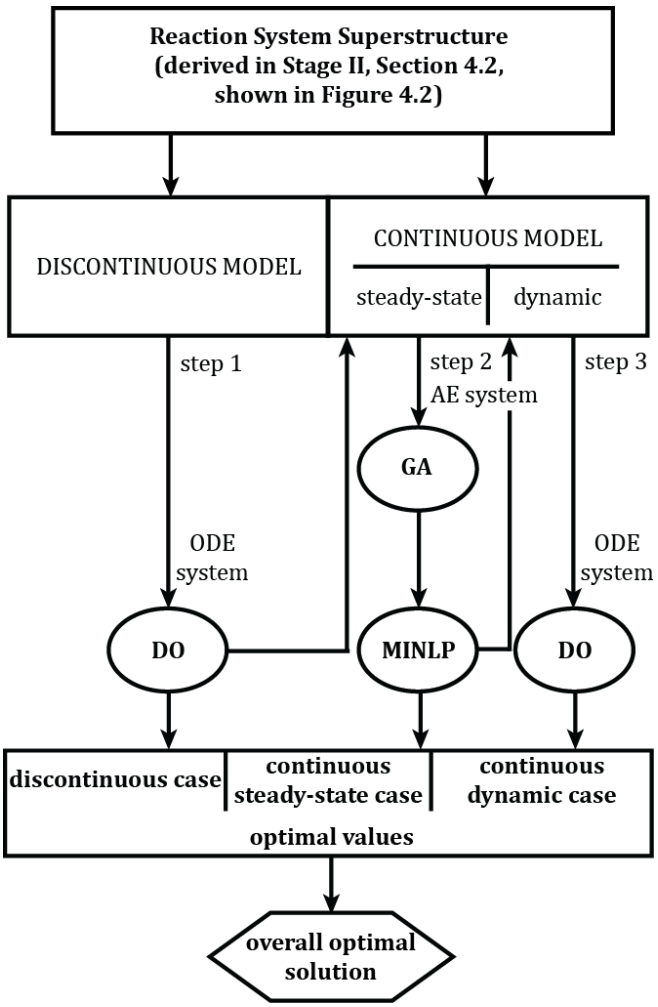

Figure 4.4 - Optimization algorithm for the reaction case study including three steps and methods: dynamic optimization (DO), genetic algorithm (GA) and mixed-integer nonlinear programming (MINLP) [2]

The optimization is performed in gPROMS (for DO and MINLP, gPROMS Modelbuilder, 2015) and Matlab (for mixed integer GA, Matlab 2015) according to numerical methods and parameters specified in Table 4.3. It should be noted that GA is used in a sequence of 50 successive runs (as part of one optimization script), with the initial population ranges taken from the previous run if it has an improved objective function value. Similarly, population sizes and generations are changed depending on the exit flag of the preceding run.

This is done in order to ensure that the optimal end solution is the closest possible to the desired global maximum and does not depend on a single combination of numerical parameters and starting population ranges. Subsequent use of deterministic optimization in gPROMS with the starting guesses from GA optimal solution gives a further increase of the objective function value of 2.7%.

Table 4.3 - Numerical methods, solvers and parameters used in the optimization of the reaction case [2]

SS case (Matlab, 2015)	
Genetic Algorithm	
Generations:	50000
StallGenLimit:	50 (fixed)
PopulationSize:	120 (starting)
TolFun:	$1 \cdot 10^{-12}$
PopInitRange:	from previous
The total number of runs:	50
Optimisation time:	11 h, 19 min, 4 s
SS case (gPROMS Modelbuilder, 2015)	
MINLP – OAERAP Algorithm	
MILPSolver:	LPSOLVE
NLPSolver:	NLPSQP
MaxIter:	200
OptimisationTolerance:	$1 \cdot 10^{-4}$
Optimisation time:	13 s
FB and DC case (gPROMS Modelbuilder, 2015)	
DO – CVP_SS Algorithm	
MaxIterations:	10000
OptimisationTolerance:	$1 \cdot 10^{-3}$
Optimisation time:	18 s
NLP – NLPSQP Algorithm	
MaxFun:	10000
MaxLineSearchSteps:	20
MaxLineSearchStepLength:	1
MinLineSearchStepLength:	$1 \cdot 10^{-5}$
NoImprovementTolerance:	$1 \cdot 10^{-12}$
OptimisationTolerance:	$1 \cdot 10^{-3}$
Optimisation time:	35 min

4.4 Results

In the fourth and final step of the optimization stage, the results are analyzed. The selected results of the optimization for different reactor cases (FB, SS, and DC) are shown in Table 4.4. Although optimization for the case SS converged to 17 segments in series (N=17), an additional optimization was performed for one segment (in which N is kept fixed to 1), just for the sake of comparing with other cases.

Table 4.4 – The optimization results for four different cases [2]

	CSTR	FB	SS	DC
N	1	1	17	17
OF, mol/m^3/h	-148	943	1243	1252
$c_{C,end}$, mol/L	3.913	3.880	3.882	3.889
V_{tot}, m^3	7.8	1.7	1.3	1.3
H_{tot}, kW	309	255	322	323

A reactor with one well-mixed segment (which equals to the module in this case), operating in the steady state, could be physically realized as a continuous stirred-tank reactor (CSTR). As could be expected from reaction engineering theory, CSTR displays the lowest efficiency, which is confirmed with the negative value of (Table 4.4). The main reason for low OF in the case of one steady-state segment (CSTR) is the required volume, which is around six times larger than for the other analyzed cases. Due to lower reactant concentrations and high demand for selectivity, the optimized steady-state CSTR without reactant B dosing requires a large reactor volume.

The fed-batch case (FB), or one segment, i.e., module with no output, has a much higher efficiency than the CSTR and requires less volume. This is due to good control of the undesired product formation achieved by reactant B dosing. The results of the simulation for optimal values for the FB case are shown in Figure 4.5a–b. The dynamic optimization (DO) was done with 20 control intervals, which can be seen in Figure 4.5c–d.

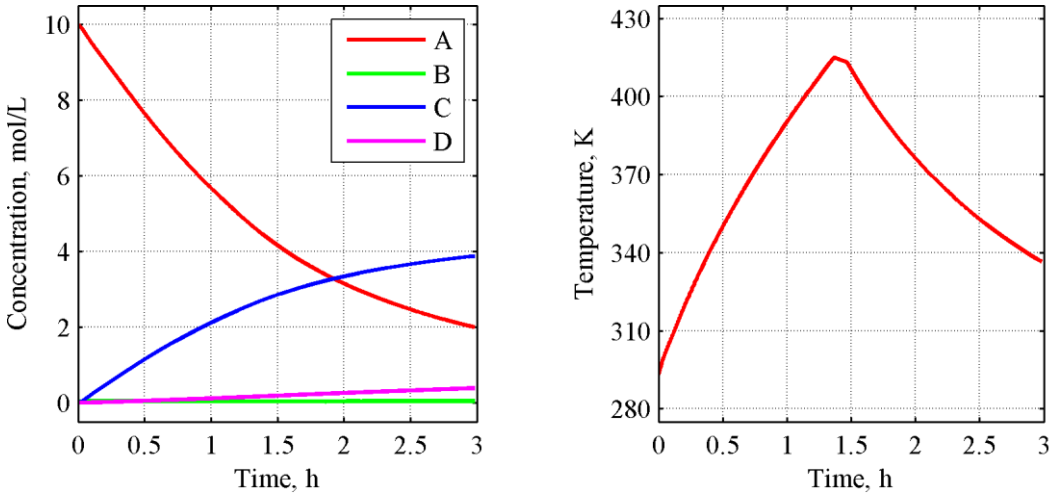

a - Concentration profiles

b - Temperature profile

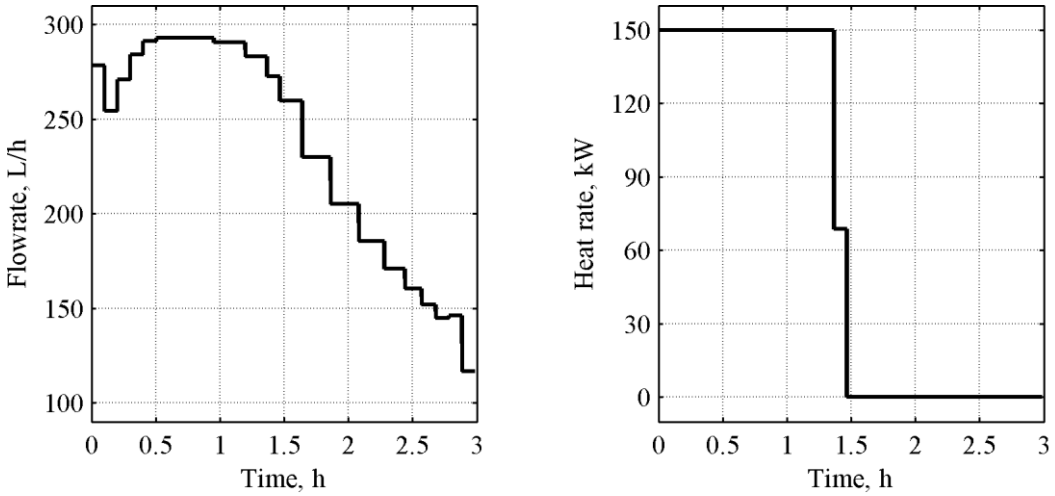

c - Input flow rate of reactant B

d - Input heat rate

Figure 4.5 – Optimization results for the FB case [2]

Reactant B is added with a higher flow rate at the beginning of a 3-hour long operation (also an optimization control variable, Table 4.2). The input flow rates of component B are ranging from 117 to 293 L/h. Heat is added only in the first half of the operation (with the maximum allowable heating rate of 150 kW), and afterward, the reaction occurs at the expense of reaction mixture temperature. As shown in Figure 4.5b, the temperature rises as heat is added to the system, all the way up to the maximum of 415 K (just below the constraint of 423.15 K). The temperature then drops as no additional heating is provided, while the endothermic reactions are still taking place.

The application of stochastic optimization (GA with integer optimization) followed by MINLP has shown that the optimal solution for the continuous steady-state case, SS, is a reactor with 17 equally sized segments of the module. As it was elaborated in the Screening stage (Section 4.1), more segments provide narrower residence time distribution, and the flow pattern approaches the plug flow. From reaction engineering theory, it is well-known that plug flow provides the highest reactant concentrations, i.e., the driving force for the reaction. This is the main reason why the optimal reactor volume is lower for the SS than for the FB case, in which the reaction mixture is more diluted. However, the optimization demonstrated that there are no additional benefits in introducing more segments above those 17. Thus, the optimal SS solution of 17 segments could be physically realized as a tubular reactor with 17 side inlet streams for reactant B. The flow through this tubular reactor would be nearly a plug flow, with some axial dispersion (corresponds to 17 well-mixed segments), which is closer to physical reality than a perfect plug flow, as some deviations from plug flow always exist.

As it can be seen from the concentration profiles (Figure 4.6a), the concentration of product C increases along the reactor (over segments) while the concentration of product D remains insignificant and within bounds set by the selectivity requirements. This is achieved by careful dosing of reactant B, i.e., low values of the inlet flow rates of B in the segments, as shown in Figure 4.6c.

Similarly, as in the FB case, the input of the reactant B flow rate decreases throughout the segments from the maximal value of 28 L/h to the minimal value of 7 L/h. Such values that correspond to a "drop-by-drop" dosing solution explain insignificant values of the concentration of product D in Figure 4.5a and 4.6a.

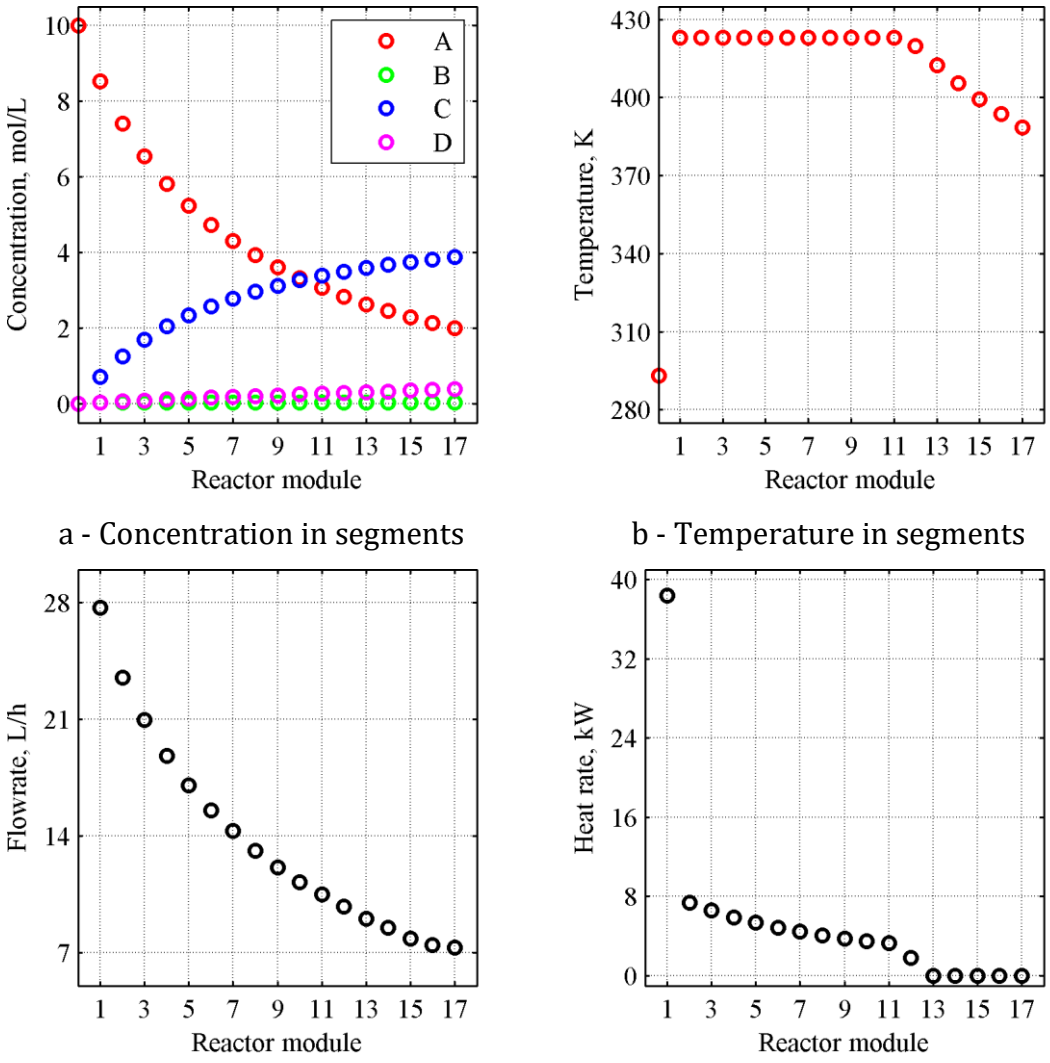

a - Concentration in segments

b - Temperature in segments

c - Input flow rates of reactant B

d - Input heat rates

Figure 4.6 – Optimization results for the SS case [2]

Another variable that was optimized was the heat input rate for each segment, shown in Figure 4.6d. The input heat rate is declining from one segment to the next, which means that the reaction mostly runs at the expense of the already present high temperature of the reaction mixture, achieved in the first segment.

From segment 13 to 17, no heat is added to the system, which would be analogous to the solution obtained for the FB case. Therefore, a decline in the temperature profile is not surprising (Figure 4.6b). However, the total heat supplied to the SS case reactor is 322 kW, while for the FB case, this input is lower by 26% (255 kW). This means that FB is energetically more efficient for this reaction system. Nevertheless, the decrease in volume from FB to SS is 30% (1.7 to 1.3 m^3), which is the main reason for the overall better performance of the SS case, depicted in the OF value (Table 4.4). It should be noted that in practice, the fed-batch reactor needs additional time for discharging and cleaning between batches. This was not penalized in the OF. Therefore, in a case that includes this time-lag in the OF, the SS case would outperform the FB case even more.

To reiterate, the dynamic continuous case (DC) is optimized around the optimal SS case by changing the input flow rates of reactant A and B and heat influx for each segment periodically. The optimized variables are the amplitudes and phases of periodic input variable functions as well as the frequency of the periodic change (Eq. 4.16-18).

The optimal control variable time profiles for the DC case are shown in Figure 4.7b-4.7f. The frequency of the change of all control variables is 4.22 rad/s. The highest obtained amplitude is for the flow rate of reactant B and heat input in the first segment, as well as the inlet flow rate of reactant A. Therefore, these three variables are shown separately from others in Figure 4.7c, 4.7e, and 4.7b, respectively. As can be seen, the input flow rate, $Q_{B,1}$, oscillates in the range of 7 L/h around the optimal steady-state value (Figure 4.7c) which corresponds to the amplitude of 23.6% while the heat input, H_1, oscillates in the range of 10 kW around the optimal steady-state value (amplitude 13.2%, Figure 4.7e). The inlet flow rate of reactant A oscillates around the optimal steady-state value with an amplitude of 10.3% (Figure 4.7b). Other flow rates of reactant B (Figure 4.7c) show different amplitudes of change for each segment, as well as a phase difference between some of them.

On the other hand, the heat input rates shown in Figure 4.7e lead to an interesting conclusion that for some segments (8, 9 and 10) there is no amplitude change, i.e., the optimal heat input is constant and corresponds to the optimal steady-state values. The total reactor volume for the DC case is held constant, so the results are comparable to other analyzed cases.

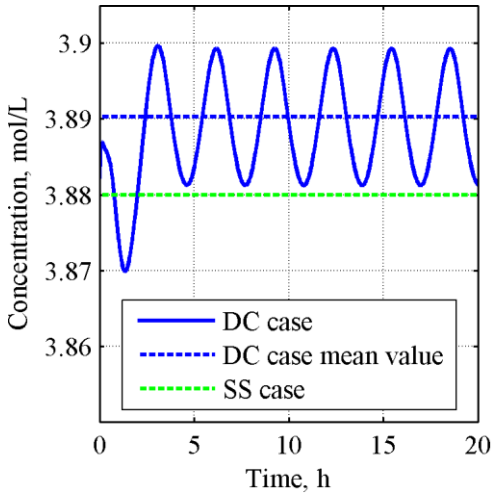

a - Concentration profile of desired product C at the reactor exit

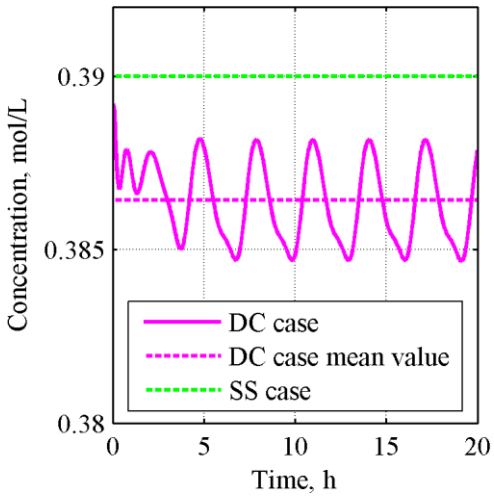

b - Concentration profile of undesired product D at the reactor exit

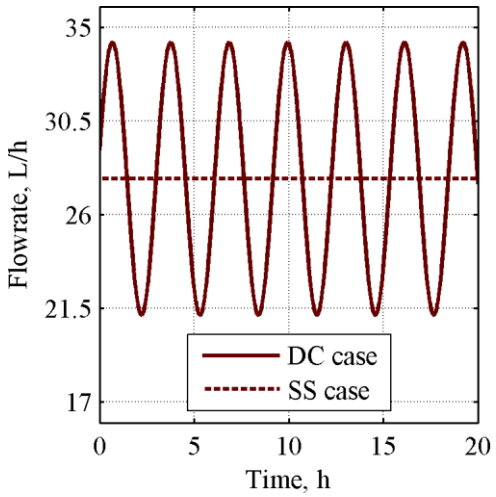

c – Input flow rate of B for segment 1

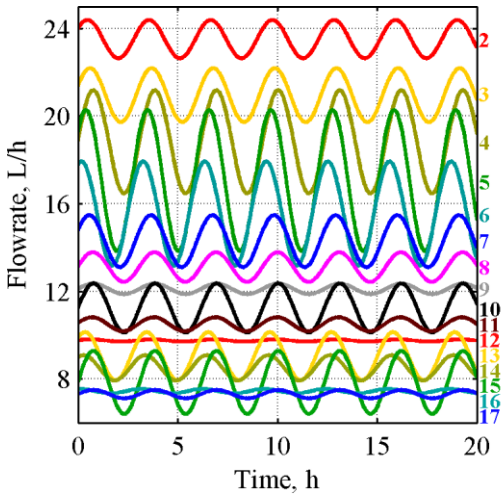

d – Input flow rates of B for seg. 2-17 (labelled on the right side of the diagram)

Figure 4.7 – Optimization results for DC case (part 1) [2]

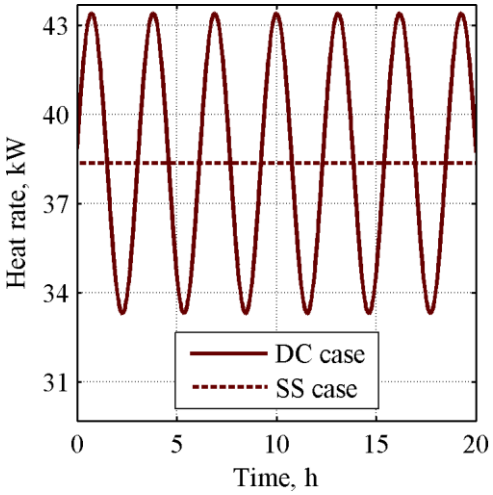

e – Input heat rate for segment 1

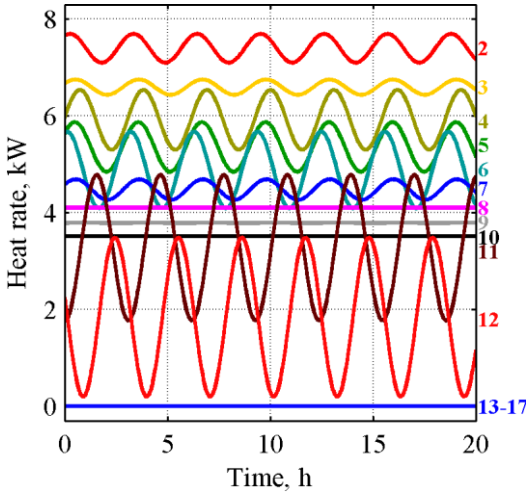

f – Input heat rate for segments 2-17 (labeled on the right side of the diagram)

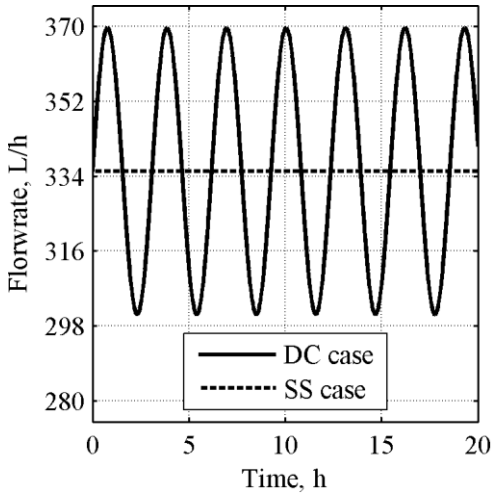

g - Input flow rate of A

Figure 4.7 - Optimization results for DC case (part 2) [2]

Figure 4.7a compares the reactor output concentrations of the desired product C for steady state (SS) and periodic case (DC). Apparently, the concentration in the DC case reactor is oscillating around a new “quasi-steady state," achieved after 2.5 hours from the start of the periodic modulations of the inputs. This concentration in DC is higher than for the SS case. However, the reactor efficiency enhancement can only be viewed via the respective increase of the component C molar flow rate, since both the volumetric flow rate and the concentration are changing.

Although the molar flow rate, which was optimized, was not plotted, it is clear from Table 4.4 that the objective function OF_{DC} is higher by only 0.7% when compared to OF_{SS}.

It should also be noted that the concentration of product D (Figure 4.7g) remains within the desired range (selectivity constraint is always satisfied). The overall heat input is the same for both continuous cases as it oscillates around the SS value. Consequently, the overall improvement may not be large enough to justify switching from the steady state to the periodic regime as the cost of dynamic operation is a lot higher and makes process control much more demanding. Therefore, for this examined reaction system, the proposed solution is a tubular reactor with a total volume of 1300 L that consists of 17 side input streams for B, operating under a steady-state condition with the values of control variables given in Figure 4.6c-d and optimal values presented in Table 4.4.

4.5 Conclusions

The ReSyPIO methodology was demonstrated on a general example of two endothermic liquid-phase parallel reactions. The Phenomena Screening analysis (stage 1) depicted potential improvements that fall into the structural, energetic, and dynamic domain of process intensification and defined a phenomenological module. Subsequent superstructure formation (stage 2) defined necessary mass and energy flow connections for the general series of segments and finally resulted in three cases, i.e., the fed-batch (FB), continuous steady-state (SS) and dynamic continuous (DC) reactors that were optimized.

Different methods were used in the optimization of the superstructure and operation regime (stage 3): dynamic optimization for the FB case, genetic algorithm and mixed integer linear programming (to ensure global minima and accurate results) for the SS case and dynamic optimization for the DC case. The objective functions were carefully adjusted to different cases, in order to have fully comparable optimization results.

The proposed solution is the reaction system that consists of 17 segments and is operated in a steady state. This system would be practically realized as a tubular reactor (plug flow with dispersion) with 17 side input streams of reactant B (which participates in both reactions).

The discontinuous or FB case, which can be realized as a simple fed-batch reactor, gives efficiency that is lower by approx. 30% than the proposed SS case, even when the time lags between batches are not accounted for (which would further decrease the objective function for the FB case).

A continuous reaction system that operates periodically around the optimal steady state (with 17 segments – tubular reactor) has shown small improvements compared to the SS case. Therefore, the DC case is discarded due to expected higher operation and control costs.

The applied methodology exemplifies a symbiosis between PI principles and PSE methods and can be efficiently applied for conceptual reactor synthesis, to demonstrate a theoretical improvement potential. In Chapter 6, the ReSyPIO methodology will be applied to an industrial case of hydrogen production through a water-gas shift reaction. Experimental investigation and results needed for the Phenomena Screening stage are presented in Chapter 5.

Nomenclature

Abbreviations

DOF	degrees of freedom
GA	genetic algorithm
MINLP	mixed-integer non-linear programming
NLP	non-linear programming
ODE	ordinary differential equation
PI	process intensification
PFR	plug-flow reactor
PSE	Process System Engineering

Variables and constants

A	the amplitude of periodic change for an input flow rate of reactant A	
Aa_l	the pre-exponential factor for reaction l	$m^3/mol/s$
$A_{Q,i}$	the amplitude of periodic change for flow rate B in segment i	
$A_{H,i}$	the amplitude of periodic change for heat input rate in segment i	
C_H	heat cost	mol/J
$c_{j,i}$	concentration for component j in segment i	mol/m^3
con	conversion	
c_p	specific heat capacity	$J/kg/K$
Ea_l	the activation energy for reaction l	J/mol
H_i	heat input rate for segment i	W
N	number of segments	
OF	objective function	$mol/m^3/s$
Q	volumetric flow rate	m^3/s
R	ideal gas constant	8.315 $J/mol/K$
sel	selectivity	

su	binary parameter (1 for presence, 0 for the absence of segment)	
t	time	s
T	temperature	K
V	segment volume	m^3
$\Delta H_{r,l}$	the heat of reaction l	J/mol
π	pi	3.14
ρ	density	kg/m^3
$\varphi_{Q,i}$	phase change between reactant B flow rate in segment i and Q_1	rad
$\varphi_{H,i}$	phase change between heat input rate in segment i and Q_1	rad
ϕ_{R1}	phenomena rate for chemical reaction R1	$mol/m^3/s$
ϕ_{R2}	phenomena rate for chemical reaction R2	$mol/m^3/s$
ω	frequency of periodic change	rad/s

Indexes

DC	dynamic continuous case
e	environment
end	at the end of the operation
FB	fed-batch case
i	segment index
in	inlet stream
j	component index (1, 2, 3 and 4 for A, B, C, and D, respectively)
l	reaction index (1 for (Eq. 1) and 2 for (Eq. 2))
max	maximum value
$mean$	mean value in time
ss	stationary value (*steady-state*)
SS	steady-state case
tot	total
out	outlet stream

5. Experimental Study on Sorption-Enhanced Water-Gas Shift Reaction

Hydrogen, an important energy carrier of the future, produces no pollution and has a high content of energy. It is formed as a direct product of the water–gas shift (WGS) reaction, which occurs in various processes for the production of hydrogen, ammonia, methanol, and different hydrocarbons, and is also a side reaction during steam reforming of hydrocarbons and Fisher–Tropsch synthesis [3]. Since it is an equilibrium reaction, it may be intensified by selective removal of the products, which can lead to higher yields and energy savings. The methodology for reactor synthesis based on process intensification concepts and application of optimization methods (ReSyPIO) that was presented in Chapter 3 will be applied on sorption-enhanced and membrane-enhanced water-gas shift reaction. Carbon dioxide will be removed through chemisorption on CaO particles, while hydrogen will be removed through the Pd-Ag membrane. The following Sections in Chapter 5 are presenting the experimental and initial modeling study, published in Applied Energy in 2016 [3].

The experimental study on water-gas shift (WGS) and sorption-enhanced water-gas shift (SE-WGS) reaction was done over six months in 2015. All experiments were conducted at the Department of Catalysis and Chemical Reaction Engineering, National Institute of Chemistry in Ljubljana, Slovenia. The experiment planning, design, execution, and analysis was done under the guidance of Blaž Likozar (Head of Department) and Andrej Pohar (Researcher and Assistant Professor) and with considerable help from Urška Kavčić (Technical Staff).

5.1 Brief Overview of The Water-Gas Shift Reaction

The water–gas shift (WGS) reaction is traditionally applied in energy-related processes for hydrogen enrichment, as well as for CO reduction in different industrial cases. It is highly crucial in reforming systems for hydrogen fuel cell applications and ammonia synthesis. Hydrogen has very high energy content and is also one of the most environmentally friendly energy sources. Fuel cells, which operate on pure hydrogen, have a rising application in energy-related domains and high importance in the research of hydrogen as the applied energy carrier of the future [330].

Plenty of WGS catalysts have been developed for the low and high-temperature range, the first being an iron-chromium catalyst developed by Bosch and Wilde in 1912 [331]. In the industry, the WGS reactor can be exploited for both ranges: the high-temperature range, which utilizes iron-oxide-based catalysts, and the low-temperature range, which utilizes copper-based catalysts [331, 332]. The reactor itself requires the largest volume in a fuel cell, primarily because of the slow kinetics at the temperatures required for a favorable equilibrium gas composition [333].

Since the WGS reaction is equilibrium-limited, one of the ways to shift the reaction towards the products' side is by removing CO_2 from the reaction mixture. This can be done by different sorption processes. Various sorption studies have been done on different types of catalysts, sorbents, reactor configurations, and operational regimes. Sedghkerdar et al. [334] showed that it is possible to achieve an outlet with 0% CO_2 and 81.7% H_2 from steam gasification by using a packed-bed with coal and CaO powder. Dou et al. [335] presented a continuous high-purity hydrogen production by sorption-enhanced steam reforming of glycerol with in situ CO_2 removal. An enriched hydrogen product of above 90% was achieved. Other in situ CO_2 capture studies involve the development of mixed catalyst-sorbent (calcium oxide) pellets [336] or use of dolomite as the sorbent in packed-beds [337].

Studies on different sorption-enhanced water–gas shift (SE–WGS) processes were also performed with potassium-promoted hydrotalcite (K–HTC) as the sorbent. These include research on pressurized bubbling fluidized-bed reactors [338], as well as both low and high-temperature pressure swing adsorption processes, which can give a 95% CO_2 recovery rate [339, 340]. The same sorbent was applied in a hybrid sorption-enhanced membrane reactor, where both CO_2 and H_2 were removed with 100% H_2 recovery [341] and a packed adsorbent-catalyst bed reactor, surrounded by a hollow fiber membrane, i.e., SE–WGS and membrane permeation [31].

By combining the sorption-enhanced reforming of hydrocarbons with CO_2 capture, the obtained energy carrier H_2 can be considered a CO_2-free fuel [342]. The CaO-based sorption process, with cyclic calcination and carbonation reactions, is one of the most prevalent technologies for CO_2 removal from gasification [343, 344]. Integrated gasification combined cycle (IGCC) is a power generation technology to convert solid fuels into electricity and IGCC with CO_2 removal is regarded as a promising option to mitigate CO_2 emission. In this case, a WGS-absorber substitutes the WGS reactors and desulfurization units and produces a hydrogen-rich stream using CaO sorbent [345]. The cyclic operation has been displayed for the case of sorption-enhanced steam methane reforming [346], and significant enhancement of the reforming process can be achieved with the CaO sorbent [347, 348].

One of the main advantages of using CaO as the sorbent is its low price, non-toxicity and no environmental impact, the possibility of use in fluidized bed reactors, the possibility of reuse in cement production, and CO_2 removal at high temperatures, where the kinetics are favored [343]. The sorbent can be regenerated with thermal decomposition at temperatures higher than 1120 K [349]. Calcium oxide can be implemented as a sorbent [350] also with the Calcium-Looping (CL) technology, or multicyclic carbonation and calcination of the sorbent in gas-solid fluidized bed reactors at high temperatures [347].

The experimental study on sorption-enhanced water-gas shift (SE-WGS) was done to gain more understanding about the enhanced process and obtain kinetic and diffusion parameters needed for the first step of the Phenomena Screening stage (data collection).

5.2 Experimental

5.2.1 Materials

For the experimental study, an iron-chromium based high-temperature catalyst, HiFUEL W210 (Alfa Aesar) was used. The catalyst was supplied in the shape of cylindrical pellets (size 5.4 x 3.6 mm). The recommended maximum operational temperature was 540 °C. The pellets were ground and sieved to the particle diameter of 160–250 μm. The small size of the catalyst particles assured negligible mass transfer resistance in its pores.

The calcium oxide sorbent particles were sieved to the same size as the catalyst, 160–250 μm, and heated to 850 °C, in order to remove any impurities. Unwashed glass beads (150–212 μm), produced by Sigma (G9018–250G, Batch #095K0141) were added as an inert. In the additional water separator unit, dodecane and silicon dioxide were applied to trap the layer of the condensed water. For the laboratory experiments, liquid water was used, as well as three gases: hydrogen, carbon monoxide, and nitrogen. Hydrogen was applied for catalyst activation, and nitrogen was used for purging the system. Concentrated sulfuric acid (19.15 M; Sigma–Aldrich) was used for qualitative analysis of the adsorbent particles, to determine the presence of carbonate.

5.2.2 Equipment and Setup

The kinetic tests were performed in an automated and computer-controlled laboratory reactor for catalytic microactivity analysis (MAR) by Process Integral Development Eng & Tech. The MAR, along with the rest of the experimental setup, is schematically shown in Figure 5.1. For the WGS and SE–WGS reactions, carbon monoxide (1) was introduced into the system and mixed with the water vapor in the blending unit (5). In its liquid form, water was kept at room temperature in a reservoir tank (6) outside of the hot box. It was injected into the hot box with a 307 HPLC Piston Pump (7) (Gilson Inc.). The flow rates of the gases introduced into the hot box (4) were controlled with mass flow controllers (MFC1–3) [3].

The water entering the hot box (4) was vaporized, since the inside temperature was held at 160 °C, with the help of an electric convection heater (8), controlled by the temperature controller, TIC1. After the mixing of the water vapor and the introduced gas in unit 5, the inlet stream was passed through a buffer vessel (9), which dampened any occurring pulsation due to evaporation.

The inlet stream was then passed through a six port VICI reactor standard bypass valve (10) and was either introduced into the reactor (11) or sent out of the MAR. The reactor was a stainless-steel tube (9 mm internal diameter, 305 mm long). The catalyst and inert/sorbent were packed inside the tube (11b) and insulated with a 15 mm layer of glass wool at the bottom (11c) and top (11d). The temperature of the packed-bed was measured with a thermocouple (TT2), and the temperature was controlled with the TIC2 controller.

After leaving the reactor tube, the outlet stream was conducted through a six-port bypass valve (10) and into the Peltier cell (13). The stream was cooled down, and water was separated inside internal storage [3].

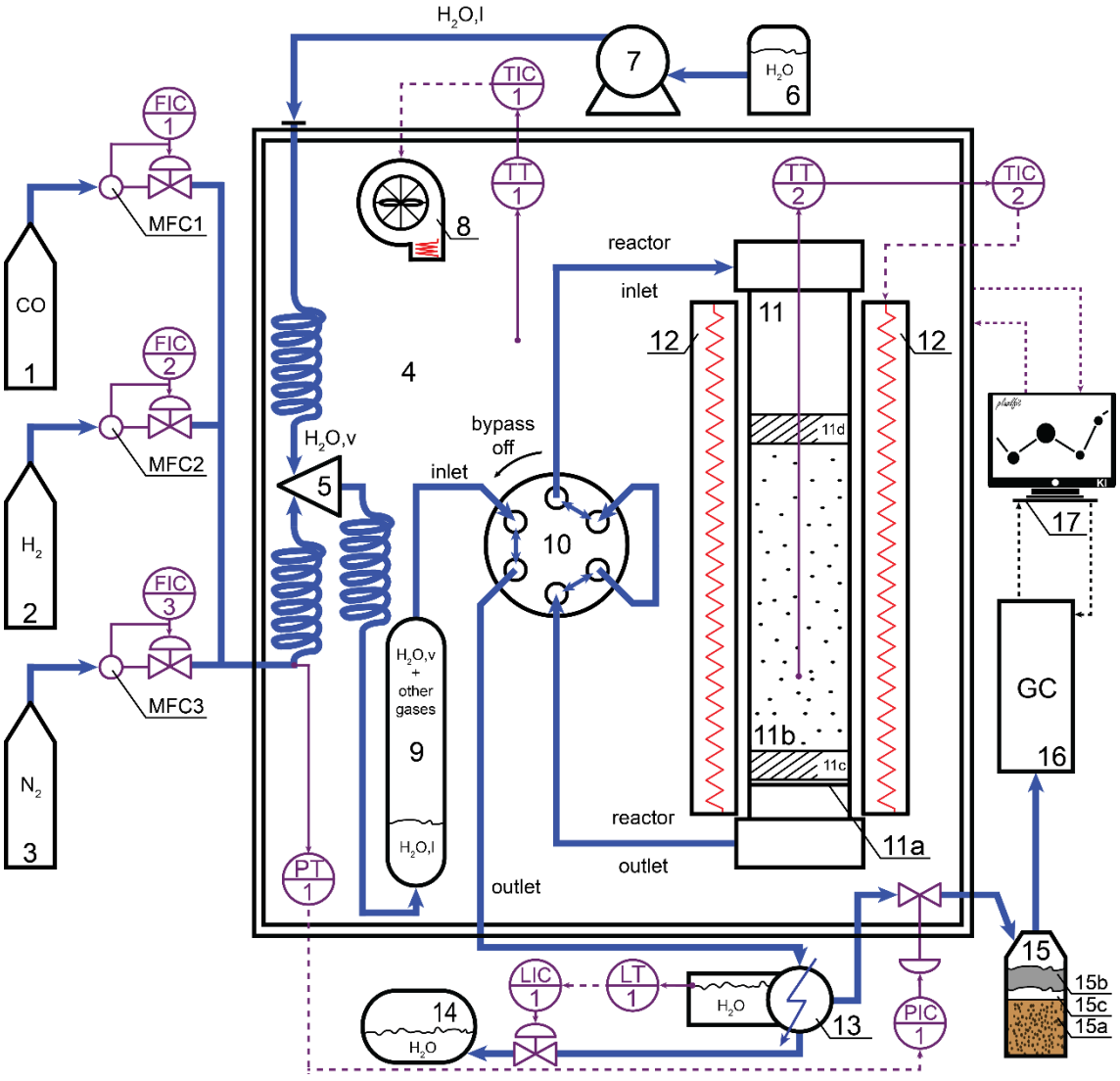

Figure 5.1 – The schematic representation of the experimental setup (MAR and auxiliary units) [3]

Blue – component flows; purple – control equipment; full black lines – units

1. CO gas storage tank, 2. H_2 gas storage tank, 3. N_2 gas storage tank, 4. Hot box, 5. Gas mixer, 6. Inlet water tank, 7. Piston pump, 8. Convection heater, 9. Pulsation dampener, 10. Six port bypass valve, 11. Reactor, 11a. Steel porous plate, 11b. Packed-bed, 11c. Glass wool bot. insul., 11d. Glass wool top insul., 12. Oven, 13. Peltier cooling cell, 14. Outlet water tank, 15. Separator vessel, 15a. SiO_2 (sand), 15b. Dodecane, 15c. Liquid water, 16. Micro GC, 17. Personal computer.

The liquid level in the storage was controlled with a level controller (LIC1), and the excess water was sent into a water tank (14) placed below the MAR. The outlet stream was then passed through the hot box outside of the MAR and into an additional separator vessel (15). The volume of the separator vessel was minimized by adding a layer of silicon dioxide at the bottom (15a) and a small layer of dodecane at the top (15b). The remaining water condensed from the outlet stream at room temperature and was trapped between the dodecane and SiO_2 (15c). The remaining gas composition was analyzed with a 490 Micro GC (16) (Agilent Technologies). The GC device had two thermal conductivity detectors and used a mixture of hydrogen and helium as the carrier gas. All GC analyses results were sent to the personal computer (17), where they were processed. All mass flow, temperature, pressure, and level controllers, as well as the pump and MAR operational parameters, were directly programmed and controlled by the computer.

5.2.3 Method and Operating Conditions

Before the start of the kinetic analysis tests on the WGS reaction, the catalyst was activated by a constant flow of hydrogen (5 mL/min, unit 2, Figure 1) for five hours, while the packed-bed (11b) was kept at 300 °C. For the WGS and SE–WGS reaction, two types of experiments were performed: steady-state and dynamic, respectively. The reaction start times were controlled by the manipulation of the bypass valve (unit 10 in Figure 5.1). For each experimental run, the bypass valve was initially turned on (i.e., Figure 5.1), and sufficient time was provided, so that the equilibrium inside the buffer vessel (9) could be achieved, and that the reactor inlet composition was constant. The reaction was then initiated by the redirection of the inlet stream into the reactor tube (11) filled with the catalyst and the inert/sorbent (11a). The stop time of each experiment run was marked by turning the bypass valve (10) on again.

The WGS reaction tests consisted of a series of steady-state runs with the packed-bed, which was filled with the catalyst and inert (11b). Glass wool was used to insulate the bed on the top (11d) and bottom (11c). The oven temperature was held constant for all relevant experimental test run repetitions.

A total of 2417 sampling tests were performed for the WGS reaction over the permitted range of operating parameters, supplied by the catalyst manufacturer (Alfa Aesar). In brief, the experiments were performed at the temperatures of 240–510 °C, flow rates of 33–302 mL/min, and H_2O to CO (STCO) ratios of 0.4–1.7. The catalyst mass and the inert to catalyst ratio were also varied [3]. The full set of operational parameters and the number of repetitions is provided in Appendix A (Table A.1).

Initially, different temperatures, flow rates, and catalyst masses were tested to make sure that the outlet composition of the components was not equal to the equilibrium values (calculated using Eq. 5.2 in Section 5.3). It was determined that the inlet flow rate of 100 mL/min, and the catalyst mass of 0.32 g, gave results which were well below the equilibrium values. Thus, most experiments were done for these parameters, by varying the inlet steam-to-carbon monoxide (STCO) ratio and the temperature.

The SE–WGS reaction experiments were dynamic, since, during the operation, the sorbent was irreversibly converted to $CaCO_3$. Before each experiment, the reactor tube (11) was purged with nitrogen (3) at room temperature to ensure that there was no carbon dioxide present inside the reactor at the beginning of the experiment. Afterward, the reactor was bypassed, and the desired initial ratio of water (7) and carbon monoxide (1) was introduced. When the equilibrium between the liquid water and the water vapor was achieved in the buffer vessel (9), the inlet gas was introduced into the reactor.

After enough time had passed (when the outlet composition results pointed to an insignificant change in value), the bypass valve (10) was turned on, which marked the experiment end time. Lastly, the catalyst was separated from the sorbent/adsorbent mixture with a magnet. The packed-bed sample was removed from the reactor and evenly distributed in a glass petri dish. For 24 experiments, total carbon (TC) analysis was performed to determine the amount of carbon inside the experiment samples, and the approximate value of the sorbent conversion, which is explained in Section 5.4. The instrument used for TC analysis was Rosemount Analytical Dohrmann DC–190. Some samples were subjected to qualitative analysis with sulfuric acid, as well as X-ray diffraction (XRD) and temperature-programmed oxidation (TPO) analysis, to determine the presence of charcoal and the carbonate. XRD analysis was performed using the PANalytical X'Pert Pro instrument, while TPO was conducted with a Micromeritics Autochem 2920 Chemisorption analyzer.

The operational parameters and the number of repetitions for the SE–WGS reaction experiments are given in Table A.2 and A.3 (Appendix A). The parameters varied were the temperature (270–510 °C), the total inlet flow rate (8–503 mL/min), the STCO ratio (0.7–1.7), the sorbent to catalyst ratio (0.3–130), and the catalyst mass (34.3–1869.5 mg).

All experimental runs for the WGS and SE–WGS reaction were automated since the Micro GC collected and analyzes samples every 3 min. Many data points (from 15 to over 300) were collected for each SE–WGS run, which improved the accuracy of the parameter estimation, described in Section 5.4.

5.3 Results

A total of 41 experiments were performed for the SE–WGS process at different temperatures, STCO, and sorbent-to-catalyst ratios, as well as reactant ratios (Table A.2 and A.3 in Appendix A). In Figure 5.2, the obtained data are shown for experiment 18 [3].

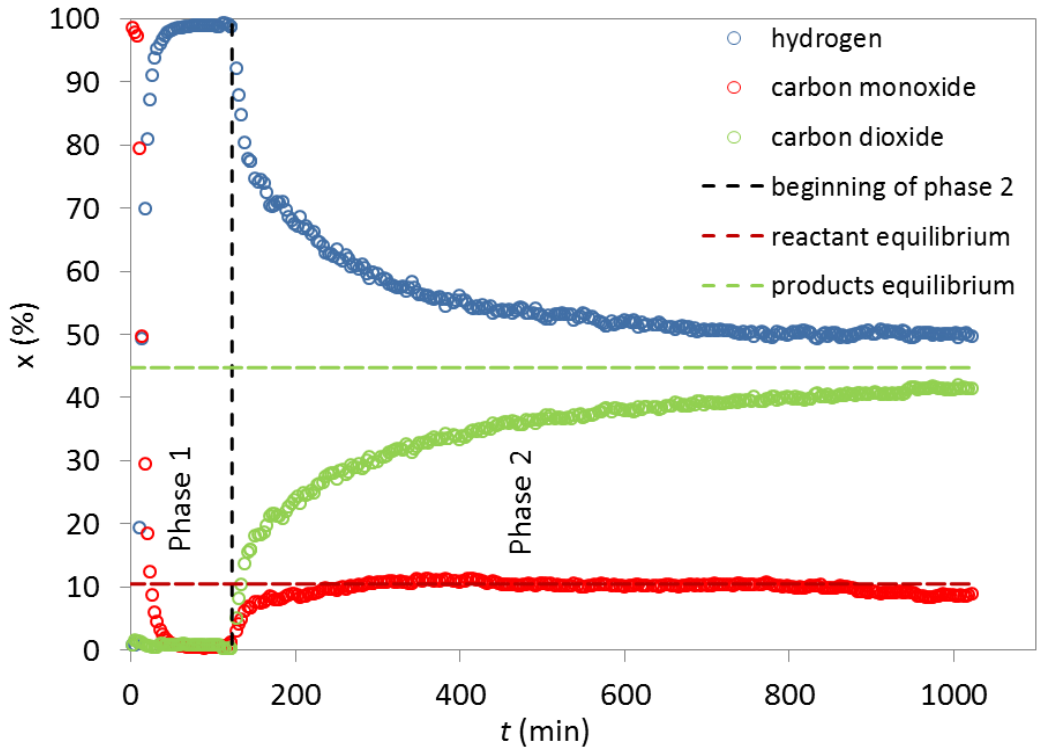

Figure 5.2 – The composition in time for experiment 18 of the SE–WGS reaction [3]

The SE–WGS experiments can be divided into 3 phases. During phase 1, CO_2 is entirely removed by the sorbent so that its concentration at the exit of the reactor is minimal. Also, the measured composition of the reactant CO is below the theoretical equilibrium values (horizontal dashed lines). In this phase, maximum hydrogen composition is obtained and maintained for another 30 min. The value and duration of this maximum depend on the total reactant flow rate, temperature, and the sorbent to catalyst ratio.

Phase 2 is the phase of the diffusion limited carbonation reaction, which begins when the sorbent surface is fully covered with $CaCO_3$ (diffusion of carbon dioxide through the outer carbonate layer) [351]. This phase is marked by decreasing hydrogen composition and increasing CO_2 composition. The sudden transition between the rapid initial reaction, followed by a much slower second stage has already been documented [352]. The last phase (3) is the time period when CO_2 is not removed by the carbonation reaction, and the gas reaches the thermodynamic equilibrium. This stage is not reached on the presented experiment, but the approach to equilibrium can be observed. Before the beginning of the experiment, when the reactor is bypassed, only carbon monoxide is detected since the water has been removed.

The total carbon mass measured in the sample for this experiment was 12%, which can be converted to 60% mass of formed carbonate. However, it has to be noted that this is only an approximate carbonization rate, as not all removed carbon dioxide is converted into carbonate. Visually, charcoal was observed in many samples, and subsequent TPO testing confirmed that carbon formation takes place during the reaction, while X-ray analysis and qualitative analytical tests with sulfuric acid reaffirmed the presence of considerable amounts of carbonate. Since it can be used only as a rough estimate, the TC analysis was applied to a few experiments only. The list of all the measured carbon mass samples can be seen in Table A.4, Appendix A.

In Figure 5.3, the equilibrium WGS and experimental SE–WGS results were compared for experiments 10–14, 17, 19, and 20. As can be seen, there is a significant difference in the maximal composition of hydrogen in the reactions with and without the sorption-enhancement in the upper range of temperatures (higher than 350 °C). For temperatures lower than 290 °C, the WGS reaction without sorption gives a higher hydrogen output, which is most probably because a higher effective catalyst area is available since it is not surrounded by the sorbent. The difference of about 60% in the hydrogen output for T > 430 °C gives a good reason for further investigation of the SE–WGS processes.

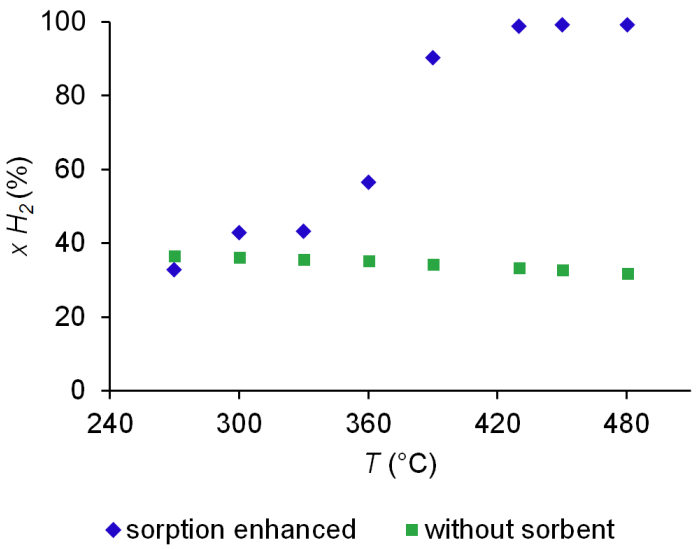

Figure 5.3 – Maximal hydrogen outlet composition for STCO ratio 1.7:1, total flow rate 33 mL/min and sorbent to catalyst ratio 9.2:1 for WGS (green) and SE–WGS (blue) [3]

5.4 Estimation of Kinetic and Diffusion Parameters

5.4.1 Water-Gas Shift

The kinetics of the water–gas shift reaction was determined at high convection conditions in order to remove the external mass transfer limitations. Additionally, the small size of the catalyst particles (160–250 μm) assured a negligible intra-particle diffusion resistance for all operational parameters, which was also confirmed using a correlation by Comiti et al. [353]. The one-dimensional mass balance (convection and reaction) equation for the packed-bed reactor, used in the model, is, therefore:

$$v \cdot \frac{dc_i(z)}{dz} = \frac{(1-\varepsilon)}{\varepsilon} \cdot r_i \tag{5.1}$$

with the boundary condition:

$$c_i(0) = c_{i,0}$$

where v is the interstitial gas velocity, c_i is the concentration of component i in the gaseous reaction mixture (CO, H_2O, CO_2 or H_2), z is the length dimension (in the direction of the flow), ε is the void fraction and r_i is the rate of reaction (positive for the products and negative for the reactants).

The chemical equilibrium constant (K_{eq}) for the WGS reaction can be calculated with the following expression [330]:

$$K_{eq} = \frac{P_{CO_2}^{eq} \cdot P_{H_2}^{eq}}{P_{CO}^{eq} \cdot P_{H_2O}^{eq}} = e^{5693.5T^{-1}+1.08ln(T)+5.44\cdot10^{-4}T-1.12\cdot10^{-7}T^2-49170T^{-2}-13.15} \tag{5.2}$$

where T is the temperature in K.

For the WGS reaction rates, a power-law equation is used [331].

$$r_i = \pm k_{WGS} \cdot P_{CO}^{a} \cdot P_{H_2O}^{b} \cdot P_{CO_2}^{c} \cdot P_{H_2}^{d} \cdot (1-\beta) \cdot \rho_{cat} \quad (5.3)$$

$$\beta = \frac{1}{K_{eq}} \cdot \frac{P_{CO_2} P_{H_2}}{P_{CO} P_{H_2O}} \quad (5.4)$$

$$k_{WGS} = A \cdot \exp\left(-\frac{E_a}{RT}\right) \quad (5.5)$$

k_{WGS} is the rate constant, P_i is the partial pressure of component i, a, b, c, and d are the reaction orders of CO, H_2O, CO_2, and H_2, respectively, β is a parameter defining the approach to equilibrium (β<1, below equilibrium, β=1 at the equilibrium), ρ_{cat} is the catalyst density, A is the pre-exponential factor, Ea is the activation energy of reaction rate constant for the WGS reaction, and R is the universal gas constant.

The high-temperature WGS experiments were performed to obtain the kinetic expressions for the process, which could be used for the sorption enhanced operation. Regression analysis was performed with the trust-region-reflective algorithm in Matlab 2015. An objective function was formulated as the sum of the absolute values of the difference between each experimental value and its model counterpart. The algorithm (function *lsqnonlin*) minimized the objective function by varying the regression parameters (kinetic constants). Several initial approximations were used to validate the detection of the global minimum.

The obtained power-law kinetic parameters with their 95% confidence intervals are presented in Table 5.1. The units of A are mol g(catalyst)$^{-1}$ s^{-1} kPa$^{-(a+b+c+d)}$, and the partial pressures of the gaseous components are in kPa. k_{WGS} is the reaction rate constant, ρ_{cat} is the catalyst density inside the reactor, R is the universal gas constant, and T is the reaction temperature (K).

Table 5.1 – The kinetic parameters obtained by regression analysis [3]

A (mol kPa$^{-(a+b+c+d)}$ g_{cat}^{-1} s^{-1})	1.11 ± 0.36
E_a (J mol^{-1})	(6.21 ± 0.06) × 10^4
a	0.38 ± 0.03
b	−0.10 ± 0.03
c	0.082 ± 0.002
d	0.082 ± 0.002

Considering that the power-law parameters c and d have the same value, a regression analysis was also performed for combined partial pressures of CO_2 and H_2 in the form:

$$r_i = \pm k_{WGS} \cdot P_{CO}^{a} \cdot P_{H_2O}^{b} \cdot \left(P_{CO_2} \cdot P_{H_2}\right)^{c} \cdot (1-\beta) \cdot \rho_{cat} \tag{5.6}$$

which resulted in the same value, c = 0.082, which was expected, since, in the equation system, both CO_2 and H_2 are produced at the same rate and have the same influence on the reaction.

As can be seen in Figure 5.4, a good agreement was obtained between the experimental data and the power-law kinetics for various temperatures and steam-to-carbon monoxide (STCO) ratios. Water was condensed prior to GC analysis. Some of the experiments were performed under the conditions that allowed for the reaction to reach the thermodynamic equilibrium, specifically the experiments at higher temperatures, which is in accordance with fast reaction kinetics.

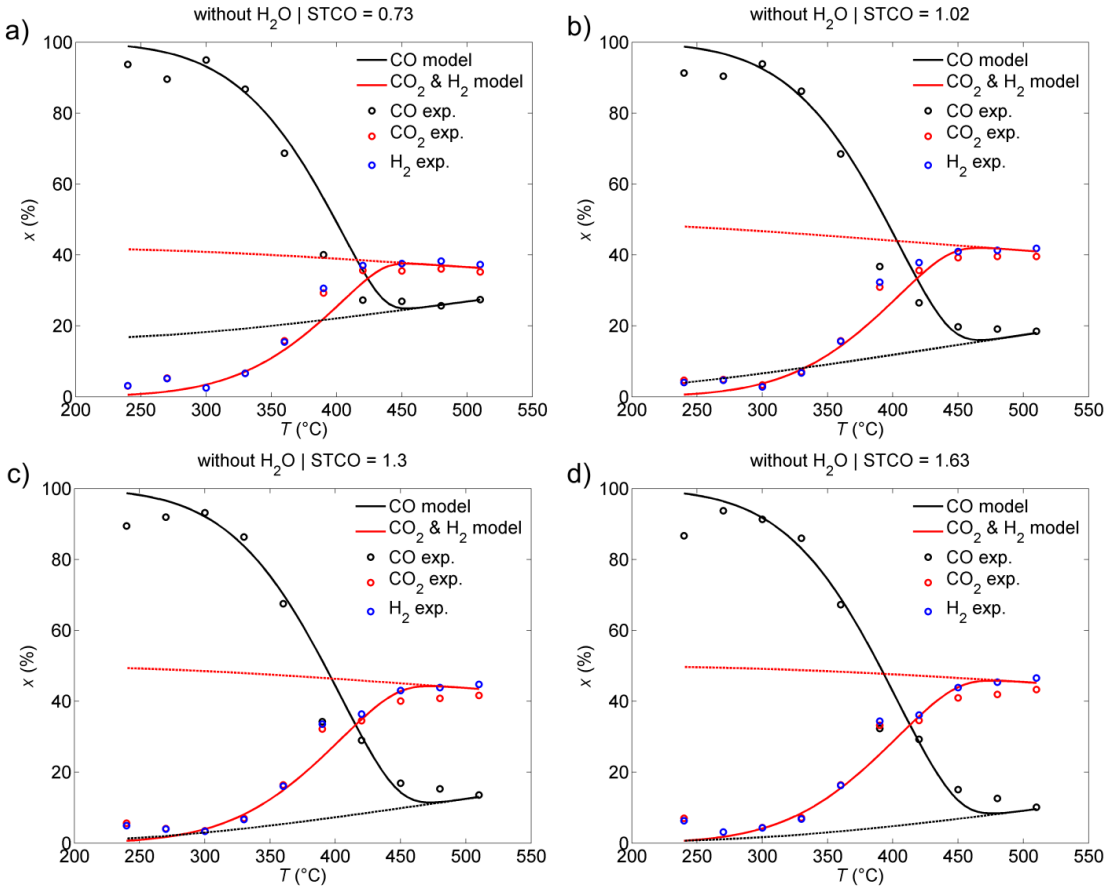

Figure 5.4 – H_2 composition vs. reaction temperature for different STCO ratios; catalyst loading: 0.3178 g; pressure: 1 atm; total flow rate: 100 mL/min. The dashed lines represent the thermodynamic equilibrium [3]

The kinetic parameters obtained are valid for the commercial iron-chromium based high-temperature catalyst, HiFUEL W210 from Alfa Aesar, and describe the catalyst activity in the temperature range of 240 – 510 °C.

The equilibrium values of the hydrogen composition that were experimentally reached at the upper-temperature range (above 450 °C) and STCO ratios (1.6:1) match the equilibrium values calculated by Eq. 5.2 within the error of 0.2%. This is slightly above the instrumental error made by the Micro GC (~0.1%).

5.4.2 Sorption-Enhanced Water-Gas Shift

Simple models of the carbonation reaction have been presented [346, 354] in the literature, while more descriptive ones include different gas-solid dynamics, such as the shrinking core model [355], grain model [356, 357], pore model [352], or the rate equation theory [358]. Apart from the different modeling approaches, the described models also vary on account of the unique morphology of the sorbents [355]. In a recent review, Perejón et al. have identified that the significant future modeling challenge is the dynamic simulation of the calcium looping process. It has been stressed that precise knowledge of the multicyclic CO_2 capture behavior is required and that it is of high relevance in order to predict the realistic process operation [347]. For modeling of the process in this work, an adaptation of the shrinking core model was used.

CaO particles react with CO_2 in the gas stream, and $CaCO_3$ is formed at the surface of the particles. Subsequently, CO_2 must diffuse through the $CaCO_3$ layer formed at the surface. This layer thickens with time as the reaction progresses, which results in increasing diffusional resistance. The front between CaO and $CaCO_3$ is at the critical radius, which changes with time by the following expression [359]:

$$-\frac{dr_c(t,z)}{dt} = \frac{c_{CO_2}/V_{m,CaO}}{\frac{r_c^2}{{R_{CaO}}^2 k_g} + \frac{(R_{CaO}-r_c)r_c}{R_{CaO}D_{e,CO_2}} + \frac{1}{k_{carb}}} \tag{5.7}$$

where r_c is the critical radius of the CaO particles, $V_{m,CaO}$ is the molar density of CaO, R_{CaO} is the radius of the CaO particles, k_g is the film mass transfer coefficient, $D_{e,CO2}$ is the apparent diffusion coefficient, and k_{carb} is the carbonization reaction rate constant.

The expression considers three mass transfer resistances: the resistance through the gas film, the resistance due to diffusion through the outer non-reacting layer, and the resistance on account of the chemical reaction ($1/k_{carb}$).

The componential material balances for the SE–WGS reaction process are:

$$\frac{\partial c_i(t,z)}{\partial t} = -v\frac{\partial c_i(t,z)}{\partial z} + \frac{(1-\varepsilon)}{\varepsilon} r_i \tag{5.8}$$

$$\frac{\partial c_{CO_2}(t,z)}{\partial t} = -v\frac{\partial c_{CO_2}(t,z)}{\partial z} + \frac{(1-\varepsilon)}{\varepsilon} r_i - \frac{(1-\varepsilon)}{\varepsilon}\frac{\rho_{CaO}}{M_{CaO}}\frac{\partial X(t,z)}{\partial t} \tag{5.9}$$

with the boundary conditions:

$$c_i\left(0 < t < t_{exp}, 0\right) = c_{i,0}$$

ρ_{CaO} is the sorbent density, and M_{CaO} is its molar mass; X represents the CaO conversion and can be calculated through the following expression:

$$X = 1 - \left(\frac{r_c}{R_{CaO}}\right)^3 \tag{5.10}$$

The gases were mixed inside the water condenser before Micro GC analysis (unit 15 on Figure 5.1). This was approximated with a continuous stirred tank reactor mathematical description. The mass balance of the gaseous species is:

$$\frac{dc_i}{dt} = \frac{\phi_v}{V}\left(c_{i,in} - c_i\right) \tag{5.11}$$

where $c_{i,in}$ is the reactor exit concentration, ϕ_v is the gas flow rate, and V is the empty volume of the condenser.

The Micro GC sampling took place every 3 minutes and lasted for 10 s. The experimental results are presented without water since it was condensed and removed before analysis. For comparison, the gas composition without water was also calculated using the model.

It is of foremost interest to know the composition of the gas at the exit of the reactor. The measuring technique, however, requires that only dry gas is analyzed, which is why a condenser was fitted after the reactor, for water condensation. In the condenser, gases are mixed to some extent, and 10 seconds of GC sampling follows. The Micro GC, therefore, analyzes the 10 s average dry gas composition, at the exit of the condenser. For the comparison between the experimental and model results, the whole sampling process was modeled, and these results were subject to regression analysis. The experimental data points are named *GC output experimental*, while the model results are *GC output model*. The actual gas composition at the exit of the reactor is also obtained with the model.

The initial simulations showed some discrepancy with the experimental data, which was found to be the consequence of the non-ideal behavior of the shrinking core particles, not accounted for by the model equations. Since the particles are not spherical but of irregular geometry, there is an initial period, when some areas of the particles are converted to $CaCO_3$, while other areas are still available for the reaction. This means that the reaction does not occur at a sharp interface, but rather along a diffuse front. In order to describe this non-ideal behavior, the effective diffusion coefficient was presumed to vary during the time. At the start of the experiment, the value of the apparent diffusion coefficient for CO_2 was $D_{e,0}$, and from that time the change was approximated as a linear decrease to the final value of D_e, which comes into effect when the whole surface of the particles is covered by $CaCO_3$. In the model, this was correlated to the conversion of the particles: at zero conversion, the apparent diffusion coefficient is $D_{e,0}$, and this value drops to D_e in a linear manner, which occurs at a specific value of sorbent conversion (discussed

below). This formulation is also following the findings of Alvarez and Abanades [360], who found that the critical $CaCO_3$ product layer thickness was only 50 nm.

The initial apparent diffusion coefficient, De_0, for all experiments at various operational conditions, was found to be 1.65×10^{-9} m^2/s through regression analysis. The high value implies that the diffusion is fast since the surface of the sorbent is available for the reaction and that the kinetics is the limiting factor. The final apparent diffusion, De_1, is temperature-dependent and described by a linear relationship (for the temperature range of the experiments performed; 360 – 480 °C):

$$De_1 = De_{1,a} \cdot T_0 + De_{1,b} = 3.342 \cdot 10^{-13} \cdot T_0 - 2.059 \cdot 10^{-10} \quad (5.12)$$

where T_0 is the temperature in K, and the units of De_1 are m^2/s. k_{carb} in eq. (5.7) is temperature-dependent according to the Arrhenius law. The estimated activation energy for the reaction-controlled regime was 72 kJ/mol [354], while the pre-exponential factor was determined to be 1.005×10^2 m/s.

The drop from the initial value of the diffusion coefficient De_0 to the final De_1 occurred at the sorbent conversion of approximately 2 – 10%, which corresponds to the time period when the surface of the sorbent was presumably fully covered with $CaCO_3$. The conversion was below 5% for cases of high sorbent to catalyst ratios (e.g., 20:1). This is most likely because the whole surface of the sorbent was not available for the reaction but blocked by other sorbent particles. The sorbent conversion is also dependent on other characteristics, such as sorbent and catalyst particle size and morphology, packing distribution [361], which cannot be accurately predicted for different reaction/sorption systems. Nevertheless, the estimate of 2 – 10% proved to be in excellent agreement with the experimental results.

The following equation was therefore used for the calculation of the apparent diffusion coefficient, *De*:

$$De = \begin{cases} De_0 + (De_1 - De_0), & X_s < X_{s,max} \\ De_1, & X_s > X_{s,max} \end{cases} \quad (5.13)$$

Sorbent conversion for which the diffusion becomes the limiting factor, $X_{s,max}$, or when the sorbent is presumably fully covered with $CaCO_3$, is calculated as:

$$X_{s,max} = X_{s,a} \cdot T_0 + X_{s,b} = 1.097 \cdot 10^{-3} \cdot T_0 - 6.387 \cdot 10^{-1} \quad (5.14)$$

As the model needs to depict processes on two different time scales: the fast water-gas shift reaction (on the scale of seconds or less) and a slow sorption process (on the scale of 10s – 100s of minutes), a short time step for integration was necessary in order to assure stability of the numerical simulations. Additionally, the pre-exponential factor for the water-gas shift reaction was raised from 0 to the correct value during the first minutes of the simulation to improve the stability of the calculations. It can be argued that perhaps this describes even more accurately the actual operation at the very beginning of the experiments since some time is needed for the catalyst to perform at 100% (initial adsorption of the species and catalyst conditioning). Apart from stability improvement, this assumption did not have a substantial effect on the final solution.

The experimental and modeling results for experiment 15, performed at 420 °C, with a total flow rate of 16 mL/min, STCO of 1.6, catalyst mass of 4.5 g, pressure of 1.5 bar and sorbent to catalyst ratio of 9.3 can be seen in Figure 5.5 (designated also as Case *c* in the subsequent text).

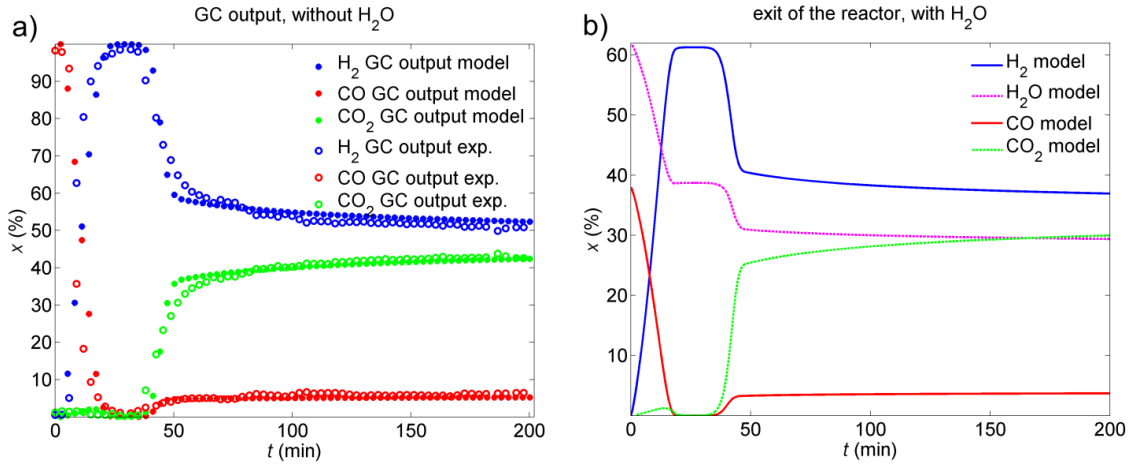

Figure 5.5 – The comparison between the experimental and simulated component compositions for exp. 15; water was condensed before analysis (a). The calculated gas composition with water vapor at the reactor exit (b) [3]

At these conditions, the whole sorbent surface was covered by $CaCO_3$ after 10% conversion. Figure 5.5a shows the gas constitution at the GC output.

Beginning from the eighteenth minute of the start of the experiment, hydrogen reached 100%, and CO content reached 0%, which lasted for 20 minutes. Steady-state was achieved after 200 minutes of operation. At that time, only a small effect of the sorbent can be noticed. The exit molar fractions are almost at the thermodynamic equilibrium. In Figure 5.5b, we can see the calculated time-dependent profiles of the gas composition at the exit of the reactor before the condensing of water. The CO_2 concentration was kept at 0 for almost 40 min, except for a small rise at the very beginning, which is documented in all the experiments and described by the model. When CO was depleted at around 20 min after the reaction started, the concentration of water stayed constant for another 20 min and was decreased again as the CO_2 was no longer reacting with the sorbent in a large extent.

Figure 5.6 presents the modeling results inside the reaction/sorption reactor during the time of the simulation. It can , how CO_2 and H_2O were depleted, and CO_2 and H_2 formed during the reaction.

CO and CO_2 values were kept at their minimum for the whole time of the sorbent-efficient process. Since CO_2 was removed from the reaction mixture, the thermodynamic equilibrium was shifted to the products' side, so more CO and H_2O were converted. Water was in excess, so it stayed at the same concentration when the CO concentration reached zero. As the sorbent conversion reached 10% at around 40 min, the sorbent outer layer was fully converted to $CaCO_3$, and the effective diffusion coefficient dropped to the lowest value of 2.58×10^{-11} m^2/s. This value is temperature-dependent, as was previously mentioned. At that time, the CO_2 diffusion was too slow for CO_2 to reach the unreacted CaO, and its concentration began to rise, while H_2O could continue to react with CO. The final partial pressures are the steady-state partial pressures for the residence time inside the sorption-enhanced reactor. At the end of the experiment, the maximal sorbent conversion almost reached 25%. If the experiments lasted longer, it could be expected that the sorbent conversion would continue to increase. Higher sorbent conversions were achieved with smaller sorbent particles and at higher temperatures [352, 362]. The final sorbent conversions achieved for the experimental range of this work are in accordance with the values found in the literature [352].

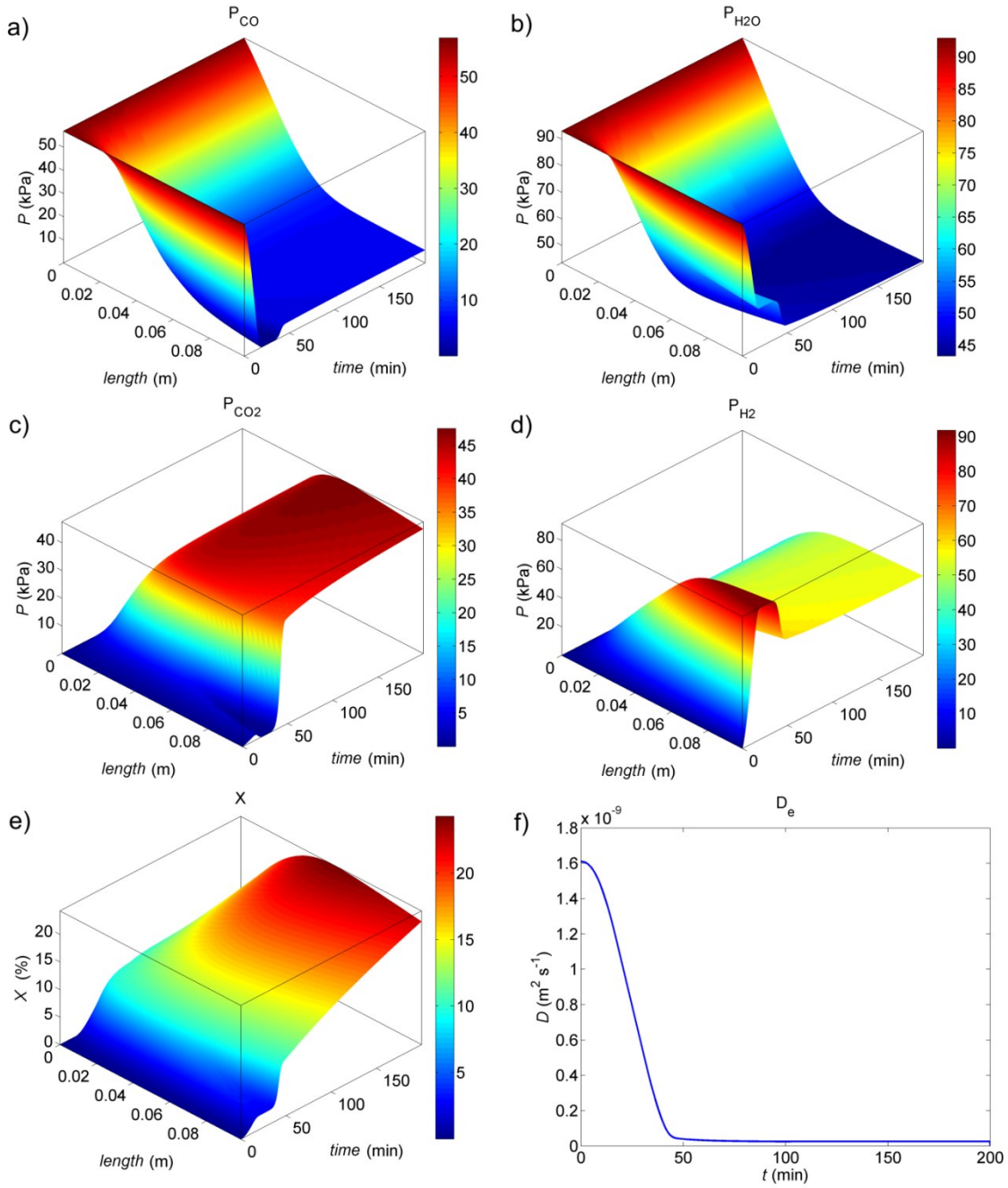

Figure 5.6 – Simulation results for exp. 15: (a-d) partial pressures (in kPa) of all components along the reactor and in time: (a)P_{CO}, (b)P_{H2O}, (c) P_{CO2} and (d) P_{H2}, (e) the sorbent conversion X , and (f) the effective diffusion coefficient of CO_2 [3]

After 200 min of the reaction/sorption time, there was only a small effect of the sorbent (the removal of CO_2 was negligible; green curve), which can be seen in Figure 5.7. The gas composition almost corresponds to the thermodynamic equilibrium, H_2 is above, and CO_2 is below the thermodynamic equilibrium line.

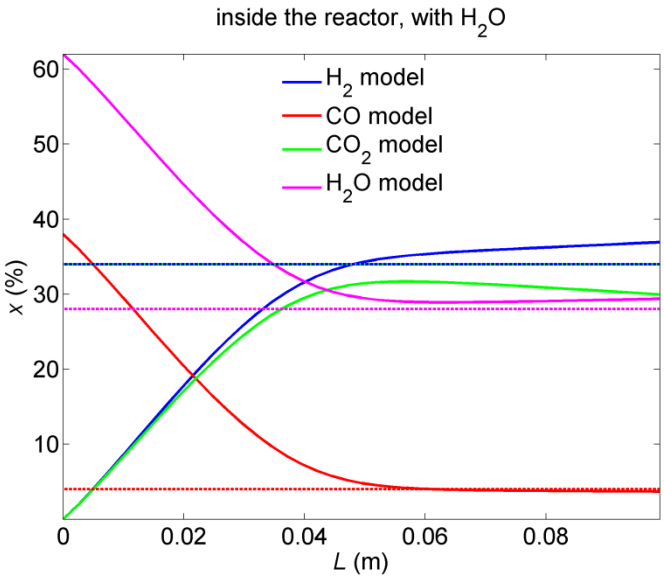

Figure 5.7 – The simulated gas composition after 200 min for exp. 15. The dashed horizontal lines represent the thermodynamic equilibrium. [3]

The results of four chosen experiments, along with the corresponding model simulations, are presented in Figure 5.8. The operational parameters for the chosen cases are presented in Table 5.2, while the operational parameters for all SE-WGS cases can be found in Tables A.3 and A.4 in Appendix A.

Table 5.2 – The operational parameters of four chosen experiments [3]

Case	Exp. №	Temp., °C	Tot. inlet flow rate, mL/min	Inlet STCO ratio	Catalyst mass, mg	Sorbent to catalyst ratio
a	3	480	67	1:1	456.3	10:1
b	11	450	33	1.7:1	479.5	9:1
c	15	420	16	1.6:1	479.6	9:1
d	27	386	8	1.2:1	250.64	20:1

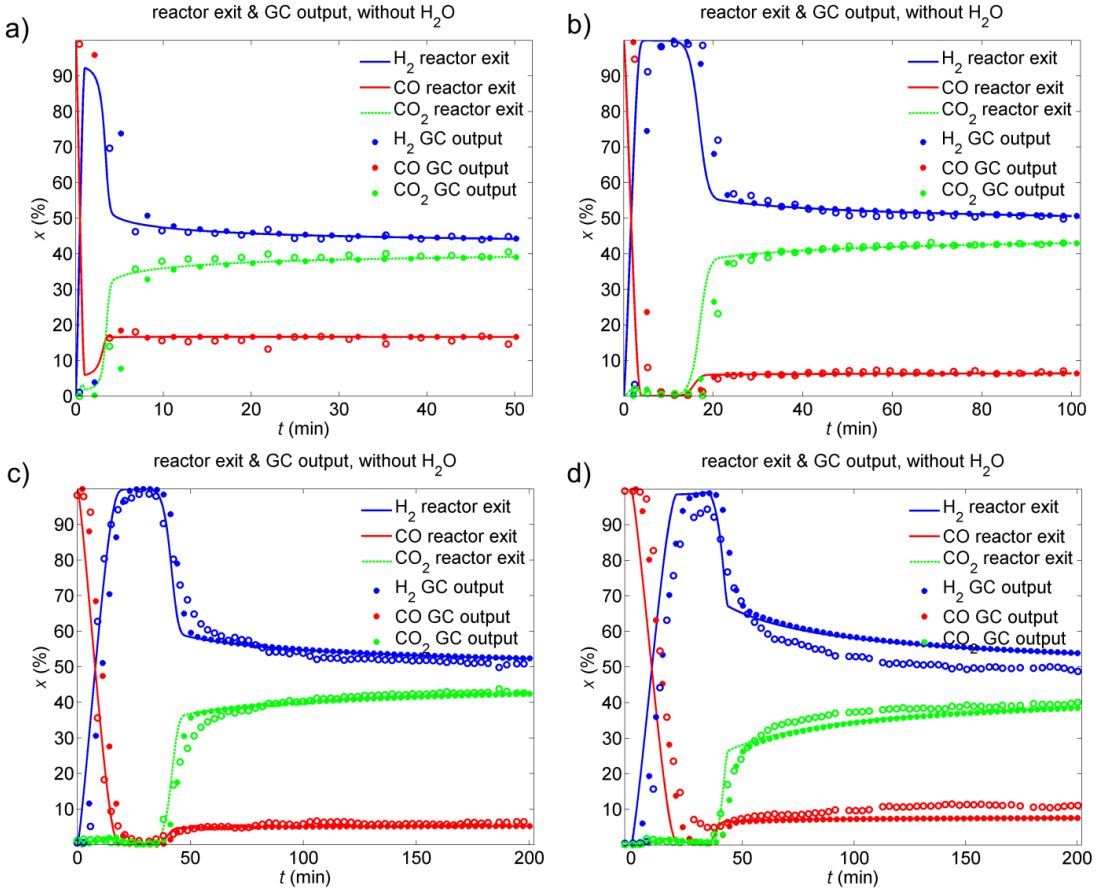

Figure 5.8 – The experimental and simulation results of the gas composition at the reactor outlet for four chosen experiments:

The model exit gas composition: line; the model GC output: full circle;

the experimental GC output: hollow circle. Water is condensed before analysis.

Cases a – d (upper left to lower right) represent Exp. 3, 11, 15 and 27, respectively. [3]

Case *a* (Figure 5.8a, Exp. 3) had a very high flow rate of 67 mL/min, which is why the sorption-enhanced process was not efficient. The sorbent to catalyst ratio was 10, and the outer layers of the sorbent were rapidly converted to $CaCO_3$, after which the reaction reached the equilibrium. The sorption process ended after approximately 3 min. In Figure 5.8b (Exp. 11), the flow rate was half of the one in Case *a*, and the successful sorption process lasted for around 18 min. Case *b* also had a higher STCO, which resulted in a lower CO content, since the equilibrium was shifted towards the products' side. Since the water was condensed at the exit of the sorption-enhanced reactor, a higher STCO is, in this sense, beneficial for the enhanced performance. Cases *c* and *d* were highly successful regarding the reaction enchantment since CO_2 was kept at almost 0% for approximately 40 min. Case *c* (Figure 5.8c, Exp. 10) was run at a higher temperature of 420 °C than Case *d* (Figure 5.8d, Exp. 27), which was run at 386 °C, which means the reaction kinetic processes were faster. This was compensated with the twice as high flow rate in case d (15.5 mL/min) (compared to 7.7 mL/min in Case *d*). For Case *d*, less catalyst and more sorbent were used. A larger amount of catalyst extends the sorbent-efficient period [316]. Since both cases were very successful, the decision on the choice of operation has to be made based on the required capacity, optimization, and overall process economics.

More experimental and simulation results for the experiments at the operational conditions corresponding to Figure 5.7 can be found in Appendix B.

5.4.3 Simulation of the Cyclic SE-WGS Process

The CaO sorption process is irreversible, so the converted sorbent from the packed bed must be replaced with a fresh sorbent in order to retain the process efficiency. The converted sorbent can be discarded or regenerated, depending on the process economics. Sorbent conversion loss with the number of cycles must be considered [363] due to particle textural changes during calcination [346], and sintering/diffusive-carbonation [364]. As shown in Sections 5.3 and 5.4.2, SE–WGS experiments can be divided into three phases. The first phase of the experiment gives the highest concentration of hydrogen (100% mole fraction) as the product CO_2 is efficiently removed from the gas, and the reaction equilibrium is shifted towards the products. If the goal is to achieve the highest hydrogen productivity and purity in the outlet stream, it is advantageous to repeat this phase cyclically, cutting off the slow phase, which is limited by the slow diffusion of CO_2 through the layers of the produced carbonates on the surface of the CO particles [362-364].

Continuous operation can be achieved by switching the flow of the reactants to a fresh catalyst/sorbent reactor bed, in a revolver-type action. The frequency of the revolving depends on the desired outlet hydrogen purity and can be selected to meet specific requirements. To illustrate this, Andrej Pohar, a colleague from the Chemical Institute of Slovenia, performed simulations for Case *c* (Figure 5.8c). In the simulations, it is assumed that fresh sorbent is present in the bed at the time of the revolving. Two simulations are presented: Cyclic simulation 1 with 50 min revolving time and Cyclic simulation 2 with 20 min revolving time.

Figure 5.9 presents the simulation results of the cyclic process. The mean outlet gas composition after the condensation of water vapor for the 50 min revolving time (Figure 5.9b) is 76.27% H_2, 16.75% CO and 6.98% CO_2, while the equilibrium gas composition (without SE–WGS) after water condensation would be 47.22% H_2, 5.57% CO and 47.22% CO_2.

The amount of produced H_2 is increased substantially, and the amount of CO_2 is drastically decreased. The mean outlet composition for the 20 min revolving time (Figure 5.9d) is 59.39% H_2, 39.36% CO, and 1.25% CO_2. In this scenario, CO_2 is kept at a very low level due to the efficient sorption process. The optimal time of one cycle is approximately 40 min for the operating conditions of the case in question. The simulation performed at that time resulted in the mean outlet composition of 78.94% H_2, 19.82% CO, and 1.24% CO_2.

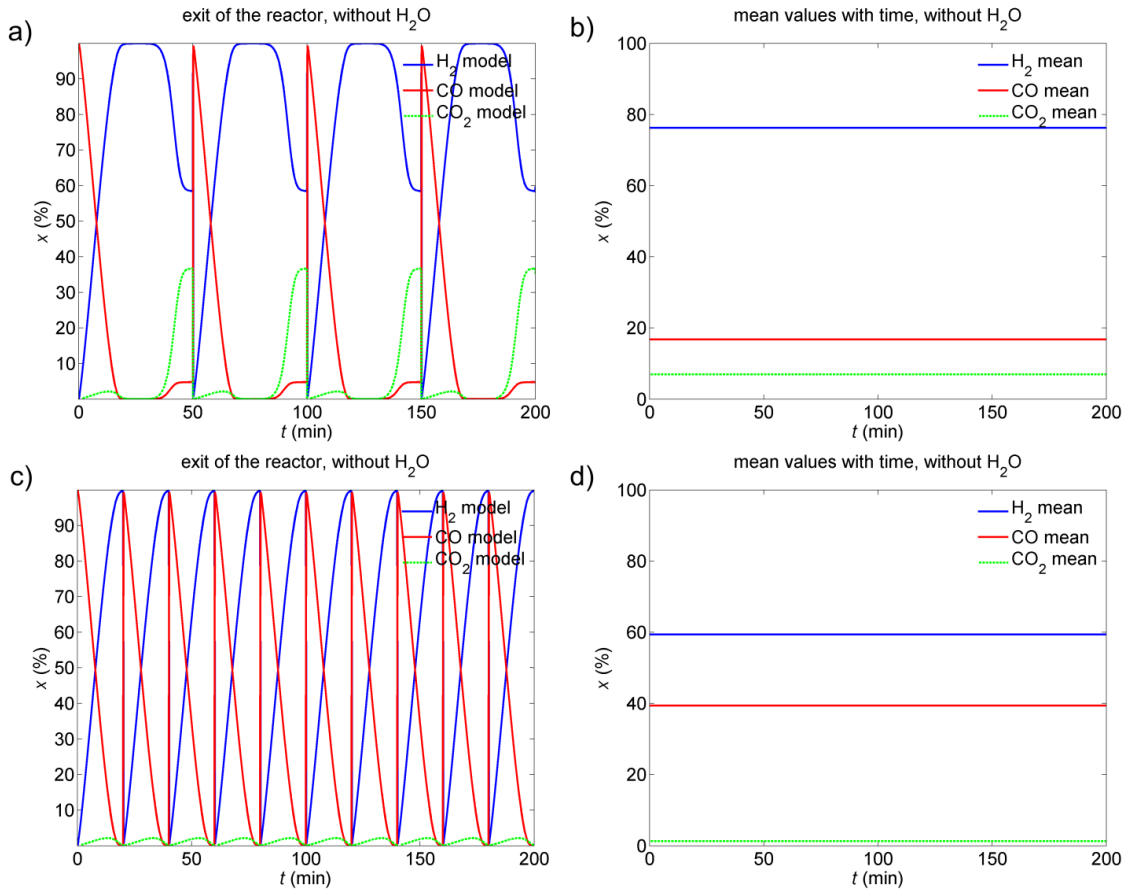

Figure 5.9 – Cyclic simulation 1: a and b; Cyclic simulation 2: c and d. Presented is the gas composition at the exit of the reactor after water condensation for Case c with fresh sorbent replacement every 50 min (a, b) and 20 min (c, d) of SE–WGS operation. [3]

5.5 Conclusions

The water-gas shift reaction can be efficiently enhanced by the removal of CO_2 from the gaseous reaction mixture, as shown by this Experimental Study, published in 2016 [3]. The removal of the product shifts the reaction equilibrium towards the products. Hydrogen production is improved, and the hydrogen molar percentage can reach a value of 100% and stay at that level during the time in which the sorbent is not fully covered with the $CaCO_3$ layer.

Diffusion of CO_2 into the sorbent particles through the formed $CaCO_3$ layer limits the sorbent efficiency. Consequently, there is insufficient CO_2 removal to affect the process before full CaO conversion is achieved. Thus, smaller CaO particles would allow for a longer sorption-enhanced process.

A higher STCO ratio is beneficial since the equilibrium is shifted towards the products, and water can be condensed at the exit of the reactor.

Very accurate dynamic results were obtained on account of the fast Micro GC analysis. The developed shrinking-core model gives valuable insight into the process specifics and allows for the prediction of operation under various process conditions and also provides the basis for further process optimization. The introduction of a sorbent conversion-dependent effective CO_2 diffusion coefficient was imperative for the description of the non-ideal shrinking-core behavior and the replication of the experimental results. This type of process intensification can be of interest for industrial H_2 production.

A revolver-type reactor design was simulated by colleagues from Slovenia for the SE–WGS continuous operation. With the optimized revolver-type system, which would also allow for sorbent regeneration, 100% hydrogen purity could be achieved continuously. However, the sorbent conversion was low (less than 10%) and the time of the sorbent replacement has to be chosen correctly to sustain high hydrogen production. Also, the revolver-type, i.e., cyclic simulations were done for a laboratory scale reactor, used for the experimental investigation of SE-WGS kinetics with low molar capacities. In order to achieve industrial-scale capacities with continuous production of hydrogen by using revolver-type configuration, many operational, control, and storage questions arise. There is also a question of the sorbent regeneration and whether it would be economically viable considering the low levels of sorbent conversion and its properties to lose capture capacity after several regeneration cycles [363]. The configuration would entail several big reactors that would revolve from active to passive duty in short cycles, with passive units being discharged and reloaded with fresh sorbent. Regeneration of sorbent of this scale would be both expensive and ineffective due to the loss of sorbent reactivity [365]. The control of such production would also be questionable and expensive as it is a case of a series of discontinuous processes in a continual fashion.

One of the ways to maintain the continuous production of hydrogen through a water-gas shift by the chemisorption-enhanced process would be to use trickling sorbent particles. In Chapter 6, the ReSyPIO methodology will be applied to such an industrial-scale process by using the experimental research data presented in this Chapter. Additional intensification options, such as membrane separation of hydrogen, will be also be considered.

6. Reactor Synthesis for Hydrogen Production Through Sorption- and Membrane-Enhanced Water-Gas Shift Reaction

In this Chapter, the methodology for reactor synthesis based on process intensification concepts and application of optimization methods (ReSyPIO) will be applied on industrial-scale hydrogen production via sorption-enhanced water-gas shift (WGS) reaction for which the kinetic and diffusion parameters were determined after extensive experimental investigation (Chapter 5). The WGS reaction is widely present in the industry as a cleanup process for the removal of carbon monoxide from reformates [366]. The WGS process is traditionally done in the industry in two types of reactors: a high-temperature shift reactor, HTSR, and a low-temperature shift reactor, LTSR [367]. The process is split into several stages. The first stage is mainly done in the HTSR (320-360 °C and up to 60 bar), favoring faster carbon monoxide conversion. The second and the following stages are done in the LTSR (190-250 °C and up to 40 bar) in order to achieve higher conversions, which are limited by the WGS equilibrium [368].

The thermodynamic limitations of the conventional WGS process can be reduced by removing one or both products, i.e., by shifting the reaction equilibrium, according to Le Chatelier's principle [369]. The principle is already in use in present-day technologies to get higher hydrogen conversion at a lower cost in terms of temperature and pressure needed for the operation, as well as the volume of the reactor itself [370]. One of the materials widely used for removing carbon dioxide is calcium oxide [3, 109-111, 347, 365, 371, 372]. Calcium oxide can be implemented as a sorbent with the Calcium-Looping (CL) technology, or multicyclic carbonation and calcination of the sorbent in gas-solid fluidized bed reactors at high temperatures [347]. However, as reported by Valverde et al., the sorbent carbonation reactivity can be recovered only partially. The sorbent capacity decreases gradually as the number of the CL cycles builds up. This can be solved by introducing an intermediate reactor between the carbonator and the calciner, where the carbonated solids are additionally carbonated at high temperature and high carbon dioxide partial pressure [365].

Wess et al. proposed an integrated process with reforming, WGS, and sorption at operating conditions of 420 °C and 1 bar. The authors concluded that the addition of the sorbent increased the production and purity of hydrogen. The used sorbent can be either sent to the recovery unit, continually regenerated [109] or not recovered at all. Martinez et al. showed that better hydrogen efficiency could be attained when sorption-enhanced reactors are designed for atmospheric pressure operations, rather than for pressurized (3 bar) conditions. This is due to lower investment and operating costs [372].

The WGS reaction also can be enhanced by selective removal of hydrogen from the reaction phase, mostly by membrane reactors [136-138, 159, 367, 368, 371, 373]. Dense metal membranes (palladium-based alloys, i.e., Pd-Ag) are usually used for high purity hydrogen-permeate streams [136]. Theoretically, Pd membranes have infinite selectivity towards hydrogen over other species. Most of the experiments for membrane reactors have been done on atmospheric reaction pressure and in the range of 0.4 to 3 bar [368]. Although higher pressures theoretically lead to higher separation fluxes (e.g., Sieverts' law) and therefore better hydrogen separation, they also result in better permeation of the reactants through the membrane. As reported by Mendes et al., at pressures higher than 4 bar, removal of the reactants occurs, which has a detrimental effect on the carbon monoxide conversion [368].

It this Chapter, a reactor structure for continuous hydrogen production via WGS at atmospheric conditions is proposed. This novel structure can include both trickling calcium-oxide sorbent for carbon dioxide removal and membrane for hydrogen separation. To date, there are several articles published where combined CO_2 sorption and H_2 membrane separation in the WGS process are considered [31, 80, 341]. This is the first time that all these phenomena are analyzed and optimized systematically and simultaneously to derive a reactor concept that could be used for WGS.

Moreover, the concept of trickling solids [108] applied to WGS is relatively new and could be favorable in terms of fixed and operational costs when compared to the sorbent fixed-bed concept.

The presence or absence of these two enhanced processes, as well as reactor structure and operating variables, are determined by applying the ReSyPIO methodology presented in Chapter 3 and demonstrated on a general reaction case in Chapter 4. This feasibility study for the new reactor concept design uses experimental data and kinetics obtained for sorption-enhanced WGS on atmospheric pressures, conducted for this work, published by Živković et al. [3] and presented in Chapter 5, and data for a Pd-Ag membrane separation published by Mendes et al. [135]. The reactor structure and operating variables are obtained by using rigorous multi-objective optimization.

The following Sections of this Chapter are part of an article that was submitted for publication in 2019 [4].

6.1 Phenomena Screening

The WGS reaction kinetics, carbon dioxide chemisorption on calcium oxide (SOR) and the Pd-based membrane separation of hydrogen (MEM) are first screened to capture the thermodynamic and kinetic limitations in the operating range for the used catalyst. The analysis is done for the atmospheric pressure since the experimental data for sorption-enhanced WGS were obtained at that pressure, and it is presumed that the Pd-based membrane is ideal, with infinite selectivity towards hydrogen. The kinetic, diffusion, and thermodynamic data for the analyzed phenomena are given in Tables 6.1–6.3.

Table 6.1 – Parameters for the WGS phenomena

Parameter	Description	Value / Units	Present in Equation
a	kinetic exponent	0.38 /	Eq. 5.3, page 112 Eq. 6.10, page 150
b	kinetic exponent	-0.10 /	Eq. 5.3, page 112 Eq. 6.10, page 150
c	kinetic exponent	0.082 /	Eq. 5.3, page 112 Eq. 6.10, page 150
d	kinetic exponent	0.082 /	Eq. 5.3, page 112 Eq. 6.10, page 150
Aa_{wgs}	pre-exponential factor	1.11 mol $kPa^{-0.444}$ $gcat^{-1}$ s^{-1}	Eq. 5.5, page 112 Eq. 6.10, page 150
Ea_{wgs}	energy of activation	$6.21 \cdot 10^4$ J mol^{-1}	Eq. 5.5, page 112 Eq. 6.10, page 150
ΔH_{wgs}	reaction enthalpy	-41.2 kJ mol^{-1}	Eq. 6.15, page 151

Table 6.2 – Parameters for the SOR phenomena

Parameter	Description	Value / Units	Present in Equation
De_0	initial apparent diffusion coefficient	$1.65 \cdot 10^{-9}$ $m^2\ s^{-1}$	Eq. 5.13, page 119 Eq. C.1, page 229
$De_{1,a}$	final apparent diffusion coefficient	$3.34 \cdot 10^{-13}$ $m^2\ K^{-1}\ s^{-1}$	Eq. 5.12, page 118 Eq. C.2, page 229
$De_{1,b}$	final apparent diffusion coefficient	$-1.15 \cdot 10^{-10}$ $m^2\ s^{-1}$	Eq. 5.12, page 118 Eq. C.2, page 229
$X_{s,a}$	sor. conv. coeff. for diffusion limited stage	$1.10 \cdot 10^{-3}$ /	Eq. 5.14, page 119 Eq. C.4, page 229
$X_{s,b}$	sor. conv. coeff. for diffusion limited stage	$-6.39 \cdot 10^{-1}$ /	Eq. 5.14, page 119 Eq. C.4, page 229
Aa_{car}	pre-exponential factor	100.5 $m\ s^{-1}$	Eq. C.6, page 229
Ea_{car}	energy of activation	$7.20 \cdot 10^4$ $J\ mol^{-1}$	Eq. C.6, page 229
ΔH_{car}	reaction enthalpy	-178.1 $kJ\ mol^{-1}$	Eq. 6.16 page 151

Table 6.3 – Parameters for the MEM phenomena

Parameter	Description	Value / Units	Present in Equation
Aa_{mem}	pre-exponential factor	$5.4 \cdot 10^{-8}$ $mol\ m\ m^{-2}\ s^{-1}\ Pa^{-0.5}$	Eq. 8 [135] Eq. 6.14, page 151
Ea_{mem}	energy of activation	$1.07 \cdot 10^4$ $J\ mol^{-1}$	Eq. 8 [135] Eq. 6.14, page 151
δ	membrane thickness	50 µm	Eq. 8 [135] Eq. 6.13 page 151

The gathered data for the WGS (Table 6.1), SOR (Table 6.2), and MEM (Table 6.3) phenomena will be used in the next three Subsections to analyze the potential for intensifying the water-gas shift process at the atmospheric pressure.

6.1.1 Water-Gas Shift Reaction (WGS)

WGS is a reversible reaction. Although it has many elementary steps, the overall reaction can be expressed as [374]:

$$CO + H_2O \rightleftharpoons CO_2 + H_2 \qquad \Delta H^0_{298} = -41.09\ kJ/mol$$

The kinetic analysis, as well as kinetic parameters estimation of the WGS with HiFUEL W210 iron-chromium catalyst, was shown in Subsection 5.3.1. Since WGS is a moderately exothermic reaction, the reactant conversion and production of hydrogen will be thermodynamically favored at low temperatures (Figure 6.1).

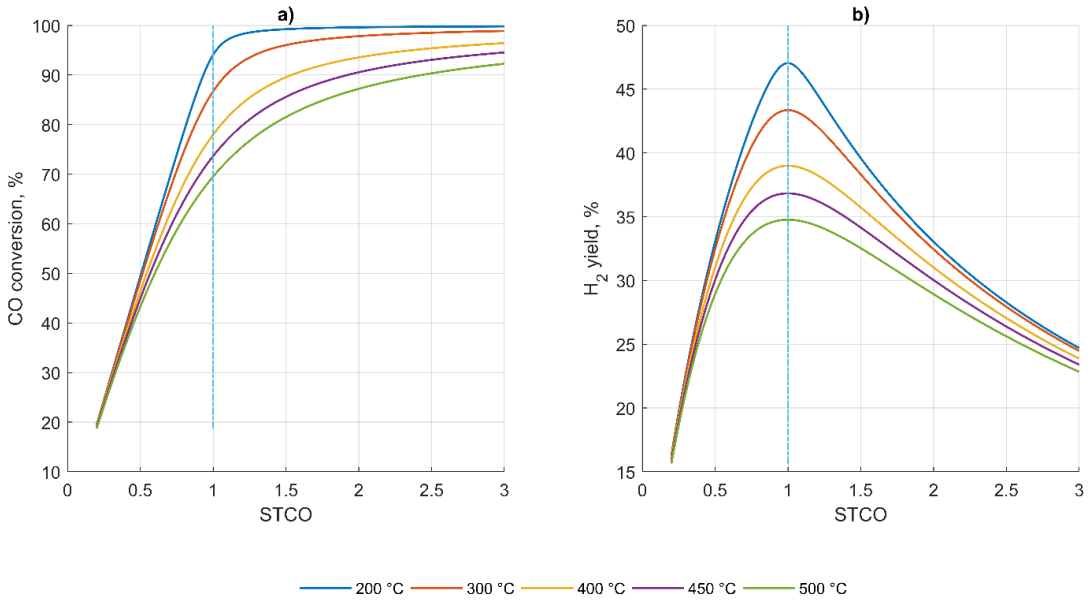

Figure 6.1 – Carbon monoxide equilibrium conversion (a) and hydrogen yield (b) for different steam to carbon monoxide (STCO) inlet ratios and gas temperatures [4]

Figure 6.1 shows that the maximum of the equilibrium hydrogen yield is achieved at the inlet reactant ratio (steam to carbon monoxide, *STCO*) of 1. The magnitude of the maximal yield increases with decreasing temperature. The gradient of the yield decrease is smaller for *STCO* ratios higher than 1 when steam is the predominantly present reactant.

Carbon monoxide conversion displays a similar trend (Figure 6.1a) except for the range of *STCO* ratios higher than 1. The maximal carbon monoxide conversions are achieved when CO is the limiting reactant.

Figure 6.2 shows the maximal WGS reaction rates for different *STCO* ratios and temperatures at 1 atm. As shown, higher temperatures and lower *STCO* ratios lead to significant increases in the reaction rate values. The WGS reaction at 500 °C is almost 80% faster than the reaction at 400 °C for the lowest *STCO* ratio. On the other hand, higher *STCO* ratio leads to slower WGS rate. At 500 °C, the maximal WGS reaction rate drops around 50%, when the *STCO* ratio is increased from 0.2 to 3.

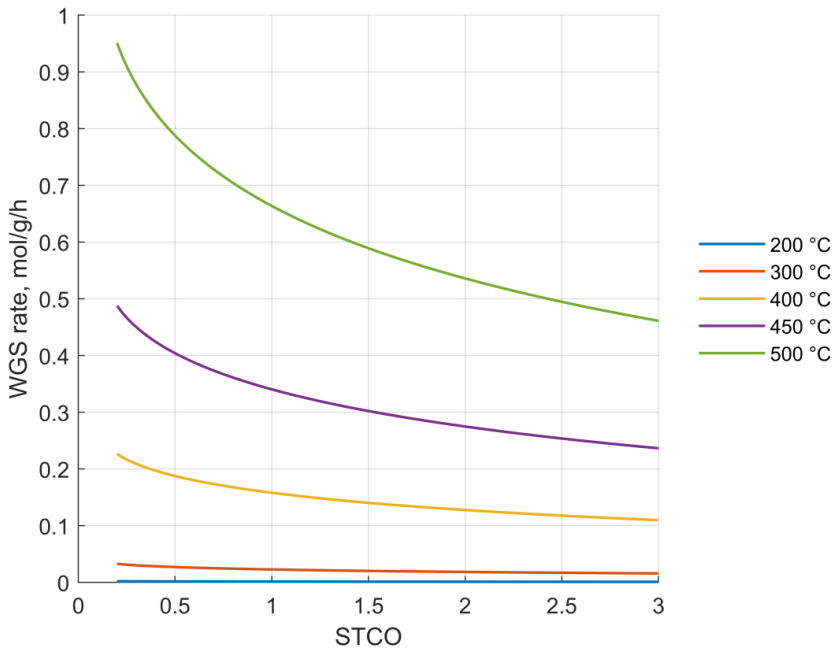

Figure 6.2 – Maximum WGS reaction rate for different steam to carbon monoxide (STCO) inlet ratios and gas temperatures [4]

The displayed reaction rate–*STCO* gradient in Figure 6.2 becomes less pronounced at lower temperatures. At temperatures below 300 °C, the gradient becomes negligible, with the difference in rates for the lowest and highest *STCO* ratio of just a few percentages.

The displayed opposite directions of the thermodynamic and kinetic favorability of hydrogen production were also corroborated by research of WGS done over the past decades [111, 368, 374, 375]. These different effects are the main reason for the enhancement of the reaction rate by selective removal of the product at less favorable equilibrium conditions. Also, the higher reaction rate requires lower residence time, and thus, the lower cost associated with the reactor volume.

6.1.2 Carbon Dioxide Chemisorption (SOR)

One way to intensify the WGS reaction is by removing carbon dioxide, as the product. In Subsection 5.3.2, kinetic, and diffusion data for sorption-enhanced WGS (SEWGS) with calcium-oxide as the sorbent in a packed bed reactor was provided [3]. It was shown that at temperatures above 350 °C, the hydrogen molar fraction could reach 100% in the outlet stream during a particular time interval. The hydrogen fraction remains 100% as long as the surface of the sorbent particles is not fully covered with the $CaCO_3$ layer [3]. The chemisorption is therefore favored at higher temperatures, and the sorbent needs to be regenerated before reuse. Since the aim is to synthesize a reactor for continuous production of hydrogen, using flowing sorbent particles is an alternative. This way, the need for fewer parallel units is expected, which would significantly reduce the fixed costs [109, 347, 365].

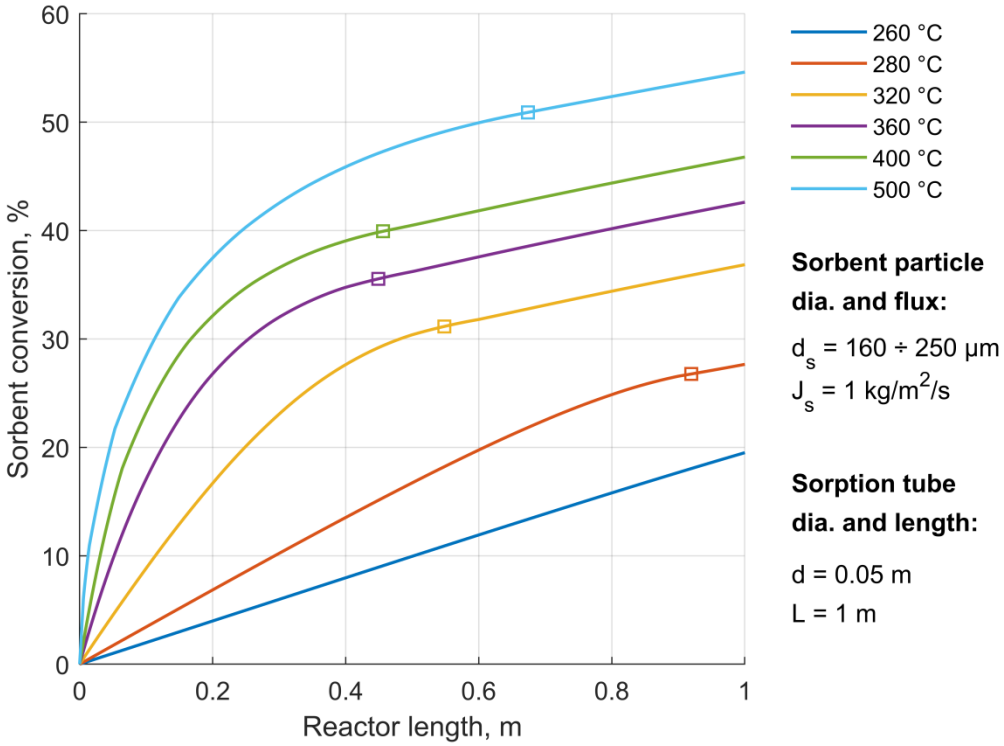

Figure 6.3 – Sorbent conversion for different gas temperatures and respective diffusion limited stages (□) [4]

Figure 6.3 presents the sorbent conversion for different gas temperatures at 1 atm. The details on the sorbent particles that are trickling down the tube with structured support (ε = 0.15) are given in the legend of Figure 6.3. The solids hold-up is calculated by using correlations taken from Nikačević et al. [376, 377]. In Figure 6.3, the squares mark the position at which the sorption goes from the kinetic to the diffusion-limited stage. The diffusion stage starts when the sorbent surface is presumably fully covered with the formed calcium carbonate layer, as shown in Chapter 5. The diffusion-limited stage is characterized by lower (linear form) sorption rates with respect to distance from the reactor inlet. This is in contrast to higher (exponential), kinetically limited stage rate. Figure 6.3 shows how the sorption rate depends on temperature. At temperatures below 280 °C, the chemisorption rate will be lower, and the diffusion-limited stage will not be reached. As the gas temperature increases, the diffusion-limited stage will be reached closer to the reactor inlet. However, this is true just up to 350 °C, when an opposite trend occurs, and the stage limited by diffusion starts farther away in the reactor even though the chemisorption reaction rate is higher. This can be explained by thicker calcium carbonate layers formed at higher temperatures before diffusion becomes the limiting factor.

6.1.3 Hydrogen Removal Through Palladium Membrane (MEM)

The other possibility for reaction enhancement would be a separation of hydrogen via the palladium-silver (Pd-Ag) membrane. The membrane is presumed to be ideal with infinite selectivity towards hydrogen. The kinetic data is taken from Mendes et al. since the authors have conducted an extensive experimental study on enhancing the WGS reaction with Pd-based membrane reactors [135]. The membrane uses a sweep co-current nitrogen inert gas on the permeate side. The analysis is done for atmospheric pressure conditions. In Figure 6.4, the separation flux of hydrogen through the membrane vs. molar fraction of hydrogen is shown. As expected, higher temperatures and hydrogen fractions lead to higher separation rates. The separation flux at 500 °C is over 60% higher than the one at 200 °C, in a hydrogen-rich stream (fraction of hydrogen higher than 0.8).

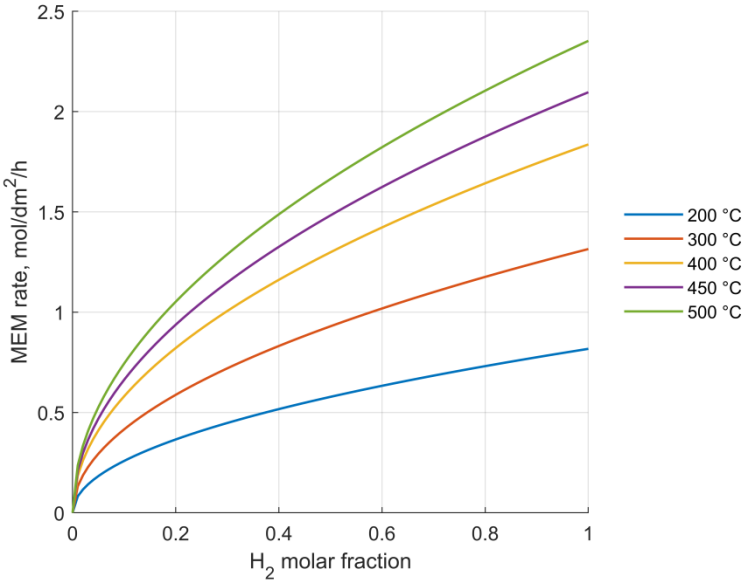

Figure 6.4 – Hydrogen separation flux through Pd-Ag membrane for different retentate molar fractions and gas temperatures [4]

6.1.4 Phenomenological Module Creation

By analyzing the WGS, SOR, and MEM phenomena, the following conclusions are made:

1) The highest hydrogen yield with non-enhanced WGS reaction can be achieved for STCO ratio of 1;
2) The WGS reaction is faster at higher temperatures but with significantly lower hydrogen yields;
3) The SOR and MEM separation are favored at higher temperatures and higher concentrations of carbon dioxide and hydrogen, respectively;
4) Shifting the equilibrium of the WGS reaction by using SOR and MEM separation can lead to increased (above equilibrium) hydrogen conversion at higher temperatures.

In order to create a phenomenological module, the initial layout of phases needs to be determined. In Figure 6.5, an example of an initial phenomenological module is given.

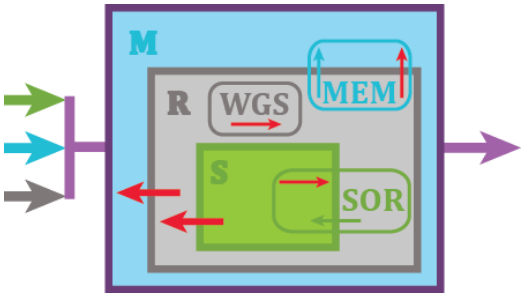

Figure 6.5 – Initial phenomenological module for sorption- and membrane-enhanced water-gas shift reaction

The module shown in Figure 6.5 has two gaseous phases, R or the reaction phase (a gray area) and M or membrane sweep gas phase (blue area). It also has a solid sorbent, the S phase (green area).

Three analyzed phenomena occur in these phases: water-gas shift reaction (WGS) only in the R phase, chemisorption (SOR) in the S phase with a transfer to/from the R phase and membrane separation (MEM) in the M phase and transfer from the R phase.

Since both WGS and SOR are exothermic processes, cooling might be needed for the R phase. All of the defined phases have separate inputs: gray, green, and blue arrow. However, the phenomenological module created in this way leads to optimized scenarios where only the equilibrium WGS values are obtained. This is due to the fact that the WGS reaction has not been intensified. The equilibrium shift is not achieved despite having both hydrogen and carbon monoxide removal because the inert (nitrogen) and hydrogen that make the sweep stream or the M phase, have low heat capacities and cannot cool the R phase in a desirable way. As a result, thermodynamically, smaller carbon monoxide conversions are favored (Figure 6.1a). As stated in Section 6.1.1, for high carbon monoxide conversions, low temperatures are needed, for which the WGS rates are low. This can be solved by adding another phase (W), that will be used for cooling of the R phase (Figure 6.6).

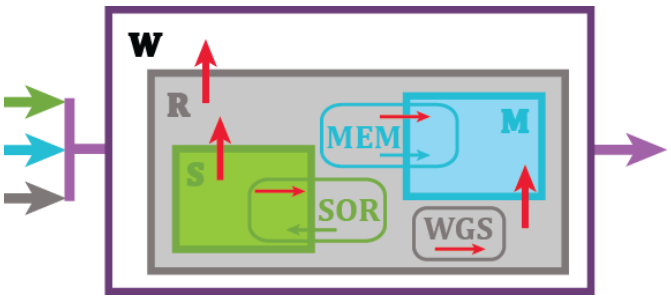

Figure 6.6 – Correctly created phenomenological module for sorption- and membrane-enhanced water-gas shift reaction

Thus, the final module has four phases (W, R, S, and M) with three phenomena in them (WGS, SOR, and MEM). Energy transfer is also present, and in Figure 6.6, it is depicted as a transfer from R to W, S to R, and R to the M phase.

The heat will be generated by the WGS reaction (red arrow inside the WGS phenomena rectangle) and carbonization reaction (red arrow inside the SOR phenomena rectangle).

Mixing of two hydrogen streams, from the R phase through the membrane with the M phase sweep gas, also needs to be accounted in the energy balance (red arrow inside MEM phenomena). The phenomenological module shown in Figure 6.6 will be further split into segments and used for the creation of the reactor superstructure in Subsection 6.2.1.

6.2 Reactor Structure and Mathematical Modeling

6.2.1 Reactor Structure

The reactor superstructure that will be used in the optimization of hydrogen production, which entails all three previously analyzed phenomena (WGS, SOR, and MEM) is shown in Figure 6.7. The reactor consists of a number of phenomenological modules, *Nm* (Figure 6.7a), that may differ in the presence or absence of the phenomena, which will be determined in optimization. The modules that were defined in Section 6.1 (Figure 6.6) are connected in series where the reaction inlet stream into a WGS module, F_R, consists of a fresh supply of the reactants and inert, F_R^{in}, and the outlet stream from the previous module (gray arrows). The proposed structure allows co-feeding of the fresh feed at every stage, i.e., module, with the reactant inlet ratio (*STCO*), flow rate (F_R^{in}), and temperature (T_R) being optimization variables. Each module can also have an independent feed of sorbent (green arrows) with an inlet temperature T_s^{in} which is optimized. The presence or absence of the sorbent feed and therefore SOR phenomena is determined by optimizing the sorbent mass flux, *Js*. In the modules in which membrane separation is present, inert gas sweep streams (blue arrows) are provided.

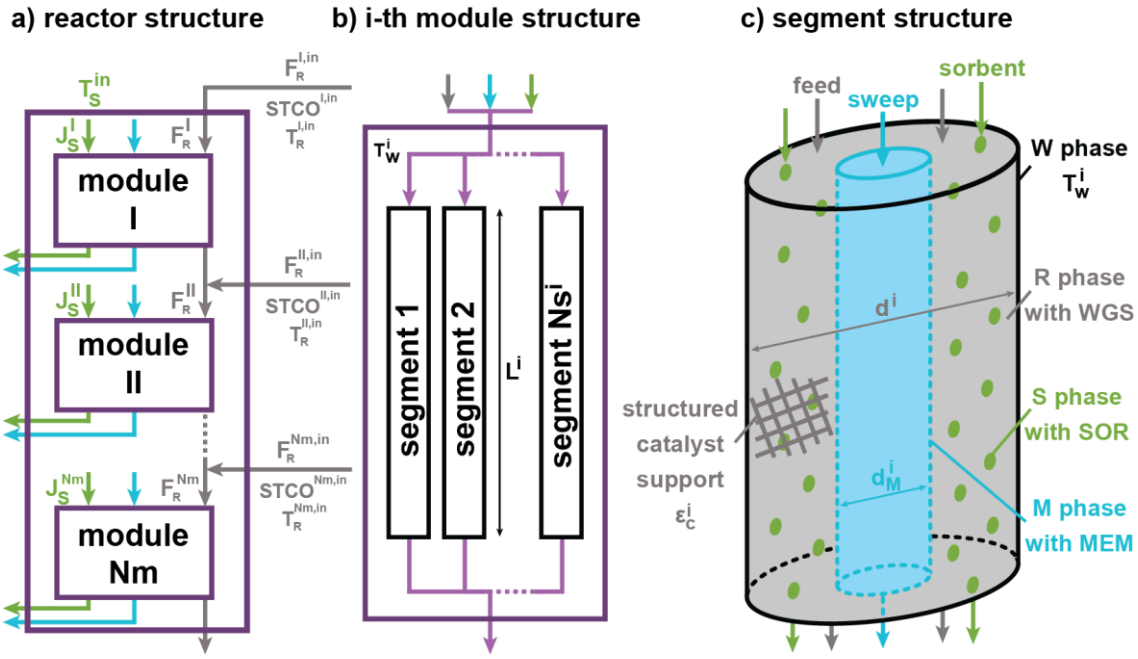

Figure 6.7 – Schematic diagram for the reactor structure (a), i^{th} module structure (b) and module/segment structure (c) [4]

Each module consists of a number of parallel segments, *Ns*, of the same length, *L* (Figure 6.7b). *Ns* and *L* are optimized to get different velocities in the module and the corresponding residence times needed for the WGS, SOR, and MEM phenomena. According to the proposed ReSyPIO methodology, if the optimization results with a solution in which all modules contain the same phenomena, then the modules are considered to be segments of a single module, connected both in series and in parallel.

Each segment is split into four different phases (Figure 6.7c). It has the same layout as the phenomenological module defined in Figure 6.6, Subsection 6.1.4. The structure of the module/segment is set in such a way to decouple the heating/cooling processes from the MEM phenomena, as explained above. This allows for potential scenarios in which the presence of only WGS reaction will be optimal or the WGS in combination with the SOR and MEM phenomena. In general, the modules can have one solid and three gaseous phases, or less, depending on the results of the optimization.

As stated in Subsection 6.1.4, the first gaseous phase is shown with a gray area in Figure 6.6 and 6.7c. It is the reaction (shortly R) phase where WGS proceeds due to catalyst coating on the structured support. The presence or complete absence of the WGS reaction is controlled by optimizing the amount of catalyst in each module, represented by its volumetric fraction, ε_c. The second gaseous phase is the sweeping nitrogen and permeated hydrogen stream. It is shortly called the M phase and placed inside the R phase (blue tube area in Figure 6.7c). The outer wall of the inner tube (the M phase) is made of Pd-Ag membrane. Its diameter, d_M, is optimized to allow the absence or presence of MEM separation.

The heat exchange medium, which is assumed to be pressurized steam, is placed on the outside of the R phase for necessary cooling or heating for the WGS and SOR processes. It is the third gaseous phase that surrounds the outer wall (W), shown in black color in Figure 6.7c. The diameter of the outer wall, d, is optimized for each module. The temperature of the wall, T_w, is constant and optimized for each module.

Apart from the three gaseous phases, a module/segment can also contain a solid phase (green circles in Figure 6.7c). It is the sorption (S) phase consisting of calcium oxide particles on which the chemisorption takes place. Since the chemisorption requires carbon dioxide from the R phase, the sorbent particles are trickling down the tube with structured catalyst support (i.e., Kerapak or similar). The phases, which are all flowing in a co-current direction, are referred to as R, M, W, and S in all equations and figures.

6.2.2 Mathematical Model

The experiments and simulations done while determining kinetic parameters of the WGS reaction [3], showed an insignificant pressure drop through the bed, which is why the pressure is assumed to be constant in the current model. The kinetics of the sorption-enhanced WGS reaction that was determined at high convection conditions is also applied here. Thus, all external mass and heat transfer limitations are considered to be negligible. It is assumed that the structured support is coated with a thin layer of catalyst so that all mass transfer resistances in the pores can be neglected. Furthermore, the support, which occupies 15% of the reaction volume, is made of aluminum with high thermal conductivity. This is the reason why heat transfer resistances in the support are neglected. The sorbent particles are of the same size (160–250 μm) as in the experimental measurements (Chapter 5) when it was assumed that mass transfer resistance in the particles and through the gas film could be neglected [3]. The inner wall of the segment is made of a 50 μm thick Pd-Ag membrane assuring insignificant heat conduction resistances across the membrane. The heat exchange medium is pressurized saturated steam, so it is assumed that its temperature is constant along the reactor segment. Since all reactions occur at low pressure (1 atm) and high temperatures (250–500 °C), the gases are considered to be ideal.

The following assumptions are defined for the reactor mathematical model:

1) The reaction is occurring at atmospheric pressure;
2) The mass and heat transfer resistances in the sorbent particles and through the gas film surrounding sorbent particles are negligible;
3) The fresh sorbent is supplied at the inlet of each module;
4) The maximal separation driving force across the membrane is considered (the partial pressure of hydrogen in the permeate is equal to zero);
5) The pressure drop in the reactor is negligible;

6) The mass and heat transfer resistances around the structured support and in its pores can be neglected;
7) The heat conduction resistance across the membrane is negligible;
8) The temperature of the segment wall does not change along the segment length and is equal to the temperature of heat exchange medium, T_w (can vary between different segments, in accordance with the optimization results);
9) All gases are considered to have ideal behavior and follow the ideal gas law;
10) The plug flow pattern of all flowing phases is assumed (co-current flow).

One segment, which will have the same layout as its module (Figure 6.6), is displayed in more details in Figure 6.8.

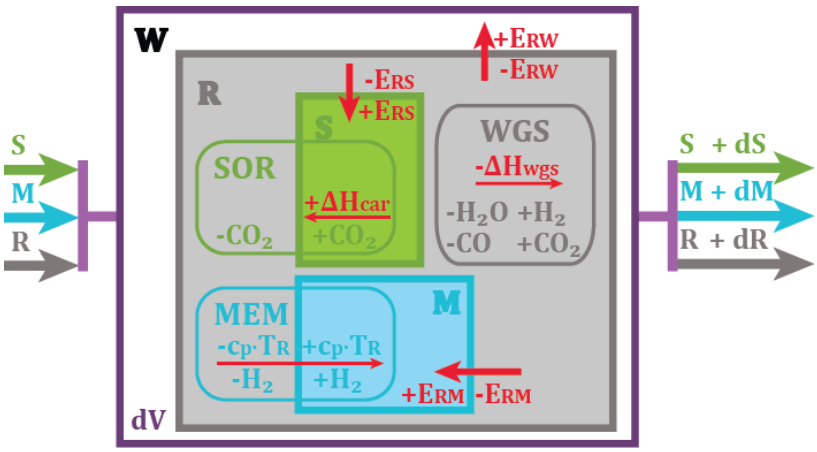

Figure 6.8 – Graphical representation of one segment for module i with the material and energy flows

A reactor segment of module *i*, displayed in Figure 6.8, is mathematically represented by the following set of equations:

a) Component material balances for the R phase:

$$\frac{dF^i_{CO,R}}{dV^i} = -\phi^i_{WGS} \tag{6.1}$$

$$\frac{dF^i_{H_2O,R}}{dV^i} = -\phi^i_{WGS} \tag{6.2}$$

$$\frac{dF_{CO_2,R}^i}{dV^i} = \phi_{WGS}^i - \phi_{SOR}^i \tag{6.3}$$

$$\frac{dF_{H_2,R}^i}{dV^i} = \phi_{WGS}^i - \phi_{MEM}^i \tag{6.4}$$

$$\frac{dF_{N_2,R}^i}{dV^i} = 0 \tag{6.5}$$

$$F_R^i = \sum_{n=1}^{5} F_n^i \tag{6.6}$$

where ϕ_{WGS}^i, ϕ_{SOR}^i and ϕ_{MEM}^i are the corresponding rates for the WGS, SOR and MEM phenomena, respectively:

$$\phi_{WGS}^i = \rho_c \cdot r_{wgs}^i \cdot \frac{dV_c^i}{dV^i} \tag{6.7}$$

$$\phi_{SOR}^i = \frac{\rho_s}{M_s} \cdot \frac{d\dot{V}_s^i}{dV^i} \tag{6.8}$$

$$\phi_{MEM}^i = J_M^i \cdot \frac{dA_m^i}{dV^i} \tag{6.9}$$

The WGS reaction rate, r_{wgs}^i, is defined with the following equations [3]:

$$r_{wgs}^i = Aa_{wgs} \cdot e^{-Ea_{wgs}/R/T_R^i} \cdot {p_{CO}^i}^{0.385} \cdot {p_{H_2O}^i}^{-0.104} \cdot {p_{CO_2}^i}^{0.082} \cdot {p_{H_2}^i}^{0.082} \cdot \left(1 - \beta^i\right) \tag{6.10}$$

$$\beta^i = \frac{1}{K_{eqb}^i} \cdot \frac{p_{CO_2}^i \cdot p_{H_2}^i}{p_{CO}^i \cdot p_{H_2O}^i} \tag{6.11}$$

b) Material balance equation for the S phase, shrinking core model [3]:

$$\frac{dr_s^i}{dV^i} = -\frac{c_{CO_2}^i}{\pi \cdot {r_r^i}^2} \cdot \frac{M_s^i}{\rho_s^i} \cdot \frac{1}{u_s^i} \cdot \frac{1}{\frac{\left(r_{CaO} - r_s^i\right) \cdot r_s^i}{r_{CaO} \cdot De^i} + \frac{1}{k_{car}^i}} \tag{6.12}$$

c) Material balance equations for the M phase (Sieverts' law) [135]:

$$J_M^i = \frac{k_{mem}^i}{\delta}\left({p_{H_2}^i}^n - {p_{H_2,M}^i}^n\right) \tag{6.13}$$

$$k_{mem}^i = Aa_{mem} \cdot e^{-Ea_{mem}/R/T_R^i} \tag{6.14}$$

where $n = 0.5$ (ideal membrane with infinite selectivity towards hydrogen) and ${p_{H_2,M}^i}^n \approx 0$ (maximum driving force).

d) Energy balance equations for the R, S, and M phases:

$$\frac{d\dot{H}_R^i}{dV^i} = -\phi_{WGS}^i \cdot \Delta H_{wgs} - \phi_{MEM}^i \cdot c_{p,H_2}^i \cdot T_R^i - \mathrm{E}_{RW}^i - \mathrm{E}_{RS}^i - \mathrm{E}_{RM}^i \tag{6.15}$$

$$\frac{d\dot{H}_S^i}{dV^i} = \phi_{SOR}^i \cdot \Delta H_{car} + \mathrm{E}_{RS}^i \tag{6.16}$$

$$\frac{d\dot{H}_M^i}{dV^i} = \phi_{MEM}^i \cdot c_{p,H_2}^i \cdot T_R^i + \mathrm{E}_{RM}^i \tag{6.17}$$

where $\dot{H}_R^i$, $\dot{H}_S^i$ and $\dot{H}_M^i$ are the enthalpy rates for phases R, S, and M, respectively:

$$\dot{H}_R^i = F_R^i \cdot c_{p,R}^i \cdot T_R^i \tag{6.18}$$

$$\dot{H}_S^i = J_S^i \cdot A_h^i \cdot \frac{c_{p,S}^i}{M_S^i} \cdot T_S^i \tag{6.19}$$

$$\dot{H}_M^i = F_M^i \cdot c_{p,M}^i \cdot T_M^i \tag{6.20}$$

and E_{RW}^i, E_{RS}^i and E_{RM}^i are the corresponding heat transfer rates between the adjacent phases R and W, R and S, and R and M:

$$\mathrm{E}_{RW}^i = U_{RW}^i \cdot \left(T_R^i - T_W^i\right) \cdot \frac{dA_R^i}{dV^i} \tag{6.21}$$

$$\mathrm{E}_{RS}^{i} = U_{RS}^{i} \cdot \left(T_{R}^{i} - T_{S}^{i}\right) \cdot \frac{dA_{S}^{i}}{dV^{i}} \tag{6.22}$$

$$\mathrm{E}_{RM}^{i} = U_{RM}^{i} \cdot \left(T_{R}^{i} - T_{M}^{i}\right) \cdot \frac{dA_{M}^{i}}{dV^{i}} \tag{6.23}$$

The additional differential equations are defined as:

$$\frac{dV_{c}^{i}}{dV^{i}} = \varepsilon_{c}^{i} \tag{6.24}$$

$$\frac{dA_{R}^{i}}{dV^{i}} = \frac{2}{r_{R}^{i}} \tag{6.25}$$

$$\frac{dA_{M}^{i}}{dV^{i}} = \varepsilon_{M}^{i} \cdot \frac{2}{r_{M}^{i}} \tag{6.26}$$

$$\frac{du_{S}^{i}}{dV^{i}} = -\frac{J_{S}^{i} \cdot A_{h}^{i}}{\varepsilon_{S}^{i} \cdot {\rho_{S}^{i}}^{2} \cdot A_{R}^{i}} \cdot \frac{d\rho_{S}^{i}}{dV^{i}} \tag{6.27}$$

$$\frac{d\rho_{S}^{i}}{dV^{i}} = \left(\rho_{CaCo_{3}} - \rho_{CaO}\right) \cdot \frac{dX_{s}^{i}}{dV^{i}} \tag{6.28}$$

$$\frac{dX_{s}^{i}}{dV^{i}} = -3 \cdot \frac{{r_{CaO}^{i}}^{2}}{{R_{CaO}}^{3}} \cdot \frac{dr_{CaO}^{i}}{dV^{i}} \tag{6.29}$$

$$\frac{d\dot{V}_{S}^{i}}{dV^{i}} = A_{R}^{i} \cdot \frac{d\left(u_{S}^{i} \cdot X_{s}^{i} \cdot \varepsilon_{S}^{i}\right)}{dV^{i}} \tag{6.30}$$

All additional model equations and correlations are given in Appendix D, while the values of the corresponding parameters are given in Appendix E.

6.2.3 Model Validation

The overall model comprises the WGS reaction, CO_2 chemisorption on CaO sorbent particles, and H_2 removal through the Pd-Ag membrane. All phenomena present in the model were validated separately with experimental data from our research [3] and Mendes et al. [135]. The agreement can be seen in Figure 6.9 (a – WGS; b – sorption-enhanced WGS; c, d – membrane separation). Sorption-enhanced WGS validation was performed with a stationary sorbent bed.

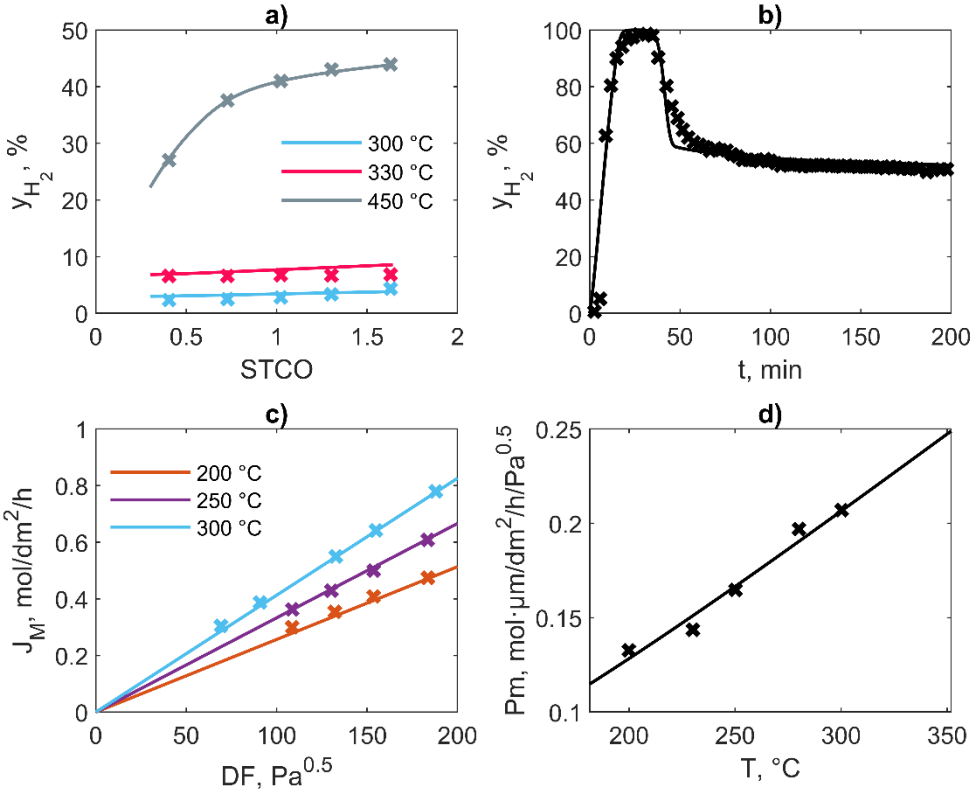

Figure 6.9 – Agreement between the model (line) and experimental data (x) for WGS (a), sorption-enhanced WGS (b) and membrane separation (c and d) [4]

6.3 Optimization

6.3.1 Objective Functions

The goal of the applied ReSyPIO methodology is to optimize and analyze which reactor structure, operational parameters, and presence of which phenomena (WGS, SOR, and MEM) give the highest possible hydrogen yield at the lowest reactor cost indicators. Since this is a feasibility study with no specific economic objective function, different physical variables related to the WGS, SOR, and MEM costs are quantified. The variables representing the main reactor costs are the amount of catalyst used (Fe-Cr mass, the main WGS cost), inlet sorbent flow rate (CaO mass flux, the main SOR cost), total membrane surface (Pd-Ag area, the main MEM cost) and the reactor volume (the main reactor cost). These variables cannot be summed up without corresponding economic data (i.e., prices) and can only be viewed separately related to the hydrogen yield.

In order to define a single objective function that combines all before-mentioned costs for the WGS, SOR and MEM processes, the main cost indicators are expressed as the fractions of the respective volumes in the reactor segment volume, V^i. As explained in Section 6.2.1, the reactor segment (Figure 6.7c) consists of three phases R, S, and M, where the WGS, SOR, and MEM processes occur. Each of these processes and their respective phases require a certain fraction of the module/segment volume. The catalyst mass, which is related to the catalyst volume, is directly proportional to the volumetric fraction of the catalyst in the segment, ε_c (Eq. 6.24). The total membrane area, shown in Eq. 6.26, is proportional to the volumetric fraction of the M phase (inner tube) in the segment volume, ε_M. The SOR main costs are related to the sorbent flow rate and are also directly proportional to the sorbent hold-up, i.e., the volumetric fraction of the sorbent (S phase) in the segment volume, ε_S (Eq. 6.30).

Therefore, the total reactor volume and the sum of the volumetric fractions for the catalyst, sorbent, and membrane can be used to represent the costs for all three analyzed phenomena (WGS, SOR, and MEM). The single objective function relating the desired yield and the costs, that is to be maximized, could be defined as:

$$OF = \frac{Y_{H_2}}{\sum_{i=1}^{Nm}\left[\left(\varepsilon_c^i + \varepsilon_M^i + \varepsilon_S^i\right) \cdot V_{seg}^i\right]} = \frac{Y_{H_2}}{\sum_{i=1}^{Nm}\left(V_c^i + V_m^i + V_s^i\right)} \tag{6.31}$$

The objective function defined with Eq. 6.31 can mathematically lead to scenarios with minimal volumes for the catalyst, sorbent, and membrane (close to zero), for which the limit of *OF* would be infinite, irrespective of the value of the yield (not equal to zero). Also, in cases where both the yield and the costs approach zero, the limit of Eq. 6.31 would be mathematically undefined. To circumvent this problem, two objective functions are used for the optimization instead of one. These objective functions are called Benefit and Cost functions:

$$Benefit = Y_{H_2} \tag{6.32}$$

$$Cost = \sum_{i=1}^{Nm}\left(V_c^i + V_m^i + V_s^i\right) \tag{6.33}$$

The goal is to achieve the highest possible yield (maximum of *Benefit*, defined by Eq. 6.32) at the lowest expense of the catalyst, sorbent, and membrane (minimum of *Cost*, defined by Eq. 6.33). In order to get sets of optimal results irrespective of the scale of the problem, multi-objective optimization (MO) is used to solve the problem [108, 325-327]. MO gives solutions named as Pareto optimal set. Any solution within the set cannot be regarded as a better solution than the others. Also, none of the solutions in the set are worse than other solutions. All solutions of the set are connected by a curve called Pareto optimal front. At any point along this curve, one objective function can be improved at the cost of the other objective function [325]. Applied to this study, higher hydrogen yield (*Benefit*) can be achieved at a higher cost of the volumes (*Cost*), and vice versa, lower cost of the volumes can be used at the expense of the lower attained hydrogen yield.

6.3.2 Optimization Cases, Variables and Constraints

The optimization is performed separately for Cases with a different number of modules, *Nm*, connected in series (Figure 6.7a, Section 6.2.1). The list of optimized Cases and their names are given in Table 6.4. Five intensified Cases with a different number of modules, *Nm*, are optimized. The Base Case or the reactor with only WGS present and no SOR and MEM phenomena is also optimized.

Table 6.4 – Optimization Cases [4]

Case Name	Nm	Possible Phenomena
Base Case	1	WGS
Case 1	1	WGS, SOR, MEM
Case 2	2	WGS, SOR, MEM
Case 3	3	WGS, SOR, MEM
Case 4	4	WGS, SOR, MEM
Case 5	5	WGS, SOR, MEM

The optimized variables for each Case are listed in Table 6.5. The structural and geometric optimization variables are: the number of segments for each module (Ns^i, Figure 6.7b), the segment length (L^i, Figure 6.7b) and diameter (d^i, the outer tube in Figure 6.7c), segment's M phase inner diameter ($d_M{}^i$, the inner tube diameter in Figure 6.7c) and the catalyst fraction of the solid structured support ($\varepsilon_c{}^i$, dark gray grid in Figure 6.7c). The operational optimization variables are: the temperature of the module heat exchange medium or the W phase ($T_w{}^i$, Figure 6.7b and 6.7c), the molar inlet flow rate into each module ($F^{i,\,in}$), the module steam to carbon monoxide inlet ratio ($STCO^{i,in}$), the module sorbent or S phase mass flux ($J_S{}^i$), the module inlet temperature of the R phase ($T_R{}^{i,in}$), the reactor inlet temperature of the sorbent ($T_S{}^{in}$), all shown in Figure 6.7a. The optimized variables and their lower and upper bounds are given in Table 6.5.

Table 6.5 – Pareto optimization variables [4]

Variable	Lower Bound	Upper Bound
Ns^i	100	1e6
L^i, m	0.1	2
d^i, m	0.05	0.5
$d_M{}^i$, m	0	0.5
$\varepsilon_c{}^i$	0	1
$F^{i,in}$, mol/s	0	100
$STCO^{i,in}$	0.1	3
$J_S{}^i$, kg/m^2/s	0	3
$T_R{}^{i,in}$, °C	150	520
$T_S{}^{in}$, °C	150	520
$T_{w,}{}^{i,in}$, °C	150	520

In order to compare Cases with a different number of modules, *Nm*, and the presence or absence of different phenomena, the total inlet flow rate is fixed to 100 mol/s (corresponding to industrial-scale reactor capacity). Parameters that are not optimized are the module inlet inert flow rate (10 mol/s) and the operating pressure (1 atm).

Two optimization constraints are defined:

1) The gas temperature in the R phase cannot surpass the maximally allowed temperature for the operating catalyst, HiFUEL W210 ($T_{max} < 540$ °C); and

2) The outer tube diameter with the R phase must be larger than the inner tube diameter with the M phase (the specified difference is $d\text{-}d_m > 5$ *mm*), to accommodate the WGS (structured Kerapak packing) and SOR phenomena (trickling sorbent particles).

6.3.3 Optimization Algorithms and Criteria

The multi-objective optimizations are performed in Matlab 2018b by using a non-dominated sorting genetic algorithm, also called controlled, elitist genetic algorithm (a variant of NSGA-II). NSGA-II, the criteria of which are listed in Table 6.6, can maintain satisfactory convergence of the non-dominated front and an appropriate spread of the solutions [108].

Table 6.6 – Pareto optimization criteria [4]

NSGA-II Criteria	**Name**	**Value**
Number of variables	Nvars	$9 \cdot Nm + 1$
Population size	Pop	$10 \cdot Nvars$
Max. number of generations	Gen	$200 \cdot Pop$
Max. stall generations	StallGenLimit	50
Pareto tolerance	TolFun	$1 \cdot 10^{-3}$
Parallel computing	UseParallel	true

6.4 Results and Discussion

The Pareto fronts for all optimized Cases (Table 6.4) and Cost values (sum of volumes, Eq. 6.33) up to 10 m^3 are shown in Figure 6.10. The base case, which contains only the WGS reaction, gives the lowest maximum Yield function, up to 46%. Case 1 shows a significant drop in the Cost function (more than 55%, relatively) when compared to the Base Case, for the same Yield. Case 2 shows a further drop in Cost, up to 50% relatively, for hydrogen Yield above 48%, when compared to Case 1. Case 3 shows a smaller improvement compared to Case 2 in Cost (up to 0.5 m^3) while Cases 4–5 do not show any improvements compared to Case 3. The intensified Cases 2–5 can achieve Yield up to the theoretical maximum of 50% (which corresponds to 100% conversion of the limiting reactant), but with high costs (~10m^3). In the following analysis, Cases with four and five modules will not be considered, as they give similar results as Case 3, with fewer modules.

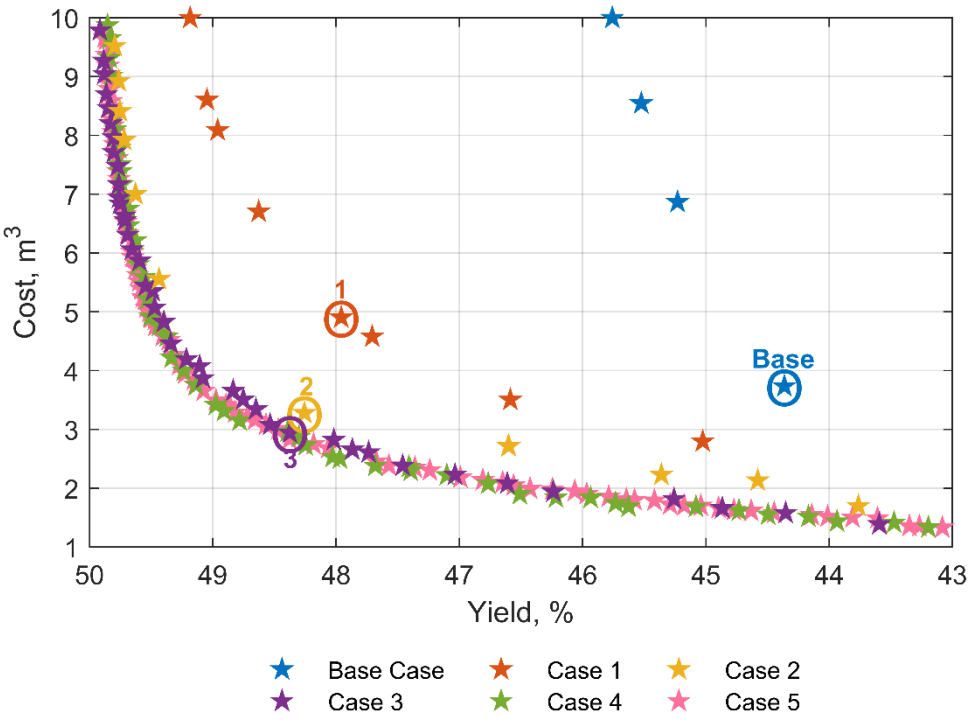

Figure 6.10 – Pareto fronts for the analyzed Cases and chosen solutions [4]

Solutions that are selected for further analysis have Cost below 5 m^3. They are marked in Figure 6.10 with numbers (for Cases 1–3) and word Base (for the Base Case). Solutions with similar Yields or close Pareto points are selected for further analysis, to investigate how the presence of different phenomena (WGS, SOR, and MEM), as well as reactor structure and operating conditions, contribute to the overall decrease in the Cost value and increase in Yield.

Table 6.7 – Pareto optimization results for the Base Case and Cases 1-3 [4]

Case	**Base**	**1**	**2**		**3**		
Module i	**I**	**I**	**I**	**II**	**I**	**II**	**III**
Reactor structure optimization variables							
Ns^i	362	4771	422	2295	429	1539	3230
L^i, m	1.01	0.32	0.24	0.59	0.35	0.61	0.37
d^i, m	0.332	0.127	0.093	0.144	0.115	0.117	0.098
d_M^i, m	/	0.022	0.008	0.012	0.006	0.008	0.003
ε_c^i	0.12	0.14	0.14	0.03	0.12	0.02	0.05
Operating condition optimization variables							
$F^{i,in}$, mol/s	100	100	64.9	35.1	65.8	22.7	11.5
$STCO^i$	0.94	1.00	0.74	1.66	0.80	1.69	1.21
J_s^i,	/	1.20	1.79	1.26	1.86	0.30	2.36
$T_R^{i,in}$, °C	462	483	482	488	482	477	475
T_s^{in}, °C	/	482	482			482	
T_w^i, °C	258	472	472	474	472	473	473
Constraint variables							
$T_{R,max}^i$, °C	492	535	507	488	529	477	479
d^i-d_M^i, m	0.33	0.105	0.084	0.132	0.109	0.110	0.095
Yield and Cost function value							
Y, %	44.36	47.96	48.26		48.37		
Cost, m^3	3.73	4.90	3.28		2.94		
Gas and sorbent mean residence time							
τ^i, s	6.95	4.86	0.17	5.65	0.43	2.45	2.49
τ_s^i, s	/	25.5	30.7	57.7	48.0	77.6	29.1

The values for optimization variables, constraints values, Yield, and Cost are given in Table 6.7. Breakdown of the Cost function is shown in Figure 6.11.

Instead of showing the volumetric fractions of the catalyst, sorbent, and membrane, the main costs indicators for WGS, SOR, and MEM phenomena are analyzed in this breakdown. The main cost indicators are the catalyst mass, sorbent mass flow rate, membrane area, and total reactor volume. They are directly related to the corresponding volumetric fractions, as discussed in Subsection 6.3.1.

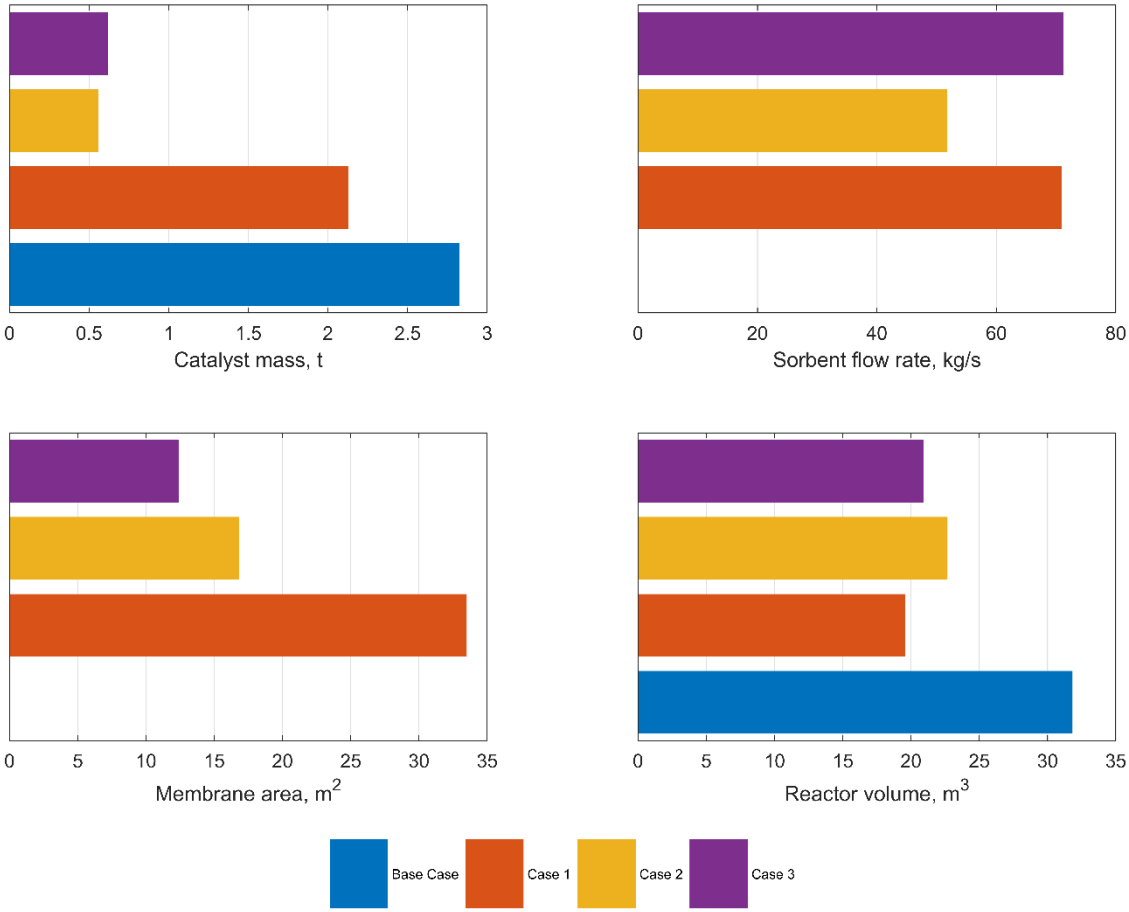

Figure 6.11 – Reactor cost indicators for the Base Case and Cases 1-3: catalyst mass, sorbent flow rate, membrane area and reactor volume [4]

The following statements can be made by comparing the results in Table 6.7 and Figure 6.11:

1) The needed catalyst mass decreases for more than 75% when two or more modules are used (Cases 2 and 3) when compared to the Base Case;
2) The catalyst mass also decreases with the inclusion of the SOR and MEM phenomena (up to 80% for Case 2, when compared to the Base Case);
3) The membrane area decreases with the increase of the number of modules, *Nm*, and is more than 50% smaller for Cases 2 and 3, when compared to Case 1;
4) The intensified Cases 1–3 with SOR and MEM use significantly smaller reactors than the Base Case reactor (relatively 30% smaller);
5) The Base Case reactor achieves lower Yield than the reactors for the intensified Cases 1–3 (relatively around 3.5%);
6) Even though the sorbent total mass flux decreases with the increase of the number of modules, *Nm*, the sorbent consumption, reflected in the total sorbent mass flow rate, seems to be independent on *Nm*.

Further analysis on how the reactor structure, operating conditions, presence of the SOR, and MEM phenomena improves the reactor efficiency will be given in the following Subsections.

6.4.1 Operating Conditions and the Reactor Structure

The temperature profiles in the R phase shown in Figure 6.12 point to two different scenarios in the Base Case and the intensified Cases 1–3.

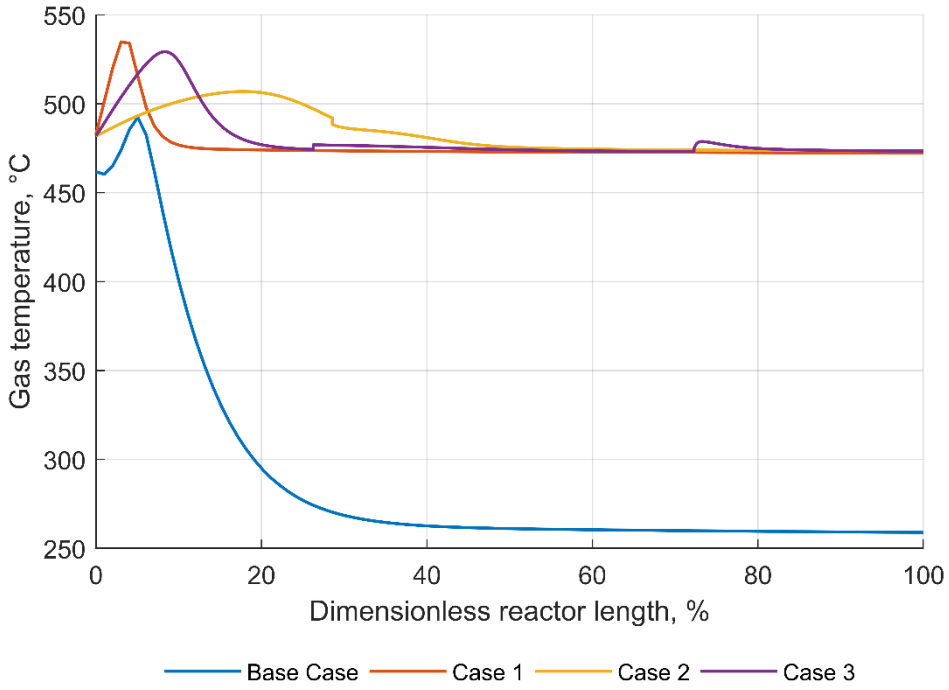

Figure 6.12 – The gas temperature in the R phase for Base Case and Cases 1-3 [4]

The optimized Base Case results with a 20 °C lower inlet gas temperature and more than 200 °C lower coolant temperature than Cases 1–3. The high inlet temperature is needed for the short and fast kinetic WGS reaction stage at the beginning (Figure 6.2, Subsection 6.1.1). However, high temperatures do not favor more hydrogen production (Figure 6.1b) and, since there are no additional enhancing phenomena present in the Base Case, a large reactor and low coolant temperature is needed to cool the R phase for more than 200 °C once the reaction has evolved. As a result, a different operating temperature, larger reactor, and more catalyst are needed when only the WGS reaction (Base Case) is considered. On the other hand, the Base Case coolant temperature also requires considerably less heating energy, since it is 55% lower than the coolant temperatures for the intensified Cases 1–3.

The Base Case result corresponds to the traditional arrangement of the WGS reactors: HTSR as the first reactor favoring CO conversion, and LTSR as the second reactor favoring higher hydrogen yield [367]. When the temperature profiles in Figure 6.12 are compared, the profile corresponding to Case 2 is the most uniform one, with the smallest difference between the maximal and the minimal temperature of the R phase. There are no visible peaks that could cause possible hot spots and potential issues for temperature control [378]. More uniform profiles for the intensified Cases 1–3 when compared to the Base Case can also be explained by the higher temperatures needed for the SOR and MEM phenomena, as discussed in Subsections 6.1.2 and 6.1.3.

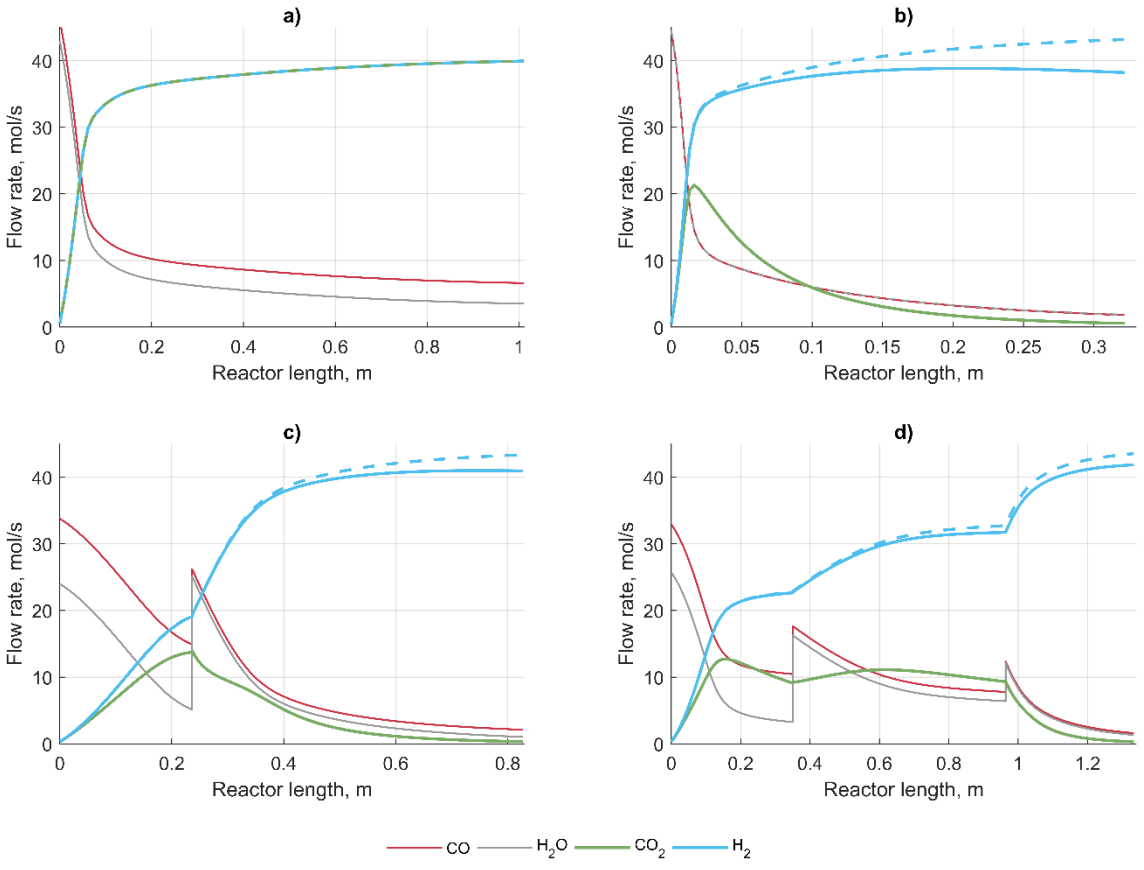

Figure 6.13 – The component molar flow rates (solid lines) in the reaction (R) phase and the total hydrogen flow rate including the flow rate in the inner permeate tube (dashed line) for the Base case (a) and Cases 1–3 (b–d, respectively) [4]

When the component molar flow rates in the R phase (outer tube) are compared (Figure 6.13), two scenarios are visible for the *STCO* inlet ratio. These scenarios depend on the number of modules, *Nm*. The reactor with one module (Base Case and Case 1) has equal molar flow rates of both reactants at the inlet (*STCO=1*, Table 6.7) since this value gives the highest possible hydrogen yield (the maximum in Figure 6.1b). This was confirmed by Jang et al. (2012), who state that hydrogen productivity increases drastically when the *STCO* ratio is around one, as WGS is an equimolar reaction [369]. The reactors with more than one module result in a higher content of carbon monoxide at the inlet (*STCO<1*), as lower *STCO* ratios lead to faster WGS reaction (Figure 6.2). In order to compensate for the surplus of carbon monoxide at the outlet of module I, *STCO* inlet in module II is around 1.7 (*STCO>1*) for Cases 2 and 3. A parallel can be drawn with the traditional WGS process, which is conducted in two or three-stage catalytic converters with water being injected between the stages to adjust the *STCO* ratio [368]. To reiterate, the inlet into module II is obtained as a sum of the optimized inlet feed, and the outlet from module I. Mixing of these two streams results in an almost equal ratio of both reactants at the inlet of module II (Figure 6.13c and d). The benefit of having more modules is the reduction of catalyst consumption and the total reactor volume. The ability to use lower *STCO* ratios near the reactor inlet increases the WGS reaction rate in module I and decreases the R phase residence time and, subsequently, the module volume. This is also confirmed by comparing the number of segments, reactor length, and diameter values in Table 6.7. The first module for Cases 2 and 3 comprises less than 8% of the total reactor volume, while the other modules comprise more than 92%.

6.4.2 Chemisorption and Membrane Separation

The sorbent consumption, i.e., the mass flow rate of the sorbent does not show a clear trend between Cases 1–3 (Figure 6.11), as it is the same for Cases 1 and 3 and 27% smaller for Case 2. However, the sorbent conversion is higher in the reactors with more modules, as shown in Figure 6.14.

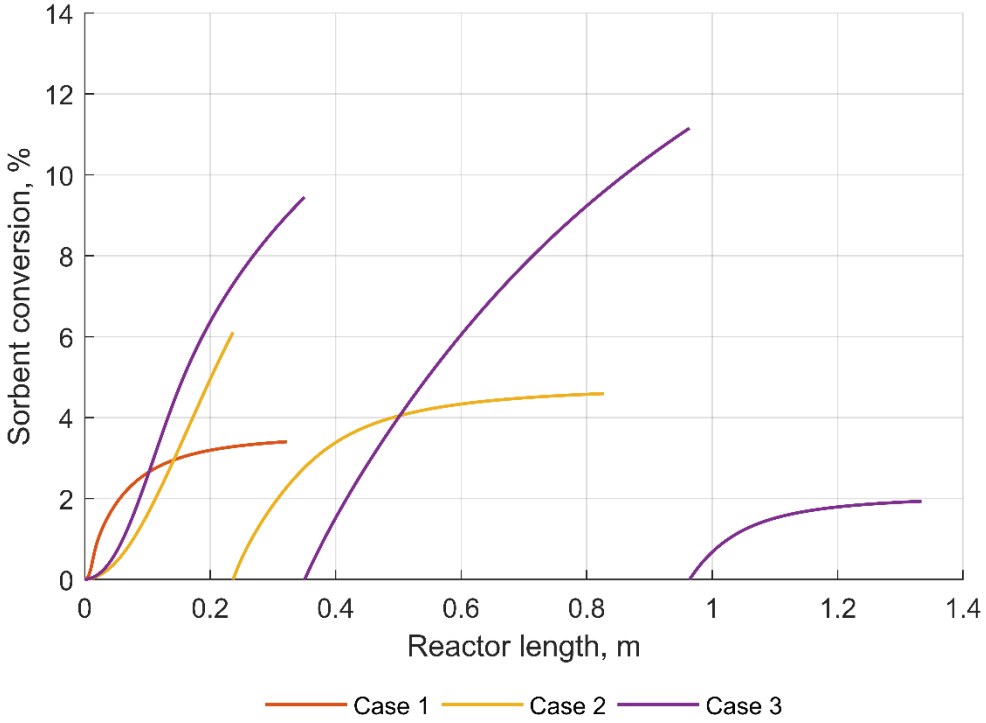

Figure 6.14 – Sorbent conversion for Cases 1–3 [4]

The higher sorbent conversion is due to the increase of the residence time of the S phase, τ_S (Table 6.7), which is a function of the sorbent hold-up and optimization variables (cross-section area and sorbent flux, Eq. D.12 in Appendix D). When the conversion profiles are compared in Figure 6.14, the last module for each Case has a profile that qualitatively matches the one with both diffusion and kinetically limited stages. These stages, as explained in Subsection 6.1.2 and Figure 6.3, are marked with exponential and linear zones corresponding to the kinetic and diffusion-limited sorption stage, respectively.

The modules other than the last one, or module I of Cases 2 and 3, and module II of Case 3, have the CaO conversion profile that seems to have only the exponential stage, corresponding to the kinetically limited stage. When analyzing the CO_2 molar profiles in Figure 6.13b–d, at the outlet of the intermediate modules (module I in Case 2 and 3 and module II in Case 3), it can be seen that CO_2 is not completely removed from the R phase. On the other hand, CO_2 is completely removed at the outlet of the last module for each Case (which is also the reactor outlet). Complete CO_2 removal is something that was achieved in experiments as well when sorption-enhanced WGS was analyzed in a reactor with a packed bed [3]. It is worth noting that, although the sorbent conversion rises as the number of modules increases, the conversion levels are still low (less than 12%). The sorption costs include the costs for "fresh" sorbent and partly used sorbent. As stated by Wess et al., the used sorbent can be [109]:

1) regenerated in a separate unit, i.e., CaL technology [365];
2) continuously regenerated, i.e., fluid catalytic cracking [109] and circulating fluidized bed riser [110]; or
3) not recovered at all (either storage or use in other industries).

The first two options have problems with heat management needed to regenerate the sorbent, and the decaying sorbent capacity after a few cycles. The third option leads to better energetic efficiency since no heat is needed for the recovery, and there are zero CO_2 emissions. Considering the beforementioned, the relatively low sorbent conversion in our Cases, as well as relatively low calcium oxide prices and high availability, the third option could be suggested. However, this should be investigated in a more detailed, economic analysis.

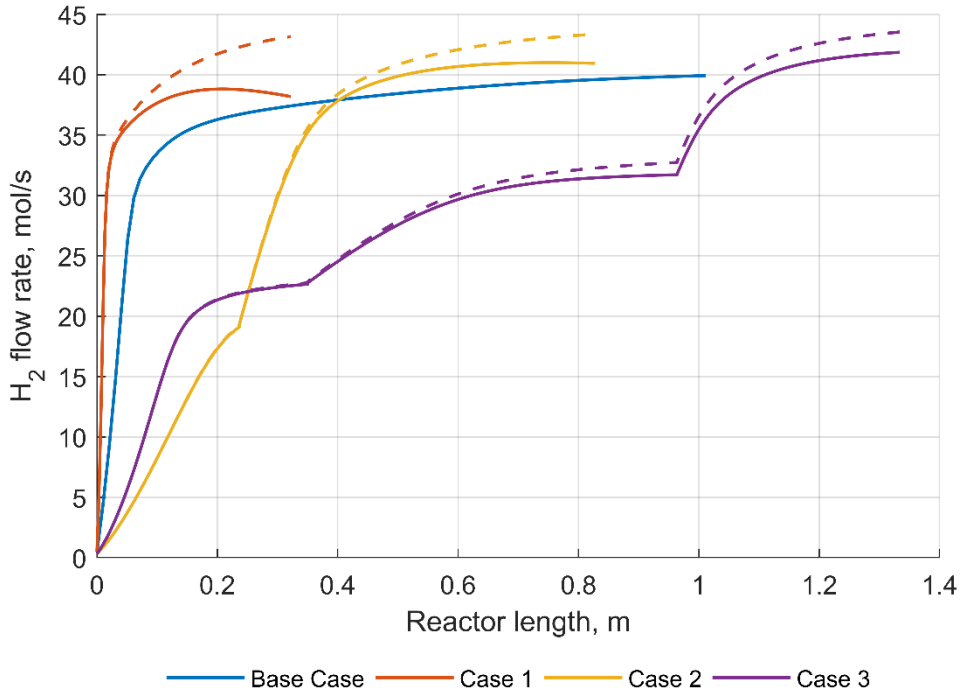

Figure 6.15 – Total hydrogen molar flow rate (dashed lines), and the flow rate in the R phase (solid lines) for Base Case and Cases 1-3 [4]

Contribution of the membrane separation to higher hydrogen Yield can be observed by comparing the total (R+M) and the R phase hydrogen molar flow rate profiles (Figure 6.15). The separated hydrogen flow rate in the inner tube (M) is added to the R phase hydrogen flow rate to calculate the total hydrogen produced. By comparing the profiles in Figure 6.15, a conclusion can be made that the membrane is better utilized in the reactor with fewer modules, although, at a much higher price in the membrane area (Figure 6.11). In the reactor with just one module (Case 1), the permeated hydrogen comprises more than 11% of the total hydrogen flow rate. It leads to 96% of carbon monoxide conversion, which is slightly higher than 93.5% achieved by Basile et al. at the same atmospheric pressure [368]. However, Basile et al. used a temperature of 331 °C, which is significantly lower than 470+ °C for Case 1. As explained in Subsection 6.1.3, lower temperatures lead to lower MEM fluxes. In cases with more than one module, the fraction of the permeated hydrogen in the total hydrogen flow rate drops to less than 6% for Case 3.

Hydrogen separation via the Pd-Ag membrane is expensive [379], both to implement (cost of the membrane and fabrication) and control (operational costs). Altogether, modest removal and its effect on equilibrium obtained in Cases 2 and 3 suggest that the MEM phenomena can be excluded without a significant loss in the total outlet hydrogen flow rate, which will considerably decrease the total costs. The results presented in Figure 6.13 demonstrate that the mixture at the reactor outlet mainly consists of H_2 (93 mol%, excluding the inert for Case 3), since CO_2 is removed by sorption, and the reactants are converted almost completely. This is favorable from the separation point of view, even without the membrane.

6.4.3 Proposed Structure and Operating Conditions

According to the results presented in Section 6.4 (Figure 6.11), Case 2 is proposed for the conceptual design of the reactor for hydrogen production via WGS reaction on atmospheric pressure. Case 2 is selected due to the lowest catalyst mass required for the WGS reaction (552 kg), the lowest sorbent consumption (51.6 kg/s) and significantly lower total reactor volume of 22.6 m^3 when compared to non-intensified Base Case. This proposed reactor structure consists of two modules. The first module (0.24 m in length) has 422 segments or tubes, and the second module (0.59 m in length) has 2295 tubes. The conversion of carbon monoxide is 95% or 64% higher relative to the equilibrium conversion at the same operating conditions. The main stream exiting the reactor has a very high molar fraction of hydrogen (92.2%), environmentally undesired carbon dioxide in traces (0.7%) and 7.1% of the reactants (excluding the inert). Both modules should include the SOR phenomena, i.e., the trickling sorbent particles. The inlet operational variables for the proposed Case are listed in Table 6.7. The presence of the MEM phenomena does not contribute considerably to the H_2 yield and purity at the outlet of the R phase, as shown in Figures 6.13 and 6.15, while the costs of the membrane are rather high. This result suggests that the membrane could be excluded from the reactor. However, both reactor cases (with and without membrane separation) could be analyzed in the next stage of the reactor design and optimization, which should include more detailed cost analysis (with prices).

Considering the analysis done in this section, the following relevant results and explanations are emphasized:

1) *The first benefit of using the SOR and MEM enhanced processes is a higher hydrogen yield, lower reactor volume, and lower catalyst consumption when compared to the non-enhanced WGS (Base Case).*

When compared to the Base Case, the intensified WGS in the reactor with one module (Case 1) gives a higher yield with 25% less catalyst, and 39% reduced reactor volume. However, it also comes with additional costs in sorbent consumption (70.8 kg/s) and membrane fabrication and operation (33.5 m^2). Higher yield, lower reactor volume, and lower catalyst mass are the results of exceeding of the thermodynamic limitations of the conventional WGS process. These limitations are overcome by removing one (CO_2) or both products (CO_2 and H_2) and by a subsequent shifting of the reaction equilibrium, according to Le Chatelier's principle.

2) *The second benefit of using the SOR and MEM enhanced processes is a more balanced reaction temperature profile when compared to the non-enhanced WGS (Base Case).*

In the absence of reaction intensification, the Base Case firstly needs a high temperature for the faster reaction rate and a subsequent significant drop in temperature to exceed the equilibrium limitations and force the reaction towards higher carbon monoxide conversion. Substantial temperature differences can be undesirable from the point of view of temperature control.

3) *Having more than one module is beneficial for the enhancement of the WGS reaction.*

Additional modules allow for feeds of different STCO ratios and feed flow rates to be introduced into separate locations in the reactor. This way, the WGS reaction can be carried out at a higher rate in the first, smaller module. The higher rate is achieved with a lower STCO ratio (around 1) and at thermodynamically less favorable conditions. In the second module, the high STCO ratio favors better carbon monoxide conversion at kinetically less favorable conditions. The outcome is a shorter residence time and significantly reduced catalyst mass. The reduction in the catalyst mass for Case 2 is 74% relative to the intensified WGS with just one module (Case 1) and 80% relative to the non-enhanced Base Case.

6.4.4 Pressure Drop Considerations

Since the Pareto optimization runs discussed in Section 6.3 were done for isobaric conditions, a simulation with pressure drop is performed. The results of the simulation show whether the pressure drop is negligible as assumed in Section 6.2 and whether it will affect any crucial results. Additional model equations for pressure drop are included [377]:

$$\frac{dp_R^i}{dV^i} = -\left(\frac{dp_{sp}^i}{dV^i} + \frac{dp_{mp}^i}{dV^i}\right) \tag{6.34}$$

$$\frac{dp_{sp}^i}{dV^i} = \frac{1}{A_h^i} \cdot \left(\frac{A}{Re_p'^{,i}} + B\right) \cdot \frac{{u_R^i}^2 \cdot \rho_R^i}{d_{eq}^i} \cdot \frac{1-\varepsilon_R^i}{{\varepsilon_R^i}^3} \tag{6.35}$$

$$\frac{dp_{mp}^i}{dV^i} = \frac{1}{A_h^i} \cdot \frac{3}{4} \cdot c_D^i \cdot \frac{\beta_{dyn}^i \cdot \rho_R^i \cdot {u_{rel}^i}^2}{2 \cdot R_{CaO} \cdot \varepsilon_R^i} \tag{6.36}$$

where dp_{sp}^i/dV^i is the pressure drop in the segment of module *i* due to structured packing and dp_{mp}^i/dV^i is the pressure drop due to the moving sorbent particles.

The total pressure in the R phase drops from 1 atm at the reactor inlet to 0.995 atm at the reactor outlet, which is a 0.5 % change. No visible changes are detected in any of the profiles shown in Figures 6.11–6.15 or in the values in Table 6.6. It is, therefore, reasonable to assume that the fifth assumption (negligible pressure change) in Subsection 6.2.2 is valid.

6.4.5 Reaction Pressure as Optimization Variable

Case 2 without membrane separation (MEM) was recommended as the reactor structure in Subsection 6.4.3. This was due to the low contribution of the MEM phenomena to the overall hydrogen molar flow rate output, as demonstrated in Figure 6.15. Since the driving force for hydrogen separation depends on the partial pressure of hydrogen in the reaction (R) phase (Eq. 6.13), it is expected that the MEM flux rate will increase with the rise of the total pressure in the R phase. Separation dependence on pressure was also reported in many published articles [30, 31, 135, 368, 371]. In this Subsection, the previously optimized Cases will be compared to a new Case (Case 2*), with two modules and additional optimization variable, the R phase pressure (Table 6.8). The goal is to explore whether higher pressure would lead to a significant contribution of the MEM phenomena in the overall hydrogen molar flow rate output and how the reactor efficiency and cost indicators would change.

Table 6.8 – Optimization Case 2 and Previously Optimized Cases*

Case Name	Nm	R Phase Pressure, atm	Possible Phenomena
Base Case	1	1	WGS
Case 1	1	1	WGS, SOR, MEM
Case 2	2	1	WGS, SOR, MEM
Case 3	3	1	WGS, SOR, MEM
Case 4	4	1	WGS, SOR, MEM
Case 2*	2	up to 4	WGS, SOR, MEM

The upper bound for the new optimization variable, the R phase pressure, is set to 4 atm since it has been reported that at higher pressures removal of reactants can occur which lowers separation efficiency and carbon monoxide conversion [368].

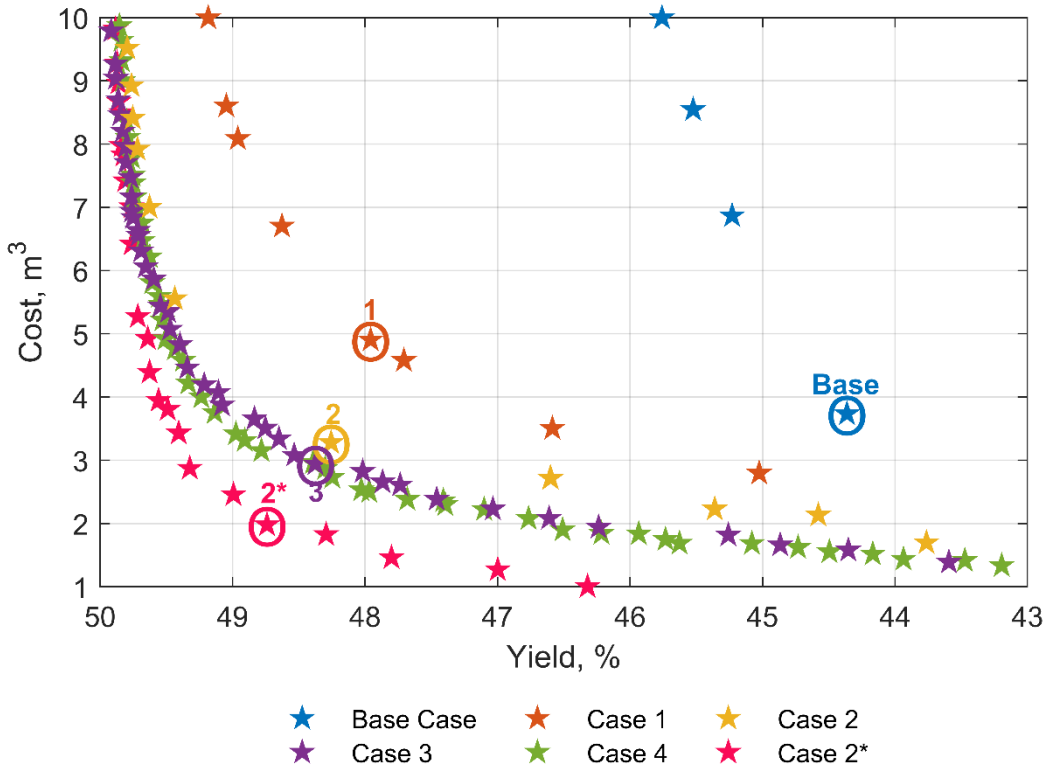

Figure 6.16 – Pareto fronts for analyzed Cases and the additional Case 2 with the chosen solutions*

The Pareto front attained for Case 2* (with pressure as optimization variable) is shown in Figure 6.16, together with the Cases obtained in Section 6.4. All solutions comprising the Case 2* front have the R phase pressure at the upper bound, 4 atm. This was expected, as pressure was not penalized in the Cost function (Eq. 6.33) and higher pressure leads to higher hydrogen yield as shown in Figure 6.16. The solution that was chosen for further analysis is shown with a number 2*. The detailed optimization results for this case are listed in Table 6.9.

The chosen point for Case 2* corresponding to 4 atm has a total Cost of 1.98 m^3 and a 48.74% Yield. Higher hydrogen yield and reduced reactor cost indicators are the direct result of the higher WGS rate due to the pressure increase (Eq. 6.10). Case 2* has significantly less volume (reactor length) and slightly higher maximal temperatures than Case 2 (corresponding to 1 atm). The residence time of the

sorbent is shorter in the reactor with higher pressure, while the module I membrane diameter is over two times bigger than the diameter for Case 1.

*Table 6.9 – Pareto optimization results for the Base Case and Cases 1, 2 and 2**

Case	Base	1	2		2*	
Module i	**I**	**I**	**I**	**II**	**I**	**II**
Reactor structure optimization variables						
Ns^i	362	4771	422	2295	141	3412
L^i, m	1.01	0.32	0.24	0.59	0.10	0.14
d^i, m	0.332	0.127	0.093	0.144	0.087	0.157
d_M^i, m	/	0.022	0.008	0.012	0.045	0.010
ε_c^i	0.12	0.14	0.14	0.03	0.15	0.11
Operating condition optimization variables						
$F^{i,in}$, mol/s	100	100	64.9	35.1	27.8	72.2
$STCO^i$	0.94	1.00	0.74	1.66	0.62	1.18
J_s^i,	/	1.20	1.79	1.26	0.36	1.17
$T_R^{i,in}$, °C	462	483	482	488	482	488
T_s^{in}, °C	/	482	482		482	
T_w^i, °C	258	472	472	474	472	401
Constraint variables						
$T_{R,max}^i$, °C	492	535	507	488	503	533
d^i-d_M^i, m	0.33	0.105	0.084	0.132	0.042	0.147
Yield and Cost function value						
Y, %	44.36	47.96	48.26		48.74	
Cost, m^3	3.73	4.90	3.28		1.98	
Gas and sorbent mean residence time						
τ^i, s	6.95	4.86	0.17	5.65	0.15	10.9
τ_s^i, s	/	25.5	30.7	57.7	14.4	12.8

The inlet STCO ratio and temperature trends remain the same as before, with lower values in the first module, and higher values in the second module. When the temperature profiles of the R phase are analyzed (Figure 6.17), the temperature gradient inside the reactor is much greater for the case with 4 atm, when compared to the intensified Cases at 1 atm. However, the gradient is still smaller than the one for the Base Case. The sorbent conversion profile for Case 2*, which is shown in Figure 6.18, remains similar to a kinetically limited stage in the first module and diffusion limited stage in the second module. However, lower sorbent conversion is

observed at 4 atm. This is as a result of the significantly lower particle residence time (Table 6.9) when compared to the intensified Cases for 1 atm.

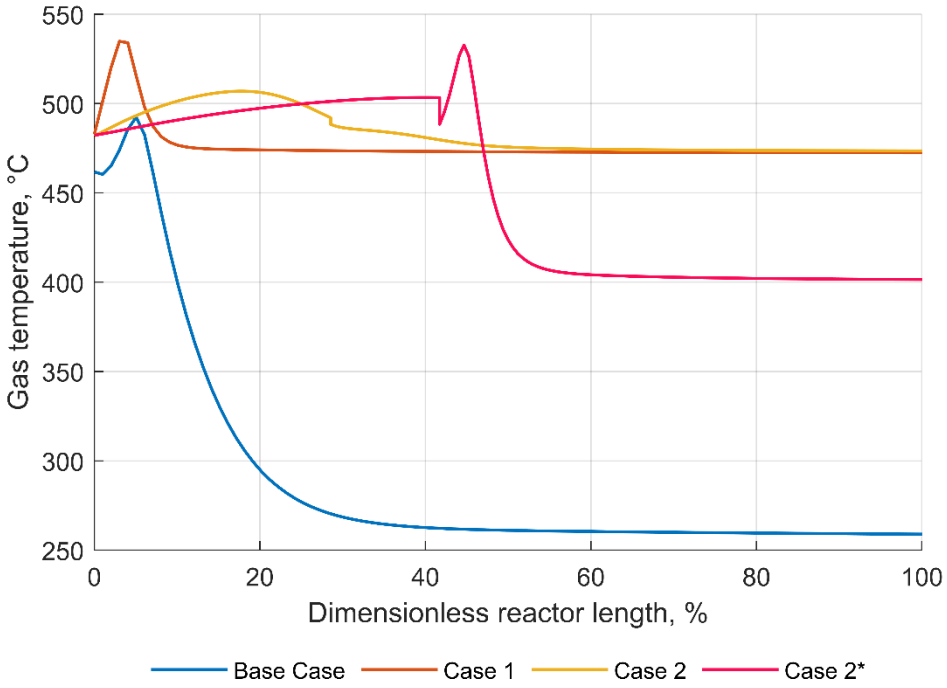

*Figure 6.17 – The gas temperature in the R phase for the Base Case and Cases 1,2, and 2**

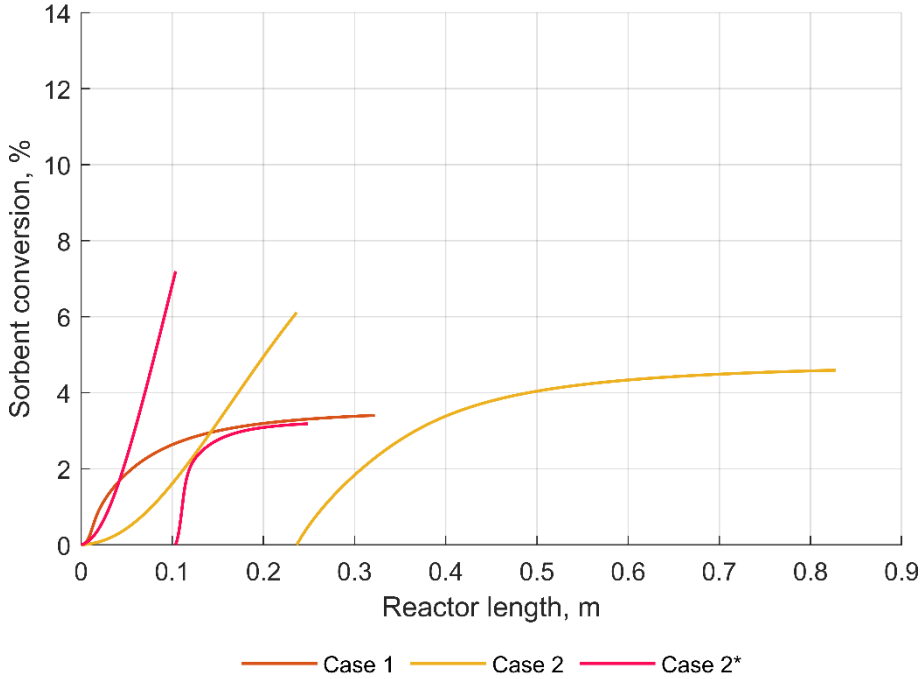

*Figure 6.18 – Sorbent conversion for the Cases 1, 2, and 2**

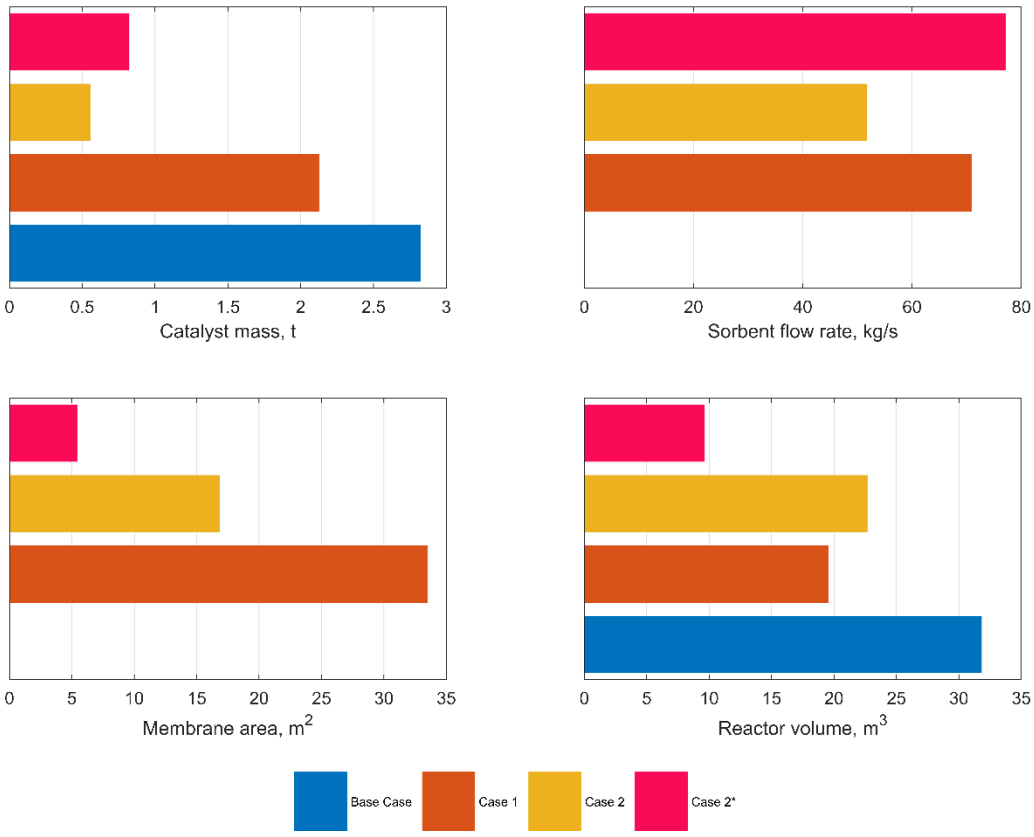

Figure 6.19 – Reactor cost indicators for the Base Case and Cases 1, 2, and 2: catalyst mass, sorbent flow rate, membrane area, and reactor volume*

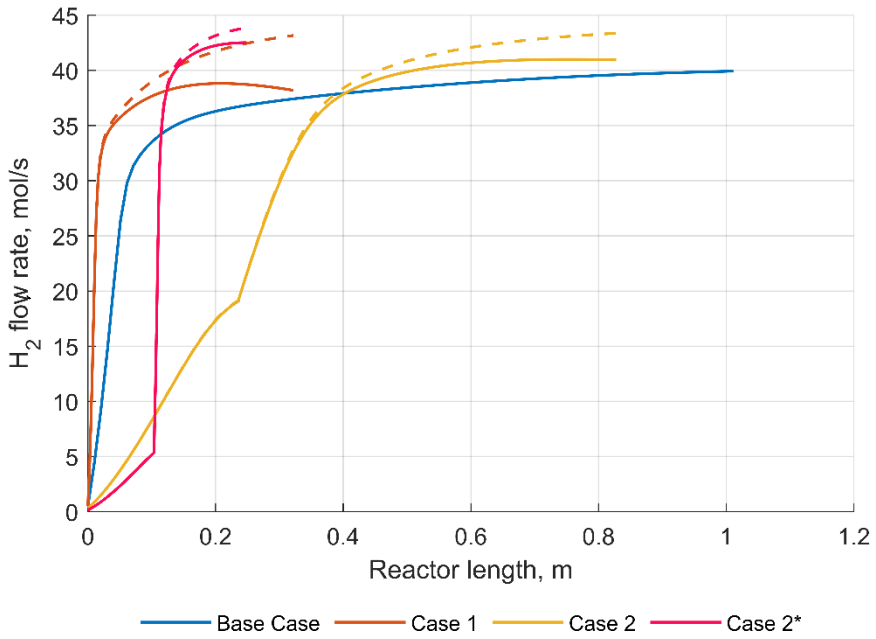

*Figure 6.20 – Total hydrogen molar flow rate (dashed lines), and the flow rate in the R phase (solid lines) for the Base Case and Cases 1, 2, and 2**

When the reactor cost indicators are compared (Figure 6.19), Case 2* corresponding to the total pressure of 4 atm has significantly lower total reactor volume (more than double) than the Cases at 1 atm. The lower volume is due to higher WGS rates and lower residence time needed for the reaction. The membrane area is also smaller, more than three times when compared to Case 2. The cost indicators that are higher for Case 2* are the sorbent flow rate and the catalyst mass. The increased sorbent usage is as a result of the smaller reactor and the reduced particle residence time. Case 2* gives a higher yield when compared to Case 2, but with the increased catalyst and sorbent usage. The most important finding comes from Figure 6.20 that shows the hydrogen molar flow rate profiles. The profiles do not show considerable improvement in membrane separation for the 4 atm Case when compared to the 1 atm Cases. As visible in Figure 6.20, the M phase hydrogen flow rate is only a few percentage points of the R phase hydrogen flow rate for Case 2*. Since the MEM phenomena contribution remains rather small, higher reaction pressure optimization did not change the previous conclusion stated in Subsection 6.4.3. Moreover, all of the pressure optimization values are on their upper bounds, suggesting the excess of degrees of freedom and that pressure would need to be penalized, i.e., included in the Cost function. Higher hydrogen yields were expected, but the question remains at what price regarding the construction and operation.

6.5 Conclusions

In this Chapter, the ReSyPIO methodology was successfully applied to synthesize a reactor system for an industrial reaction case. Due to the thorough analysis, the application led to answers how the reactor structure, operational conditions, and presence of sorption- and membrane-enhancing processes affect the hydrogen production through water-gas shift reaction at atmospheric conditions. After the detailed analysis of the enhancing phenomena, a pseudo-homogeneous one-dimensional model was developed for a rigorous optimization. Multi-objective optimization was efficiently exploited, in which the Benefit function was defined as the hydrogen yield at the exit of the reactor, and the Cost function as the sum of the volume fractions for catalyst, sorbent particles, and membrane, multiplied by the total reactor volume (representing the reactor cost indicators). The defined reactor superstructure allowed for co-feeding of fresh feed at different reactor locations, determined in the optimization. Several reactor designs and operational parameters were optimized.

The results of the multi-objective optimization analysis showed that inclusion of chemisorption and membrane separation led to higher hydrogen yields, lower reactor volumes, and decreased catalyst consumption. The enhanced processes were also accompanied by better-balanced temperature profiles when compared to the non-intensified water-gas shift process. By adding additional fresh reactant streams with determined composition along the reactor, the catalyst consumption and reactor volume decreased even further. In the end, it was concluded that the high-capacity reactor containing two modules, two different reactant supply streams and CaO sorbent particles trickling down the structured catalyst bed (sorption-enhanced water-gas shift process) gives the highest hydrogen yield at the lowest reactor cost indicators.

Nomenclature

Abbreviations

$HTSR$	the high-temperature shift reactor
$LTSR$	the low-temperature shift reactor
MEM	hydrogen removal through Palladium membrane
SOR	carbon dioxide chemisorption
WGS	water-gas-shift reaction

Variables and constants

a	specific area	m^{-1}
A	area	m^2
$Benefit$	Benefit objective function	mol/s
c	concentration	mol/m^3
c_p	isobaric heat capacity	$J/mol/K$
$Cost$	Cost objective function	m^3
d	diameter	m
DF	driving force	$Pa^{0.5}$
F	molar flow rate	mol/s
g	gravitational acceleration constant	9.80665 m/s^2
h	heat transfer coefficient	$W/m^2/K$
$\dot{H}$	rate of heat transfer	J/s
J_M	membrane separation (M phase) molar flux	$mol/m^2/s$
J_S	sorbent (S phase) mass flux	$kg/m^2/s$
L	length	m
M	molar mass	kg/mol
Nm	number of modules	
Ns	number of segments	
$Nvars$	number of variables	
OF	single objective function	$1/m^3$
$STCO$	steam to carbon monoxide ratio	
p	pressure	Pa
Pm	permeability	$mol \cdot m/m^2/s/Pa^{0.5}$
r	radius	m

R	universal gas constant	$8.314462175\ J/mol/K$
r_{CaO}	unreacted sorbent particle radius	m
R_{CaO}	fresh sorbent particle radius	$160-250\ \mu m$
t	time	s
T	temperature	T
u	velocity	m/s
U	overall heat transfer coefficient	$W/m^2/s$
V	volume	m^3
$\dot{V}$	volumetric flow rate	m^3/s
X	conversion	
y	molar fraction	
Y	Yield	
z	the distance along the total reactor length	m
ε	volumetric fraction	
λ	conductivity	$W/m/K$
μ	viscosity	$Pa\cdot s$
ρ	density	kg/m^3
φ	component between-influence factor	
τ	residence time	s
E	heat transfer rate per segment volume	$J/m^3/s$
ϕ_{MEM}	membrane separation phenomena rate	$mol/m^3/s$
ϕ_{SOR}	chemisorption phenomena rate	$mol/m^3/s$
ϕ_{WGS}	water gas shift reaction phenomena rate	$mol/m^3/s$

Water gas shift reaction parameters [3]

Aa_{wgs}	pre-exponential factor	$molkPa^{-a-b-c-d}/g/s$
Ea_{wgs}	activation energy	kJ/mol
k_{wgs}	Arrhenius' water gas shift reaction rate	$molkPa^{-a-b-c-d}/g/s$
r_{wgs}	water gas shift reaction rate	$mol/g/s$
ΔH_{wgs}	reaction enthalpy	kJ/mol

Carbonization reaction and diffusion parameters [3]

Aa_{car}	pre-exponential factor	m/s
De_0	diffusion parameter	m^2/s

Ea_{car}	activation energy	kJ/mol
k_{car}	Arrhenius' carbonization reaction rate	m/s
ΔH_{car}	reaction enthalpy	kJ/mol

Membrane separation parameters [135]

Aa_{mem}	pre-exponential factor	$molm/m^2/s/Pa^{0.5}$
Ea_{mem}	activation energy	kJ/mol
k_{mem}	Arrhenius' membrane separation rate	$molm/m^2/s/Pa^{0.5}$
δ	membrane thickness	μm

Viscosity parameters [380, 381]

$v2, v3$	NIST model parameters
$va, vb, v1$	Sutherland model parameters

Isobaric heat capacity parameters [380]

c_{pA}, c_{pB} …	Shomate equation parameters

Conductivity parameters [380]

$l1, l2, l3$	NIST model parameters

Non-dimensional numbers and coefficients

Ar	Archimedes number
c_D	shape resistance coefficient
Fe	the ratio between mass flow rates of S and R phase
Fm	Federov's number
Ke	the ratio between kinetic energy of sorbent and R
Pr	Prandtl number
Re	Reynolds number
Re'	modified Reynolds number

Subscript indexes

0	reference value	
c	catalyst	
dyn	dynamic	
e	effective	
eq	equivalent	
eqb	equilibrium	
er	effective radial	
$frac$	the fraction of the structure	
h	hydraulic	
ine	inert (N_2)	
m, n	component	m, n
M	M phase	
max	maximum	
$mean$	mean value	
mp	moving particle	
R	R phase	
rel	relative	
Rs	expressed on the Rankine scale (1 °R = 1 K · 9/5)	
s	sorbent particle	
S	S phase	
$stat$	static	
sp	structured (Kerapak) packing	
v	void fraction for pseudo-homogenous system	
W	W phase	
λ	conductivity index	
μ	viscosity index	

Superscript indexes

i	module index	$i = I, II, III, \ldots$
in	inlet	
Nm	total number of modules	
out	outlet	
tot	total for all segments in one or all modules	

7. Final Conclusions

A new methodology for reactor synthesis based on process intensification concepts and application of optimization methods (ReSyPIO) was proposed and applied to a general and an industrially relevant reaction case. In the general reaction case, the proposed solution is the reaction system that consists of 17 segments and is operated in a steady state. This system is practically realized as a tubular reactor with 17 side input streams for the dosed reactant and optimal distribution of heat supply. In the industrial, water-gas shift reaction case, the application of ReSyPIO methodology results in a large-capacity reactor that contains two modules, having different reactant supply, and CaO sorbent particle streams, trickling down the structured catalyst bed, or a sorption-enhanced water-gas shift process. The ReSyPIO methodology provides recommendations for the reactor structure, operating conditions, and in the general reaction case, the operational regime of the analyzed reaction. As demonstrated in Chapters 4 and 6, the ReSyPIO methodology successfully applies the principles from all four domains of process intensification:

Structure domain – it provides a combination of phase and segment layouts of different sizes interconnected in different ways and examines the PI options for miniaturization (Chapter 4) and utilization of structural inserts (catalyst supports) (Chapter 6);

Synergetic domain – it allows for the presence of multiple phenomena that have synergetic contributions, such as a combination of reaction and separation (Chapter 4 and 6);

Dynamic domain – it determines the operational regime (steady-state vs. dynamic, Chapter 4) and examines forced periodic operation (Chapter 4);

Energetic domain – it optimizes the energy flows/rates in the system (Chapter 4 and 6).

More detailed and specific conclusions, related to the ReSyPIO methodology and the applied examples, have been given in Chapters 4, 5, and 6.

The main advantages of the developed methodology are:

1) Judgments in the reactor selection and design, i.e., decision making, are based on a systematic analysis and optimization, and not solely the result of heuristics and experience (i.e., "what comes to mind").
2) Theoretically, the ReSyPIO methodology allows for an infinite number of structural, synergetic, dynamic, and energetic variations. Therefore, some judgments have to be made by the designers, according to their best knowledge and experience. However, those selections are limited to the ones that are physically viable and (in some cases) more important.
3) The ReSyPIO methodology allows for simultaneous optimization of both the structure and the operational regime, which is rare among methodologies presented in the literature.
4) The ReSyPIO methodology is general enough and conceptual, meaning that it can be applied to various reaction cases and processes, from different chemical and process industries.
5) The optimization results can give a valuable insight into the phenomena which could lead to new layouts, subsequent optimization, and possibly to novel solutions. The ReSyPIO methodology consists of reverse stages and steps, meaning that, if the optimization results point to wrong or inferior layouts, new ones can be created.
6) The ReSyPIO methodology is not confined to a few numerical methods that can be used, and its results do not have to rely on specific and economic parameters, i.e., variable prices. Other numerical methods, aside from the presented ones, can be used and implemented.

The application of the ReSyPIO methodology has also shown several shortcomings:

1) The ReSyPIO methodology relies on the validity and breadth of the experimental data. It is highly sensitive to unavailability or/and uncertainty of experimental information, i.e., physical and chemical parameters, similar to all other first principles modeling approaches.
2) The result of the application, i.e., the recommendation for the reactor design, largely depends on the quality and availability of the numerical and optimization solvers.
3) Matlab 2018b numerical solvers can be used only for simple reactor structures. The simple structure has up to 10 complex modules (more than two phases and several phenomena) or up to several hundred simple modules (a combination of one phase and several phenomena or two phases and two phenomena). Optimization of more complex superstructures and dynamic operational regimes requires the use of more sophisticated software, which could be more costly and time demanding.
4) The application of the ReSyPIO methodology can be time-consuming as it requires experiment data collection, thorough analysis, modeling, and optimization.
5) The ReSyPIO methodology is applied on the feasibility or screening level. The following detailed optimization-based reactor design in which process control (or controllability) is included might show that the previous recommendations are not viable, functional or they do not provide the predicted efficiency and process enhancement.

Nevertheless, with everyday advances in numerical solvers, creation of new stochastic and hybrid stochastic-deterministic algorithms, the ReSyPIO methodology could evolve and become applicable to the more complex structure and module layouts. Integration with analytical Process System Engineering methods, e.g., the Nonlinear Frequency Response Method, might prove to be valuable when simultaneously determining the reactor structure and the operational regime.

References

1. Kahneman, D., *Maps of Bounded Rationality: Psychology for Behavioral Economics.* American Economic Review, 2003. **93**(5): p. 1449–1475.
2. Živković, L.A. and N.M. Nikačević, *A method for reactor synthesis based on process intensification principles and optimization of superstructure consisting of phenomenological modules.* Chemical Engineering Research & Design, 2016. **113**: p. 189–205.
3. Živković, L.A., A. Pohar, B. Likozar, and N.M. Nikačević, *Kinetics and reactor modeling for CaO sorption-enhanced high-temperature water-gas shift (SE-WGS) reaction for hydrogen production.* Applied Energy, 2016. **178**: p. 844–855.
4. Živković, L.A., A. Pohar, B. Likozar, and N.M. Nikačević, *Reactor Conceptual Design by Optimization for Hydrogen Production through Sorption- and Membrane-enhanced Water–Gas Shift Reaction.* Chemical Engineering Science, 2019. ***under minor revision after review***.
5. Stephanopoulos, G. and G.V. Reklaitis, *Process systems engineering: From Solvay to modern bio- and nanotechnology.: A history of development, successes and prospects for the future.* Chemical Engineering Science, 2011. **66**(19): p. 4272–4306.
6. Reay, D., C. Ramshaw, and A. Harvey, *Process Intensification: Engineering for Efficiency, Sustainability and Flexibility*. 2011: Butterworth-Heinemann.
7. Herder, P.M., A.L. Turk, E. Subrahmanian, and A.W. Westerberg, *Challenges for process systems engineering in infrastructure design.* Computers & Chemical Engineering, 2000. **24**(2): p. 1775–1780.
8. Nikačević, N.M., A.E.M. Huesman, P.M.J. Van Den Hof, and A.I. Stankiewicz. *New optimization-based approach to process synthesis - Towards the full integration of process design, operation and control*. in *AIChE 2013 National Spring Meeting*. 2011. Chicago, IL, USA.
9. Moulijn, J.A., A. Stankiewicz, J. Grievink, and A. Górak, *Process intensification and process systems engineering: A friendly symbiosis.* Computers & Chemical Engineering, 2008. **32**(1): p. 3–11.
10. Luyben, W.L., *Chemical Reactor Design and Control*. 2007: Wiley.
11. Alvarado-Morales, M., M.K.A. Hamid, G. Sin, K.V. Gernaey, J.M. Woodley, and R. Gani, *A model-based methodology for simultaneous design and control of a bioethanol production process.* Computers & Chemical Engineering, 2010. **34**(12): p. 2043–2061.
12. Zondervan, E., N. Nikacevic, H. Khajuria, E.N. Pistikopoulos, and A.B. de Haan, *Integrated Operation and Design of a Simulated Moving Bed Reactor.* Computer Aided Chemical Engineering, 2012. **30**: p. 642–646.

13. Freund, H. and K. Sundmacher, *Towards a methodology for the systematic analysis and design of efficient chemical processes: Part 1. From unit operations to elementary process functions.* Chemical Engineering and Processing, 2008. **47**(12): p. 2051–2060.
14. Bird, R.B., W.E. Stewart, and E.N. Lightfoot, *Transport Phenomena*. 2007: Wiley.
15. McCabe, W.L., P. Harriott, and J.C. Smith, *Unit Operations of Chemical Engineering*. 2005: McGraw-Hill Higher Education.
16. Smith, J.M., *Chemical Engineering Kinetics*. 1981: McGraw-Hill Inc.,US.
17. Scriven, L.E. *When Chemical Reactors Were Admitted and Earlier Roots of Chemical Engineering*. 2003. 11–28.
18. Levenspiel, O., *Chemical reaction engineering.* 1999: Wiley.
19. Gilles, E.D., *Quasi-stationäres verhalten von wandernden brennzonen.* Chemical Engineering Science, 1974. **29**(5): p. 1211–1216.
20. Gilles, E.D., G. Eigenberger, and W. Ruppel, *Relaxation oscillations in chemical reactors.* AlChE Journal, 1978. **24**(5): p. 912–920.
21. Achenie, L., V. Venkatasubramanian, and R. Gani, *Computer Aided Molecular Design*. Vol. 12. 2002: Elsevier Science.
22. Leszczynski, Z., *Role of chemical engineering and chemical process machinery in industrial application and in process intensification.* Przemsyl Chemiczny, 1973. **52**(3): p. 161–163.
23. Ramshaw, C., *HIGEE Distillation—An Example of Process Intensification.* Chemical Engineer London, 1983. **389**: p. 13–14.
24. Stankiewicz, A.I. *Process Intensification in Europe*. in *Infotag: Prozessintensivierung: Ansichten der Industrie*. 2006. Frankfurt am Main, Germany: DECHEMA
25. Moulijn, J.A., Stankiewicz, A., *Re-engineering the Chemical Processing Plant: Process Intensification*. 2004, New York: Marcel Dekker.
26. Keil, P.D.D.h.c.F.J., *Modeling of Process Intensification*. 2007, Weinheim: Wiley-VCH.
27. Stankiewicz, A.I. and J.A. Moulijn, *Process Intensification: Transforming Chemical Engineering.* Chemical Engineering Progress, 2000. **96**(1): p. 22–33.
28. Nikačević, N., M. Jovanović, and M. Petkovska, *Enhanced ammonia synthesis in multifunctional reactor with in situ adsorption.* Chemical Engineering Research and Design, 2011. **89**(4): p. 398–404.
29. Bayat, M., M. Hamidi, Z. Dehghani, M.R. Rahimpour, and A. Shariati, *Hydrogen/methanol production in a novel multifunctional reactor with in situ adsorption: modeling and optimization.* International Journal of Energy Research, 2014. **38**(8): p. 978–994.
30. Dittmeyer, R., V. Höllein, and K. Daub, *Membrane reactors for hydrogenation and dehydrogenation processes based on supported palladium.* Journal of Molecular Catalysis A: Chemical, 2001. **173**(1): p. 135–184.

31. Garcia-Garcia, F.R., M. Leon, S. Ordonez, and K. Li, *Studies on water-gas-shift enhanced by adsorption and membrane permeation.* Catalysis Today, 2014. **236**: p. 57–63.
32. Buchaly, C., P. Kreis, and A. Górak, *Hybrid separation processes—Combination of reactive distillation with membrane separation.* Chemical Engineering and Processing, 2007. **46**(9): p. 790–799.
33. Marquardt, W., S. Kossack, and K. Kraemer, *A Framework for the Systematic Design of Hybrid Separation Processes* *Supported by the Deutsche Forschungsgemeinschaft (German Research Foundation), DAAD (German Academic Exchange Service) and FUNDAYACUCHO, and Bayer Technology Services.* Chinese Journal of Chemical Engineering, 2008. **16**(3): p. 333–342.
34. Berry, D.A. and K.M. Ng, *Synthesis of crystallization–distillation hybrid separation processes.* AlChE Journal, 1997. **43**(7): p. 1751–1762.
35. Franke, M., A. Görak, and J. Strube, *Design and optimization of hybrid separation processes.* Chemie Ingenieur Technik, 2004. **76**(3): p. 199–210.
36. Lucia, A., A. Amale, and R. Taylor, *Energy Efficient Hybrid Separation Processes.* Industrial & Engineering Chemistry Research, 2006. **45**(25): p. 8319–8328.
37. Mitsos, A., N. Asprion, C.A. Floudas, M. Bortz, M. Baldea, D. Bonvin, A. Caspari, and P. Schäfer, *Challenges in process optimization for new feedstocks and energy sources.* Computers & Chemical Engineering, 2018. **113**: p. 209–221.
38. Bhat, S.A. and J. Sadhukhan, *Process intensification aspects for steam methane reforming: An overview.* AlChE Journal, 2009. **55**(2): p. 408–422.
39. Van Gerven, T. and A. Stankiewicz, *Structure, Energy, Synergy, Time—The Fundamentals of Process Intensification.* Industrial & Engineering Chemistry Research, 2009. **48**(5): p. 2465–2474.
40. Keil, F.J., *Process intensification.* Reviews in Chemical Engineering, 2018. **34**(2): p. 135–200.
41. Commenge, J.-M., L. Falk, J.-P. Corriou, and M. Matlosz, *Analysis of Microstructured Reactor Characteristics for Process Miniaturization and Intensification.* Chemical Engineering & Technology, 2005. **28**(4): p. 446–458.
42. Charpentier, J.-C., *Process Intensification by Miniaturization.* Chemical Engineering & Technology, 2005. **28**(3): p. 255–258.
43. Jensen, K.F., *Microreaction Engineering—Is Small Better.* Chemical Engineering Science, 2001. **56**(2): p. 293–303.
44. Mills, P.L., D.J. Quiram, and J.F. Ryley, *Microreactor technology and process miniaturization for catalytic reactions—A perspective on recent developments and emerging technologies.* Chemical Engineering Science, 2007. **62**(24): p. 6992–7010.

45. Mbodji, M., J.M. Commenge, L. Falk, D. Di Marco, F. Rossignol, L. Prost, S. Valentin, R. Joly, and P. Del-Gallo, *Steam methane reforming reaction process intensification by using a millistructured reactor: Experimental setup and model validation for global kinetic reaction rate estimation.* Chemical Engineering Journal, 2012. **207-208**: p. 871–884.
46. Kiwi-Minsker, L. and A. Renken, *Microstructured reactors for catalytic reactions.* Catalysis Today, 2005. **110**(1): p. 2–14.
47. Klemm, E., H. Döring, A. Geisselmann, and S. Schirrmeister, *Microstructured Reactors in Heterogenous Catalysis.* Chemical Engineering & Technology, 2007. **30**(12): p. 1615–1621.
48. Wörz, O., K.P. Jäckel, T. Richter, and A. Wolf, *Microreactors, a new efficient tool for optimum reactor design.* Chemical Engineering Science, 2001. **56**(3): p. 1029–1033.
49. Gourdon, C., S. Elgue, and L. Prat, *What are the needs for Process Intensification?* Oil & Gas Science and Technology - Revue d'IFP Energies nouvelles, 2015. **70**(3): p. 463–473.
50. Sohrabi, S., M. Keshavarz Moraveji, and D. Iranshahi, *A review on the design and development of photocatalyst synthesis and application in microfluidic reactors: Challenges and opportunities.* Reviews in Chemical Engineering, 2019.
51. Hessel, V., H. Löwe, and F. Schönfeld, *Micromixers—a review on passive and active mixing principles.* Chemical Engineering Science, 2005. **60**(8): p. 2479–2501.
52. Ottino, J.M. and S. Wiggins, *Applied physics. Designing optimal micromixers.* Science, 2004. **305**(5683): p. 485–486.
53. Alm, B., U. Imke, R. Knitter, U. Schygulla, and S. Zimmermann, *Testing and simulation of ceramic micro heat exchangers.* Chemical Engineering Journal, 2008. **135**: p. S179–S184.
54. Henning, T., J.J. Brandner, and K. Schubert, *Characterisation of electrically powered micro-heat exchangers.* Chemical Engineering Journal, 2004. **101**(1): p. 339–345.
55. Ookawara, S., T. Ishikawa, and K. Ogawa, *Applicability of a Miniaturized Micro-Separator/Classifier to Oil-Water Separation.* Chemical Engineering & Technology, 2007. **30**(3): p. 316–321.
56. Wan, Y.S.S., J.L.H. Chau, A. Gavriilidis, and K.L. Yeung, *Design and fabrication of zeolite-based microreactors and membrane microseparators.* Microporous and Mesoporous Materials, 2001. **42**(2): p. 157–175.
57. Kreutzer, M.T., F. Kapteijn, and J.A. Moulijn, *Shouldn't catalysts shape up?: Structured reactors in general and gas–liquid monolith reactors in particular.* Catalysis Today, 2006. **111**(1): p. 111–118.
58. Kapteijn, F., T.A. Nijhuis, J.J. Heiszwolf, and J.A. Moulijn, *New non-traditional multiphase catalytic reactors based on monolithic structures.* Catalysis Today, 2001. **66**(2): p. 133–144.
59. Roy, S., T. Bauer, M. Al-Dahhan, P. Lehner, and T. Turek, *Monoliths as multiphase reactors: A review.* AlChE Journal, 2004. **50**(11): p. 2918–2938.

60. Giani, L., G. Groppi, and E. Tronconi, *Mass-Transfer Characterization of Metallic Foams as Supports for Structured Catalysts.* Industrial & Engineering Chemistry Research, 2005. **44**(14): p. 4993–5002.
61. Patcas, F.C., G.I. Garrido, and B. Kraushaar-Czarnetzki, *CO oxidation over structured carriers: A comparison of ceramic foams, honeycombs and beads.* Chemical Engineering Science, 2007. **62**(15): p. 3984–3990.
62. Scheffler, F., A. Zampieri, W. Schwieger, J. Zeschky, M. Scheffler, and P. Greil, *Zeolite covered polymer derived ceramic foams: novel hierarchical pore systems for sorption and catalysis.* Advances in Applied Ceramics, 2005. **104**(1): p. 43–48.
63. de Campos, V.J.M. and R.M. Quinta-Ferreira, *Structured catalysts for partial oxidations.* Catalysis Today, 2001. **69**(1): p. 121–129.
64. Ellenberger, J. and R. Krishna, *Counter-current operation of structured catalytically packed distillation columns: pressure drop, holdup and mixing.* Chemical Engineering Science, 1999. **54**(10): p. 1339–1345.
65. Chinthaginjala, J.K., K. Seshan, and L. Lefferts, *Preparation and Application of Carbon-Nanofiber Based Microstructured Materials as Catalyst Supports.* Industrial & Engineering Chemistry Research, 2007. **46**(12): p. 3968–3978.
66. Tribolet, P. and L. Kiwi-Minsker, *Palladium on carbon nanofibers grown on metallic filters as novel structured catalyst.* Catalysis Today, 2005. **105**(3): p. 337–343.
67. Vandewalle, L.A., R. Van de Vijver, K.M. Van Geem, and G.B. Marin, *The role of mass and heat transfer in the design of novel reactors for oxidative coupling of methane.* Chemical Engineering Science, 2019. **198**: p. 268–289.
68. Zhang, Q., M. Liu, and A. Zeng, *Performance enhancement of pressure-swing distillation process by the combined use of vapor recompression and thermal integration.* Computers & Chemical Engineering, 2019. **120**: p. 30–45.
69. Aguiar, P., D. Chadwick, and L. Kershenbaum, *Modelling of an indirect internal reforming solid oxide fuel cell.* Chemical Engineering Science, 2002. **57**(10): p. 1665–1677.
70. Heidebrecht, P. and K. Sundmacher, *Conceptual design of the integration of the reforming process in high temperature fuel cells.* Journal of Power Sources, 2005. **145**(1): p. 40–49.
71. Kolios, G., J. Frauhammer, and G. Eigenberger, *Autothermal fixed-bed reactor concepts.* Chemical Engineering Science, 2000. **55**(24): p. 5945–5967.
72. Bac, S., S. Keskin, and A.K. Avci, *Modeling and simulation of water-gas shift in a heat exchange integrated microchannel converter.* International Journal of Hydrogen Energy, 2018. **43**(2): p. 1094–1104.
73. Schumacher, K., N. Engelbrecht, R.C. Everson, M. Friedl, and D.G. Bessarabov, *Steady-state and transient modelling of a microchannel reactor for coupled ammonia decomposition and oxidation.* International Journal of Hydrogen Energy, 2019. **44**(13): p. 6415–6426.

74. Friedle, U. and G. Veser, *A counter-current heat-exchange reactor for high temperature partial oxidation reactions: I. Experiments.* Chemical Engineering Science, 1999. **54**(10): p. 1325–1332.
75. Ellzey, J.L., E.L. Belmont, and C.H. Smith, *Heat recirculating reactors: Fundamental research and applications.* Progress in Energy and Combustion Science, 2019. **72**: p. 32–58.
76. Grünewald, M. and D.W. Agar, *Intensification of Regenerative Heat Exchange in Chemical Reactors Using Desorptive Cooling.* Industrial & Engineering Chemistry Research, 2004. **43**(16): p. 4773–4779.
77. Stankiewicz, A., *Energy Matters: Alternative Sources and Forms of Energy for Intensification of Chemical and Biochemical Processes.* Chemical Engineering Research and Design, 2006. **84**(7): p. 511–521.
78. Chen, J.Y., M. Pan, C. He, B.J. Zhang, and Q.L. Chen, *New Gasoline Absorption–Stabilization Process for Separation Intensification and Flowsheet Simplification in Refineries.* Industrial & Engineering Chemistry Research, 2018. **57**(43): p. 14707–14717.
79. Tian, Y., S.E. Demirel, M.M.F. Hasan, and E.N. Pistikopoulos, *An overview of process systems engineering approaches for process intensification: State of the art.* Chemical Engineering and Processing, 2018. **133**: p. 160–210.
80. Soria, M.A., C. Roch, S. Tosti, A. Mendes, and L.M. Madeira, *COx free hydrogen production through water-gas shift reaction in different hybrid multifunctional reactors.* Chemical Engineering Journal, 2019. **356**: p. 727–736.
81. Baldea, M., *From process integration to process intensification.* Computers & Chemical Engineering, 2015. **81**: p. 104–114.
82. Dahmen, M. and W. Marquardt, *Model-Based Formulation of Biofuel Blends by Simultaneous Product and Pathway Design.* Energy Fuels, 2017. **31**(4): p. 4096–4121.
83. Krishna, R., *Reactive separations: more ways to skin a cat.* Chemical Engineering Science, 2002. **57**(9): p. 1491–1504.
84. Stankiewicz, A., *Reactive separations for process intensification: an industrial perspective.* Chemical Engineering and Processing, 2003. **42**(3): p. 137–144.
85. Sundmacher, K., A. Kienle, and A. Seidel-Morgenstern, *Integrated Chemical Processes: Synthesis, Operation, Analysis and Control*. 2006, Weinheim: Wiley-VCH.
86. Kim, Y.-h., L.K. Park, S. Yiacoumi, and C. Tsouris, *Modular Chemical Process Intensification: A Review.* Annual Review of Chemical and Biomolecular Engineering, 2017. **8**(1): p. 359–380.
87. Marín, P., F.V. Díez, and S. Ordóñez, *Reverse flow reactors as sustainable devices for performing exothermic reactions: Applications and engineering aspects.* Chemical Engineering and Processing, 2019: p. 175–189.

88. Gupta, J., M. Agarwal, and A.K. Dalai, *Intensified transesterification of mixture of edible and nonedible oils in reverse flow helical coil reactor for biodiesel production.* Renewable Energy, 2019. **134**: p. 509–525.
89. Górak, A. and A. Hoffmann, *Catalytic distillation in structured packings: Methyl acetate synthesis.* AlChE Journal, 2001. **47**(5): p. 1067–1076.
90. Schoenmakers, H.G. and B. Bessling, *Reactive and catalytic distillation from an industrial perspective.* Chemical Engineering and Processing, 2003. **42**(3): p. 145–155.
91. Sundmacher, K. and U. Hoffmann, *Development of a new catalytic distillation process for fuel ethers via a detailed nonequilibrium model.* Chemical Engineering Science, 1996. **51**(10): p. 2359–2368.
92. Gorissen, H.J., *A general approach for the conceptual design of counter-current reactive separations.* Chemical Engineering Science, 2003. **58**(3): p. 809–814.
93. Da Cruz, F.E. and V.I. Manousiouthakis, *Process intensification of reactive separator networks through the IDEAS conceptual framework.* Computers & Chemical Engineering, 2017. **105**: p. 39–55.
94. Muthia, R., A.G.T. Reijneveld, A.G.J. van der Ham, A.J.B. Ten Kate, G. Bargeman, S.R.A. Kersten, and A.A. Kiss, *Novel method for mapping the applicability of reactive distillation.* Chemical Engineering and Processing, 2018. **128**: p. 263–275.
95. Pattison, R.C., C. Tsay, and M. Baldea, *Pseudo-transient models for multiscale, multiresolution simulation and optimization of intensified reaction/separation/recycle processes: Framework and a dimethyl ether production case study.* Computers & Chemical Engineering, 2017. **105**: p. 161–172.
96. Weinfeld, J.A., S.A. Owens, and R.B. Eldridge, *Reactive dividing wall columns: A comprehensive review.* Chemical Engineering and Processing, 2018. **123**: p. 20–33.
97. Almeida-Rivera, C.P., P.L.J. Swinkels, and J. Grievink, *Designing reactive distillation processes: present and future.* Computers & Chemical Engineering, 2004. **28**(10): p. 1997–2020.
98. Shah, M., A.A. Kiss, E. Zondervan, and A.B. de Haan, *Evaluation of configuration alternatives for multi-product polyester synthesis by reactive distillation.* Computers & Chemical Engineering, 2013. **52**: p. 193–203.
99. Dragomir, R.M. and M. Jobson, *Conceptual design of single-feed kinetically controlled reactive distillation columns.* Chemical Engineering Science, 2005. **60**(18): p. 5049–5068.
100. Zondervan, E., M. Shah, and A.B. De Haan, *Optimal Design of a Reactive Distillation Column.* Chemical Engineering Transactions, 2011. **24**: p. 295–300.
101. Tanskanen, J., V.J. Pohjola, and K.M. Lien, *Phenomenon driven process design methodology: Focus on reactive distillation.* Computers & Chemical Engineering, 1995. **19**: p. 77–82.
102. Günther, A., S.A. Khan, M. Thalmann, F. Trachsel, and K.F. Jensen, *Transport and reaction in microscale segmented gas–liquid flow.* Lab Chip, 2004. **4**(4): p. 278–286.

103. Kashid, M.N. and D.W. Agar, *Hydrodynamics of liquid–liquid slug flow capillary microreactor: Flow regimes, slug size and pressure drop.* Chemical Engineering Journal, 2007. **131**(1): p. 1–13.
104. Kreutzer, M.T., F. Kapteijn, J.A. Moulijn, and J.J. Heiszwolf, *Multiphase monolith reactors: Chemical reaction engineering of segmented flow in microchannels.* Chemical Engineering Science, 2005. **60**(22): p. 5895–5916.
105. Elsner, M.P., C. Dittrich, and D.W. Agar, *Adsorptive reactors for enhancing equilibrium gas-phase reactions—two case studies.* Chemical Engineering Science, 2002. **57**(9): p. 1607–1619.
106. Sheikh, J., L.S. Kershenbaum, and E. Alpay, *Analytical basis for separation enhanced reaction in continuous flow processes.* Chemical Engineering Science, 1998. **53**(16): p. 2933–2939.
107. Xiu, G.-h., P. Li, and A.E. Rodrigues, *New generalized strategy for improving sorption-enhanced reaction process.* Chemical Engineering Science, 2003. **58**(15): p. 3425–3437.
108. Bayat, M., Z. Dehghani, M. Hamidi, and M.R. Rahimpour, *Methanol synthesis via sorption-enhanced reaction process: Modeling and multi-objective optimization.* Journal of the Taiwan Institute of Chemical Engineers, 2014. **45**(2): p. 481–494.
109. Wess, R., F. Nores-Pondal, M. Laborde, and P. Giunta, *Single stage H-2 production, purification and heat supply by means of sorption-enhanced steam reforming of glycerol. A thermodynamic analysis.* Chemical Engineering Science, 2015. **134**: p. 86–95.
110. Phuakpunk, K., B. Chalermsinsuwan, S. Putivisutisak, and S. Assabumrungrat, *Parametric study of hydrogen production via sorption enhanced steam methane reforming in a circulating fluidized bed riser.* Chemical Engineering Science, 2018. **192**: p. 1041–1057.
111. Stevens, R.W., A. Shamsi, S. Carpenter, and R. Siriwardane, *Sorption-enhanced water gas shift reaction by sodium-promoted calcium oxides.* Fuel, 2010. **89**(6): p. 1280–1286.
112. García-Lario, A.L., G.S. Grasa, and R. Murillo, *Performance of a combined CaO-based sorbent and catalyst on H2 production, via sorption enhanced methane steam reforming.* Chemical Engineering Journal, 2015. **264**: p. 697–705.
113. Hamidi, M., F. Samimi, and M.R. Rahimpour, *Dimethyl ether synthesis in a gas–solid–solid trickle flow reactor with continuous adsorbent regeneration.* Journal of the Taiwan Institute of Chemical Engineers, 2015. **47**: p. 105–112.
114. Agrawal, S. and K.D.P. Nigam, *Modeling of coiled tubular chemical reactor.* Chemical Engineering Journal, 2001. **84**(3): p. 437–444.
115. Sawyers, D.R., M. Sen, and H.-C. Chang, *Effect of chaotic interfacial stretching on bimolecular chemical reaction in helical-coil reactors.* Chemical Engineering Journal, 1996. **64**(1): p. 129–139.
116. Saxena, A.K. and K.D.P. Nigam, *Coiled configuration for flow inversion and its effect on residence time distribution.* AlChE Journal, 1984. **30**(3): p. 363–368.

117. Mizzi, B., M. Meyer, L. Prat, F. Augier, and D. Leinekugel-Le-Cocq, *General design methodology for reactive liquid–liquid extraction: Application to dicarboxylic acid recovery in fermentation broth.* Chemical Engineering and Processing, 2017. **113**: p. 20–34.
118. Djas, M. and M. Henczka, *Reactive extraction of carboxylic acids using organic solvents and supercritical fluids: A review.* Separation and Purification Technology, 2018. **201**: p. 106–119.
119. Barecka, M.H., M. Skiborowski, and A. Górak, *A novel approach for process retrofitting through process intensification: Ethylene oxide case study.* Chemical Engineering Research and Design, 2017. **123**: p. 295–316.
120. Kelkar, V.V. and K.M. Ng, *Design of reactive crystallization systems incorporating kinetics and mass-transfer effects.* AlChE Journal, 1999. **45**(1): p. 69–81.
121. Tsuge, H., Y. Tanaka, S. Yoshizawa, and T. Kuraishi, *Reactive Crystallization Behaviour of Calcium Phosphate with and Without Whey Protein Addition.* Chemical Engineering Research and Design, 2002. **80**(1): p. 105–110.
122. Fino, D., N. Russo, G. Saracco, and V. Specchia, *Multifunctional Filter for Treatment of the Flue Gases from Municipal Waste Incinerators.* Industrial & Engineering Chemistry Research, 2005. **44**(25): p. 9542–9548.
123. Hoffmann, U. and T. Rieckmann, *Reduction of diesel particulate emissions by catalytic filtration.* Chemical Engineering & Technology, 1994. **17**(3): p. 149–160.
124. Bade, S. and U. Hoffmann, *Development of a new reactor for combined comminution and chemical reaction.* Chemical Engineering Communications, 1996. **143**(1): p. 169–193.
125. Kaupp, G., J. Schmeyers, M.R. Naimi-Jamal, H. Zoz, and H. Ren, *Reactive milling with the Simoloyer®: environmentally benign quantitative reactions without solvents and wastes.* Chemical Engineering Science, 2002. **57**(5): p. 763–765.
126. Ganzeveld, K.J. and L.P.B.M. Janssen, *Twin screw extruders as polymerization reactors for a free radical homo polymerization.* The Canadian Journal of Chemical Engineering, 1993. **71**(3): p. 411–418.
127. Moad, G., *The synthesis of polyolefin graft copolymers by reactive extrusion.* Progress in Polymer Science, 1999. **24**(1): p. 81–142.
128. Falk, T. and A. Seidel-Morgenstern, *Comparison between a fixed-bed reactor and a chromatographic reactor.* Chemical Engineering Science, 1999. **54**(10): p. 1479–1485.
129. Mazzotti, M., B. Neri, D. Gelosa, and M. Morbidelli, *Dynamics of a Chromatographic Reactor: Esterification Catalyzed by Acidic Resins.* Industrial & Engineering Chemistry Research, 1997. **36**(8): p. 3163–3172.
130. Pal, P. and P. Dey, *Process intensification in lactic acid production by three stage membrane integrated hybrid reactor system.* Chemical Engineering and Processing, 2013. **64**: p. 1–9.
131. Coronas, J. and J. Santamaría, *Catalytic reactors based on porous ceramic membranes.* Catalysis Today, 1999. **51**(3): p. 377–389.

132. Klose, F., T. Wolff, S. Thomas, and A. Seidel-Morgenstern, *Concentration and residence time effects in packed bed membrane reactors.* Catalysis Today, 2003. **82**(1): p. 25–40.
133. Tsotsis, T.T., A.M. Champagnie, S.P. Vasileiadis, Z.D. Ziaka, and R.G. Minet, *Packed bed catalytic membrane reactors.* Chemical Engineering Science, 1992. **47**(9): p. 2903–2908.
134. Hamedi, H., M. Ehteshami, S.A. Mirbagheri, S.A. Rasouli, and S. Zendehboudi, *Current Status and Future Prospects of Membrane Bioreactors (MBRs) and Fouling Phenomena: A Systematic Review.* The Canadian Journal of Chemical Engineering, 2019. **97**(1): p. 32–58.
135. Mendes, D., V. Chibante, J.M. Zheng, S. Tosti, F. Borgognoni, A. Mendes, and L.M. Madeira, *Enhancing the production of hydrogen via water-gas shift reaction using Pd-based membrane reactors.* International Journal of Hydrogen Energy, 2010. **35**(22): p. 12596–12608.
136. Gallucci, F., E. Fernandez, P. Corengia, and M.V. Annaland, *Recent advances on membranes and membrane reactors for hydrogen production.* Chemical Engineering Science, 2013. **92**: p. 40–66.
137. Mahecha-Botero, A., T. Boyd, A. Gulamhusein, N. Comyn, C.J. Lim, J.R. Grace, Y. Shirasaki, and I. Yasuda, *Pure hydrogen generation in a fluidized-bed membrane reactor: Experimental findings.* Chemical Engineering Science, 2008. **63**(10): p. 2752–2762.
138. Gil, A.G., Z.T. Wu, D. Chadwick, and K. Li, *A catalytic hollow fibre membrane reactor for combined steam methane reforming and water gas shift reaction.* Chemical Engineering Science, 2015. **137**: p. 364–372.
139. Hua, T., S. Li, F. Li, Q. Zhou, and B.S. Ondon, *Microbial electrolysis cell as an emerging versatile technology: a review on its potential application, advance and challenge.* Journal of Chemical Technology & Biotechnology, 2019.
140. Scott, K., *Process intensification: An electrochemical perspective.* Renewable & Sustainable Energy Reviews, 2018. **81**: p. 1406–1426.
141. Cecilia, R., U. Kunz, and T. Turek, *Possibilities of process intensification using microwaves applied to catalytic microreactors.* Chemical Engineering and Processing, 2007. **46**(9): p. 870–881.
142. Jachuck, R.J.J., D.K. Selvaraj, and R.S. Varma, *Process intensification: oxidation of benzyl alcohol using a continuous isothermal reactor under microwave irradiation.* Green Chemistry, 2006. **8**(1): p. 29–33.
143. Rao, D.P., A. Bhowal, and P.S. Goswami, *Process Intensification in Rotating Packed Beds (HIGEE): An Appraisal.* Industrial & Engineering Chemistry Research, 2004. **43**(4): p. 1150–1162.
144. Gogate, P.R. and A.B. Pandit, *Sonophotocatalytic reactors for wastewater treatment: A critical review.* AlChE Journal, 2004. **50**(5): p. 1051–1079.
145. Van Gerven, T., G. Mul, J. Moulijn, and A. Stankiewicz, *A review of intensification of photocatalytic processes.* Chemical Engineering and Processing, 2007. **46**(9): p. 781–789.

146. Hume, A.P., L.R. Weatherley, and J. Petera, *Trajectories of charged drops in a liquid–liquid system.* Chemical Engineering Journal, 2003. **95**(1): p. 171–177.

147. Noor, Z., M. Dogru, and G.L. Akay, S. R., *Process intensification in water-in-crude oil separation by simultaneous application of electric field and novel micro-porous polymeric demulsifiers*, in *7th World Congress of Chemical Engineering*. 2005, 5th European Congress of Chemical Engineering: Glasgow. p. 231–232.

148. Horst, C., U. Kunz, A. Rosenplänter, and U. Hoffmann, *Activated solid–fluid reactions in ultrasound reactors.* Chemical Engineering Science, 1999. **54**(13): p. 2849–2858.

149. Keil, F.J. and K.M. Swamy, *Reactors for sonochemical engineering-present status.* Reviews in Chemical Engineering, 1999. **15**(2): p. 85–155.

150. Iliuta, I. and F. Larachi, *Theory of trickle-bed magnetohydrodynamics under magnetic-field gradients.* AlChE Journal, 2003. **49**(6): p. 1525–1532.

151. Munteanu, M.C., I. Iliuta, and F. Larachi, *Process Intensification in Artificial Gravity.* Industrial & Engineering Chemistry Research, 2005. **44**(25): p. 9384–9390.

152. Gogate, P.R. and A.B. Pandit, *A review and assessment of hydrodynamic cavitation as a technology for the future.* Ultrasonics Sonochemistry, 2005. **12**(1): p. 21–27.

153. Sampath Kumar, K. and V.S. Moholkar, *Conceptual design of a novel hydrodynamic cavitation reactor.* Chemical Engineering Science, 2007. **62**(10): p. 2698–2711.

154. Zou, N., Q. Nie, X. Zhang, G. Zhang, J. Wang, and P. Zhang, *Electrothermal regeneration by Joule heat effect on carbon cloth based MnO2 catalyst for long-term formaldehyde removal.* Chemical Engineering Journal, 2019. **357**: p. 1–10.

155. Lei, Z., C. Li, and B. Chen, *Extractive Distillation: A Review.* Separation & Purification Reviews, 2003. **32**(2): p. 121–213.

156. Lelkes, Z., P. Lang, B. Benadda, and P. Moszkowicz, *Feasibility of extractive distillation in a batch rectifier.* AlChE Journal, 1998. **44**(4): p. 810–822.

157. Ohs, B., J. Lohaus, and M. Wessling, *Optimization of membrane based nitrogen removal from natural gas.* Journal of Membrane Science, 2016. **498**: p. 291–301.

158. Koch, K., D. Sudhoff, S. Kreiß, A. Górak, and P. Kreis, *Optimisation-based design method for membrane-assisted separation processes.* Chemical Engineering and Processing, 2013. **67**: p. 2–15.

159. Voncken, R.J.W., I. Roghair, and M.V. Annaland, *Mass transfer phenomena in fluidized beds with horizontally immersed membranes: A numerical investigation.* Chemical Engineering Science, 2018. **191**: p. 369–382.

160. Charcosset, C., *Review: Purification of proteins by membrane chromatography.* Journal of Chemical Technology & Biotechnology, 1998. **71**(2): p. 95–110.

161. Feng, X., C.Y. Pan, J. Ivory, and D. Ghosh, *Integrated membrane/adsorption process for gas separation.* Chemical Engineering Science, 1998. **53**(9): p. 1689–1698.

162. Ghosh, T.K., H.D. Lin, and A.L. Hines, *Hybrid adsorption-distillation process for separating propane and propylene.* Industrial & Engineering Chemistry Research, 1993. **32**(10): p. 2390–2399.
163. Kumar, R., T.C. Golden, T.R. White, and A. Rokicki, *Novel Adsorption Distillation Hybrid Scheme for Propane/Propylene Separation.* Separation Science and Technology, 1992. **27**(15): p. 2157–2170.
164. Curcio, E. and E. Drioli, *Membrane Distillation and Related Operations—A Review.* Separation & Purification Reviews, 2005. **34**(1): p. 35–86.
165. Lawson, K.W. and D.R. Lloyd, *Membrane distillation.* Journal of Membrane Science, 1997. **124**(1): p. 1–25.
166. Lutze, P. and A. Gorak, *Reactive and membrane-assisted distillation: Recent developments and perspective.* Chemical Engineering Research and Design, 2013. **91**(10): p. 1978–1997.
167. Bart, H.J., *Prozessintensivierung durch reaktive Carrier bei Reaktivextraktion und -sorption.* Chemie Ingenieur Technik, 2005. **77**(11): p. 1773–1783.
168. Huang, Y.-S., K. Sundmacher, Z. Qi, and E.-U. Schlünder, *Residue curve maps of reactive membrane separation.* Chemical Engineering Science, 2004. **59**(14): p. 2863–2879.
169. Qi, Z. and K. Sundmacher, *The impact of interfacial mass transfer on the feasible products of countercurrent reactive separation processes.* Separation and Purification Technology, 2004. **34**(1): p. 201–211.
170. Wasewar, K.L., V.G. Pangarkar, A.B.M. Heesink, and G.F. Versteeg, *Intensification of enzymatic conversion of glucose to lactic acid by reactive extraction.* Chemical Engineering Science, 2003. **58**(15): p. 3385–3393.
171. Scharzec, B., T. Waltermann, and M. Skiborowski, *A Systematic Approach towards Synthesis and Design of Pervaporation-Assisted Separation Processes.* Chemie Ingenieur Technik, 2017. **89**(11): p. 1534–1549.
172. Draxler, J. and R. Marr, *Emulsion liquid membranes part I: Phenomenon and industrial application.* Chemical Engineering and Processing, 1986. **20**(6): p. 319–329.
173. Sastre, A.M., A. Kumar, J.P. Shukla, and R.K. Singh, *Improved Techniques in Liquid Membrane Separations: An Overview.* Separation and Purification Methods, 1998. **27**(2): p. 213–298.
174. Rogers, R.D. and K.R. Seddon, *Ionic Liquids–Solvents of the Future?* Science, 2003. **302**(5646): p. 792–793.
175. Wasserscheid, P., *Continuous reactions using ionic liquids as catalytic phase.* Journal of Industrial and Engineering Chemistry, 2007. **13**(3): p. 325–338.
176. Zhang, X., C. Liu, Q. Ren, X. Qiu, B. Xu, X. Zhou, Y. Xie, H. Lou, M.C. Ali, H. Gao, Y. Bai, and S. Zhang, *Green chemical engineering in China.* Reviews in Chemical Engineering, 2019.
177. Darr, J.A. and M. Poliakoff, *New Directions in Inorganic and Metal-Organic Coordination Chemistry in Supercritical Fluids.* Chemical Reviews, 1999. **99**(2): p. 495–542.

178. Savage, P.E., S. Gopalan, T.I. Mizan, C.J. Martino, and E.E. Brock, *Reactions at supercritical conditions: Applications and fundamentals.* AlChE Journal, 1995. **41**(7): p. 1723–1778.
179. Schwuger, M.-J., K. Stickdorn, and R. Schomaecker, *Microemulsions in Technical Processes.* Chemical Reviews, 1995. **95**(4): p. 849–864.
180. Watarai, H., *Microemulsions in separation sciences.* Journal of Chromatography A, 1997. **780**(1): p. 93–102.
181. Albanese, D., *New Applications of Phase Transfer Catalysis in Organic Synthesis.* Mini-Reviews in Organic Chemistry, 2006. **3**(3): p. 195–217.
182. Behr, A., G. Henze, and R. Schomäcker, *Thermoregulated Liquid/Liquid Catalyst Separation and Recycling.* Advanced Synthesis & Catalysis, 2006. **348**(12-13): p. 1485–1495.
183. Arizmendi-Sánchez, J.A. and P.N. Sharratt, *Phenomena-based modularisation of chemical process models to approach intensive options.* Chemical Engineering Journal, 2008. **135**(1): p. 83–94.
184. Baldea, M. and T.F. Edgar, *Dynamic process intensification.* Current Opinion in Chemical Engineering, 2018. **22**: p. 48–53.
185. Matros, Y.S., *Forced unsteady-state processes in heterogeneous catalytic reactors.* The Canadian Journal of Chemical Engineering, 1996. **74**(5): p. 566–579.
186. Nikačević, N., B. Todić, M. Mandić, M. Petkovska, and D.B. Bukur, *Optimization of forced periodic operations in milli-scale fixed bed reactor for Fischer-Tropsch synthesis.* Catalysis Today, 2018.
187. Benner, P., A. Seidel-Morgenstern, and A. Zuyev, *Periodic switching strategies for an isoperimetric control problem with application to nonlinear chemical reactions.* Appl. Math. Modell., 2019. **69**: p. 287–300.
188. Nikolić, D., A. Seidel-Morgenstern, and M. Petkovska, *Periodic Operation with Modulation of Inlet Concentration and Flow Rate. Part I: Nonisothermal Continuous Stirred-Tank Reactor.* Chemical Engineering & Technology, 2016. **39**(11): p. 2020–2028.
189. Petkovska, M. and A. Seidel-Morgenstern, *Evaluation of periodic processes*, in *Periodic Operation of Reactors*, P.L. Silveston and R.R. Hudgins, Editors. 2013, Butterworth-Heinemann: Elsevier.
190. Grossmann, I.E. and M.M. Daichendt, *New trends in optimization-based approaches to process synthesis.* Computers & Chemical Engineering, 1996. **20**(6): p. 665–683.
191. Lutze, P., R. Gani, and J.M. Woodley, *Process intensification: A perspective on process synthesis.* Chemical Engineering and Processing, 2010. **49**(6): p. 547–558.
192. Roth, T., P. Kreis, and A. Górak, *Process analysis and optimisation of hybrid processes for the dehydration of ethanol.* Chemical Engineering Research and Design, 2013. **91**(7): p. 1171–1185.

193. Patel, M.P., N. Shah, and R. Ashe, *Robust optimisation methodology for the process synthesis of continuous technologies.* Computer Aided Chemical Engineering, 2011. **29**: p. 351–355.
194. Van Goethem, M.W.M., S. Barendregt, J. Grievink, J.A. Moulijn, and P.J.T. Verheijen, *Towards synthesis of an optimal thermal cracking reactor.* Chemical Engineering Research and Design, 2008. **86**(7A): p. 703–712.
195. Recker, S., C.M. Gordon, A. Peace, C. Redepenning, and W. Marquardt, *Systematic Design of a Butadiene Telomerization Process: The Catalyst Makes the Difference.* Chemie Ingenieur Technik, 2017. **89**(11): p. 1479–1489.
196. Harmsen, G.J., *Industrial best practices of conceptual process design.* Chemical Engineering and Processing, 2004. **43**(5): p. 671–675.
197. Montolio-Rodriguez, D., P. Linke, D. Linke, and M.Z. Stijepovic, *Optimal conceptual design of processes with heterogeneous catalytic reactors.* Chemical Engineering Journal, 2010. **163**(3): p. 438–449.
198. Gürsel, I.V., Q. Wang, T. Noël, and V. Hessel, *Process-Design Intensification – Direct Synthesis of Adipic Acid in Flow.* Chemical Engineering Transactions, 2012. **29**: p. 565–570.
199. Vural-Gürsel, I., Q. Wang, T. Noël, V. Hessel, and J.T. Tinge, *Improving Energy Efficiency of Process of Direct Adipic Acid Synthesis in Flow Using Pinch Analysis.* Industrial & Engineering Chemistry Research, 2013. **52**(23): p. 7827–7835.
200. Gavrila, I.S. and P. Iedema, *Phenomena-driven process design, a knowledge-based approach.* Computers & Chemical Engineering, 1996. **20**: p. S103–S108.
201. Diaconescu, R., R.Z. Tudose, and S. Curteanu, *A case study for optimal reactor networks synthesis: styrene polymerization.* Polymer-Plastics Technology and Engineering, 2002. **41**(2): p. 297–326.
202. Blahušiak, M., A.A. Kiss, K. Babic, S.R.A. Kersten, G. Bargeman, and B. Schuur, *Insights into the selection and design of fluid separation processes.* Separation and Purification Technology, 2018. **194**: p. 301–318.
203. Cheng, H., C. Liu, J. Zhang, L. Chen, B. Zhang, and Z. Qi, *Screening deep eutectic solvents for extractive desulfurization of fuel based on COSMO-RS model.* Chemical Engineering and Processing, 2018. **125**: p. 246–252.
204. Papadopoulos, A.I., P. Seferlis, and P. Linke, *A framework for the integration of solvent and process design with controllability assessment.* Chemical Engineering Science, 2017. **159**: p. 154–176.
205. Scheffczyk, J., P. Schäfer, L. Fleitmann, J. Thien, C. Redepenning, K. Leonhard, W. Marquardt, and A. Bardow, *COSMO-CAMPD: A framework for integrated design of molecules and processes based on COSMO-RS.* Molecular Systems Design & Engineering, 2018. **3**(4): p. 645–657.

206. Schilling, J., D. Tillmanns, M. Lampe, M. Hopp, J. Gross, and A. Bardow, *From molecules to dollars: integrating molecular design into thermo-economic process design using consistent thermodynamic modeling.* Molecular Systems Design & Engineering, 2017. **2**(3): p. 301–320.

207. Struebing, H., S. Obermeier, E. Siougkrou, C.S. Adjiman, and A. Galindo, *A QM-CAMD approach to solvent design for optimal reaction rates.* Chemical Engineering Science, 2017. **159**: p. 69–83.

208. Bardow, A., K. Steur, and J. Gross, *Continuous-Molecular Targeting for Integrated Solvent and Process Design.* American Chemical Society, 2010. **49**(6): p. 2834–2840.

209. Waltermann, T., T. Grueters, and M. Skiborowski, *Optimization of extractive distillation – integrated solvent selection and energy integration.* Computer Aided Chemical Engineering, 2018. **44**: p. 187–192.

210. Skiborowski, M., *Process synthesis and design methods for process intensification.* Current Opinion in Chemical Engineering, 2018. **22**: p. 216–225.

211. Li, X. and A. Kraslawski, *Conceptual process synthesis: past and current trends.* Chemical Engineering and Processing, 2004. **43**(5): p. 583–594.

212. Peschel, A., H. Freund, and K. Sundmacher, *Methodology for the Design of Optimal Chemical Reactors Based on the Concept of Elementary Process Functions.* Industrial & Engineering Chemistry Research, 2010. **49**(21): p. 10535–10548.

213. Achenie, L.K.E. and L.T. Biegler, *A superstructure based approach to chemical reactor network synthesis.* Computers & Chemical Engineering, 1990. **14**(1): p. 23–40.

214. Kokossis, A.C. and F. Christodoulos A., *Optimization of complex reactor networks—I. Isothermal operation.* Chemical Engineering Science, 1990. **45**(3): p. 595–614.

215. Kokossis, A.C. and C.A. Floudas, *Optimization of complex reactor networks—II. Nonisothermal operation.* Chemical Engineering Science, 1994. **49**(7): p. 1037–1051.

216. Marcoulaki, E.C. and A.C. Kokossis, *Scoping and screening complex reaction networks using stochastic optimization.* AlChE Journal, 1999. **45**(9): p. 1977–1991.

217. Schweiger, C.A. and C.A. Floudas, *Optimization Framework for the Synthesis of Chemical Reactor Networks.* Industrial & Engineering Chemistry Research, 1999. **38**(3): p. 744–766.

218. Smith, E.M.B. and C.C. Pantelides, *Design of reaction/separation networks using detailed models.* Computers & Chemical Engineering, 1995. **19**: p. 83–88.

219. Anantasarn, N., U. Suriyapraphadilok, and D.K. Babi, *A computer-aided approach for achieving sustainable process design by process intensification.* Computers & Chemical Engineering, 2017. **105**: p. 56–73.

220. Tian, Y. and E.N. Pistikopoulos, *Synthesis of Operable Process Intensification Systems—Steady-State Design with Safety and Operability Considerations.* Industrial & Engineering Chemistry Research, 2018. **58**(15): p. 6049–6068.

221. Glasser, D., C. Crowe, and D. Hildebrandt, *A geometric approach to steady flow reactors: the attainable region and optimization in concentration space.* Industrial & Engineering Chemistry Research, 1987. **26**(9): p. 1803–1810.
222. Horn, F. *Attainable and non-attainable regions in chemical reaction technique*. in *3rd European Symposium on Chemical Reaction Engineering*. 1964. London: Pergamon Press.
223. Glasser, D. and D. Hildebrandt, *Reactor and process synthesis.* Computers & Chemical Engineering, 1997. **21**: p. S775–S783.
224. Feinberg, M. and D. Hildebrandt, *Optimal reactor design from a geometric viewpoint—I. Universal properties of the attainable region.* Chemical Engineering Science, 1997. **52**(10): p. 1637–1665.
225. Glasser, D., D. Hildebrandt, and S. Godorr, *The Attainable Region for Segregated, Maximum Mixed, and Other Reactor Models.* Industrial & Engineering Chemistry Research, 1994. **33**(5): p. 1136–1144.
226. Glasser, B., D. Hildebrandt, and D. Glasser, *Optimal mixing for exothermic reversible reactions.* Industrial & Engineering Chemistry Research, 1992. **31**(6): p. 1541–1549.
227. Hildebrandt, D. and D. Glasser, *The attainable region and optimal reactor structures.* Chemical Engineering Science, 1990. **45**(8): p. 2161–2168.
228. Hildebrandt, D., D. Glasser, and C.M. Crowe, *Geometry of the attainable region generated by reaction and mixing: with and without constraints.* Industrial & Engineering Chemistry Research, 1990. **29**(1): p. 49–58.
229. And, A.L. and L.T. Biegler*, *Synthesis of Optimal Chemical Reactor Networks.* Industrial & Engineering Chemistry Research, 1996. **35**(4): p. 1344–1353.
230. Achenie, L.E.K. and L.T. Biegler, *Algorithmic synthesis of chemical reactor networks using mathematical programming.* Industrial & Engineering Chemistry Fundamentals, 1986. **25**(4): p. 621–627.
231. Achenie, L.K.E. and L.T. Biegler, *Developing targets for the performance index of a chemical reactor network: isothermal systems.* Industrial & Engineering Chemistry Research, 1988. **27**(10): p. 1811–1821.
232. Kokossis, A.C. and C.A. Floudas, *Synthesis of isothermal reactor—separator—recycle systems.* Chemical Engineering Science, 1991. **46**(5): p. 1361–1383.
233. Utikar, R.P. and V.V. Ranade, *Intensifying Multiphase Reactions and Reactors: Strategies and Examples.* ACS Sustainable Chemistry & Engineering, 2017. **5**(5): p. 3607–3622.
234. Mehta, V.L. and A. Kokossis, *Development of novel multiphase reactors using a systematic design framework.* Computers & Chemical Engineering, 1997. **21**: p. S325–S330.
235. Mehta, V.L., *Synthesis and optimisation of multiphase reactor networks*, in *Department of Process Integration*. 1998, UMIST: Manchester, UK. p. 267.

236. Mehta, V.L. and A.C. Kokossis, *Nonisothermal synthesis of homogeneous and multiphase reactor networks.* AlChE Journal, 2000. **46**(11): p. 2256–2273.
237. Pattison, R.C., A.M. Gupta, and M. Baldea, *Equation-oriented optimization of process flowsheets with dividing-wall columns.* AlChE Journal, 2016. **62**(3): p. 704–716.
238. Triantafyllou, C. and R. Smith, *The Design and Optimisation of Fully Thermally Coupled Distillation Columns.* Chemical Engineering Research and Design, 1992. **70**: p. 118–132.
239. Sargent, R.W.H. and K. Gaminibandara, *Optimum Design of Plate Distillation Columns*, in *Optimization in Action*, D. LCW, Editor. 1976, Academic Press: London. p. 267–314.
240. Agrawal, R., *Synthesis of Distillation Column Configurations for a Multicomponent Separation.* Industrial & Engineering Chemistry Research, 1996. **35**(4): p. 1059–1071.
241. Christiansen, A.C., S. Skogestad, and K. Lien, *Complex distillation arrangements: Extending the petlyuk ideas.* Computers & Chemical Engineering, 1997. **21**: p. S237–S242.
242. Floudas, C.A. and G.E. Paules, *A mixed-integer nonlinear programming formulation for the synthesis of heat-integrated distillation sequences.* Computers & Chemical Engineering, 1988. **12**(6): p. 531–546.
243. Aggarwal, A. and C.A. Floudast, *Synthesis of heat integrated nonsharp distillation sequences.* Computers & Chemical Engineering, 1992. **16**(2): p. 89–108.
244. Bauer, M.H. and J. Stichlmair, *Superstructures for the mixed integer optimization of nonideal and azeotropic distillation processes.* Computers & Chemical Engineering, 1996. **20**: p. S25–S30.
245. Caballero, J.A. and I.E. Grossmann, *Aggregated Models for Integrated Distillation Systems.* Industrial & Engineering Chemistry Research, 1999. **38**(6): p. 2330–2344.
246. Dünnebier, G. and C.C. Pantelides, *Optimal Design of Thermally Coupled Distillation Columns.* Industrial & Engineering Chemistry Research, 1999. **38**(1): p. 162–176.
247. Papalexandri, K.P. and E.N. Pistikopoulos, *Generalized modular representation framework for process synthesis.* AlChE Journal, 1996. **42**(4): p. 1010–1032.
248. Shah, P.B. and A.C. Kokossis, *Knowledge based models for the analysis of complex separation processes.* Computers & Chemical Engineering, 2001. **25**(4): p. 867–878.
249. Shah, P.B. and A.C. Kokossis, *New synthesis framework for the optimization of complex distillation systems.* AlChE Journal, 2002. **48**(3): p. 527–550.
250. Peschel, A., F. Karst, H. Freund, and K. Sundmacher, *Analysis and optimal design of an ethylene oxide reactor.* Chemical Engineering Science, 2011. **66**(24): p. 6453–6469.
251. Peschel, A., B. Hentschel, H. Freund, and K. Sundmacher, *Design of optimal multiphase reactors exemplified on the hydroformylation of long chain alkenes.* Chemical Engineering Journal, 2012. **188**: p. 126–141.
252. Krishna, R. and S.T. Sie, *Strategies for multiphase reactor selection.* Chemical Engineering Science, 1994. **49**(24, Part A): p. 4029–4065.

253. Kelkar, V.V. and K.M. Ng, *Screening multiphase reactors for nonisothermal multiple reactions.* AlChE Journal, 2000. **46**(2): p. 389–406.

254. Kaiser, N.M., R.J. Flassig, and K. Sundmacher, *Reactor-network synthesis via flux profile analysis.* Chemical Engineering Journal, 2018. **335**: p. 1018–1030.

255. Xie, M. and H. Freund, *Optimal reactor design and operation taking catalyst deactivation into account.* Chemical Engineering Science, 2018. **175**: p. 405–415.

256. Xie, M. and H. Freund, *Rigorous design of multiphase reactors: Identification of optimal conditions for mass transfer limited reactions.* Chemical Engineering and Processing, 2018. **124**: p. 174–185.

257. Demirel, S.E., J. Li, and M.M.F. Hasan, *Systematic process intensification using building blocks.* Computers & Chemical Engineering, 2017. **105**: p. 2–38.

258. Li, J., S.E. Demirel, and M.M.F. Hasan, *Process Integration Using Block Superstructure.* Industrial & Engineering Chemistry Research, 2018. **57**(12): p. 4377–4398.

259. Kuhlmann, H. and M. Skiborowski, *Optimization-Based Approach To Process Synthesis for Process Intensification: General Approach and Application to Ethanol Dehydration.* Industrial & Engineering Chemistry Research, 2017. **56**(45): p. 13461–13481.

260. Kuhlmann, H., H. Veith, M. Möller, K.-P. Nguyen, A. Górak, and M. Skiborowski, *Optimization-Based Approach to Process Synthesis for Process Intensification: Synthesis of Reaction-Separation Processes.* Industrial & Engineering Chemistry Research, 2018. **57**(10): p. 3639–3655.

261. Tula, A.K., M.R. Eden, and R. Gani, *Process synthesis, design and analysis using a process-group contribution method.* Computers & Chemical Engineering, 2015. **81**: p. 245–259.

262. Tula, A.K., D.K. Babi, J. Bottlaender, M.R. Eden, and R. Gani, *A computer-aided software-tool for sustainable process synthesis-intensification.* Computers & Chemical Engineering, 2017. **105**: p. 74–95.

263. Klatt, K.-U. and W. Marquardt, *Perspectives for process systems engineering—Personal views from academia and industry.* Computers & Chemical Engineering, 2009. **33**(3): p. 536–550.

264. Demirel, S.E., J. Li, and M.M.F. Hasan, *A General Framework for Process Synthesis, Integration, and Intensification.* Industrial & Engineering Chemistry Research, 2019. **58**(15): p. 5950–5967.

265. Biegler, L.T. and I.E. Grossmann, *Retrospective on optimization.* Computers & Chemical Engineering, 2004. **28**(8): p. 1169–1192.

266. Tsay, C., R.C. Pattison, M.R. Piana, and M. Baldea, *A survey of optimal process design capabilities and practices in the chemical and petrochemical industries.* Computers & Chemical Engineering, 2018. **112**: p. 180–189.

267. Biegler, L.T., *New directions for nonlinear process optimization.* Current Opinion in Chemical Engineering, 2018. **21**: p. 32–40.

268. Kiss, A.A., C.S. Bildea, and J. Grievink, *Dynamic modeling and process optimization of an industrial sulfuric acid plant.* Chemical Engineering Journal, 2010. **158**(2): p. 241–249.
269. Zondervan, E., M. Nawaz, A.B. de Haan, J.M. Woodley, and R. Gani, *Optimal design of a multi-product biorefinery system.* Computers & Chemical Engineering, 2011. **35**(9): p. 1752–1766.
270. Peschel, A., A. Jörke, K. Sundmacher, and H. Freund, *Optimal reaction concept and plant wide optimization of the ethylene oxide process.* Chemical Engineering Journal, 2012. **207-208**: p. 656–674.
271. Capón-García, E., A.D. Bojarski, A. Espuña, and L. Puigjaner, *Multiobjective evolutionary optimization of batch process scheduling under environmental and economic concerns.* AlChE Journal, 2013. **59**(2): p. 429–444.
272. Oliva, D.G., G. Guillén-Gosálbez, J.M. Mateo-Sanz, and L. Jiménez-Esteller, *MILP-based clustering method for multi-objective optimization: Application to environmental problems.* Computers & Chemical Engineering, 2013. **56**: p. 202–217.
273. Xu, B., R. Qi, W. Zhong, W. Du, and F. Qian, *Optimization of p-xylene oxidation reaction process based on self-adaptive multi-objective differential evolution.* Chemometrics and Intelligent Laboratory Systems, 2013. **127**: p. 55–62.
274. Zamarripa, M.A., A.M. Aguirre, C.A. Méndez, and A. Espuña, *Mathematical programming and game theory optimization-based tool for supply chain planning in cooperative/competitive environments.* Chemical Engineering Research and Design, 2013. **91**(8): p. 1588–1600.
275. Ng, R.T.L., D.K.S. Ng, and R.R. Tan, *Systematic Approach for Synthesis of Integrated Palm Oil Processing Complex. Part 2: Multiple Owners.* Industrial & Engineering Chemistry Research, 2013. **52**(30): p. 10221–10235.
276. García-Sánchez, L.N., R. Vázquez-Román, C. Díaz-Ovalle, and M.S. Mannan, *A Multiobjective-driven Approach to Reduce Risk in Process Layouts.* Chemical Engineering Transactions, 2013. **31**: p. 643–648.
277. Mandić, M., V. Dikić, M. Petkovska, B. Todić, D.B. Bukur, and N.M. Nikačević, *Dynamic analysis of millimetre-scale fixed bed reactors for Fischer-Tropsch synthesis.* Chemical Engineering Science, 2018. **192**: p. 434–447.
278. Brzić, D. and M. Petkovska, *Some practical aspects of nonlinear frequency response method for investigation of adsorption equilibrium and kinetics.* Chemical Engineering Science, 2012. **82**: p. 62–72.
279. Currie, R., D. Nikolic, M. Petkovska, and D.S.A. Simakov, *CO2 Conversion Enhancement in a Periodically Operated Sabatier Reactor: Nonlinear Frequency Response Analysis and Simulation-based Study.* Israel Journal of Chemistry, 2018. **58**(6-7): p. 762–775.
280. Ilić, M., M. Petkovska, and A. Seidel-Morgenstern, *Nonlinear frequency response functions of a chromatographic column—A critical evaluation of their potential for estimation of single solute adsorption isotherms.* Chemical Engineering Science, 2007. **62**(5): p. 1269–1281.

281. Ilić, M., M. Petkovska, and A. Seidel-Morgenstern, *Nonlinear frequency response method for estimation of single solute adsorption isotherms. Part I. Theoretical basis and simulations.* Chemical Engineering Science, 2007. **62**(16): p. 4379–4393.

282. Ilić, M., M. Petkovska, and A. Seidel-Morgenstern, *Nonlinear frequency response method for estimation of single solute adsorption isotherms. Part II.* Chemical Engineering Science, 2007. **62**(16): p. 4394–4408.

283. Ilić, M., M. Petkovska, and A. Seidel-Morgenstern, *Determination of competitive adsorption isotherms applying the nonlinear frequency response method. Part I. Theoretical analysis.* Journal of Chromatography A, 2009. **1216**(33): p. 6098–6107.

284. Marković, A., A.-S. Morgenstern, and M. Petkovska, *Evaluation of the potential of periodically operated reactors based on the second order frequency response function.* Chemical Engineering Research and Design, 2008. **86**(7): p. 682–691.

285. Nikolić, D., M. Felischak, A. Seidel-Morgenstern, and M. Petkovska, *Periodic Operation with Modulation of Inlet Concentration and Flow Rate Part II: Adiabatic Continuous Stirred-Tank Reactor*. Chemical Engineering & Technology, 2016. **39**(11): p. 2126–2134.

286. Nikolić, D. and M. Petkovska, *Evaluation of Performance of Periodically Operated Reactors for Single Input Modulations of General Waveforms.* Chemie Ingenieur Technik, 2016. **88**(11): p. 1715–1722.

287. Nikolić, D., A. Seidel-Morgenstern, and M. Petkovska, *Nonlinear frequency response analysis of forced periodic operation of non-isothermal CSTR with simultaneous modulation of inlet concentration and inlet temperature.* Chemical Engineering Science, 2015. **137**: p. 40–58.

288. Petkovska, M., *Nonlinear FR-ZLC method for investigation of adsorption equilibrium and kinetics.* Adsorption, 2008. **14**(2-3): p. 223–239.

289. Petkovska, M. and D.D. Do, *Use of Higher-Order Frequency Response Functions for Identification of Nonlinear Adsorption Kinetics: Single Mechanisms under Isothermal Conditions.* Nonlinear Dynamics, 2019. **21**(4): p. 353–376.

290. Petkovska, M. and A. Marković, *Fast Estimation of Quasi-Steady States of Cyclic Nonlinear Processes Based on Higher-Order Frequency Response Functions. Case Study: Cyclic Operation of an Adsorption Column.* Industrial & Engineering Chemistry Research, 2006. **45**(1): p. 266–291.

291. Petkovska, M., D. Nikolić, A. Marković, and A. Seidel-Morgenstern, *Fast evaluation of periodic operation of a heterogeneous reactor based on nonlinear frequency response analysis.* Chemical Engineering Science, 2010. **65**(11): p. 3632–3637.

292. Petkovska, M., D. Nikolić, and A. Seidel-Morgenstern, *Nonlinear Frequency Response Method for Evaluating Forced Periodic Operations of Chemical Reactors.* Israel Journal of Chemistry, 2018. **58**(6-7): p. 663–681.

293. Petkovska, M. and A. Seidel-Morgenstern, *Nonlinear frequency response of a chromatographic column. Part I: Application to estimation of adsorption isotherms with inflection points.* Chemical Engineering Communications, 2005. **192**(10): p. 1300–1333.

294. Wang, Y. and M.D. LeVan, *Master curves for mass transfer in bidisperse adsorbents for pressure-swing and volume-swing frequency response methods.* AlChE Journal, 2011. **57**(8): p. 2054–2069.

295. Brzić, D. and M. Petkovska, *A Study of Applicability of Nonlinear Frequency Response Method for Investigation of Gas Adsorption Based on Numerical Experiments.* Industrial & Engineering Chemistry Research, 2013. **52**(46): p. 16341–16351.

296. Mutavdžin, I., A. Seidel-Morgenstern, and M. Petkovska, *Estimation of competitive adsorption isotherms based on nonlinear frequency response experiments using equimolar mixtures–numerical analysis for racemic mixtures.* Chemical Engineering Science, 2013. **89**: p. 21–30.

297. Faizollahzadeh Ardabili, S., B. Najafi, S. Shamshirband, B. Minaei Bidgoli, R.C. Deo, and K.-w. Chau, *Computational intelligence approach for modeling hydrogen production: a review.* Engineering Applications of Computational Fluid Mechanics, 2018. **12**(1): p. 438–458.

298. Ley, S.V., *The Engineering of Chemical Synthesis: Humans and Machines Working in Harmony.* Angewandte Chemie International Edition, 2018. **57**(19): p. 5182–5183.

299. Mohammadi, Y., M.R. Saeb, A. Penlidis, E. Jabbari, F. J. Stadler, P. Zinck, and K. Matyjaszewski, *Intelligent Machine Learning: Tailor-Making Macromolecules.* Polymers, 2019. **11**(4): p. 579.

300. Keshtegar, B. and S. Heddam, *Modeling daily dissolved oxygen concentration using modified response surface method and artificial neural network: a comparative study.* Neural Computing and Applications, 2018. **30**(10): p. 2995–3006.

301. Venkatasubramanian, V., *The promise of artificial intelligence in chemical engineering: Is it here, finally?* AlChE Journal, 2019. **65**(2): p. 466–478.

302. Drawert, B., B. Jacob, Z. Li, T.-M. Yi, and L. Petzold, *A hybrid smoothed dissipative particle dynamics (SDPD) spatial stochastic simulation algorithm (sSSA) for advection–diffusion–reaction problems.* Journal of Computational Physics, 2019. **378**: p. 1–17.

303. Nikačević, N.M., A.E.M. Huesman, P.M.J. Van den Hof, and A.I. Stankiewicz, *Opportunities and challenges for process control in process intensification.* Chemical Engineering and Processing, 2012. **52**: p. 1–15.

304. Nikačević, N.M., P.M.J. Van den Hof, and A. Stankiewicz. *New approach to conceptual reactor design based on dynamic optimization*. in *NPS – 10*. 2010. Veldhoven, The Netherlands.

305. Nikačević, N.M., A.E.M. Huesman, P.M.J. Van den Hof, and A. Stankiewicz. *New optimization-based approach to chemical reactor synthesis-towards the full integration of reactor design, operation and control*. in *International Conference on Chemical Reactors, CHEMREACTOR – 19*. 2011. Vienna, Austria.

306. Nikačević, N.M., A.E.M. Huesman, P.M.J. Van den Hof, and A. Stankiewicz. *Novel approach to process synthesis based on dynamic optimization and exploitation of process intensification principles*. in *3rd European Process Intensification Conference (EPIC)*. 2011. Manchester, UK.

307. Almeida-Rivera, C.P. and J. Grievink, *Process Design Approach for Reactive Distillation Based on Economics, Exergy, and Responsiveness Optimization.* Industrial & Engineering Chemistry Research, 2008. **47**(1): p. 51–65.

308. Shah, M., A.A. Kiss, E. Zondervan, and A.B. de Haan, *A systematic framework for the feasibility and technical evaluation of reactive distillation processes.* Chemical Engineering and Processing, 2012. **60**: p. 55–64.

309. Harmsen, G.J., *Reactive distillation: The front-runner of industrial process intensification: A full review of commercial applications, research, scale-up, design and operation.* Chemical Engineering and Processing, 2007. **46**(9): p. 774–780.

310. Huesman, A., P. Van Den Hof, and A. Stankiewicz. *On the essential role of process control in process intensification*. in *The 2nd European Process Intensification Conference – EPIC 2*. 2009. Venice, IT.

311. Huesman, A.E.M., O.H. Bosgra, and P.M.J. Van den Hof, *Towards the systematic design of actuation for process systems.* IFAC Proceedings Volumes, 2010. **43**(5): p. 469–474.

312. Huesman, A.E.M., O.H. Bosgra, and P.M.J. Van den Hof. *Integrating MPC and RTO in the Process Industry by Economic Dynamic Lexicographic Optimization; An Open-Loop Exploration*. in *AICHE Annual Meeting*. 2008. Philadelphia, USA.

313. Adris, A.M., S.S.E.H. Elnashaie, and R. Hughes, *A fluidized bed membrane reactor for the steam reforming of methane.* The Canadian Journal of Chemical Engineering, 1991. **69**(5): p. 1061–1070.

314. Gallucci, F., M. Van Sintannaland, and J.A.M. Kuipers, *Theoretical comparison of packed bed and fluidized bed membrane reactors for methane reforming.* International Journal of Hydrogen Energy, 2010. **35**(13): p. 7142–7150.

315. Sarić, M., Y.C. van Delft, R. Sumbharaju, D.F. Meyer, and A. de Groot, *Steam reforming of methane in a bench-scale membrane reactor at realistic working conditions.* Catalysis Today, 2012. **193**(1): p. 74–80.

316. Xie, M., Z. Zhou, Y. Qi, Z. Cheng, and W. Yuan, *Sorption-enhanced steam methane reforming by in situ CO2 capture on a CaO–Ca9Al6O18 sorbent.* Chemical Engineering Journal, 2012. **207-208**: p. 142–150.

317. Fischer, C.D. and O.A. Iribarren, *Improvements in the Design of the Ammonia Synthesis Process Implementing Counter Current Gas Permeation Modules.* Industrial & Engineering Chemistry Research, 2012. **51**(50): p. 16410–16418.

318. Westerterp, K.R. and M. Kuczynski, *A model for a countercurrent gas—solid—solid trickle flow reactor for equilibrium reactions. The methanol synthesis.* Chemical Engineering Science, 1987. **42**(8): p. 1871–1885.
319. Bayat, M., M. Heravi, and M.R. Rahimpour, *Sorption enhanced process by integrated heat-exchanger reactor assisted by fluidization concept for methanol synthesis.* Chemical Engineering and Processing: Process Intensification, 2016. **110**: p. 30–43.
320. Farsi, M. and A. Jahanmiri, *Methanol production in an optimized dual-membrane fixed-bed reactor.* Chemical Engineering and Processing, 2011. **50**(11): p. 1177–1185.
321. Hashimoto, K., M. Kawase, and P.L. Silveston, *Simulated Moving Bed Chromatographic Reactors*, in *Periodic Operation of Chemical Reactors*. 2013, Butterworth-Heinemann: Oxford, UK.
322. Shore, G., M. Tsimerman, and M.G. Organ, *Gold film-catalysed benzannulation by Microwave-Assisted, Continuous Flow Organic Synthesis (MACOS).* The Beilstein Journal of Organic Chemistry, 2009. **5**(1): p. 35.
323. Lomel, S., L. Falk, J.M. Commenge, J.L. Houzelot, and K. Ramdani, *The Microreactor: A Systematic and Efficient Tool for the Transition from Batch to Continuous Process?* Chemical Engineering Research and Design, 2006. **84**(5): p. 363–369.
324. Wiles, C. and P. Watts, *Translation of microwave methodology to continuous flow for the efficient synthesis of diaryl ethers via a base-mediated SNAr reaction.* The Beilstein Journal of Organic Chemistry, 2011. **7**(1): p. 1360–1371.
325. Mamaghani, A.H., B. Najafi, A. Shirazi, and F. Rinaldi, *Exergetic, economic, and environmental evaluations and multi-objective optimization of a combined molten carbonate fuel cell-gas turbine system.* Applied Thermal Engineering, 2015. **77**: p. 1–11.
326. Rajesh, J.K., S.K. Gupta, G.P. Rangaiah, and A.K. Ray, *Multi-objective optimization of industrial hydrogen plants.* Chemical Engineering Science, 2001. **56**(3): p. 999–1010.
327. Rajesh, J.K., S.K. Gupta, G.P. Rangaiah, and A.K. Ray, *Multiobjective optimization of steam reformer performance using genetic algorithm.* Industrial & Engineering Chemistry Research, 2000. **39**(3): p. 706–717.
328. Linke, P. and A. Kokossis, *On the robust application of stochastic optimisation technology for the synthesis of reaction/separation systems.* Computers & Chemical Engineering, 2003. **27**(5): p. 733–758.
329. Parulekar, S.J., *Systematic performance analysis of continuous processes subject to multiple input cycling.* Chemical Engineering Science, 2003. **58**(23): p. 5173–5194.
330. Choi, Y. and H.G. Stenger, *Water Gas Shift Reaction Kinetics and Reactor Modeling for Fuel Cell Grade Hydrogen.* Journal of Power Sources, 2003. **124**(2): p. 432–439.

331. Ovesen, C.V., B.S. Clausen, B.S. Hammershøi, G. Steffensen, T. Askgaard, I. Chorkendorff, J.K. Nørskov, P.B. Rasmussen, P. Stoltze, and P. Taylor, *A Microkinetic Analysis of the Water–Gas Shift Reaction under Industrial Conditions.* Journal of Catalysis, 1996. **158**(1): p. 170–180.

332. Gokhale, A.A., J.A. Dumesic, and M. Mavrikakis, *On the mechanism of low-temperature water gas shift reaction on copper.* Journal of the American Chemical Society, 2008. **130**(4): p. 1402–1414.

333. Koryabkina, N.A., A.A. Phatak, W.F. Ruettinger, R.J. Farrauto, and F.H. Ribeiro, *Determination of kinetic parameters for the water–gas shift reaction on copper catalysts under realistic conditions for fuel cell applications.* Journal of Catalysis, 2003. **217**(1): p. 233–239.

334. Sedghkerdar, M.H., E. Mostafavi, and N. Mahinpey, *Sorbent enhanced hydrogen production from steam gasification of coal integrated with CO2 capture.* International Journal of Hydrogen Energy, 2014. **39**(30): p. 17001–17008.

335. Dou, B., Y. Song, C. Wang, H. Chen, M. Yang, and Y. Xu, *Hydrogen production by enhanced-sorption chemical looping steam reforming of glycerol in moving-bed reactors.* Applied Energy, 2014. **130**: p. 342–349.

336. Mostafavi, E., N. Mahinpey, and V. Manovic, *A novel development of mixed catalyst–sorbent pellets for steam gasification of coal chars with in situ CO2 capture.* Catalysis Today, 2014. **237**: p. 111–117.

337. Noor, T., M.V. Gil, and D. Chen, *Production of fuel-cell grade hydrogen by sorption enhanced water gas shift reaction using Pd/Ni–Co catalysts.* Applied Catalysis B, 2014. **150-151**: p. 585–595.

338. Byun, C.K., S.J. Kwon, H.B. Im, H.S. Ahn, H.J. Ryu, and K.B. Yi, *Novel method for investigation of a K–Mg-based CO2 sorbent for sorption-enhanced water–gas shift reaction.* Renewable Energy, 2016. **87**: p. 415–421.

339. Najmi, B., O. Bolland, and K.E. Colombo, *A systematic approach to the modeling and simulation of a Sorption Enhanced Water Gas Shift (SEWGS) process for CO2 capture.* Separation and Purification Technology, 2016. **157**: p. 80–92.

340. Boon, J., P.D. Cobden, H.A.J. van Dijk, and M. van Sint Annaland, *High-temperature pressure swing adsorption cycle design for sorption-enhanced water–gas shift.* Chemical Engineering Science, 2015. **122**: p. 219–231.

341. Soria, M.A., S. Tosti, A. Mendes, and L.M. Madeira, *Enhancing the low temperature water-gas shift reaction through a hybrid sorption-enhanced membrane reactor for high-purity hydrogen production.* Fuel, 2015. **159**: p. 854–863.

342. Hafizi, A., M.R. Rahimpour, and S. Hassanajili, *High purity hydrogen production via sorption enhanced chemical looping reforming: Application of 22Fe2O3/MgAl2O4 and 22Fe2O3/Al2O3 as oxygen carriers and cerium promoted CaO as CO2 sorbent.* Applied Energy, 2016. **169**: p. 629–641.

343. Kotyczka-Moranska, M., G. Tomaszewicz, and G. Labojko, *Comparison of different methods for enhancing CO2 capture by CaO-based sorbents. Review.* Physicochemical Problems of Mineral Processing, 2012. **48**: p. 70–90.

344. Fernández, J.R. and J.C. Abanades, *Chapter Three - Reactor Design for Sorption-Enhanced Reforming Using CaCu Chemical Loops.* Advances in Chemical Engineering, 2017. **51**: p. 207–260.

345. Chen, S., W. Xiang, D. Wang, and Z. Xue, *Incorporating IGCC and CaO sorption-enhanced process for power generation with CO2 capture.* Applied Energy, 2012. **95**: p. 285–294.

346. Li, Z.-s. and N.-s. Cai, *Modeling of Multiple Cycles for Sorption-Enhanced Steam Methane Reforming and Sorbent Regeneration in Fixed Bed Reactor.* Energy Fuels, 2007. **21**(5): p. 2909–2918.

347. Perejon, A., L.M. Romeo, Y. Lara, P. Lisbona, A. Martinez, and J.M. Valverde, *The Calcium-Looping technology for CO2 capture: On the important roles of energy integration and sorbent behavior.* Applied Energy, 2016. **162**: p. 787–807.

348. Liu, W., H. An, C. Qin, J. Yin, G. Wang, B. Feng, and M. Xu, *Performance Enhancement of Calcium Oxide Sorbents for Cyclic CO2 Capture—A Review.* Energy & Fuels, 2012. **26**(5): p. 2751–2767.

349. Halikia, I., L. Zoumpoulakis, E. Christodoulou, and D. Prattis, *Kinetic study of the thermal decomposition of calcium carbonate by isothermal methods of analysis.* European Journal of Mineral Processing and Environmental Protection, 2001. **1**: p. 89–102.

350. Nouri, S.M.M., H. Ale Ebrahim, and B. Naser Nejad, *Preparation of a Nano CaO Sorbent for Improvement the Capacity for CO2 Capture Reaction.* Synthesis and Reactivity in Inorganic, Metal-Organic, and Nano-Metal Chemistry, 2015. **45**(6): p. 828–833.

351. Yu, C.-t., H.-t. Kuo, and Y.-m. Chen, *Carbon dioxide removal using calcium aluminate carbonates on titanic oxide under warm-gas conditions.* Applied Energy, 2016. **162**: p. 1122–1130.

352. Bhatia, S.K. and D.D. Perlmutter, *Effect of the product layer on the kinetics of the CO2-lime reaction.* AlChE Journal, 1983. **29**(1): p. 79–86.

353. Comiti, J., E. Mauret, and M. Renaud, *Mass transfer in fixed beds: proposition of a generalized correlation based on an energetic criterion.* Chemical Engineering Science, 2000. **55**(22): p. 5545–5554.

354. Lee, D.K., *An apparent kinetic model for the carbonation of calcium oxide by carbon dioxide.* Chemical Engineering Journal, 2004. **100**(1): p. 71–77.

355. Johnsen, K., J.R. Grace, S.S.E.H. Elnashaie, L. Kolbeinsen, and D. Eriksen, *Modeling of Sorption-Enhanced Steam Reforming in a Dual Fluidized Bubbling Bed Reactor.* Industrial & Engineering Chemistry Research, 2006. **45**(12): p. 4133–4144.

356. Stendardo, S. and P.U. Foscolo, *Carbon dioxide capture with dolomite: A model for gas–solid reaction within the grains of a particulate sorbent.* Chemical Engineering Science, 2009. **64**(10): p. 2343–2352.

357. Wang, H., Z. Li, X. Fan, and N. Cai, *Rate-Equation-Based Grain Model for the Carbonation of CaO with CO2.* Energy & Fuels, 2017. **31**(12): p. 14018–14032.

358. Li, Z., H. Sun, and N. Cai, *Rate Equation Theory for the Carbonation Reaction of CaO with CO2.* Energy Fuels, 2012. **26**(7): p. 4607–4616.

359. Nikulshina, V., M.E. Gálvez, and A. Steinfeld, *Kinetic analysis of the carbonation reactions for the capture of CO2 from air via the Ca(OH)2–CaCO3–CaO solar thermochemical cycle.* Chemical Engineering Journal, 2007. **129**(1): p. 75–83.

360. Alvarez, D. and J.C. Abanades, *Determination of the Critical Product Layer Thickness in the Reaction of CaO with CO2.* Industrial & Engineering Chemistry Research, 2005. **44**(15): p. 5608–5615.

361. Hughes, R.W., D. Lu, E.J. Anthony, and Y. Wu, *Improved Long-Term Conversion of Limestone-Derived Sorbents for In Situ Capture of CO2 in a Fluidized Bed Combustor.* Industrial & Engineering Chemistry Research, 2004. **43**(18): p. 5529–5539.

362. Gupta, H. and L.-S. Fan, *Carbonation–Calcination Cycle Using High Reactivity Calcium Oxide for Carbon Dioxide Separation from Flue Gas.* Industrial & Engineering Chemistry Research, 2002. **41**(16): p. 4035–4042.

363. Grasa, G.S. and J.C. Abanades, *CO2 Capture Capacity of CaO in Long Series of Carbonation/Calcination Cycles.* Industrial & Engineering Chemistry Research, 2006. **45**(26): p. 8846–8851.

364. Valverde, J.M., *A model on the CaO multicyclic conversion in the Ca-looping process.* Chemical Engineering Journal, 2013. **228**: p. 1195–1206.

365. Valverde, J.M., P.E. Sanchez-Jimenez, and L.A. Perez-Maqueda, *Calcium-looping for post-combustion CO2 capture. On the adverse effect of sorbent regeneration under CO2.* Applied Energy, 2014. **126**: p. 161–171.

366. Baier, T. and G. Kolb, *Temperature control of the water gas shift reaction in microstructured reactors.* Chemical Engineering Science, 2007. **62**(17): p. 4602–4611.

367. LeValley, T.L., A.R. Richard, and M.H. Fan, *The progress in water gas shift and steam reforming hydrogen production technologies - A review.* International Journal of Hydrogen Energy, 2014. **39**(30): p. 16983–17000.

368. Mendes, D., A. Mendes, L.M. Madeira, A. Iulianelli, J.M. Sousa, and A. Basile, *The water-gas shift reaction: from conventional catalytic systems to Pd-based membrane reactors - a review.* Asia-Pacific Journal of Chemical Engineering, 2010. **5**(1): p. 111–137.

369. Jang, H.M., K.B. Lee, H.S. Caram, and S. Sircar, *High-purity hydrogen production through sorption enhanced water gas shift reaction using K2CO3-promoted hydrotalcite.* Chemical Engineering Science, 2012. **73**: p. 431–438.
370. Rostrup-Nielsen, J.R. and T. Rostrup-Nielsen, *Large-scale hydrogen production.* Cattech, 2002. **6**(4): p. 150–159.
371. Barelli, L., G. Bidini, F. Gallorini, and S. Servili, *Hydrogen production through sorption-enhanced steam methane reforming and membrane technology: A review.* Energy, 2008. **33**(4): p. 554–570.
372. Martinez, I., M.C. Romano, P. Chiesa, G. Grasa, and R. Murillo, *Hydrogen production through sorption enhanced steam reforming of natural gas: Thermodynamic plant assessment.* International Journal of Hydrogen Energy, 2013. **38**(35): p. 15180–15199.
373. Chen, H., M. Cao, L. Zhao, J. Ciora, Richard J., P.K.T. Liu, V.I. Manousiouthakis, and T.T. Tsotsis, *Experimental Study of an Intensified Water–Gas Shift Reaction Process Using a Membrane Reactor/Adsorptive Reactor Sequence.* Industrial & Engineering Chemistry Research, 2018. **57**(41): p. 13650–13660.
374. Smith, R.J.B., M. Loganathan, and M.S. Shantha, *A Review of the Water Gas Shift Reaction Kinetics.* International Journal of Chemical Reactor Engineering, 2010. **8**.
375. Holladay, J.D., J. Hu, D.L. King, and Y. Wang, *An overview of hydrogen production technologies.* Catalysis Today, 2009. **139**(4): p. 244-260.
376. Nikačević, N.M., *Multiphase flow dynamics in gas – flowing solids – fixed bed contactors*. 2008, University of Belgrade: Faculty of Technology and Metallurgy.
377. Nikačević, N.M., M. Petkovska, and M.P. Duduković, *Solids flow pattern in gas-flowing solids-fixed bed contactors. Part I Experimental.* Chemical Engineering Science, 2009. **64**(10): p. 2501–2509.
378. Karafyllis, I. and P. Daoutidis, *Control of hot spots in plug flow reactors.* Computers & Chemical Engineering, 2002. **26**(7-8): p. 1087–1094.
379. Koros, W.J. and R. Mahajan, *Pushing the limits on possibilities for large scale gas separation: which strategies?* Journal of Membrane Science, 2001. **181**(1): p. 141–141.
380. NIST, T.N.I.o.S.a.T. 2019 2019/03/04/; Available from: https://www.nist.gov.
381. Sutherland, W., *LII. The viscosity of gases and molecular force.* London, Edinburgh, and Dublin Philosophical Magazine and Journal of Science, 1893. **36**(223): p. 507–531.
382. Groppi, G. and E. Tronconi, *Honeycomb supports with high thermal conductivity for gas/solid chemical processes.* Catalysis Today, 2005. **105**(3-4): p. 297–304.
383. Rajan, K.S., K. Dhasandhan, S.N. Srivastava, and B. Pitchumani, *Studies on gas-solid heat transfer during pneumatic conveying.* International Journal of Heat and Mass Transfer, 2008. **51**(11-12): p. 2801–2813.

384. Whitaker, S., *Forced convection heat transfer correlations for flow in pipes, past flat plates, single cylinders, single spheres, and for flow in packed beds and tube bundles.* AIChE Journal, 1972. **18**(2): p. 361–371.

385. Froment, G.F., K.B. Bischoff, and J. De Wilde, *Chemical Reactor Analysis and Design, 3rd Edition*. 2010: Wiley.

386. Jacobs, G.K., D.M. Kerrick, and K.M. Krupka, *The high-temperature heat capacity of natural calcite (CaCO3).* Physics and Chemistry of Minerals, 1981. **7**(2): p. 55–59.

Appendices

Appendix A Conditions for Water-Gas Shift and Sorption-Enhanced Water-Gas Shift Experiments

Table A.1 – Operating conditions for WGS reaction experiments [3]

Exp. №	Temp., °C	Tot. inlet flow rate, mL/min	Inlet STCO ratio	Catalyst mass, mg	Inert to catalyst ratio	Number of runs
1-5	270	33	1.7:1 1.4:1 1.1.1 0.7.1 0.4:1	485.5	9.2:1	84
6-10	300					96
11-15	330					95
16-20	360					98
21-25	390					110
26-30	420					104
31-35	450					82
36-40	480					110
41	480	66	1:1			18
42		200				19
43		302				19
44	240	200	1.6:1	360.3	14.3:1	19
45-49	270		1.6:1 1.3:1 1:1			121
50-54	300		0.7:1 0.4:1			123
55-56	330		0.7:1 0.4:1			42

Table A.2 – Operating conditions for WGS reaction experiments [3]

Exp. №	Temp., °C	Tot. inlet flow rate, mL/min	Inlet STCO ratio	Catalyst mass, mg	Inert to catalyst ratio	Number of runs
57-61	240	100	1.6:1	317.8	7.9:1	139
62-66	270					128
67-71	300					132
72-76	330		1.3:1			131
77-81	360		1:1			138
82-86	390					126
87-91	420		0.7:1			128
92-96	450		0.4:1			131
97-101	480					112
102-106	510					112

Table A.3 – Operating experimental conditions for SE–WGS reaction [3]

Exp. №	Temp., °C	Tot. inlet flow rate, mL/min	Inlet STCO ratio	Catalyst mass, mg	Sorbent to catalyst ratio	Number of data points*
1	351	200	1:1	372.7	9:1	15
2	480	200	1:1	532.7	9:1	57
3	480	67	1:1	456.3	10:1	57
4	480	33	1:1	51.7	102:1	58
5	350	33	1:1	54.1	98:1	97
6	480	33	1:1	50.7	66:1	119
7	480	503	1:1	35.1	56:1	33
8	479	503	1:1	1869.5	0.3:1	24
9	480	33	1.7:1	34.3	130:1	48
10	480	33	1.7:1	485.5	9:1	43
11	450	33	1.7:1	479.5	9:1	40
12	428	33	1.7:1	483.2	9:1	81
13	390	33	1.7:1	481	10:1	65
14	360	33	1.7:1	486.8	9:1	54
15	420	16	1.6:1	479.6	9:1	281
16	446	33	1.4:1	486	9:1	6
17	330	33	1.7:1	490	9:1	24
18	510	8	1.6:1	490.7	12:1	310
19	300	33	1.7:1	469.4	10:1	30
20	270	33	1.7:1	494.6	10:1	43

* This number refers only to points gathered during the second and third phase of the experiment, which was used for parameter estimation.

Table A.4 – Operating experimental conditions for SE–WGS reaction [3]

Exp. №	Temp., °C	Tot. inlet flow rate, mL/min	Inlet STCO ratio	Catalyst mass, mg	Sorbent to catalyst ratio	Number of data points*
21	390	8	1.6:1	216.1	28:1	275
22	390	200	1.6:1	288.6	14:1	56
23	386	8	1.6:1	496.9	12:1	295
24	390	200	1.6:1	603.6	6:1	15
25	390	200	1.6:1	601.2	6:1	38
26	300	100	1.3:1	509.8	10:1	47
27	386	8	1.2:1	250.64	20:1	254
28	360	100	1.3:1	500.99	10:1	59
29	360	8	1.2:1	250.44	20:1	286
30	480	100	0.7:1	509.8	10:1	52
31	360	100	1.3:1	500.8	1:1	70
32	360	57	1054:1	500.62	1:1	117
33	360	100	1.3:1	501.07	14:1	193
34	360	100	1.3:1	250.22	28:1	52
35	360	100	1.3:1	501.04	10:1	480
36	360	100	1.3:1	501.3	10:1	139
37	360	100	1.6:1	501.41	10:1	212
38	359	100	1:1	501	10:1	164
39	360	97	0.7:1	501.2	10:1	218
40	360	100	1.2:1	501.3	10:1	171
41	360	100	0.7:1	501.4	10:1	225

* This number refers only to points gathered during the second and third phase of the experiment, which was used for parameter estimation.

Table A.5 – Carbon mass percentage in the analyzed experiment samples [3]

Exp. №	C mass, %	Exp. №	C mass, %	Exp. №	C mass, %
4	7.51	13	6.14	22	4.27
5	3.26	14	3.50	23	5.67
6	9.04	16	5.11	25	4.03
7	6.91	17	1.71	26	1.44
9	7.14	18	12.00	27	4.67
10	8.34	19	1.32	28	2.29
11	6.74	20	1.32	29	3.98
12	5.90	21	4.68	30	1.72

Appendix B Additional Simulation Results for Cases a, b and d

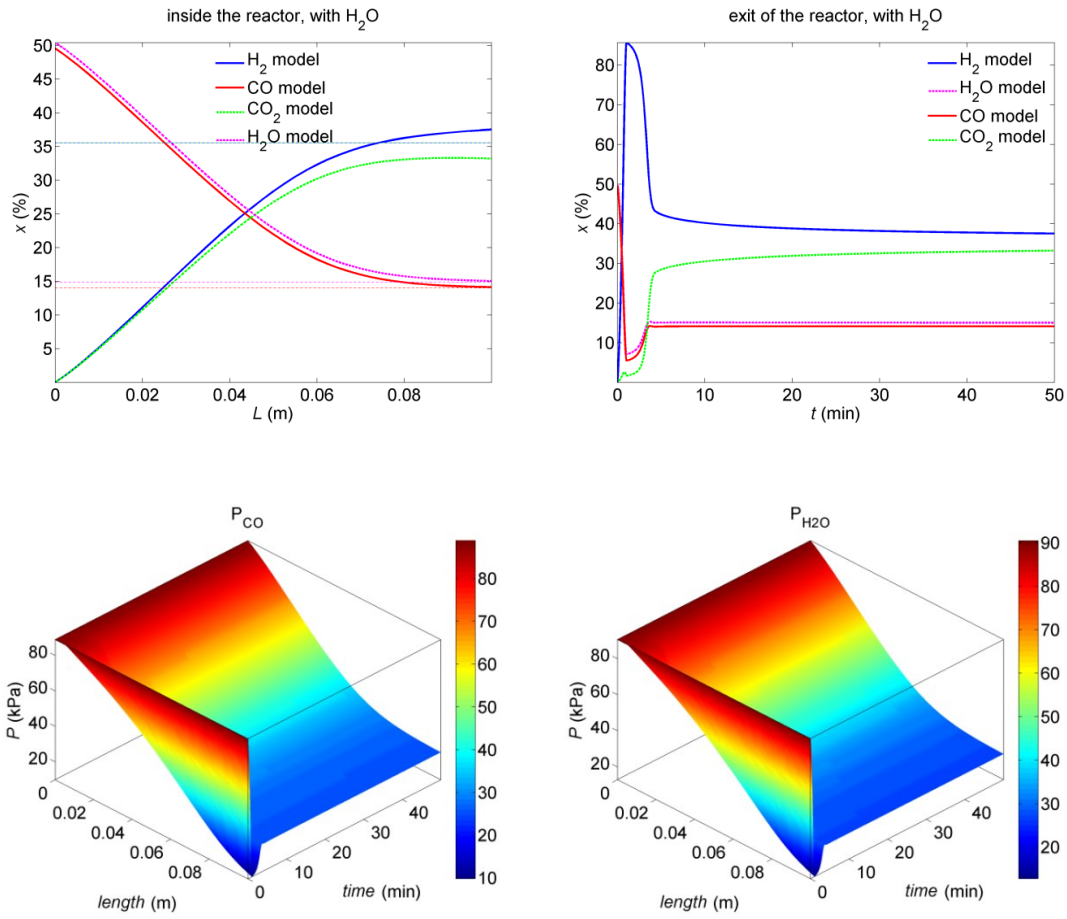

Figure B.1 – Additional simulation results for Case a [3]

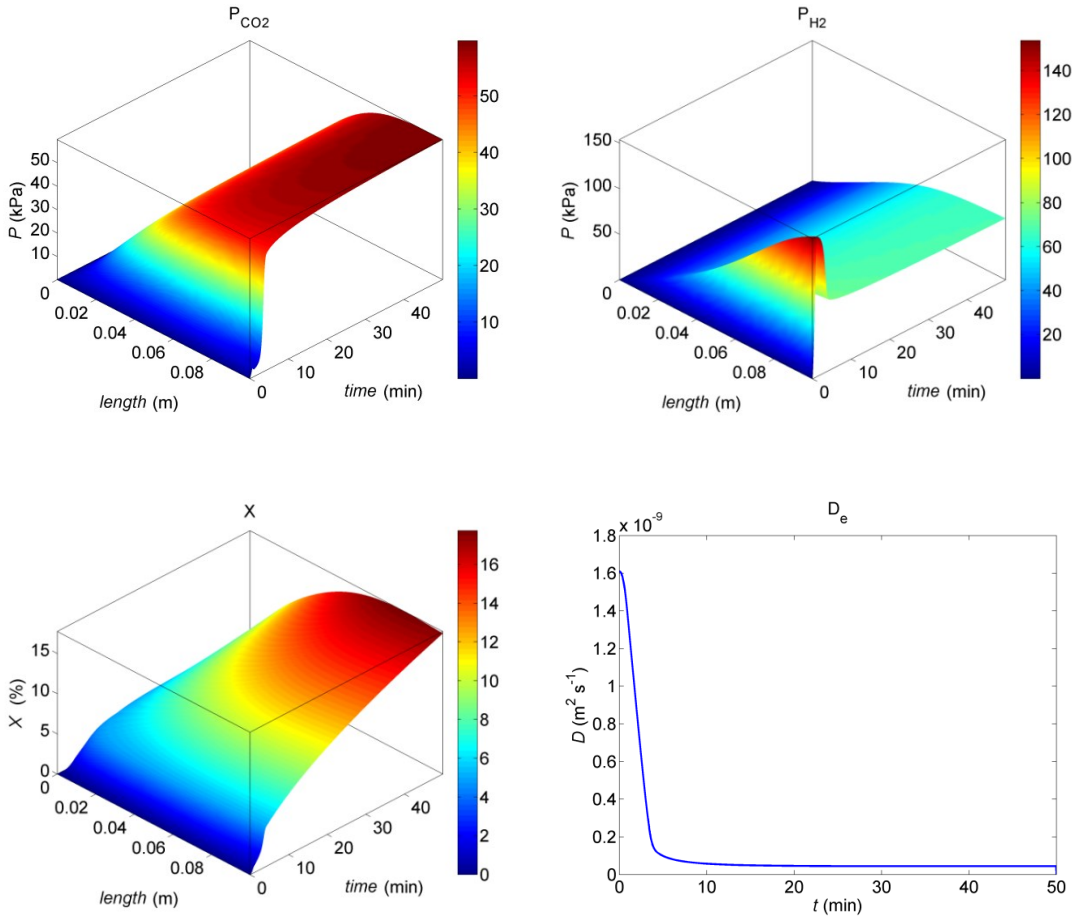

Figure B.2 – Additional simulation results for Case a [3]

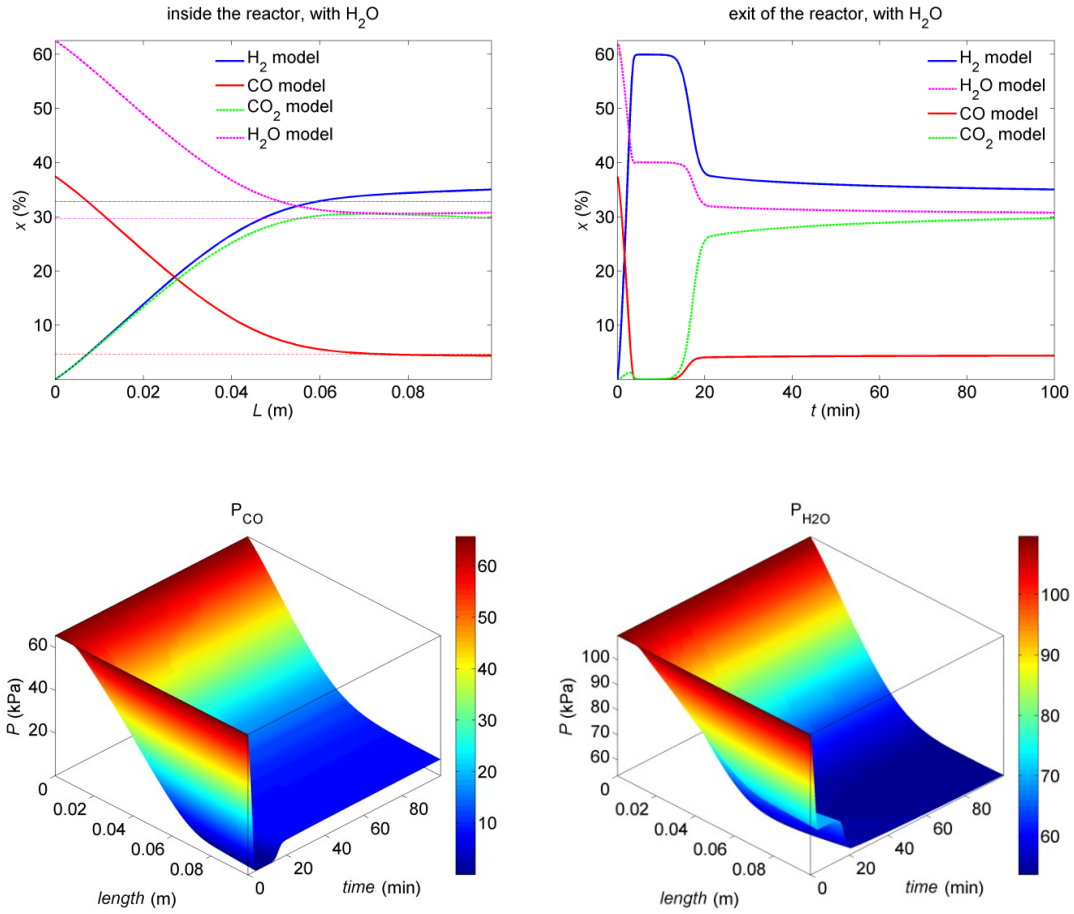

Figure B.3 – Additional simulation results for Case b [3]

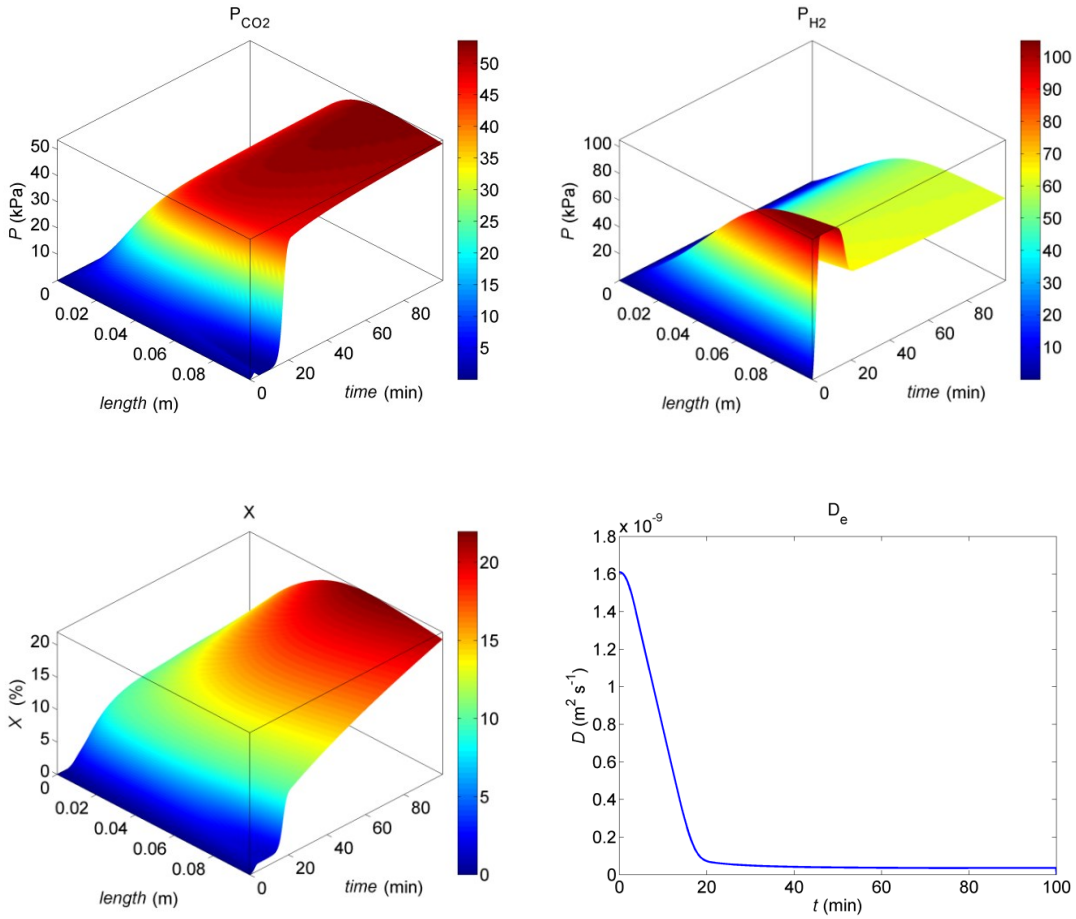

Figure B.4 – Additional simulation results for Case b [3]

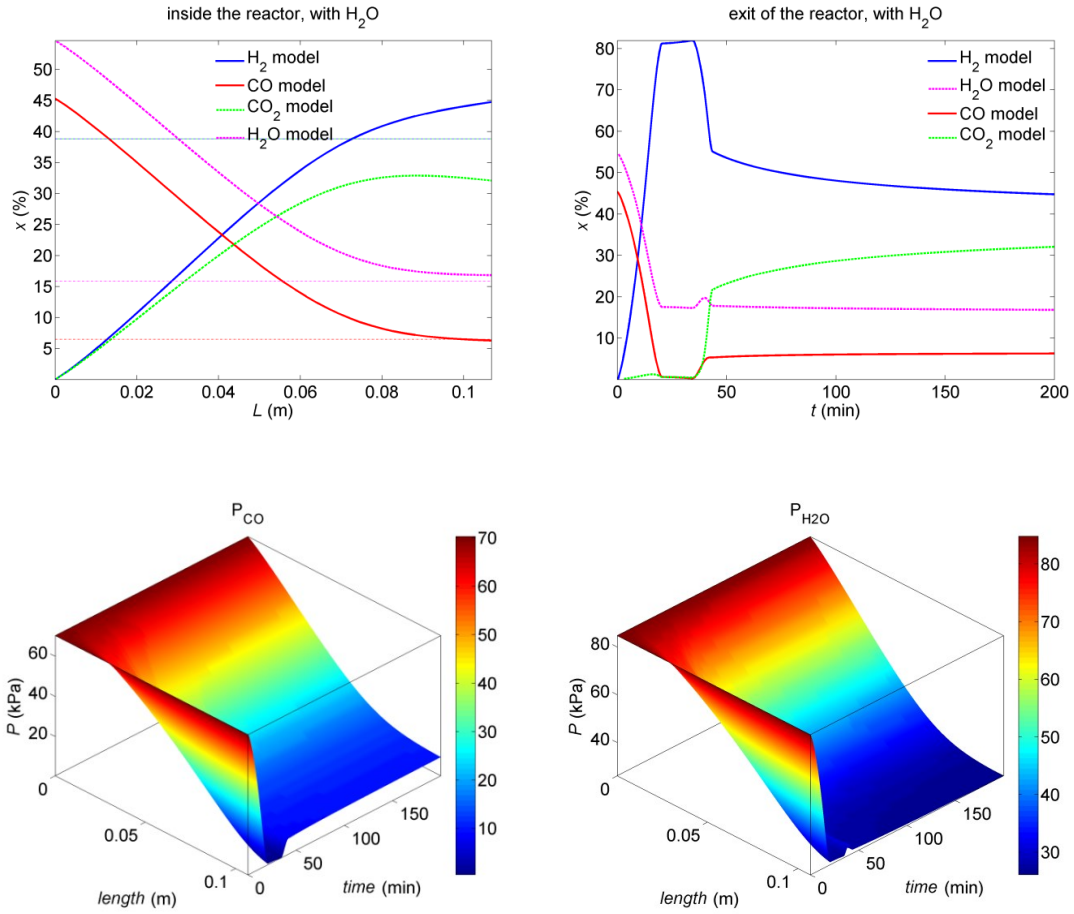

Figure B.5 – Additional simulation results for Case d [3]

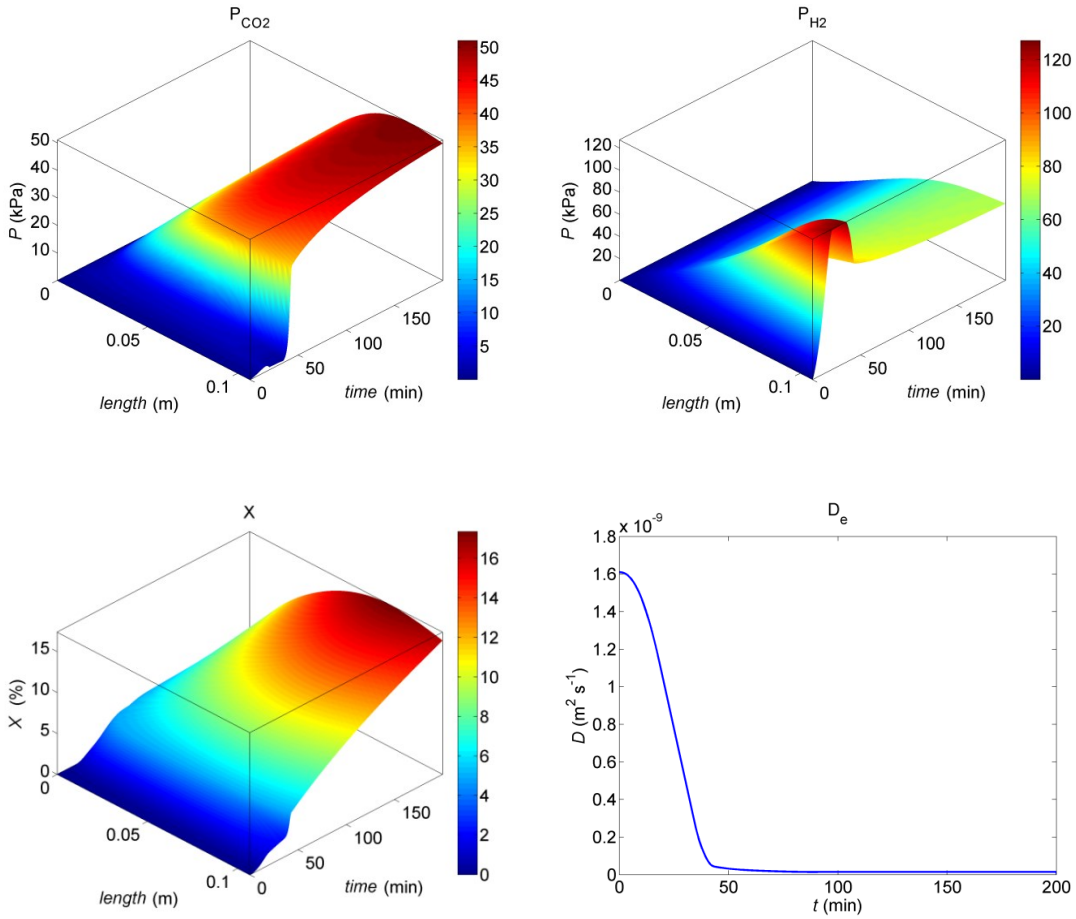

Figure B.6 – Additional simulation results for Case d [3]

Appendix C Additional Model Equations

Material Balance Parameters and Variables

Kinetic and diffusion parameters for chemisorption and sorbent conversion [3]:

$$De^i = \begin{cases} De_0^i + \left(De_1^i - De_0^i\right), & X_s^i < X_{s,max}^i \\ De_1^i, & X_s^i > X_{s,max}^i \end{cases} \tag{C.1}$$

$$De^i \approx \frac{1}{1 + e^{100 \cdot \left(1 - \frac{X_s^i}{X_{s,max}^i}\right)}} \cdot De_1^i + \frac{1}{1 + e^{100 \cdot \left(1 - X_{s,max}^i / X_s^i\right)}} \cdot \left[De_0^i + \left(De_1^i - De_0^i\right) \cdot X_s^i / X_{s,max}^i\right] \tag{C.2}$$

$$De_1^i = De_{1,a} \cdot T_R^i + De_{1,b} \tag{C.3}$$

$$X_{s,max}^i = X_{s,a} \cdot T_R^i + X_{s,b} \tag{C.4}$$

$$X_s^i = 1 - \left(\frac{r_{CaO}^i}{R_{CaO}}\right)^3 \tag{C.5}$$

$$k_{car}^i = Aa_{car} \cdot e^{-Ea_{car}/R/T_R^i} \tag{C.6}$$

Water-gas-shift (WGS) reaction equilibrium correlation [3]:

$$K_{eqb}^i = e^{\frac{5693.5}{T_R^i} + 1.077 \cdot \log\left(T_R^i\right) + 5.44 \cdot 10^{-4} T_R^i - 1.125 \cdot 10^{-7} {T_R^i}^2 - 4.917 \cdot 10^4 {T_R^i}^{-2} - 13.148} \tag{C.7}$$

Sorbent hold-up and velocity equations [376, 377]:

$$d_{eq}^{i} = \frac{6 \cdot \left(1 - \varepsilon_{sp}^{i}\right)}{a_s + 4/d_h^i} \tag{C.8}$$

$$\beta_{dyn}^{i} = 9.67 \cdot {Re_{sp}^{i}}^{1.123} \cdot {Ar^{i}}^{-0.486} \cdot {Ke^{i}}^{0.453} \cdot \left(\frac{d_{eq}^{i}}{d_h^i}\right)^{-0.647} \cdot \left(1 - \varepsilon_{sp}^{i}\right)^{-0.404} \cdot {\varepsilon_{sp}^{i}}^{0.726} / 100 \tag{C.9}$$

$$\beta_{stat}^{i} \approx 0 \tag{C.10}$$

$$\varepsilon_S^i = \beta_{dyn}^{i} + \beta_{stat}^{i} \tag{C.11}$$

$$u_S^i = \frac{J_S^i \cdot A_h^i}{\rho_S^i \cdot \varepsilon_S^i \cdot A_R^i} \tag{C.12}$$

Energy Balance Parameters and Variables

Heat transfer coefficient equations and the corresponding correlations:

$$\frac{1}{U_{RM}^{i}} \approx \frac{d_h^i}{4 \cdot \lambda_{er}^{i}} + \frac{1}{h_{RM}^{i}} \tag{C.13}$$

$$\frac{1}{U_{RW}^{i}} \approx \frac{1}{h_{RW}^{i}} + \frac{d_h^i}{4 \cdot \lambda_{er}^{i}} \tag{C.14}$$

$$\frac{1}{U_{RS}^{i}} \approx \frac{1}{h_{RS}^{i}} \tag{C.15}$$

Effective radial conductivity [382]:

$$\lambda_{er}^{i} = \lambda_{e,sp}^{i} \approx \lambda_{sp}^{i} \cdot \left(\left(1 - \sqrt{\varepsilon_v^i}\right) + \frac{\sqrt{\varepsilon_v^i}}{\left(1 - \sqrt{\varepsilon_v^i}\right) + \frac{\lambda_R^i}{\lambda_{sp}^i} \cdot \sqrt{\varepsilon_v^i}} \right) \tag{C.16}$$

Structured catalyst support conductivity (binomial fit for *NIST* [380] aluminum data):

$$\lambda_{sp}^{i} = \lambda_{Al}^{i} = -5 \cdot 10^{-5} \cdot {T_R^i}^2 + 5 \cdot 10^{-3} \cdot T_R^i + 246 \tag{C.17}$$

Correlation for heat transfer between R and S phase [383]:

$$h_{RS}^{i} = 8.2951 \cdot 10^{-7} \cdot {Re_s^i}^{5.3365} \cdot {F_m^i}^{-1.3863} \cdot {Fe^i}^{-5.0530} \cdot \frac{\lambda_R^i}{2 \cdot R_{CaO}} \tag{C.18}$$

Correlation for heat transfer between R and M phase [384]:

$$h_{RM}^{i} = 1.86 \cdot {Re_{sb}^i}^{1/3} \cdot {Pr^i}^{1/3} \cdot \left(\frac{L^i}{2 \cdot r_M^i}\right)^{-1/3} \cdot \left(\frac{\mu_{H_2,M}^i}{\mu_{H_2,R}^i}\right)^{0.14} \cdot \frac{\lambda_M^i}{2 \cdot r_M^i} \tag{C.19}$$

Correlation for heat transfer between R and W phase [385]:

$$h_{RW}^{i} = \frac{10.21}{{d_h^i}^{4/3}} \cdot \lambda_{e,sp}^{i} + 0.033 \cdot Re_R^i \cdot Pr_R^i \cdot \frac{\lambda_R^i}{d_{eq}^i} \tag{C.20}$$

Viscosity equations

For CO and CO_2 components, Sutherland model is used [381]:

$$\mu_m^i = \mu_{0,m} \cdot \frac{va_m}{vb_m^i} \cdot \left(\frac{T_{Rs}^i}{T_{Rs,0}}\right)^{3/2} \cdot 10^{-3} \tag{C.21}$$

$$va_m = 0.555 \cdot T_{R,0} + v1_m \tag{C.22}$$

$$vb_m^i = 0.555 \cdot T_{R,r}^i + v1_m \tag{C.23}$$

For H_2, N_2, and steam, the linear fit of *NIST* experimental data is used [380]:

$$\mu_m^i = v2_m \cdot T^i + v3_m \tag{C.24}$$

For the gaseous mixture:

$$\varphi_{\mu,mn}^i = \frac{\left[1 + \left(\frac{\mu_m^i}{\mu_n^i}\right)^{1/2} \cdot \left(\frac{M_n}{M_m}\right)^{1/4}\right]^2}{\left[8 \cdot \left(1 + \frac{M_m}{M_n}\right)\right]^{1/2}} \tag{C.25}$$

$$\mu^i = \sum_m \frac{y_m^i \cdot \mu_m^i}{\sum_n y_n^i \cdot \varphi_{\mu,mn}^i} \tag{C.26}$$

Isobaric heat capacity equations

For all gaseous components and CaO, parameters for Shomate equations are taken from *NIST* [380]:

$$c_{p,m}^{i} = c_{pA,m} + c_{pB,m} \cdot \frac{T^{i}}{1000} + c_{pC,m} \cdot \left(\frac{T^{i}}{1000}\right)^{2} + c_{pD,m} \cdot \left(\frac{T^{i}}{1000}\right)^{3} + c_{pE,m} / \left(\frac{T^{i}}{1000}\right)^{2} \tag{C.27}$$

For $CaCO_3$, calcite [386]:

$$c_{p,CaCO_3}^{i} = -184.79 + 0.32322 \cdot T_S^{i} - 3688200 / {T_S^{i}}^{2} - 1.2974 \cdot 10^{-4} \cdot {T_S^{i}}^{2} + 3883.5 \cdot {T_S^{i}}^{-0.5} \tag{C.28}$$

For R (*n=5*) and M (*n=2*) phase gas:

$$c_p^{i} = \sum_{m=1}^{n} y_m^{i} \cdot c_{p,m}^{i} \tag{C.29}$$

For the S phase:

$$c_{p,S}^{i} = X_s^{i} \cdot c_{p,CaCO_3}^{i} + \left(1 - X_s^{i}\right) c_{p,CaO}^{i} \tag{C.30}$$

Conductivity equations

For gaseous components, binomial fit for *NIST* experimental data is used [380]:

$$\lambda_m^i = l1_m \cdot T^{i^2} + l2_m \cdot T^i + l3_m \tag{C.31}$$

For the gaseous mixture:

$$\varphi_{\lambda,mn}^i = \frac{\left[1 + \left(\frac{\lambda_m^i}{\lambda_n^i}\right)^{1/2} \cdot \left(\frac{M_n}{M_m}\right)^{1/4}\right]^2}{\left[8 \cdot \left(1 + \frac{M_m}{M_n}\right)\right]^{1/2}} \tag{C.32}$$

$$\lambda^i = \sum_m \frac{y_m^i \cdot \lambda_m^i}{\sum_n y_n^i \cdot \varphi_{\lambda,mn}^i} \tag{C.33}$$

Non-dimensional numbers, intermediate and other variables

$$Re_R^i = \frac{F_R^i \cdot M_R^i \cdot d_{eq}^i}{A_h^i \cdot \mu_R^i} \tag{C.34}$$

$$Pr_R^i = \frac{c_{p,R}^i \cdot \mu_R^i}{\lambda_R^i} \tag{C.35}$$

$$Fm = \frac{J_S^i \cdot A_h^i}{F_R^i \cdot M_R^i} \tag{C.36}$$

$$Fe^i = 2 \cdot R_{CaO} \cdot \left[\frac{4 \cdot g \cdot {\rho_R^i}^2}{3 \cdot {\mu_R^i}^2} \cdot \left(\frac{\rho_S^i}{\rho_R^i} - 1\right)\right]^{1/3} \tag{C.37}$$

$$Ar = \frac{(2 \cdot R_{CaO})^3 \cdot \left(\rho_S^i - \rho_R^i\right) \cdot \rho_R^i \cdot g}{{\mu_R^i}^2} \tag{C.38}$$

$$Re_{sp}^i = \frac{d_{eq}^i \cdot u_R^i \cdot \rho_R^i}{\mu_R^i} \tag{C.39}$$

$$Ke^i = \frac{{J_S^i}^2}{\rho_S^i \cdot \rho_R^i \cdot {u_R^i}^2} \tag{C.40}$$

$$Re_{sp}^{\prime,i} = \frac{d_{eq}^i \cdot u_R^i \cdot \rho_R^i}{\varepsilon_{sp}^i \cdot \mu_R^i} \tag{C.41}$$

$$Re_s^i = \frac{2 \cdot R_{CaO} \cdot u_{rel}^i \cdot \rho_R^i}{\mu_R^i} \tag{C.42}$$

$$c_D^i = \frac{24}{Re_S^i} \cdot \left(1 + 0.173 \cdot {Re_S^i}^{0.6567}\right) + \frac{0.413}{1 + 16300 \cdot {Re_S^i}^{-1.09}} \tag{C.43}$$

$$\varepsilon_R^i = 1 - \varepsilon_{sp}^i - \varepsilon_S^i - \varepsilon_M^i \tag{C.44}$$

$$\varepsilon_v^i = 1 - \varepsilon_{sp}^i \tag{C.45}$$

$$y_n^i = \frac{F_n^i}{F_R^i} \tag{C.46}$$

$$p_n^i = y_n^i \cdot p_R^i \tag{C.47}$$

$$M_R^i = \sum_{n=1}^{5} \left(M_n \cdot y_n^i\right) \tag{C.48}$$

$$M_M^i = \sum_{n=1}^{2} \left(M_n \cdot y_n^i\right) \tag{C.49}$$

$$A_h^i = \left({r_R^i}^2 - {r_M^i}^2\right) \cdot \pi \tag{C.50}$$

$$\rho_R^i = \frac{p_R^i \cdot M_R^i}{R \cdot T_R^i} \tag{C.51}$$

$$u_R^i = \frac{F_R^i \cdot R \cdot T_R^i}{p_R^i \cdot A_h^i} \tag{C.52}$$

$$d_h^i = 2 \cdot \left(r_R^i - r_M^i\right) \tag{C.53}$$

$$u_{rel}^i = u_R^i - u_S^i \tag{C.54}$$

$$M_S^i = X_s^i \cdot M_{CaCO_3} + \left(1 - X_s^i\right) \cdot M_{CaO} \tag{C.55}$$

$$\rho_S^i = X_s^i \cdot \rho_{CaCO_3} + \left(1 - X_s^i\right) \cdot \rho_{CaO} \tag{C.56}$$

Segment inlet/outlet variables and total carbon monoxide conversion

$$y_{ine}^{i,in} = 0.1 \tag{C.57}$$

$$y_{CO_2}^{i,in} = 0.005 \tag{C.58}$$

$$y_{H_2}^{i,in} = 0.005 \tag{C.59}$$

$$y_{CO}^{i,in} = \frac{1}{1 + STCO^{i,in}} - \frac{y_{H_2}^{i,in}}{2} - \frac{y_{CO_2}^{i,in}}{2} - \frac{y_{ine}^{i,in}}{2} \tag{C.60}$$

$$y_{H_2O}^{i,in} = 1 - y_{CO}^{i,in} - y_{H_2}^{i,in} - y_{CO_2}^{i,in} - y_{ine}^{i,in} \tag{C.61}$$

$$F_R^i = \frac{F_R^{i-1,out} \cdot Ns^{i-1} + F_R^{i,in}}{Ns^i} \tag{C.62}$$

$$T_R^i = \frac{F_R^{i-1,out} \cdot Ns^{i-1} \cdot M_R^{i-1,out} \cdot c_{p,R}^{i-1,out} \cdot T_{R,i}^{i-1,out} + F_R^{i,in} \cdot FM_R^{i,in} \cdot c_p^{i,in} \cdot T^{i,in}}{F_R^{i-1,out} \cdot Ns^{i-1} \cdot M_R^{i-1,out} \cdot c_{p,R}^{i-1,out} + F_R^{i,in} \cdot FM_R^{i,in} \cdot c_p^{i,in}} \tag{C.63}$$

$$F_n^i = \frac{F_R^{i-1,out} \cdot Ns^{i-1} \cdot y_{n,R}^{i-1,out} + F_R^{i,in} \cdot y_n^{i,in}}{Ns^i} \tag{C.64}$$

$$y_n^i = \frac{F_n^i}{F_R^{i,}} \tag{C.65}$$

$$F_M^i = F_M^{in}/Ns^i \tag{C.66}$$

$$X_{CO} = \frac{\sum_{i=1}^{Nm}\left(F_R^i \cdot y_{CO}^i \cdot Ns^i\right) - F_R^{Nm,out} \cdot y_{CO,R}^{Nm,out} \cdot Ns^{Nm}}{\sum_{i=1}^{Nm}\left(F_R^i \cdot y_{CO}^i \cdot Ns^i\right)} \tag{C.67}$$

Appendix D Parameter Values

Viscosity is calculated by using equations (C.21–C.26). Sutherland model (C.21) [381] and *NIST* fitted parameters (C.24) [380] are given in Table D.1.

Table D.1: Viscosity parameters [4]

m	$v1_{mj}$	$v2_m$	$v3_m$	T_0 (°R)	$\mu_{0,m}$ (cP)
CO	118			518.67	0.01720
CO_2	240			527.67	0.01480
H_2		$1.5712 \cdot 10^{-8}$	$4.8759 \cdot 10^{-6}$		
H_2O		$4.1262 \cdot 10^{-8}$	$-3.3468 \cdot 10^{-6}$		
N_2		$3.2347 \cdot 10^{-8}$	$1.0086 \cdot 10^{-5}$		

Isobaric heat capacity is calculated by using equations (C.27–C.30). Shomate equation (C.27) parameters [380] are given in Table D.2.

Table D.2: Shomate equation parameters [4]

m	$c_{A,m}$	$c_{B,m}$	$c_{C,m}$	$c_{D,m}$	$c_{E,m}$
CO	25.56759	6.096130	4.054656	-2.671301	0.131021
CO_2	24.99735	55.18696	-33.69137	7.948387	-0.136638
H_2	33.066178	-11.363417	11.432816	-2.772874	-0.158558
H_2O	30.09200	6.832514	6.793435	-2.534480	0.082139
N_2	19.50583	19.88705	-8.598535	1.369784	0.527601
CaO	49.95403	4.887916	-0.352056	0.046187	-0.825097

Conductivity is calculated by using equations (C.31–C.36). *NIST* binomial fit parameters (C.31) are given in Table D.3 [380].

Table D.3: Conductivity parameters [4]

m	$l1_m$	$l2_m$	$l3_m$
CO	-3.5692·10^{-8}	8.9536·10^{-5}	2.9568·10^{-3}
CO_2	-1.6240·10^{-8}	9.8509·10^{-5}	-1.1704·10^{-2}
H_2	3.1820·10^{-8}	4.4086·10^{-4}	5.2115·10^{-2}
H_2O	4.5502·10^{-8}	5.5900·10^{-5}	-3.4951·10^{-3}
N_2	-4.8047·10^{-9}	6.3090·10^{-5}	7.7960·10^{-3}

Water gas shift reaction parameters [3]:

Aa_{wgs}	pre-exponential factor	$1.109\ molkPa^{-a-b-c-d}/g$
Ea_{wgs}	activation energy	$62.1\ kJ/mol$
ΔH_{wgs}	reaction enthalpy	$-41.2\ kJ/mol$

Carbonization reaction and diffusion parameters [3]:

Aa_{car}	pre-exponential factor	$100.5\ m/s$
De_0	initial apparent diffusion parameter	$1.65 \cdot 10^{-9} m^2/s$
De_{1a}	final apparent diffusion parameter	$3.34 \cdot 10^{-13} m^2/K/s$
De_{1b}	final apparent diffusion parameter	$-1.15 \cdot 10^{-10} m^2/s$
$X_{s,a}$	diffusion limited sorbent conversion parameter	$1.10 \cdot 10^{-3} 1/K$
$X_{s,b}$	diffusion limited sorbent conversion parameter	$-6.39 \cdot 10^{-1}$
Ea_{car}	activation energy	$72.0\ kJ/mol$
ΔH_{car}	reaction enthalpy	$-178.1\ kJ/mol$

Membrane separation parameters [135]:

Aa_{mem}	pre-exponential factor	$5.4 \cdot 10^{-8}\ molm/m^2/s$
Ea_{mem}	activation energy	$10.72\ kJ/mol$
δ	membrane thickness	$50\ \mu m$

Biography of the Author

Luka Živković was born in Belgrade on the 21st of March, 1984. He graduated at the Department of Chemical Engineering, on Faculty of Technology and Metallurgy of the University of Belgrade, with the average grade 9.64/10. His final thesis on the undergraduate studies was titled: "Application of Nonlinear Frequency Response Method in the Kinetics Investigation of the Electrochemical Hydrogen Reaction – Theoretical Analysis."

Luka Živković is employed in Faculty of Technology and Metallurgy from 2012, where he takes participation in research activities. He was a visiting researcher at Chemical Institute in Ljubljana (Slovenia) and Max-Planck Institute for dynamics of complex technical systems in Magdeburg (Germany).

Luka Živković enrolled in Ph.D. studies at the Faculty of Technology and Metallurgy in 2011 at the Department of Chemical Engineering. He is the co-author of three papers in the leading international journal (M21).

Прилог 1.

Изјава о ауторству

Име и презиме аутора Лука Живковић

Број индекса 4049/2011

Изјављујем

да је докторска дисертација под насловом

Методологија за синтезу реактора заснована на концептима интензификације процеса и примени метода оптимизације

- резултат сопственог истраживачког рада;
- да дисертација у целини ни у деловима није била предложена за стицање друге дипломе према студијским програмима других високошколских установа;
- да су резултати коректно наведени и
- да нисам кршио/ла ауторска права и користио/ла интелектуалну својину других лица.

Потпис аутора

У Београду, 17.05.2019. године

Лука Живковић

Прилог 2.

Изјава о истоветности штампане и електронске верзије докторског рада

Име и презиме аутора Лука Живковић

Број индекса 4049/2011

Студијски програм хемијско инжењерство

Наслов рада Методологија за синтезу реактора заснована на концептима интензификације процеса и примени метода оптимизације

Ментор Проф. Др Никола Никачевић

Изјављујем да је штампана верзија мог докторског рада истоветна електронској верзији коју сам предао/ла ради похрањена у **Дигиталном репозиторијуму Универзитета у Београду.**

Дозвољавам да се објаве моји лични подаци везани за добијање академског назива доктора наука, као што су име и презиме, година и место рођења и датум одбране рада.

Ови лични подаци могу се објавити на мрежним страницама дигиталне библиотеке, у електронском каталогу и у публикацијама Универзитета у Београду.

Потпис аутора

У Београду, 17.05.2019. године

Прилог 3.

Изјава о коришћењу

Овлашћујем Универзитетску библиотеку „Светозар Марковић“ да у Дигитални репозиторијум Универзитета у Београду унесе моју докторску дисертацију под насловом:

Методологија за синтезу реактора заснована на концептима интензификације процеса и примени метода оптимизације

која је моје ауторско дело.

Дисертацију са свим прилозима предао/ла сам у електронском формату погодном за трајно архивирање.

Моју докторску дисертацију похрањену у Дигиталном репозиторијуму Универзитета у Београду и доступну у отвореном приступу могу да користе сви који поштују одредбе садржане у одабраном типу лиценце Креативне заједнице (Creative Commons) за коју сам се одлучио/ла.

1. Ауторство (CC BY)

2. Ауторство – некомерцијално (CC BY-NC)

3. Ауторство – некомерцијално – без прерада (CC BY-NC-ND)

4. Ауторство – некомерцијално – делити под истим условима (CC BY-NC-SA)

5. Ауторство – без прерада (CC BY-ND)

6. Ауторство – делити под истим условима (CC BY-SA)

(Молимо да заокружите само једну од шест понуђених лиценци.
Кратак опис лиценци је саставни део ове изјаве).

Потпис аутора

У Београду, 17.05.2019. године

Јука Живковић

1. **Ауторство**. Дозвољавате умножавање, дистрибуцију и јавно саопштавање дела, и прераде, ако се наведе име аутора на начин одређен од стране аутора или даваоца лиценце, чак и у комерцијалне сврхе. Ово је најслободнија од свих лиценци.

2. **Ауторство – некомерцијално**. Дозвољавате умножавање, дистрибуцију и јавно саопштавање дела, и прераде, ако се наведе име аутора на начин одређен од стране аутора или даваоца лиценце. Ова лиценца не дозвољава комерцијалну употребу дела.

3. **Ауторство – некомерцијално – без прерада**. Дозвољавате умножавање, дистрибуцију и јавно саопштавање дела, без промена, преобликовања или употребе дела у свом делу, ако се наведе име аутора на начин одређен од стране аутора или даваоца лиценце. Ова лиценца не дозвољава комерцијалну употребу дела. У односу на све остале лиценце, овом лиценцом се ограничава највећи обим права коришћења дела.

4. **Ауторство – некомерцијално – делити под истим условима**. Дозвољавате умножавање, дистрибуцију и јавно саопштавање дела, и прераде, ако се наведе име аутора на начин одређен од стране аутора или даваоца лиценце и ако се прерада дистрибуира под истом или сличном лиценцом. Ова лиценца не дозвољава комерцијалну употребу дела и прерада.

5. **Ауторство – без прерада**. Дозвољавате умножавање, дистрибуцију и јавно саопштавање дела, без промена, преобликовања или употребе дела у свом делу, ако се наведе име аутора на начин одређен од стране аутора или даваоца лиценце. Ова лиценца дозвољава комерцијалну употребу дела.

6. **Ауторство – делити под истим условима**. Дозвољавате умножавање, дистрибуцију и јавно саопштавање дела, и прераде, ако се наведе име аутора на начин одређен од стране аутора или даваоца лиценце и ако се прерада дистрибуира под истом или сличном лиценцом. Ова лиценца дозвољава комерцијалну употребу дела и прерада. Слична је софтверским лиценцама, односно лиценцама отвореног кода.

Оцена извештаја о провери оригиналности докторске дисертације

На основу Правилника о поступку провере оригиналности докторских дисертација које се бране на Универзитету у Београду и налаза у извештају генерисаном од стране софтвера IThenticate којим је извршена провера оригиналности докторске дисертације „**Методологија за синтезу реактора заснована на концептима интензификације процеса и примени метода оптимизације (енг. A methodology for reactor synthesis based on process intensification concepts and application of optimization methods)**“ аутора и кандидата **Луке Живковића**, констатујем да подударање текста износи 42%. Од тога већина подударности (око 26%) долази од предходно публикованих резултата докторанда, проистеклих из саме дисертације, што је у складу са чланом 9. Правилника. Остале подударности (око 16%) простичу у највећој мери из научних радова коју су представљени и анализирани у прегледу литературе. Сви научни радови из извештаја су адекватно цитирани и наведени у списку литературе. За велику већину радова из литературе подударност је до 50 речи, сем за неколицину научних радова, који су кључни за дисертацију (где подударност не прелази 250 речи). Напоменуо бих да је већа подударност од уобичајене за докторске дисертације са Универзитета у Београду последица тога да је ова дисертација написана на енглеском језику.

На основу анализе и свега изнетог, а у складу са чланом 8. Став 2. Правилника о поступку провере оригиналности докторских дисертација које се бране на Универзитету у Београду, изјављујем да извештај указује на оригиналност докторске дисертације, те се прописани поступак припреме за њену одбрану може наставити.

Београд, 20.6.2019.

Ментор

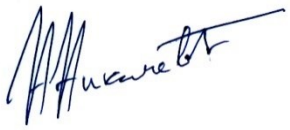

Др Никола Никачевић, редовни професор

Универзитет у Београду, Технолошко-металуршки факултет